THEORY OF OPTICAL RECTIFICATION IN A TRAVELLING WAVE STRUCTURE

A DISSERTATION

SUBMITTED TO THE DEPARTMENT OF ELECTRONICS AND ELECTRICAL ENGINEERING

OF GLASGOW UNIVERSITY

IN PARTIAL FULFILLMENT OF THE REQUIREMENTS

FOR THE DEGREE OF

DOCTOR OF PHILOSOPHY

By

Karsten Bubke

November 2001

Abstract

This thesis is concerned with the interaction of an optical wave with a microwave in a waveguiding structure coupled by a second order nonlinearity. Emphasis is laid upon the generation of ultrashort electrical transients via optical rectification (OR) as well as cascading effects due to the interplay of OR and the linear electro-optic effect.

A simple transmission line model is introduced to explain qualitatively the basic physical mechanisms of an externally induced polarisation in a travelling wave structure. For a quantitative description, evolution equations for the overall interaction between the microwave and the optical wave based on a coupled mode formalism are developed. The basic properties of the structure under consideration are discussed and techniques for their evaluation are introduced. A set of corresponding parameters for typical structures is estimated and used for calculations throughout the thesis. The generation of electrical signals from optical waves via OR is discussed in detail for the cases of single and mixed polarization optical modes in the structure. The self phase modulation due to cascading of OR and the electro-optic effect is elucidated.

It is shown that continuous wave solutions of the conservative system are modulationally unstable in a large range of relevant system parameters. The possibility of formation of solitary waves due to the mutual interaction of optical wave and microwave is considered in the context of long wave short wave interaction. Basic properties of bright stationary solutions and their excitation are discussed. The possibility of formation of solitons due to microwave self-interaction is illuminated.

The linear stability of bright solitary waves is investigated. The observed oscillations and radiation of perturbed propagated bound states are explained by the existence of discrete, quasi-bound internal modes of the stationary solutions. Collision scenarios are addressed.

Publications

Refereed Journal Papers

- K. Bubke, U. Peschel, and D. C. Hutchings, "**Mixed polarization optical rectification in semiconductor waveguides,**" to be published in JOSA B, November 2001.

- U. Peschel, K. Bubke, D. C. Hutchings, and F. Lederer, "**Temporal solitary waves due to optical rectification and the electro-optic effect,**" Opt. Lett., vol.26, no.14, pp. 1090-1092, 2001.

- U. Peschel, K. Bubke, D. C. Hutchings, J. M. Arnold, and J. S. Aitchison, "**Optical rectification in a travelling wave geometry,**" Phys. Rev. A, vol. 60, no. 6, pp. 4918-4926, 1999.

Conference Contributions

- K. Bubke, U.Peschel, and D. C. Hutchings, "**Modulational Instability in Optical-Microwave Generation,**" LEOS Annual Meeting, San Diego, USA, 2001.

- K. Bubke, U.Peschel, F. Lederer, and D. C. Hutchings, "**Internal modes of solitary waves in optical-microwave interaction,**" QEP 15, Glasgow, 2001.

- K. Bubke, U.Peschel, and D. C. Hutchings, "**Mixed polarization optical rectification in semiconductor waveguides,**" OSA Meeting NLGW, Clearwater, USA, 2001.

- U. Peschel, F. Lederer, K. Bubke, and D. C. Hutchings, "**Solitons in electro-optic modulators,** " CLEO Europe, Nice, 2000.

- K. Bubke, D. C. Hutchings, U. Peschel, and J. M. Arnold, "**Transmission line model for optical rectification in a travelling wave structure,** " PIERS, Cambridge, USA, 2000.

- K. Bubke, U. Peschel, and D. C. Hutchings, "**Oscillations and stability of solitons due to cascading of optical rectification and the electro-optical effect,**" OSA Meeting NLO, Hawaii, 2000.

- K. Bubke, U. Peschel, and D. C. Hutchings, "**KdV solitons on GaAs transmission lines due to the intrinsic second order nonlinearity,**" OSA Meeting NLGW, Dijon, 1999.

- U. Peschel, K. Bubke, D. C. Hutchings, and J. S. Aitchison, "**Pulse propagation and soliton formation using optical rectification,**" OSA Meeting NLGW, Dijon, 1999.

- K. Bubke, U. Peschel, and D. C. Hutchings, "**Nonlinear wave propagation and solitons in semiconductor transmission lines due to the intrinsic second-order nonlinearity,**" QEP 14, Manchester, 1999.

Acknowledgements

The completion of a thesis relies greatly on contributions in various forms from many different people and this thesis is no exception. First of all I would like to thank my supervisor Dave Hutchings for his encouragement, guidance and for always being there when help was needed. I can't thank Ulf Peschel enough who gave me the best start in a PhD one can imagine. His constant help and inexhaustible ideas made this thesis come to fruition. I am also indebted to John Arnold for many useful discussions, critical comments and suggestions related to the work presented here.

Thanks a lot to Valentine Loyo-Maldonado for discussing many practical aspects. I would also like to thank Daniele Modotto, first of all for answering all those stupid questions I wouldn't dare to ask anyone else and secondly for being such an enjoyable flatmate. Thanks to Gaby Slavcheva for listening and the many coffee breaks. I should also express my best thanks to the team at the IFTO in Jena, in particular Dirk Michaelis and Christoph Etrich, who made my stay there fruitful and enjoyable.

Special thanks to Mark Sorel for not allowing me to become a complete nerd in particular when writing up this thesis. Also thanks to John Arnold and Catrina Bryce for giving me time to finish the thesis. Very special thanks to Henrik Gollee for a critical reading of the manuscript.

On the personal side, there are a number of people who made my stay in Glasgow an enjoyable and remarkable time of my life, among them Thomas Schauer, Henrik Gollee, Luc Froehly, Pierre Pottier, Khalil Zeaiter, Franck Robert, and Sonja and Nikola Dragojlovic.

Most importantly, I would like to thank my parents and grandparents for giving me the best start in life I could have hoped for.

Contents

List of Tables

List of Figures

1 Introduction

1.1 Motivation and Historical Preamble

The terahertz (THz) region of the electromagnetic spectrum, located midway between microwaves and visible light, presents a new challenging area of research. The motivation to explore this new territory arises from numerous potential applications, among them THz spectroscopy [1], THz imaging [2] and high bandwidth data transmission [3]. However, apart from the applied points of view this relatively new range of science offers a large field of new interesting physical effects to be discovered.

Associated with THz investigations is the need for new THz technologies and techniques, ranging from sources and detectors to structures for guidance. The lack of miniaturised, reliable, and low cost power sources operating in the THz range was often referred to as the "terahertz gap" in the past. An attempt to bridge this gap which proved to be very successful was the introduction of ultrafast optoelectronic techniques in the early eighties [4]. Here, rather than controlling and detecting light by electrical signals as is the case in optical communications, the reverse was applied, i.e. ultrafast optical pulses generate and detect high speed electrical signals.

Two basic principles have been used extensively for the purpose of both generation and detection of THz radiation. These are photoconducting and electro-optic effects. The generation of THz signals using photoconducting materials is based on the concept of optical electron-hole injection in semiconductors. The photoconductive switch, invented by Auston in the early 80's [5], is a prominent example. The combination of a photoconducting gap between biased coplanar striplines, excited by an ultrashort optical pulse, with substrate lenses to couple the radiation in and out of the switch [1] made these devices extremely efficient for the generation of THz beams which can be propagated similarly to light beams. Although it is possible to generate relatively short electrical pulses by using photoconductive switching, the carrier lifetime of the medium poses a fundamental limitation on the response time.

The second principle, where those effects can be potentially avoided, is Optical Rectification (OR). OR is traditionally referred to as the generation of a static electric polarisation from a high power optical beam in a medium with a second order nonlinearity. The first observation of OR was reported as early as 1962, when Bass *et al.* demonstrated that a high

power laser pulse passing trough a KDP crystal placed between metal electrodes gives rise to a voltage across the electrodes [6, 7]. The signal was found to be proportional to the laser power and further to have the same time dependence as the envelope of the optical power. While early interest in OR was mainly concerned with the generation of a static induced field, e.g. for the characterisation of high power optical beams [8], with the development of picosecond and femtosecond high power pulsed lasers in the 1970's interest focussed mainly on the generation of THz radiation. Here the difference frequency mixing of the nearly degenerate Fourier components of an ultrashort optical pulse in a nonlinear medium with a near-instantaneous response generates microwave frequencies ranging potentially from zero to several THz, depending on the optical pulse width.

Early experiments demonstrated that the OR-induced polarisation in a nonlinear dielectric indeed radiates in a broad spectrum of frequencies ranging from microwaves, millimeterwaves into the infrared [9]. During the 1980's and 90's, generation as well as detection techniques based on electro-optic effects steadily improved and a number of materials, electro-optic crystals as well as semiconductors, were shown to be suitable materials for the efficient generation of THz signals [10]. To date, OR in bulk material is a well developed technique which can produce tunable, narrow-bandwidth, coherent THz radiation covering a frequency range up to 40 THz [11, 12, 13].

However, apart from the generation of ultrashort electrical transients, OR is also interesting from another point of view. OR is the inverse process of the linear electro-optic effect, in which the optical polarisibility of crystals with a second order nonlinearity is modified by applying a static or quasistatic field. Both mechanisms, i.e. OR and the electro-optic effect, can give rise to cascading effects which are well known from the interaction of a fundamental with its second harmonic via the second order nonlinearity (SHG cascading). In fact, a number of effects which are usually related to Kerr (i.e. third order) nonlinearities have been intensively investigated for SHG cascading in the last decade, among them self phase modulation, modulational instability and soliton formation (for a review, see [14, 15]).

Whereas self phase modulation in electro-optic crystals has been predicted as early as 1972 by Gustafson *et al.* [16], the cascading effect via OR was only recently demonstrated experimentally by Bosshardt and co-workers [17]. Some theoretical work has been undertaken in recent years to explore these effects in more detail [18, 19, 20, 21, 22, 23, 24]. However, the topic is still far from exhausted and not too many, theoretical as well as experimental, results are available yet.

1.2 Subject of this Thesis

Whereas OR in bulk materials has been used for nearly one decade now for the generation of THz electrical pulses, an attractive implementation would be a waveguiding structure where

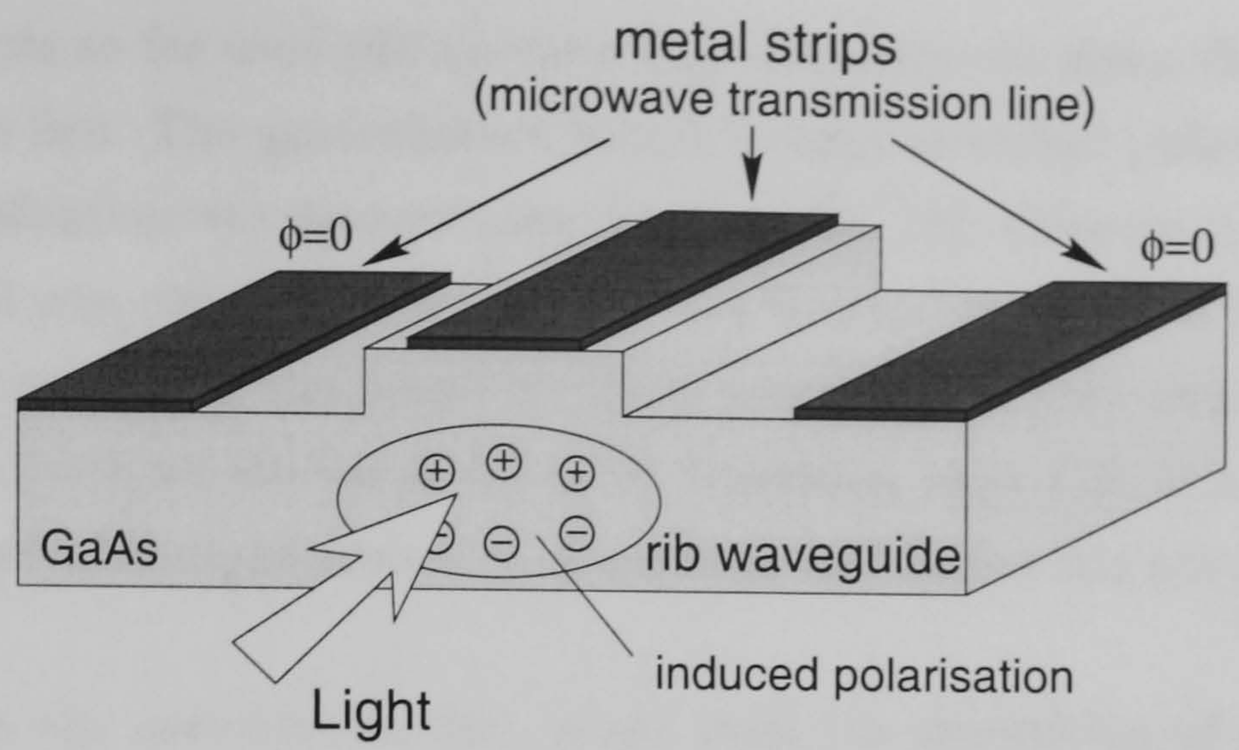

Figure 1.1: Schematic of an example structure for optical rectification in a waveguiding structure combining an optical rib waveguide with a microwave transmission line.

the optical and electric fields propagate in parallel. There are a number of advantages which could result from such a scheme:

- A travelling wave structure allowing the guidance of both the optical wave and the microwave can lead to a large effective conversion as the optical wave can steadily give energy into the microwave along the way.

- The confinement of both waves allows high effective nonlinearities avoiding effects such as optical diffraction.

- The microwave and the optical wave are guided by different structures which can be engineered separately. This implies the possibility of velocity matching by, for example, periodic loading of the microwave transmission line. This principle is well known from electro-optic modulators [25].

- The microwave is directly induced in a microwave transmission line leading to on-chip generation of ultrashort microwave signals. In this way a semiconductor laser with a carefully designed nonlinear waveguide could provide the basis for a one chip integrated THz source.

An example structure as considered in this thesis is shown in Fig. 1.1. A rib waveguide for the optical wave is combined with a typical microwave transmission line, here a coplanar waveguide. The optical wave is injected into the optical waveguide and induces a microwave signal in the transmission line which is guided and constantly amplified. Such a device is in principle very similar to a travelling wave optical modulator [26]. A suitable material for the substrate could be a semiconductor like GaAs. Not only is the fabrication technology for both optical devices and microwave integrated circuits based on the AlGaAs-system well-developed to date, but also GaAs provides a relatively high second order nonlinearity.

The propagation of picosecond and subpicosecond pulses on lithographically defined transmission lines has been a subject of intense research in recent years (for a review, see [27]).

Most of the attempts so far used photoconducting techniques to inject the electric transient in the transmission line. The generation of subpicosecond electrical pulses in a transmission line by optical rectification was demonstrated recently [28, 29]. Whereas in those experiments the electrical signal was coupled externally into the transmission line, a first attempt of applying a travelling wave structure based on GaAs was reported very recently [30]. However, the excitation of ultrashort electrical pulses by travelling wave OR in a properly designed waveguide combined with sophisticated measurement techniques has not been demonstrated yet.

As indicated in the previous Section, apart from the generation of electrical signals a structure as depicted in Fig. 1.1 might offer a number of physical effects arising from the *mutual* interaction of the optical wave with the microwave, i.e. cascading effects. Therefore it is interesting to explore if similar effects as predicted and partially demonstrated in SHG cascading can potentially occur in an optical-microwave travelling wave structure, for example modulational instability or soliton formation.

The theory describing a structure as shown in Fig. 1.1 is currently incomplete. This thesis is aimed to provide a theoretical framework considering a number of effects which might be observed by OR in a travelling wave structure. In particular, the following essential points are addressed:

- The basic physics of the conversion process in a travelling wave structure is explained by means of simple models.

- An appropriate set of evolution equations for a quantitative description of the overall conversion process is developed for the propagating fields in the structure. The generation of ultrashort electrical signals is discussed for a number of different scenarios. Relevant parameters of typical structures based on the AlGaAs-system are estimated and used in calculations.

- It is shown that the cascading of OR and the electro-optic effect in a waveguiding structure can potentially lead to self phase modulation (SPM), modulational instability (MI) and soliton formation. Further we elaborate on the stability properties of bright soliton solutions.

1.3 Outline

In **Chapter 2**, the basic theory of optical rectification and the electro-optic effect in media with a second order nonlinearity is introduced. The concept of a nonlinear polarisation and basic physical effects are explained.

Chapters 3-6 contain the main contributions of this thesis. Here, the reader can find the discussion of a variety of effects related to the interaction of a microwave with an optical

wave in a travelling wave structure. Whereas Chapters 3 and 4 are mainly devoted to the generation of electrical signals, Chapters 5 and 6 consider special effects arising from the mutual interaction of both waves under influence of dispersion.

- In **Chapter 3**, a simple transmission line model is introduced to explain qualitatively the basic physical mechanism of an externally induced polarisation in a travelling wave structure. Different scenarios, i.e. pulsed and continuous wave excitation, are discussed under consideration of practical boundary conditions. The important case of a modulation of the nonlinearity is explained.

- **Chapter 4** gives a detailed quantitative analysis of the mutual interaction between microwave and optical wave. Evolution equations based on a coupled mode formalism are derived. The basic properties of the structure under consideration are discussed and techniques for their evaluation are introduced. A set of corresponding parameters for typical structures is estimated and used for calculations throughout the thesis. The different modes of action of the electro-optic effect are shortly explained. The generation of electrical signals due to optical rectification is discussed in detail for the single and mixed-polarisation case. Different phenomena arising from the cascading of OR and the electro-optic effect are elucidated.

- In **Chapter 5**, the possibility of soliton formation due to cascading of OR and the electro-optic effect is considered in the context of long wave short wave interaction. It is shown that continuous wave solutions are modulational unstable in a wide range of system parameters. Basic properties of bright soliton solutions and their excitation are considered. The formation of solitons due to microwave self-interaction is shortly addressed.

- **Chapter 6** investigates the linear stability of bright soliton solutions. The observed oscillations and radiation of perturbed propagated solitons is explained by the existence of quasi-bound internal modes of the stationary solutions. Collision scenarios are shortly addressed.

Conclusions and recommendations for future work are presented in the final **Chapter 7**.

In order to make the thesis more self-contained, Appendices A-E contain additional material. In particular, **Appendices A** and **B** contain detailed derivations of essential equations used in Chapters 3 and 4. The discretisation scheme for the optical mode solver used for the calculation of overlap integrals can be found in **Appendix C**. Basic properties of the AlGaAs system are addressed in **Appendix D**. The approximate equations used for a discussion of microwave losses are reproduced in **Appendix E**. Finally, the example structures and the corresponding set of parameters estimated for a quantitative analysis can be found in **Appendix F**.

2 Principles of Optical Rectification

Before starting the main part of this thesis, some basic aspects of nonlinear optics related to optical rectification (OR) which are essential for the material in upcoming Chapters will be reviewed. This includes the concept of nonlinear polarisation and the relationship between OR and the electro-optic effect. Furthermore, we will contemplate on the induced polarisation and voltage due to OR in a plate capacitor arrangement, which comes close to the structures considered in this thesis. A detailed treatment of fundamentals of nonlinear optics can be found in standard textbooks [31, 32].

2.1 Nonlinear Polarisation

The application of an electrical field to a dielectric medium results in the induction of electric dipoles, for example by distortion of the charges bound to the molecules or the alignment of polar particles. This effect can be described by introduction of a polarisation $\mathbf{P}$, defined as the dipole moment per unit volume. Electric field $\mathbf{E}$ and polarisation in the dielectric are usually combined to give the dielectric displacement $\mathbf{D}$,

$$\mathbf{D} = \varepsilon_0 \mathbf{E} + \mathbf{P} \,, \tag{2.1}$$

where ε_0 is the free space permittivity. The polarisation is in general a complicated nonlinear function of the electric field and can be written as a convolution integral in the time domain,

$$\begin{aligned} \mathbf{P}(t) = \varepsilon_0 & \int_{-\infty}^{t} \boldsymbol{\chi}^{(1)}(t-t') \cdot \mathbf{E}(t')\, dt' \\ & + \varepsilon_0 \int_{-\infty}^{t}\int_{-\infty}^{t} \boldsymbol{\chi}^{(2)}(t-t', t-t'') : \mathbf{E}(t')\mathbf{E}(t'')\, dt'\, dt'' \,, \\ & + \varepsilon_0 \int_{-\infty}^{t}\int_{-\infty}^{t}\int_{-\infty}^{t} \boldsymbol{\chi}^{(3)}(t-t', t-t'', t-t''') \vdots \mathbf{E}(t')\mathbf{E}(t'')\mathbf{E}(t''')\, dt'\, dt''\, dt'' + \ldots \,. \end{aligned} \tag{2.2}$$

Here $\boldsymbol{\chi}^{(n)}$ is the n-th order susceptibility tensor of rank $n+1$. In this thesis we are mainly interested in effects arising from the second order nonlinearity $\boldsymbol{\chi}^{(2)}$, which is a third rank tensor containing, in general, 27 elements. However, application of permutation symmetries

and, in most cases, crystal class symmetries reduce the number of independent elements [31]. In the following we will truncate the expansion at n=2 and hence take into account only the linear and quadratic response of the medium. To understand the effects arising from a nonlinear polarisation, it is convenient to transform the convolution integral into the frequency domain. The polarisation is then composed of contributions from the first and second order susceptibility as $\tilde{\mathbf{P}}(\omega) = \tilde{\mathbf{P}}(\omega)^{(1)} + \tilde{\mathbf{P}}(\omega)^{(2)}$ with,

$$\tilde{P}_i^{(1)}(\omega) = \varepsilon_0 \int_{-\infty}^{\infty} \tilde{\chi}_{ij}^{(1)}(\omega_1)\, \tilde{E}_j(\omega_1)\, \delta(\omega - \omega_1)\, d\omega_1 \,, \tag{2.3}$$

$$\tilde{P}_i^{(2)}(\omega) = \varepsilon_0 \int_{-\infty}^{\infty} \int_{-\infty}^{\infty} \tilde{\chi}_{ijk}^{(2)}(-\omega_3; \omega_1, \omega_2) \tilde{E}_j(\omega_1) \tilde{E}_k(\omega_2)\, \delta(\omega - \omega_1 - \omega_2)\, d\omega_1\, d\omega_2 \,. \tag{2.4}$$

Here we wrote all vectors and tensors in terms of their components and assume einstein convention, i.e. summation over the repeated indices j and k. $\delta(\omega)$ is the Dirac delta function with the following properties,

$$\delta(\omega - \omega') = 0 \quad \text{for} \quad \omega \neq \omega' \,, \quad \int_{-\infty}^{\infty} \delta(\omega - \omega') d\omega = 1 \,, \quad \int_{-\infty}^{\infty} f(\omega)\delta(\omega - \omega') d\omega = f(\omega') \,. \tag{2.5}$$

The susceptibilities in the frequency domain are defined as [31],

$$\tilde{\chi}_{ij}^{(1)}(\omega_1) = \int_{-\infty}^{\infty} \chi_{ij}^{(1)}(\tau)\, e^{i\omega_1 \tau}\, d\omega_1 \,, \tag{2.6}$$

$$\tilde{\chi}_{ijk}^{(2)}(-\omega_3; \omega_1, \omega_2) = \int_{-\infty}^{\infty} \int_{-\infty}^{\infty} \chi_{ijk}^{(2)}(\tau_1, \tau_2)\, e^{i\omega_1 \tau_1}\, e^{i\omega_2 \tau_2}\, d\omega_1 d\omega_2 \,, \tag{2.7}$$

with $\omega_3 = \omega_1 + \omega_2$. According to expression eq. (2.4), the second order susceptibility $\tilde{\chi}_{ijk}^{(2)}(-\omega_3; \omega_1, \omega_2)$ gives rise to a polarisation at the sum frequency ω_3. It is useful to elaborate more on the essential properties of the susceptibility tensor. In general, the reality condition, i.e. both electric field and polarisation in time domain are real quantities, requires,

$$\begin{aligned} \tilde{\chi}_{ij}^{(1)}(-\omega) &= \tilde{\chi}_{ij}^{(1)*}(\omega) \,, \\ \tilde{\chi}_{ijk}^{(2)}(\omega_3; -\omega_1, -\omega_2) &= \tilde{\chi}_{ijk}^{(2)*}(-\omega_3; \omega_1, \omega_2) \,. \end{aligned} \tag{2.8}$$

As indicated before, both first and second order susceptibilities are in general frequency-dependent tensors with 9 and 27 elements, respectively. However, the number of elements describing the polarisation can be reduced by application of intrinsic symmetries and, in most cases, further approximations. In a lossless medium, the linear susceptibility tensor $\tilde{\boldsymbol{\chi}}^{(1)}$ is real and symmetric,

$$\tilde{\chi}_{ij}^{(1)}(\omega) = \tilde{\chi}_{ji}^{(1)}(\omega) \,. \tag{2.9}$$

It is convenient to combine the linear susceptibility tensor with the free space permittivity giving the dielectric tensor ε_{ij},

$$\mathbf{D} = \varepsilon_0 \left(1 + \tilde{\chi}_{ij}^{(1)}\right) \mathbf{E} = \varepsilon_0 \varepsilon_{ij} \mathbf{E} \,. \tag{2.10}$$

The tensor describing the second order contribution to the displacement vector can be simplified by the following symmetries:

- **Intrinsic permutation symmetry**
  For a susceptibility $\tilde{\chi}_{ijk}^{(2)}(-\omega_3; \omega_1, \omega_2)$ the indices j and k represent a summation over the components in x, y and z direction. As the product of electric field components commutates, we can interchange j and k and the corresponding frequencies ω_1 and ω_2 as,
  $$\tilde{\chi}_{ijk}^{(2)}(-\omega_3; \omega_1, \omega_2) = \tilde{\chi}_{ikj}^{(2)}(-\omega_3; \omega_2, \omega_1) \,. \tag{2.11}$$
  This property, which is always valid, is called intrinsic permutation symmetry.

- **Overall permutation symmetry**
  If we can neglect losses, i.e. if we are far from any material resonance, overall permutation symmetry applies. This symmetry states that the frequency components together with the corresponding cartesian indices can be freely interchanged,
  $$\tilde{\chi}_{ijk}^{(2)}(-\omega_3; \omega_1, \omega_2) = \tilde{\chi}_{jik}^{(2)}(\omega_1; -\omega_3, \omega_2) = \tilde{\chi}_{kji}^{(2)}(\omega_2; \omega_1, -\omega_3) \,. \tag{2.12}$$
  In contrast to intrinsic permutation symmetry, this symmetry is only an approximation which is valid if all frequencies involved are far from material resonances.

- **Kleinmann symmetry**
  If all frequencies involved are much smaller than the lowest resonance frequency of the material, we can ignore any dispersion. As a result, all frequencies are equivalent and hence interchangeable,
  $$\tilde{\chi}_{ijk}^{(2)}(-\omega_3; \omega_1, \omega_2) = \tilde{\chi}_{ikj}^{(2)}(-\omega_3; \omega_1, \omega_2) \,. \tag{2.13}$$
  Note that Kleinmann symmetry is only an approximation which is valid in the low frequency limit.

2.2 Mixing of an Optical Wave with a DC Field

The Dirac delta function $\delta(\omega)$ in eq. (2.4) implies frequency mixing between the spectral components of the applied electric field. To get an impression of the effects which might arise by coupling of an optical wave with a static (DC) field let's assume the electric field to be composed of a monochromatic input wave at frequency ω_o and a static part $\mathbf{E}^0$,

$$\mathbf{E}(t) = \mathbf{E}^0 + [\mathbf{E}^{\omega_o} \exp(-\mathrm{i}\omega_o t) + \mathbf{E}^{\omega_o *} \exp(\mathrm{i}\omega_o t)]/2 \,. \tag{2.14}$$

The electric field in frequency domain is then given by,

$$\tilde{\mathbf{E}}(\omega) = \mathbf{E}^0\,\delta(\omega - 0) + [\mathbf{E}^{\omega_o}\,\delta(\omega - \omega_o) + \mathbf{E}^{\omega_o *}\,\delta(\omega + \omega_o)]/2\;. \tag{2.15}$$

Calculating the integrals in eq. (2.4) gives the following components for the second order polarisation,

$$\begin{aligned}
\tilde{P}_i^{(2)}(\omega) = \varepsilon_0 \Big\{ & \frac{1}{4}\tilde{\chi}_{ijk}^{(2)}(-2\omega_o;\omega_o,\omega_o)\,E_j^{\omega_o}\,E_k^{\omega_o}\,\delta(\omega - 2\omega_o) \\
& + \frac{1}{4}\tilde{\chi}_{ijk}^{(2)}(2\omega_o;-\omega_o,-\omega_o)\,E_j^{\omega_o *}\,E_k^{\omega_o *}\,\delta(\omega + 2\omega_o) \\
& + \frac{1}{2}\left[\tilde{\chi}_{ijk}^{(2)}(-\omega_o;\omega_o,0)\,E_j^{\omega_o}\,E_k^{0} + \tilde{\chi}_{ijk}^{(2)}(-\omega_o;0,\omega_o)\,E_j^{0}\,E_k^{\omega_o}\right]\delta(\omega - \omega_o) \\
& + \frac{1}{2}\left[\tilde{\chi}_{ijk}^{(2)}(\omega_o;-\omega_o,0)\,E_j^{\omega_o *}\,E_k^{0} + \tilde{\chi}_{ijk}^{(2)}(\omega_o;0,-\omega_o)\,E_j^{0}\,E_k^{\omega_o *}\right]\delta(\omega + \omega_o) \\
& + \frac{1}{4}\left[\tilde{\chi}_{ijk}^{(2)}(0;\omega_o,-\omega_o)\,E_j^{\omega_o}\,E_k^{\omega_o *} + \tilde{\chi}_{ijk}^{(2)}(0;-\omega_o,\omega_o)\,E_j^{\omega_o *}\,E_k^{\omega_o}\right]\delta(\omega - 0) \\
& + \tilde{\chi}_{ijk}^{(2)}(0;0,0)\,E_j^{0}\,E_k^{0}\delta(\omega - 0)\Big\}\;.
\end{aligned} \tag{2.16}$$

Neglecting the DC part of the input field for now, the monochromatic input at frequency ω_o gives rise to a nonlinear polarisation at frequencies $\pm 2\omega_o$ and 0, both referring to second harmonic generation (SHG) and OR. In this thesis we are mainly interested in the latter effect, i.e. the creation of a static or quasi-static electric field within the nonlinear crystal.

The interaction of both DC field and optical wave leads to a nonlinear contribution to the polarisation at the frequency of the incident optical field. It will be demonstrated in the next Section that this results in a change of the refractive index experienced by the optical wave proportional to the applied DC field. Finally, the static polarisation has an additional contribution due to a self-interaction term proportional to a susceptibility $\tilde{\chi}_{ijk}^{(2)}(0;0,0)$. As will be shown later, this can lead, in principle, to an amplitude dependent velocity of a microwave propagating in a medium with a second order nonlinearity.

In general, the susceptibilities describing the effects mentioned above can differ and further be frequency-dependent. If we are far from resonances, overall permutation symmetry applies from which follows,

$$\tilde{\chi}_{ijk}^{(2)}(0;\omega_o,-\omega_o) = \tilde{\chi}_{ijk}^{(2)}(0;-\omega_o,\omega_o) = \tilde{\chi}_{ikj}^{(2)}(0;-\omega_o,\omega_o)\;, \tag{2.17}$$

$$\tilde{\chi}_{ijk}^{(2)}(-\omega_o;\omega_o,0) = \tilde{\chi}_{ijk}^{(2)}(\omega_o;-\omega_o,0)\;,\; \tilde{\chi}_{ijk}^{(2)}(-\omega_o;0,\omega_o) = \tilde{\chi}_{ijk}^{(2)}(\omega_o;0,-\omega_o)\;. \tag{2.18}$$

Furthermore, some coefficients describing electro-optic effect and OR are related to each other,

$$\tilde{\chi}_{ijk}^{(2)}(0;\omega_o,-\omega_o) = \tilde{\chi}_{jki}^{(2)}(-\omega_o;\omega_o,0) = \tilde{\chi}_{kji}^{(2)}(-\omega_o;\omega_o,0)\;. \tag{2.19}$$

For overall permutation symmetry, the polarisation due to OR in eq. (2.16) can be written in a contracted tensor notation. If we assume the polarisation to be composed of,

$$\tilde{\mathbf{P}} = \sum_{n=0,1,2} [\mathbf{P}^{n\omega_o}\,\delta(\omega - n\omega_o) + \mathbf{P}^{n\omega_o *}\,\delta(\omega + n\omega_o)]/2\;, \tag{2.20}$$

the static part can be written as,

$$\begin{pmatrix} P_x^0 \\ P_y^0 \\ P_z^0 \end{pmatrix} = \frac{\varepsilon_0}{2} \begin{pmatrix} d_{11}\, d_{12}\, d_{13}\, d_{14}\, d_{15}\, d_{16} \\ d_{21}\, d_{22}\, d_{23}\, d_{24}\, d_{25}\, d_{26} \\ d_{31}\, d_{32}\, d_{33}\, d_{34}\, d_{35}\, d_{36} \end{pmatrix} \begin{pmatrix} E_x^{\omega_o} E_x^{\omega_o *} \\ E_y^{\omega_o} E_y^{\omega_o *} \\ E_z^{\omega_o} E_z^{\omega_o *} \\ E_y^{\omega_o} E_z^{\omega_o *} + E_z^{\omega_o} E_y^{\omega_o *} \\ E_x^{\omega_o} E_z^{\omega_o *} + E_z^{\omega_o} E_x^{\omega_o *} \\ E_x^{\omega_o} E_y^{\omega_o *} + E_y^{\omega_o} E_x^{\omega_o *} \end{pmatrix} . \tag{2.21}$$

Here the second subscript of the coefficients d_{ih} relates to the axes by $h = 1 : xx$, $2 : yy$, $3 : zz$, $4 : yz$ or zy, $5 : xz$ or zx, $6 : xy$ or yx. The elements of the d-tensor are defined as $d_{ih} = \tilde{\chi}_{ih}^{(2)}(0; \omega_o, -\omega_o)/2$. Note that, for the most general case, a notation corresponding to eq. (2.21) is possible for the electro-optic effect only if we assume Kleinmann symmetry (from which follows $\tilde{\chi}_{ijk}^{(2)}(-\omega_o; \omega_o, 0) = \tilde{\chi}_{ijk}^{(2)}(-\omega_o; 0, \omega_o)$).

In the case of excitation with a short optical pulse, the spectrum of the incoming optical wave will have a broad frequency spectrum around a central frequency ω_o with a bandwidth $\Delta\omega$ which is determined by the shape and duration of the pulse. Instead of creating a purely static field, the power spectrum of the generated electrical signal will range from 0 to $\Delta\omega$. The induced polarisation around zero frequency can then be written as,

$$\tilde{P}_i^{(2)}(\Omega) = \varepsilon_0 \int_{\omega_o - \Delta\omega/2}^{\omega_o + \Delta\omega/2} \tilde{\chi}_{ijk}^{(2)}(-\Omega; \omega, \Omega - \omega) \tilde{E}_j(\omega) \tilde{E}_k(\Omega - \omega)\, d\omega \, . \tag{2.22}$$

As the frequencies generated are very small compared to the central frequency of the incoming light pulse, this process is also referred to as optical rectification. If we are far from resonances, the second order nonlinear process reacts instantaneously and the spectrum of the generated microwave is entirely determined by the spectrum of the optical pulse. Ultrashort excitation hence allows potentially the generation of microwave signals up to the THz range.

2.3 Electro-Optic Effect

The linear electro-optic effect refers to a change in the refractive index of a material due to the presence of a DC or low-frequency electric field. In media with a second order nonlinearity, the lowest-order contribution to the refractive index change is proportional to the applied field and known as Pockels effect. Centrosymmetric materials show in lowest order an index change depending quadratically on the applied field which is often called the Kerr electro-optic or simply Kerr effect. However, in this work we are solely interested in the Pockels or linear electro-optic effect and refer to it abbreviatory as the electro-optic effect.

The electro-optic effect was discovered by Pockels at the turn of this century. Because it was convenient at that time, it was formulated in terms of changes of the coefficients of

the optical indicatrix. A description of nonlinear effects in terms of a nonlinear polarisation was later introduced by the work of Armstrong, Bloembergen *et al.* [33]. In the following we will show that the electro-optic effect can also be formulated in terms of the second order polarisation. In fact, the coefficients r_{ijk} traditionally used to describe the electro-optic effect and the susceptibility tensor $\tilde{\chi}^{(2)}_{ijk}(-\omega;\omega,0)$ are directly related to each other.

As stated earlier, the relationship between the displacement vector and the electric field at the optical frequency in a lossless, anisotropic medium can be written in terms of the real, symmetric dielectric tensor,

$$\begin{pmatrix} \tilde{D}_x^{\omega_o} \\ \tilde{D}_y^{\omega_o} \\ \tilde{D}_z^{\omega_o} \end{pmatrix} = \varepsilon_0 \begin{pmatrix} \varepsilon_{xx}\,\varepsilon_{xy}\,\varepsilon_{xz} \\ \varepsilon_{xy}\,\varepsilon_{yy}\,\varepsilon_{yz} \\ \varepsilon_{xz}\,\varepsilon_{yz}\,\varepsilon_{zz} \end{pmatrix} \begin{pmatrix} \tilde{E}_x^{\omega_o} \\ \tilde{E}_y^{\omega_o} \\ \tilde{E}_z^{\omega_o} \end{pmatrix} . \tag{2.23}$$

The dielectric tensor can always be represented in diagonal form after a transformation in principal coordinates. However, here we will consider the more general case. The polarisation state of a plane wave propagating in an anisotropic medium can be described in terms of the optical indicatrix. It is convenient to write the indicatrix in terms of the impermeability tensor η_{ij} defined as,

$$\tilde{E}_i^{\omega_o} = \frac{1}{\varepsilon_0} \sum_j \eta_{ij} \tilde{D}_j^{\omega_o} . \tag{2.24}$$

A consideration of the energy density associated with a plane wave propagating in the anisotropic medium [32] leads to the general expression of the optical indicatrix,

$$\eta_{11}x^2 + \eta_{22}y^2 + \eta_{33}z^2 + 2\eta_{23}yz + 2\eta_{13}xz + 2\eta_{12}xy = 1 . \tag{2.25}$$

Eq. (2.25) refers to an ellipsoid which can be used to determine the normal modes of propagation in the crystal under consideration. For a given propagation direction, the plane perpendicular to the wavevector through the center of the ellipsoid forms an ellipse. The semimajor and semiminor axes of this ellipse are the two possible polarisation directions of the displacement vector of a propagating plane wave, whereas their lengths determine the respective effective indices.

In the usual case the diagonal elements of the dielectric tensor will be much larger than the off-diagonal elements $\varepsilon_{ii} \gg \varepsilon_{ij}$ $(i \neq j)$. The coefficients of the optical indicatrix eq. (2.25) are then given by,

$$\begin{aligned}
\left(\frac{1}{n^2}\right)_1 &= \eta_{11} = \frac{1}{\varepsilon_{11}} \quad , \quad \left(\frac{1}{n^2}\right)_4 = \eta_{23} = \eta_{32} = -\frac{\varepsilon_{23}}{\varepsilon_{22}\varepsilon_{33}} , \\
\left(\frac{1}{n^2}\right)_2 &= \eta_{22} = \frac{1}{\varepsilon_{22}} \quad , \quad \left(\frac{1}{n^2}\right)_5 = \eta_{13} = \eta_{31} = -\frac{\varepsilon_{13}}{\varepsilon_{11}\varepsilon_{33}} , \\
\left(\frac{1}{n^2}\right)_3 &= \eta_{33} = \frac{1}{\varepsilon_{33}} \quad , \quad \left(\frac{1}{n^2}\right)_6 = \eta_{12} = \eta_{21} = -\frac{\varepsilon_{12}}{\varepsilon_{11}\varepsilon_{22}} .
\end{aligned} \tag{2.26}$$

Here we introduced the usual notation with constant coefficients $(1/n^2)_i$. Corresponding to Pockels formulation, an application of a DC electric field will change the polarisation state

of a propagating wave and hence modify the elements of the optical indicatrix. In first order. the prefactors η_{ij} depend linearly on the components of the DC electric field as,

$$\Delta\eta_{ij} = \sum_k r_{ijk} E_k^0 \approx -\frac{\Delta\varepsilon_{ij}}{\varepsilon_{ii}\varepsilon_{jj}} , \tag{2.27}$$

where we introduced the electro-optic coefficients r_{ijk}. As both tensors ε_{ij} and η_{ij} are real symmetric, the coefficients r_{ijk} must be symmetric in its first two indices. It is hence convenient to write the tensor r_{ijk} as a two-dimensional matrix r_{hk} with h defined as in eq. (2.21). The outwritten set is then given by,

$$\begin{pmatrix} \Delta(1/n^2)_1 \\ \Delta(1/n^2)_2 \\ \Delta(1/n^2)_3 \\ \Delta(1/n^2)_4 \\ \Delta(1/n^2)_5 \\ \Delta(1/n^2)_6 \end{pmatrix} = \begin{pmatrix} r_{11}\, r_{12}\, r_{13} \\ r_{21}\, r_{22}\, r_{23} \\ r_{31}\, r_{32}\, r_{33} \\ r_{41}\, r_{42}\, r_{43} \\ r_{51}\, r_{52}\, r_{53} \\ r_{61}\, r_{62}\, r_{63} \end{pmatrix} \begin{pmatrix} E_x^0 \\ E_y^0 \\ E_z^0 \end{pmatrix} . \tag{2.28}$$

To demonstrate that the electro-optic coefficients and the susceptibilities are directly related to each other, let's consider the displacement vector eq. (2.23) under influence of a DC electric field $\mathbf{E}^0$. From eq. (2.27) we obtain,

$$\tilde{D}_i^{\omega_o} = \varepsilon_0[\varepsilon_{ij} + \Delta\varepsilon_{ij}]\tilde{E}_j^{\omega_o} = \varepsilon_0\varepsilon_{ij}\tilde{E}_j^{\omega_o} - \varepsilon_0 r_{ijk}\varepsilon_{ii}\varepsilon_{jj}\tilde{E}_j^{\omega_o} E_k^0 . \tag{2.29}$$

As was demonstrated in the last Section, the interaction of a DC electric field with an optical field results in an additional polarisation at the optical frequency. The displacement vector at the optical frequency is hence composed of the linear contribution and the nonlinear polarisation,

$$\tilde{D}_i^{\omega_o} = \varepsilon_0\varepsilon_{ij}\tilde{E}_j^{\omega_o} + 2\varepsilon_0\tilde{\chi}_{ijk}(-\omega_o;\omega_o,0)\tilde{E}_j^{\omega_o} E_k^0 . \tag{2.30}$$

Comparing both expressions eqs. (2.29) and (2.30) it becomes clear that the relationship between the electro-optic coefficients r_{ijk} and the susceptibility $\tilde{\chi}_{ijk}(-\omega_o;\omega_o,0)$ is given by,

$$\tilde{\chi}_{ijk}(-\omega_o;\omega_o,0) = -\frac{1}{2} r_{ijk}\varepsilon_{ii}\varepsilon_{jj} . \tag{2.31}$$

In this thesis we will mainly use the formulation in terms of the nonlinear susceptibility. The different modes of action of electro-optic modulation of light, namely phase modulation and mode conversion, will be discussed more in detail in Section 4.4.

2.4 Optical Rectification and Induced Voltage

As was shown in the preceding Sections, the interplay between an optical wave and a static or quasi-static field in a material with a second order nonlinearity leads to the induction of

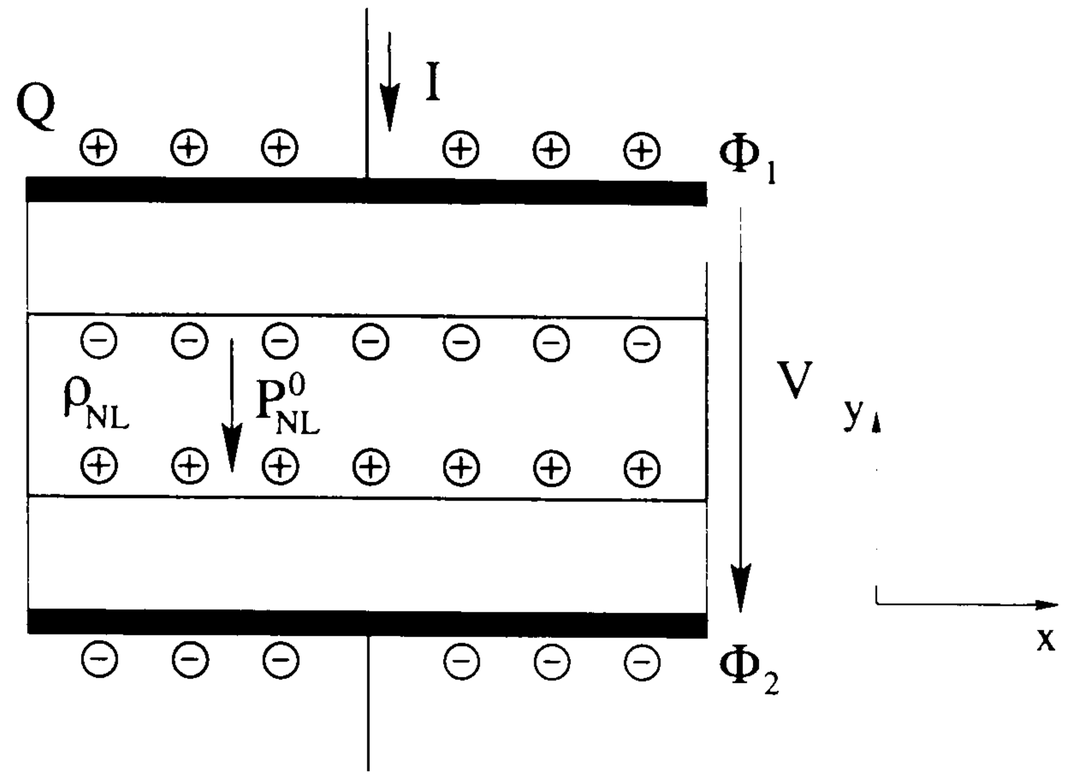

Figure 2.1: Schematic of optical rectification in a slab sandwiched between two metal electrodes,

nonlinear polarisations around the optical frequency ω_0 and zero frequency, the former giving rise to the electro-optic effect. In the derivation of the evolution equations for a travelling wave structure in Chapter 4, both additional polarisations are treated as a perturbation of propagating modes in the structure under consideration. However, in the early experiments on OR, for example by Bass et al. [6], the induced voltage in a plate capacitor arrangement was measured rather than the polarisation itself. This is not too far from the case of an optically induced polarisation in a transmission line consisting of metal strips placed on a nonlinear dielectric. Fig. 2.1 shows a simplified schematic of a dielectric sandwiched between two metal electrodes which can serve as a simple model of a piece of transmission line. In the following we will show how a static induced polarisation is related to the voltage on the metal electrodes.

An optical wave directed through the dielectric with a second order nonlinearity induces a static polarisation field $\mathbf{P}^0_{\mathrm{NL}}(x,y,z)$. Since no free charges are present in the dielectric, Gauss' law states,

$$0 = \nabla \cdot \mathbf{D} = \nabla \cdot \left[\varepsilon_0 \bar{\varepsilon}_r \mathbf{E}^0(x,y,z) + \mathbf{P}^0_{\mathrm{NL}}(x,y,z)\right] , \tag{2.32}$$

where $\mathbf{E}^0(x,y,z)$ is the static electric field and $\bar{\varepsilon}_r$ is the dielectric tensor. The action of the polarisation can be interpreted as the induction of an effective charge density ρ_{NL} in the structure,

$$\rho_{\mathrm{NL}} = -\nabla \cdot \mathbf{P}^0_{\mathrm{NL}} \quad . \tag{2.33}$$

For the static case, the electric field is curl free and can be expressed in terms of a potential $\mathbf{E}^0 = -\nabla\Phi$. Corresponding to eq. (2.32) the potential and hence the electric field in the structure is then given by the Poisson equation,

$$\nabla \cdot (\varepsilon_0 \bar{\varepsilon}_r \nabla\Phi) = -\rho_{\mathrm{NL}} = \nabla \cdot \mathbf{P}^0_{\mathrm{NL}} \quad . \tag{2.34}$$

Note that the presence of a homogeneous polarisation does not produce an electric field but only its spatial change. Furthermore, the actual induced voltage in a slab arrangement as

shown in Fig. 2.1 $V = \Phi_1 - \Phi_2$ is not fixed by eq. (2.34) but depends on the boundary conditions of the problem.

As an example, let's consider an infinitely extended waveguide with an optical CW excitation. Before the optical wave enters the waveguide there are no net charges on the conductors and hence there should not be any afterwards. The physically correct solution of the problem is consequently the voltage V_{ind} on the conductor for which the charge Q' on the conductor vanishes. The charge Q' consists of a part induced by the voltage V and one induced by the polarisation $\mathbf{P}^0_{\text{NL}}$ (denoted by Q),

$$Q' = CV + Q \quad , \tag{2.35}$$

where C is the capacitance per unit length of the structure. In an actual calculation, the potential in the structure and the charge Q on the strip could be calculated, e.g. numerically, from eq. (2.34) (see also Section 4.3.2) under the boundary condition $V = \Phi_1 - \Phi_2 = 0$. The induced voltage V_{ind} for chargefree electrodes is then given by $V_{\text{ind}} = -Q/C$. Note that, corresponding to eq. (2.34), the charge Q on the metal strip is proportional to the induced polarisation and hence to the optical power.

In this thesis we are mainly interested in transient effects in a travelling wave structure rather than in static induced voltages. Here the optical power distribution and hence the induced polarisation will depend not only on the transverse coordinates but also on time t and propagated distance z. As a result, currents flowing along the transmission line will influence the development of charges. The charges and voltages in eq. (2.35) are then functions of t and z,

$$Q'(z,t) = CV(z,t) + Q(z,t) \quad . \tag{2.36}$$

The evolution of voltage on a transmission line under influence of an induced variable polarisation will be explored in the next Chapter on the basis of a simple transmission line model.

3 Transmission Line Model

3.1 Introduction

A well known concept in microwave engineering is the characterisation of transmission lines with a set of partial differential equations known as telegraph equations [34]. As shown in Fig. 3.1, the transmission line is modeled on the basis of a uniformly and continuously distributed capacitance C' and inductance L' per unit length. The change of voltage V and current I along an infinitesimal small piece of a lossless transmission line at distance z and time t is governed by the telegraph equations,

$$\begin{aligned} \frac{\partial V}{\partial z} &= -L' \frac{\partial I}{\partial t} \,, \\ \frac{\partial I}{\partial z} &= -C' \frac{\partial V}{\partial t} \,, \end{aligned} \tag{3.1}$$

from which the wave equation in time domain can be derived as,

$$\frac{\partial^2 V}{\partial z^2} - \frac{1}{v_{\text{mic}}^2} \frac{\partial^2 V}{\partial t^2} = 0 \,, \tag{3.2}$$

where $v_{\text{mic}} = 1/\sqrt{L'C'}$ is the phase velocity of the microwave travelling along the line. The solution of the wave equation are forward and backward propagating waves V^+ and V^-,

$$V(z,t) = V^+(t - z/v_{\text{mic}}) + V^-(t + z/v_{\text{mic}}) \,, \tag{3.3}$$

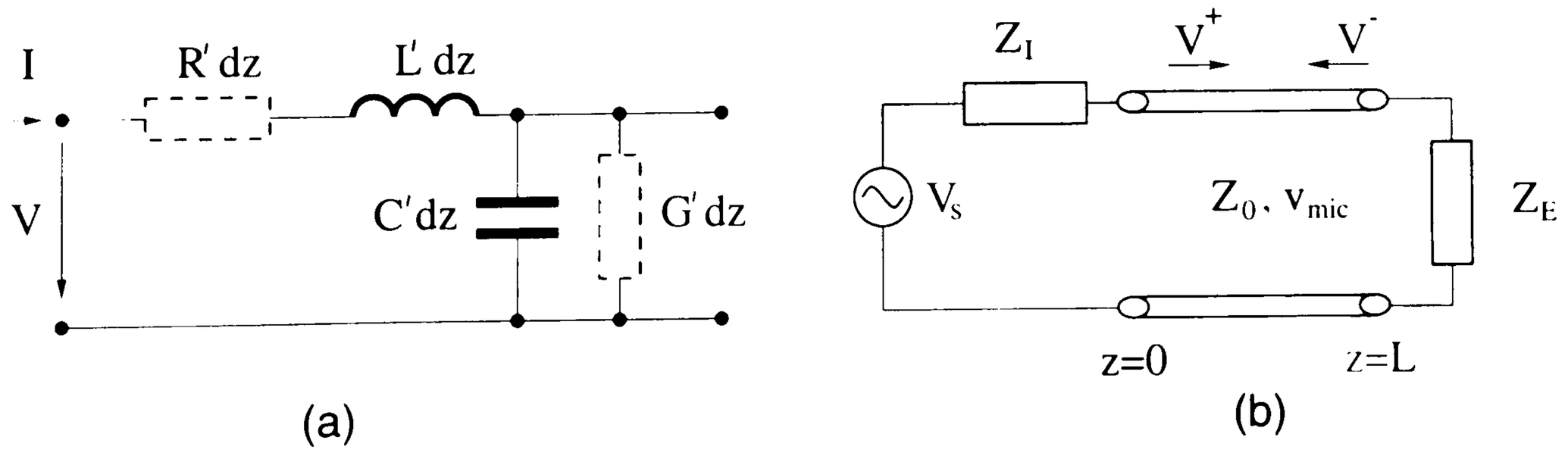

Figure 3.1: (a) Equivalent circuit of microwave transmission with line capacitance C', inductance L', resistance R' and conductance G', (b) for- and backward propagating waves V^+ and V^- are determined by boundary conditions (here voltage source V_s with impedance Z_I and load Z_E).

which are determined by applying appropriate boundary conditions at the beginning and the end of the transmission line (see Fig. 3.1).

The subject of this Chapter is the extension of this basic concept to the case of an additional induced charge in the transmission line. As optical rectification (OR) corresponds to the optical injection of a polarisation and hence space charge in the transmission line, this model gives a phenomenological description of the basic mechanisms of the generation of electrical transients from an optical pulse in a travelling wave structure. A quantitative analysis including the influence of losses, dispersion and backcoupling to the optical wave will be considered in detail in the following Chapters.

Neglecting dispersion and attenuation, the model results in a forced hyperbolic wave equation which can be solved analytically in the time domain. Here, bidirectional propagation of the microwave and hence backreflections are taken into account. In Section 3.2, the basic equations are derived and analytical solutions are given for an arbitrary charge distribution in the transmission line. The case of a travelling wave excitation is discussed in Sections 3.3 and 3.4. As a final example, the generation of electrical signals in a transmission line with periodically modulated nonlinearity is discussed in Section 3.5.

3.2 Transmission Line with Induced Charge

In the following we consider a transmission line with the equivalent circuit shown in Fig. 3.2(a). As discussed in Section 2.4, the charge Q' on the transmission line is composed of a contribution from the line capacitance C' and an externally induced charge Q as $Q'(z,t) = C'V(z,t) + Q(z,t)$. In the case of OR the additional charge Q is proportional to the optical power distribution $P_{\mathrm{opt}}(z,t)$ in the transmission line. A change of the optical power leads hence to an additional displacement current $I_{\mathrm{q}} = \partial Q/\partial t$ which can be seen as a distributed current source in the transmission line as indicated in Fig. 3.2(b). The extended telegraph equations for a lossless transmission line now read as,

$$\begin{aligned} \frac{\partial V}{\partial z} &= -L' \frac{\partial I}{\partial t} \,, \\ \frac{\partial I}{\partial z} &= -C' \frac{\partial V}{\partial t} - \frac{\partial Q}{\partial t} \,. \end{aligned} \tag{3.4}$$

From eqs. (3.4) one can easily derive forced hyperbolic wave equations for the voltage V and the current I on the transmission line,

$$\frac{\partial^2 V}{\partial z^2} - \frac{1}{v_{\mathrm{mic}}^2} \frac{\partial^2 V}{\partial t^2} = L' \frac{\partial^2 Q}{\partial t^2} \,, \tag{3.5}$$

$$\frac{\partial^2 I}{\partial z^2} - \frac{1}{v_{\mathrm{mic}}^2} \frac{\partial^2 I}{\partial t^2} = -\frac{\partial^2 Q}{\partial t \partial z} \,. \tag{3.6}$$

An equation similar to eq. (3.5) can be derived directly from Maxwells equations for the propagation of an electromagnetic field under influence of an additional polarisation neglecting the transverse field profiles [16]. The basic results of the following Sections are therefore

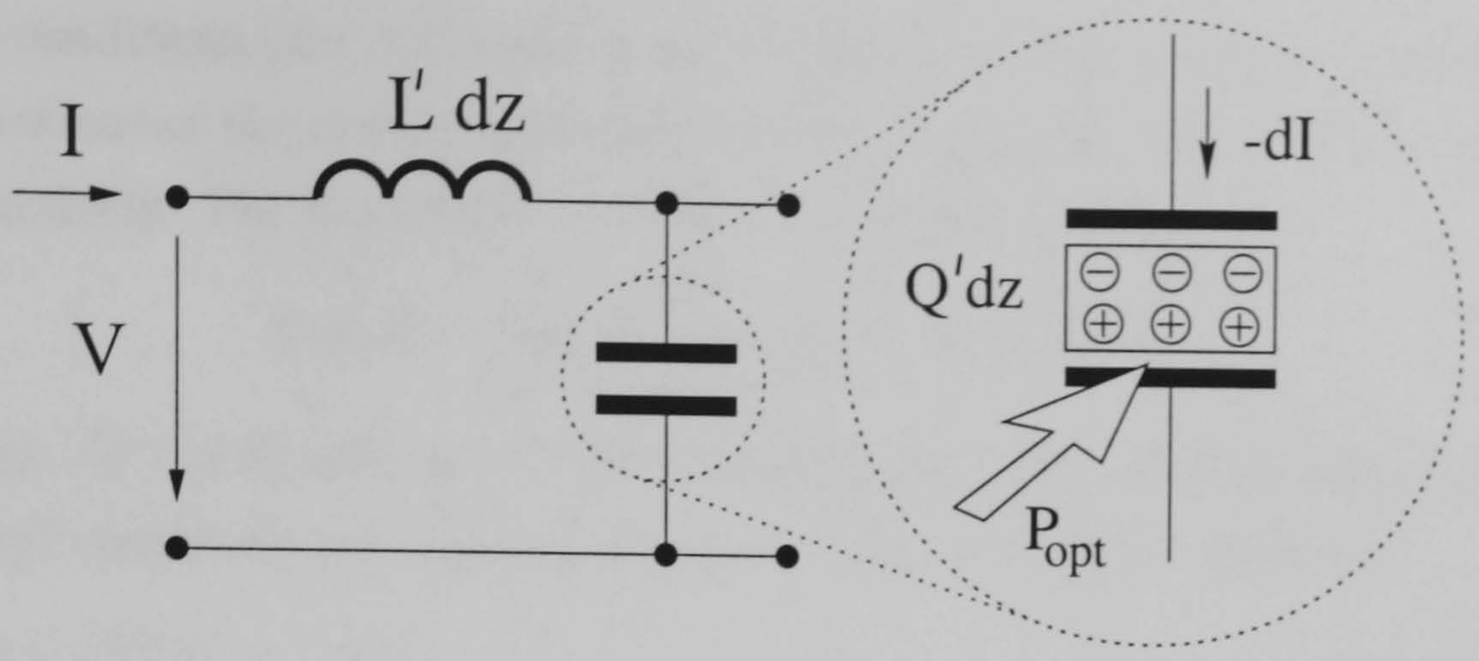

Figure 3.2: (a) Equivalent circuit of transmission line with externally induced charge distribution, the net charge Q' on the line results from the line capacitance and the induced space charge Q as $Q' = C'V + Q$, (b) transmission line with distributed current source due to displacement current $I_Q = \partial Q/\partial t$, termination with impedances Z_B and Z_E respectively.

also applicable to the propagation of plane waves in bulk material.

If the driving function is causal, i.e. $Q(z,t) = 0$ for $t \leq 0$, solutions of eqs. (3.5, 3.6) are (see Appendix A),

$$V(z,t) = V^+(t - z/v_{\mathrm{mic}}) + V^-(t + z/v_{\mathrm{mic}}) - \frac{Z_0}{2}\left\{\int_0^z \frac{\partial}{\partial t} Q[z', t - (z-z')/v_{\mathrm{mic}}]\, dz' + \int_z^L \frac{\partial}{\partial t} Q[z', t + (z-z')/v_{\mathrm{mic}}]\, dz'\right\}, \quad (3.7)$$

$$I(z,t) = I^+(t - z/v_{\mathrm{mic}}) + I^-(t + z/v_{\mathrm{mic}}) + \frac{Z_0}{2L'}\left\{\int_0^z \frac{\partial}{\partial z} Q[z', t - (z-z')/v_{\mathrm{mic}}]\, dz' + \int_z^L \frac{\partial}{\partial z} Q[z', t + (z-z')/v_{\mathrm{mic}}]\, dz'\right\}, \quad (3.8)$$

where $Z_0 = \sqrt{L'/C'}$ denotes the characteristic impedance of the transmission line and L its length. The forward and backward propagating waves $V^{\pm}$ ($I^{\pm}$) are the solutions of the source-free equation. The voltages and currents are related to each other by,

$$V^+ = Z_0 I^+ \ , \ V^- = -Z_0 I^- \ . \quad (3.9)$$

Whereas the particular integrals in eqs. (3.7, 3.8) are given by the charge distribution in the transmission line, the forward and backward propagating waves $V^{\pm}$ ($I^{\pm}$) are determined by

the boundary conditions at $z = 0$ and $z = L$. As shown in Fig. 3.2(b) we assume the general case of terminations of the transmission line by impedances Z_B and Z_E in the beginning and the end, respectively. The boundary conditions are hence given by,

$$V(0,t) = Z_B I(0,t) \ , \ V(L,t) = Z_E I(L,t) \ . \tag{3.10}$$

Introducing eqs. (3.7, 3.8) into eqs. (3.10) and using eq. (3.9), the following relationships for the forward and backward propagating waves V^+ and V^- can be derived,

$$V^+(\,t\,) = \frac{\rho_E}{\rho_B} V^+(t - 2T_{\rm m})$$

$$-\frac{1}{2} Z_0 \frac{1}{\rho_B} \int_0^L \frac{\partial}{\partial t} [Q(z', t - z'/v_{\rm mic}) + \rho_E Q(z', t + z'/v_{\rm mic} - 2T_{\rm m})]\, dz' \ , \tag{3.11}$$

$$V^-(\,t\,) = \frac{\rho_E}{\rho_B} V^-(t - 2T_{\rm m})$$

$$-\frac{1}{2} Z_0 \frac{\rho_E}{\rho_B} \int_0^L \frac{\partial}{\partial t} [Q(z', t - z'/v_{\rm mic} - 2T_{\rm m}) + \rho_B Q(z', t + z'/v_{\rm mic} - 2T_{\rm m})]\, dz' \ , \tag{3.12}$$

where $T_{\rm m} = L/v_{\rm mic}$ and ρ_B and ρ_E denote the reflection coefficients at the beginning and the end of the transmission line, respectively,

$$\rho_B = \frac{Z_B - Z_0}{Z_B + Z_0} \ , \ \rho_E = \frac{Z_E - Z_0}{Z_E + Z_0} \ . \tag{3.13}$$

The first term in eq. (3.11) can be interpreted as the forward propagating wave in a previous roundtrip which is subject to partial reflection at $z = 0$ and $z = L$. The second term represents the contribution from the source. An explicit formula for $V^+(t)$ can be derived by iterative application of eq. (3.11), i.e. we can express $V^+(t)$ in terms of $V^+(t - 2T_{\rm m})$, $V^+(t - 2T_{\rm m})$ in terms of $V^+(t - 4T_{\rm m})$ and so on. As a result, we obtain $V^+(t)$ as a summation of the contributions from the source in every roundtrip,

$$V^+(t) = -\frac{1}{2} Z_0 \frac{1}{\rho_B} \sum_{i=0}^{\infty} \left(\frac{\rho_E}{\rho_B} \right)^i$$

$$\times \int_0^L \frac{\partial}{\partial t} \{ Q(z', t - z'/v_{\rm mic} - 2iT_{\rm m}) + \rho_E Q[z', t + z'/v_{\rm mic} - 2(i+1)T_{\rm m}] \}\, dz' . \tag{3.14}$$

A similar procedure leads to an expression for the backward propagating wave $V^-(t)$,

$$V^-(t) = -\frac{1}{2} Z_0 \frac{\rho_E}{\rho_B} \sum_{i=0}^{\infty} \left(\frac{\rho_E}{\rho_B} \right)^i$$

$$\times \int_0^L \frac{\partial}{\partial t} \{ Q[z', t - z'/v_{\rm mic} - 2(i+1)T_{\rm m}] + \rho_B Q[z', t + z'/v_{\rm mic} - 2(i+1)T_{\rm m}] \}\, dz' . \tag{3.15}$$

For a given source distribution the voltage $V(z,t)$ on the transmission line can hence be calculated by first calculating V^+ and V^- and subsequent introduction into eq. (3.7).

3.3 Travelling Wave Excitation

In the following, we consider the special case of a source function which itself is a travelling wave. This corresponds to OR, where the polarisation and hence space charge is proportional to the power distribution of an optical wave travelling in the structure. Neglecting reflections at the facets, the additional charge distribution on the transmission line can be written as,

$$Q(z,t) = Q(t - z/v_{\text{opt}}) \,, \tag{3.16}$$

where v_{opt} is the group velocity of the optical pulse. Here, we assume the optical wave to propagate without dispersion, loss of energy or backcoupling due to the generated microwave. Effects arising where these approximations fail will be discussed in detail in the following Chapters.

With the source function eq. (3.16), the integrals appearing in eqs. (3.7), (3.14) and (3.15) can be evaluated explicitly for arbitrary excitations $Q(z,t)$ giving analytical expressions for the generated microwave. In the following, the evolution of the voltage on the transmission line will be discussed for typical scenarios.

3.3.1 Infinite Transmission Line

As a first example, an infinitely extended transmission line $L \to \infty$ is considered having the effect that backreflections at the end are not present. The transmission line at $z = 0$ is chosen to be open ($\rho_B = 1$) corresponding to the most likely situation in an experiment. Here and in the following, two cases are essential: these are first velocity matching, where the phase velocity of the microwave is equal to the group velocity of the optical wave and second, a mismatch between both velocities.

In the velocity matched case ($v_{\text{opt}} = v_{\text{mic}}$), eq. (3.7) simplifies to,

$$V(z,t) = -\frac{1}{2} Z_0 \frac{\partial}{\partial t} Q(t - z/v_{\text{mic}}) z - \frac{1}{2} Z_0 v_{\text{mic}} Q(t - z/v_{\text{mic}}) \,. \tag{3.17}$$

Here, the first term describes a linearly growing voltage which is proportional to the first derivative of the optical power distribution. This can be understood by the fact that the displacement current due to a change of space charge in the structure acts as a source rather than the charge itself. As shown in Fig. 3.3, for an optical pulse the microwave evolves as a quasi single cycle microwave signal. It should be noted that especially for the linearly growing part, the assumption of a nondepleted pump may fail for a large interaction length. The second term in eq. (3.17) is a static part which follows the optical power distribution and does not change during propagation. The static part can be interpreted as the instantaneously generated microwave signal reflected by the open circuit at the beginning of the line. This becomes clearer when considering a short in the beginning ($\rho_B = -1$). The corresponding voltage on the transmission line is then given by,

$$V(z,t) = -\frac{1}{2} Z_0 \frac{\partial}{\partial t} Q(t - z/v_{\text{mic}}) z \,. \tag{3.18}$$

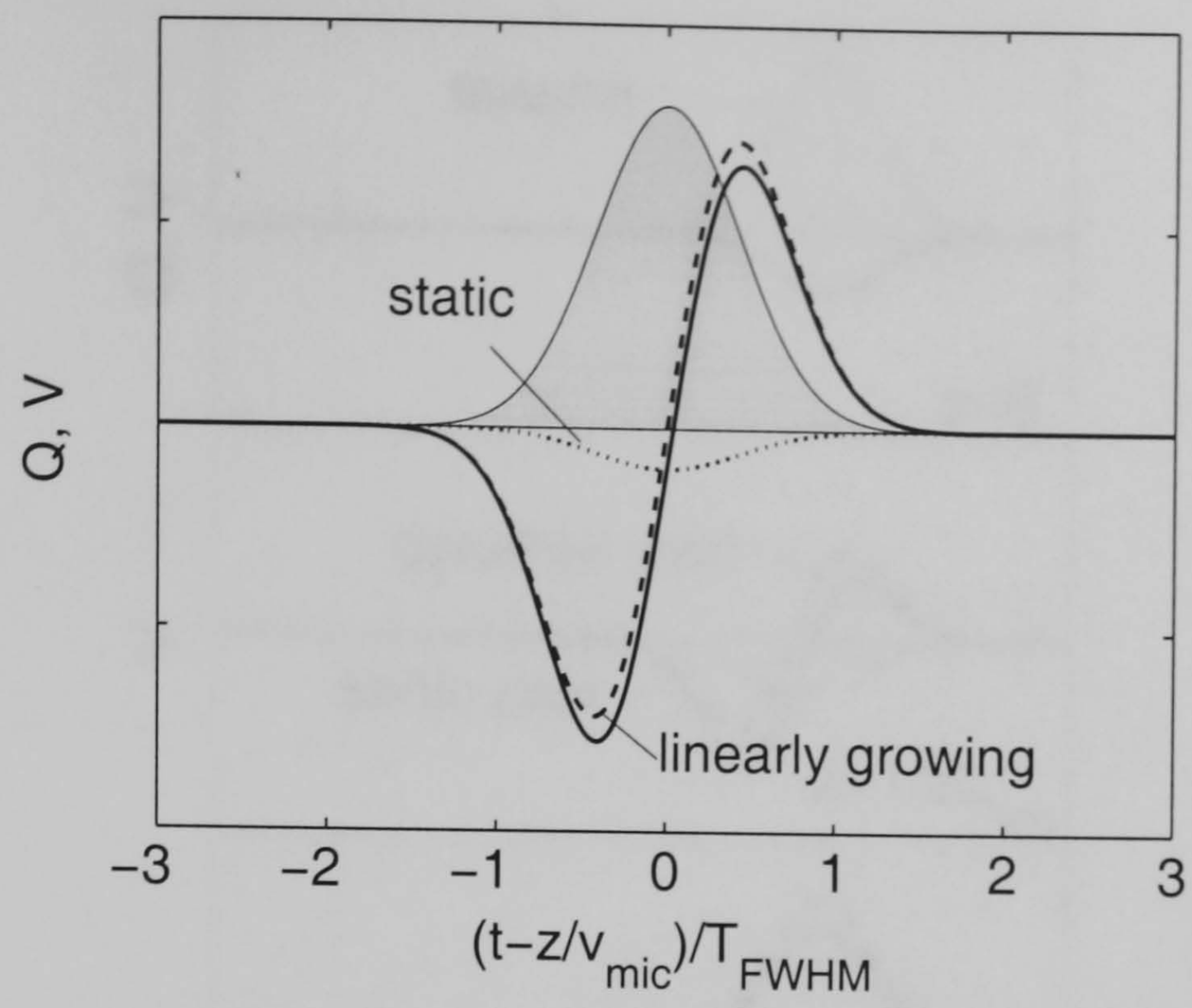

Figure 3.3: Voltage on the transmission line for velocity matching $v_{\rm opt} = v_{\rm mic}$ due to excitation with optical pulse (Gaussian, full width half maxmim $T_{\rm FWHM}$) after propagation distance $z = 5\,T_{\rm FWHM}\,v_{\rm mic}$, open ($\rho_B = 1$) at $z = 0$; solid line voltage V, dashed line linearly growing part, dotted line static part, shaded area charge distribution Q.

Whereas the linearly growing part is recovered, the static part is suppressed by the short.

For the velocity mismatched case ($v_{\rm opt} \neq v_{\rm mic}$), a similar calculation gives for the case of an open circuit at $z = 0$,

$$V(z,t) = \frac{1}{\frac{1}{v_{\rm opt}} - \frac{1}{v_{\rm mic}}} \frac{Z_0}{2} [Q(t - z/v_{\rm opt}) - Q(t - z/v_{\rm mic})] - \frac{1}{\frac{1}{v_{\rm opt}} + \frac{1}{v_{\rm mic}}} \frac{Z_0}{2} [Q(t - z/v_{\rm opt}) + Q(t - z/v_{\rm mic})] \,. \tag{3.19}$$

The first term on the right hand side can be referred to as a dynamic part. If we assume the optical excitation to be a pulse, the dynamic part is composed of two pulses following the optical power distribution which cancel each other at $z = 0$. While propagation along the transmission line one pulse travels with the optical pulse whereas the other travels with the velocity of the microwave. As shown in Fig. 3.4, we obtain a quasi single cycle pulse with growing amplitude until the pulses walk off from each other. The formation of a voltage travelling as a mirror image of the optical pulse can be understood as a microwave field generated at one slope of the optical pulse which then crosses the optical pulse due to the velocity mismatch and finally interferes destructively with the generated microwave signal at the other edge of the optical pulse. As a figure of merit a walk-off length $L_{\rm wo}$ can be defined after which there is no significant increase of microwave power,

$$L_{\rm wo} = \frac{T_{\rm FWHM}}{\left| \frac{1}{v_{\rm opt}} - \frac{1}{v_{\rm mic}} \right|} \,, \tag{3.20}$$

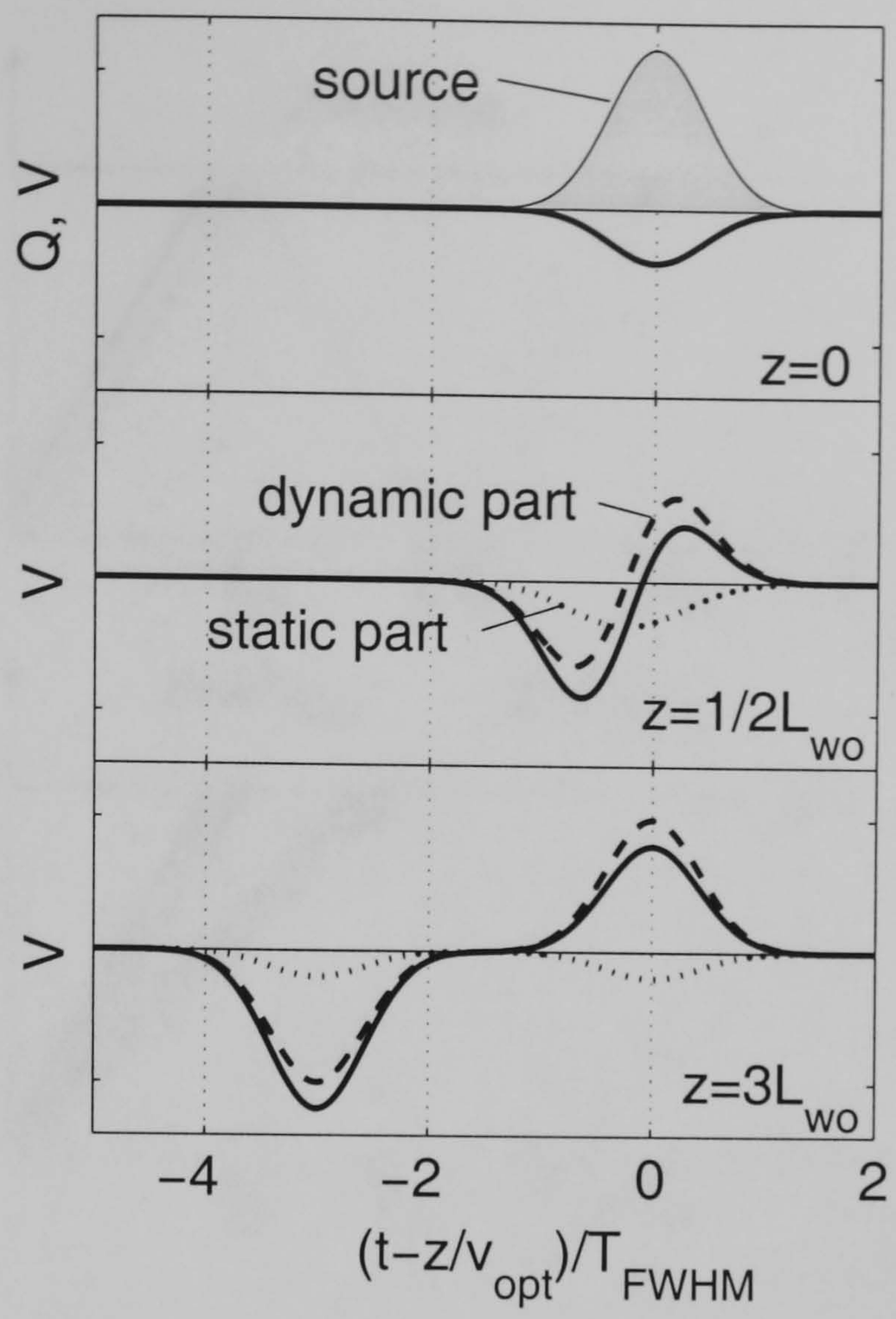

Figure 3.4: Evolution of the generated microwave signal for velocity mismatch ($v_{\mathrm{mic}}/v_{\mathrm{opt}} = 1.5$) and open circuit at $z = 0$; solid line voltage V, dashed line dynamic part and dotted line static part of V respectively. Also indicated is source Q at $z = 0$ (shaded).

where T_{FWHM} refers to the width of the optical pulse. Similar to the velocity matched case, the second term in eq. (3.19), here referred to as static part, consists of two smaller pulses which add up in the beginning and move out of each other by travelling along the transmission line. However, there is no change in microwave power of the static part along the transmission line. For a short circuit at $z = 0$ we obtain similarly,

$$V(z,t)=\frac{Z_0}{2}\left[\frac{1}{\frac{1}{v_{\mathrm{opt}}}-\frac{1}{v_{\mathrm{mic}}}}-\frac{1}{\frac{1}{v_{\mathrm{opt}}}+\frac{1}{v_{\mathrm{mic}}}}\right]\left[Q(t-z/v_{\mathrm{opt}})-Q(t-z/v_{\mathrm{mic}})\right]. \quad (3.21)$$

Again, the static part is suppressed due to the short circuit. However, the prefactor of the evolving pulses is altered due to changing boundary conditions in the beginning. Whereas the second term in the prefactor is small for slight velocity mismatch, it can become significant for large velocity mismatch between source and microwave.

3.3.2 Transmission Line with Load

In an experiment, the transmission line will be terminated with a resistance Z_E at a finite length $z = L$. In the case of a matched transmission line ($Z_E = Z_0$) and velocity matching

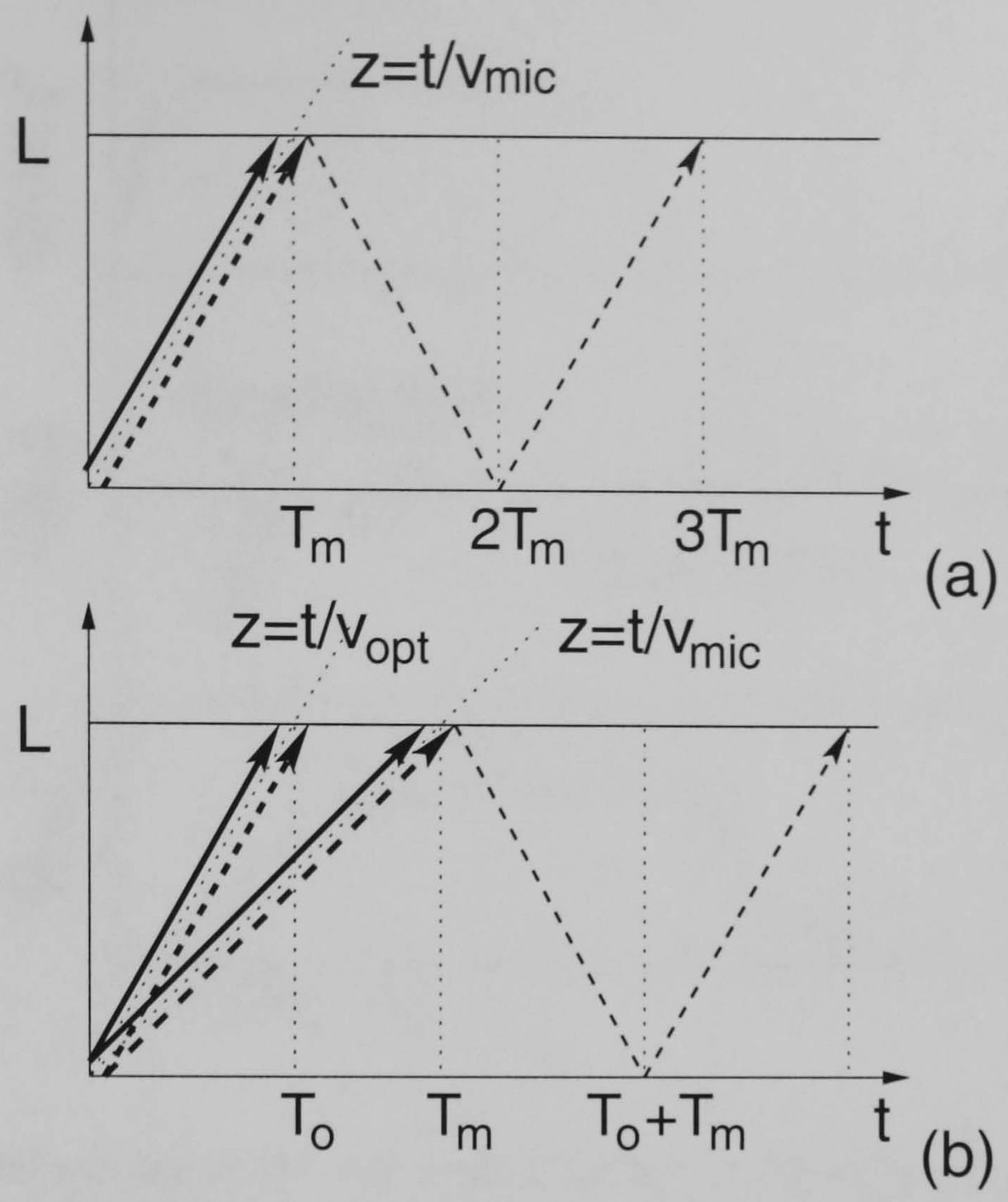

Figure 3.5: Schematic of the propagation of generated microwave in transmission line with load, (a) velocity matching, solid line linearly growing part, dashed line static part,(b) velocity mismatch, solid line dynamic part, dashed line static part (see text for details).

between both microwave and optical wave ($v_{\rm opt} = v_{\rm mic}$), the voltage distribution for an open circuit at $z = 0$ ($\rho_E = 1$) is,

$$\begin{aligned} V(z,t) = &-\frac{1}{2}Z_0\frac{\partial}{\partial t}Q(t - z/v_{\rm mic})z - \frac{1}{2}Z_0 v_{\rm mic}Q(t - z/v_{\rm mic}) \\ &+ \frac{1}{4}Z_0 v_{\rm mic}Q(t + z/v_{\rm mic} - 2T_{\rm m}) + \frac{1}{4}Z_0 v_{\rm mic}Q(t - z/v_{\rm mic} - 2T_{\rm m})\,, \end{aligned} \tag{3.22}$$

where $T_{\rm m} = L/v_{\rm mic}$. Whereas the linearly growing part is absorbed by the load, the static part is partly reflected at the end despite perfect matching of the transmission line (see Fig. 3.5). For the velocity mismatched case one obtains similarly,

$$\begin{aligned} V(z,t) = &\frac{1}{\frac{1}{v_{\rm opt}} - \frac{1}{v_{\rm mic}}}\frac{Z_0}{2}[Q(t - z/v_{\rm opt}) - Q(t - z/v_{\rm mic})] \\ &- \frac{1}{\frac{1}{v_{\rm opt}} + \frac{1}{v_{\rm mic}}}\frac{Z_0}{2}[Q(t - z/v_{\rm opt}) + Q(t - z/v_{\rm mic})] \\ &+ \frac{1}{\frac{1}{v_{\rm opt}} + \frac{1}{v_{\rm mic}}}\frac{Z_0}{2}\{Q[t + z/v_{\rm mic} - (T_{\rm m} + T_{\rm o})] + Q[t - z/v_{\rm mic} - (T_{\rm m} + T_{\rm o})]\}\,, \end{aligned} \tag{3.23}$$

where $T_{\rm o} = L/v_{\rm opt}$. Whereas the pulses travelling with the velocity of the microwave are absorbed by the load, the static term travelling with the source is again partly reflected. The

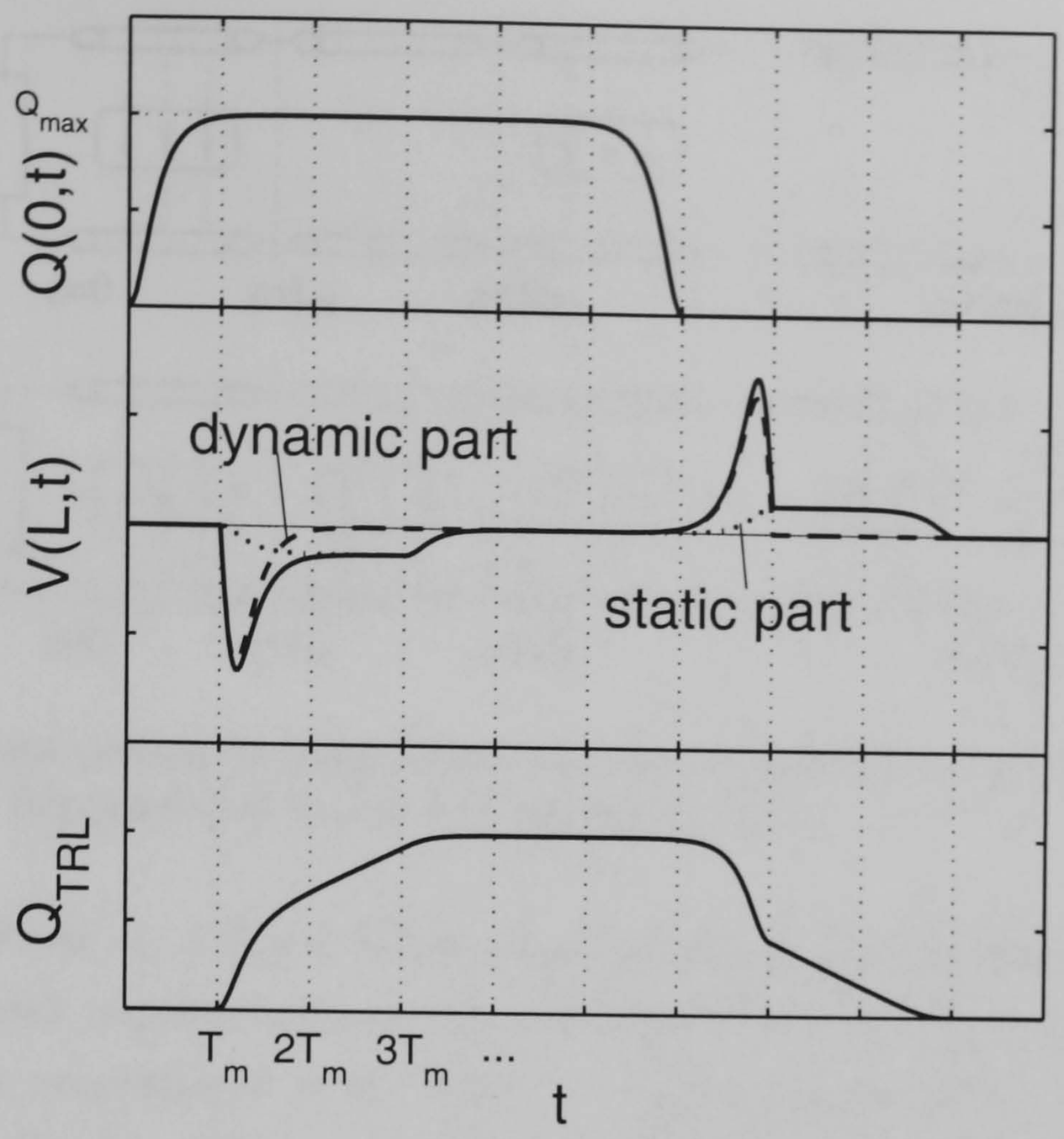

Figure 3.6: Generated voltage at the end of the transmission line $V(L,t)$ and charge Q_{TRL} on the transmission line after excitation with a CW source distribution.

reason for this somehow unexpected behaviour is the presence of a space charge at $z = L$ leading to the excitation of a backward travelling microwave which is absorbed by the load after one roundtrip. As discussed in the next subsection, the backward travelling wave is important for the charge development on the line. For terminations of the transmission line different from impedance matching the dynamic parts of the solutions are also partly reflected resulting in multiple reflections, i.e. back and forward travelling waves on the line.

3.4 Continuous Wave Source Distribution

We now turn our attention to the development of voltage and in particular the accumulation of charges on the transmission line for the case of a continuous wave (CW) source distribution. If we consider the case of an open circuit at $z = 0$ and a load Z_{E} at $z = L$, the charge on the transmission line is determined by the current flowing through the load at the end,

$$Q_{\mathrm{TRL}}(t) = \int_0^t I(L,t)\,dt = Z_{\mathrm{E}} \int_0^t U(L,t)\,dt\ . \tag{3.24}$$

As a simple example we choose a velocity matched line with a matched load at $z = L$, i.e. solution eq. (3.22) applies.

Fig. 3.6 explains the voltage and charge development for this scenario. We assume the source to be switched on at $t = 0$ resulting in a certain transient of the source function

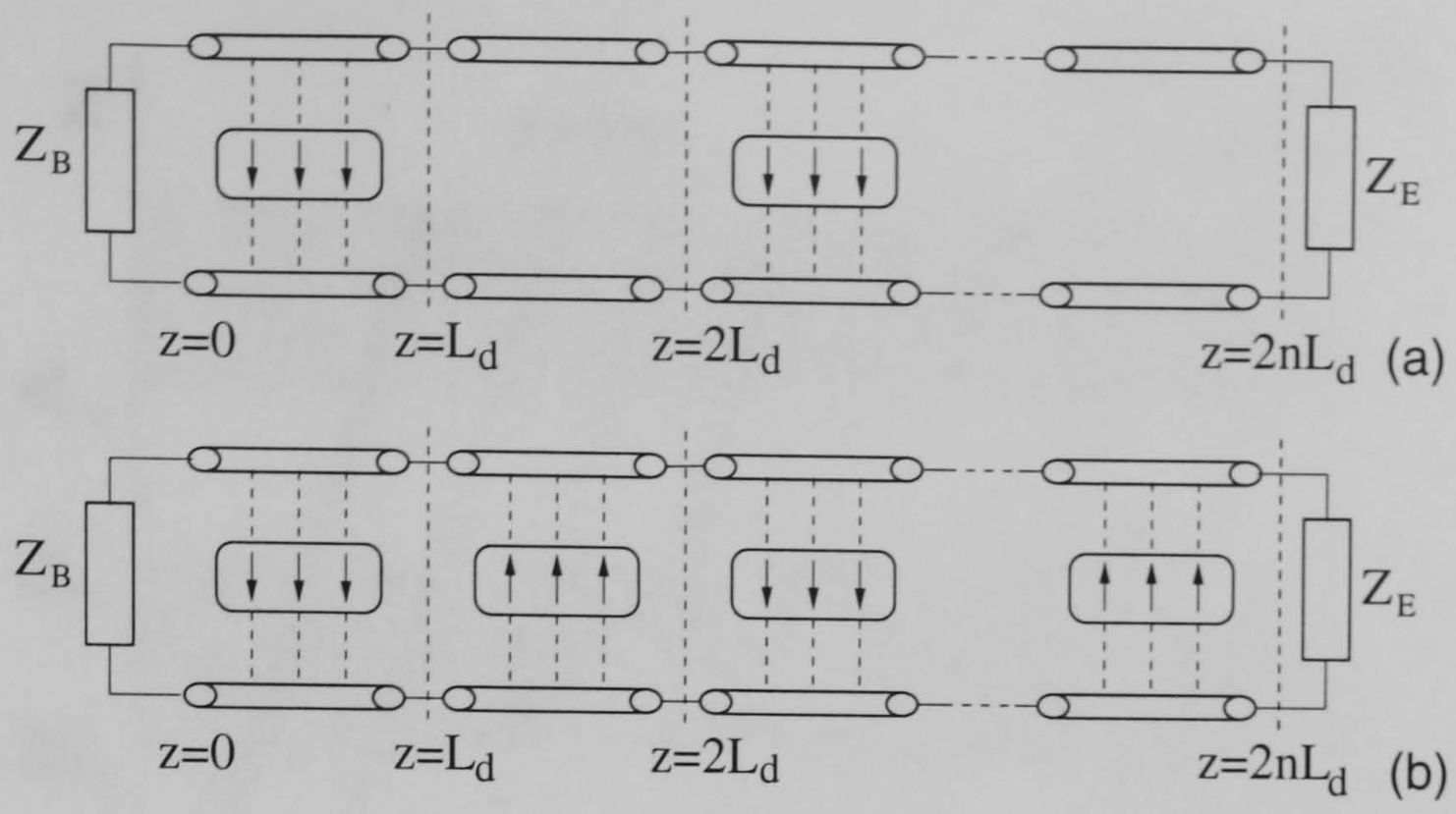

Figure 3.7: Equivalent circuits for transmission line with modulated source, (a) domains without source, (b) distributed source with alternating signs.

from 0 to $Q_{\max}$. From eq. (3.22) it follows that the voltage distribution consists of a short linearly growing peak corresponding to the derivative of the optical power transient and a quasistatic voltage proportional to Q. After $t = T_{\mathrm{m}}$ both signals arrive at the end of the transmission line, the dynamic part is absorbed by the load and the static part is partly reflected. After one roundtrip this reflected part cancels the voltage $V(L,t)$ at the end of the transmission line. This means essentially between $t = T_{\mathrm{m}}$ and shortly after $t = 3T_{\mathrm{m}}$ a voltage is present at $z = L$ leading to a current flow and hence accumulation of charge on the transmission line. Shortly after $t = 3T_{\mathrm{m}}$ the system is in a steady state. Here the charge on the transmission line and the space charge due to the presence of a CW source field cancel each other so that there is no net voltage on the transmission line. Consequently, the change of the polarisation in the transmission line leads to the generation of microwave energy and hence an accumulation of charge, not the presence of polarisation itself. When the source is switched off, the whole process reverses so that approximately after a subsequent time interval $3T_{\mathrm{m}}$ there are no charges remaining on the conductors of the transmission line. Hence, the backreflected static part plays an important role for the development and conservation of charge on the transmission line.

3.5 Modulation of the Source Distribution

The generation of microwave signals by injection of an optical pulse results in rather broad bandwidth electrical signals on the transmission line determined by the spectrum of the optical pulse. In a number of applications, a coherent, narrow bandwidth THz source might be preferable. An interesting approach to achieve this has been demonstrated recently by Lee *et al.* [13] in lithium niobate. Here periodic poling of bulk material results in domains with alternating sign in the nonlinearity, similarly as it is shown in Fig. 3.7. Using material

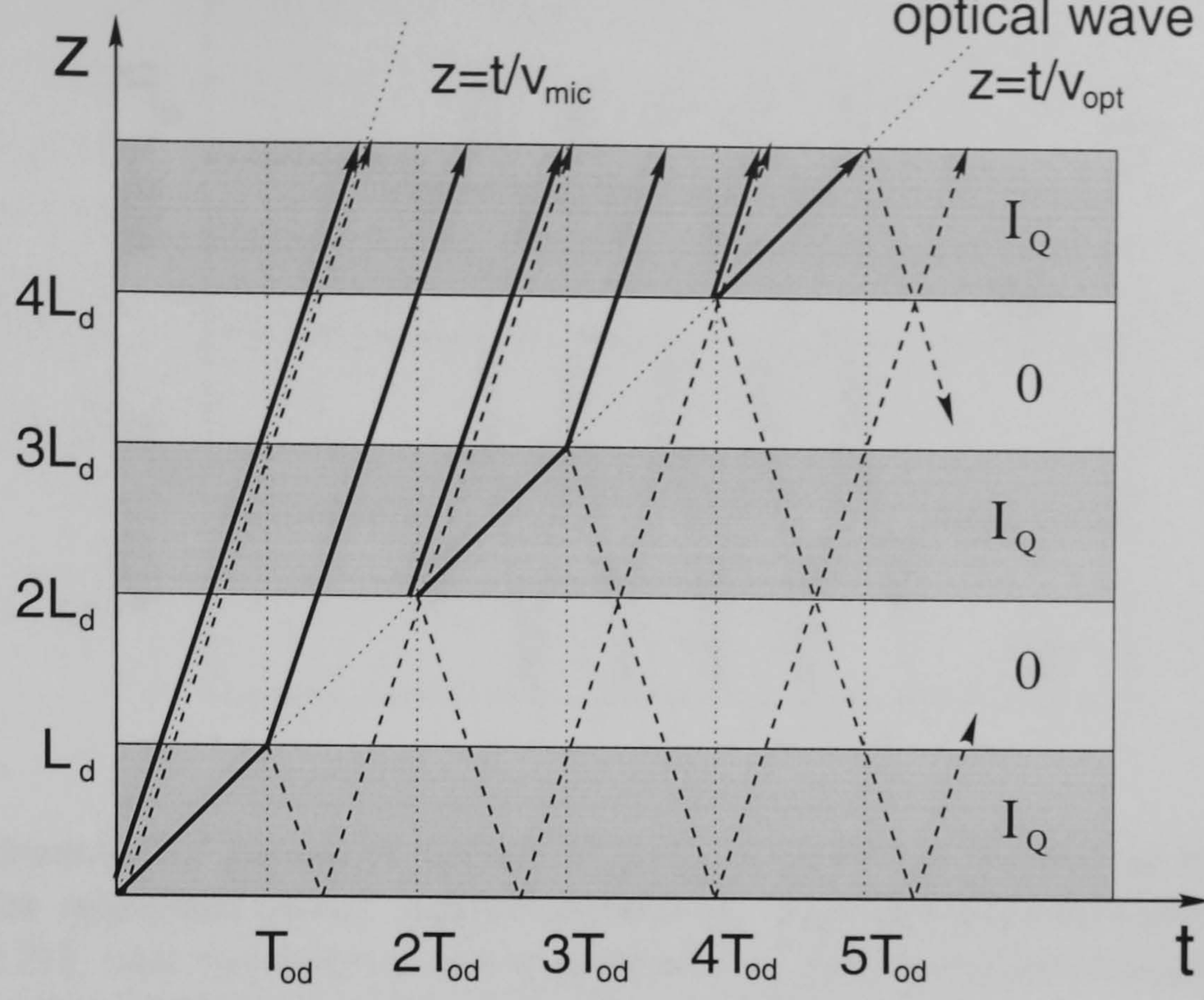

Figure 3.8: Generation of a pulse train in a network corresponding to Fig. 3.7(a), the optical wave travels with a velocity v_{opt}, solid line dynamic part of generated voltage, dashed line static part.

with slight velocity mismatch between optical wave and microwave and matching the walk-off length to the domain length of the poled material results in a train of electrical signals and hence in a narrow bandwidth THz source. As similar principles could be applied in a transmission line, the basic mechanism will be explained here by means of the transmission line model.

Fig. 3.7 shows the corresponding equivalent circuits. Two cases are considered: (a) domains with nonlinearity alternate with domains without nonlinearity and (b) the sign of the nonlinearity alternates in adjacent domains. Both cases are described as a periodic network of cells containing domains without source or a source with alternating sign.

The basic idea is illustrated in Fig. 3.8 for the case of alternate domains without nonlinearity. We assume a slight velocity mismatch between the travelling source and the microwave. As the optical pulse enters the first Section, two pulses are generated, one travelling with the optical wave and one travelling with the phase velocity of the microwave. After the domain length L_{d}, which should be comparable to the walk-off length, both pulses travel further with the phase velocity of the microwave. As the optical pulse enters the second domain with nonlinearity, this process repeats so that after passing a number of cells a train of microwave pulses is obtained. This corresponds to a narrow bandwidth electrical signal with a midfrequency depending on the velocity mismatch as well as the the length L_{d} of one cell,

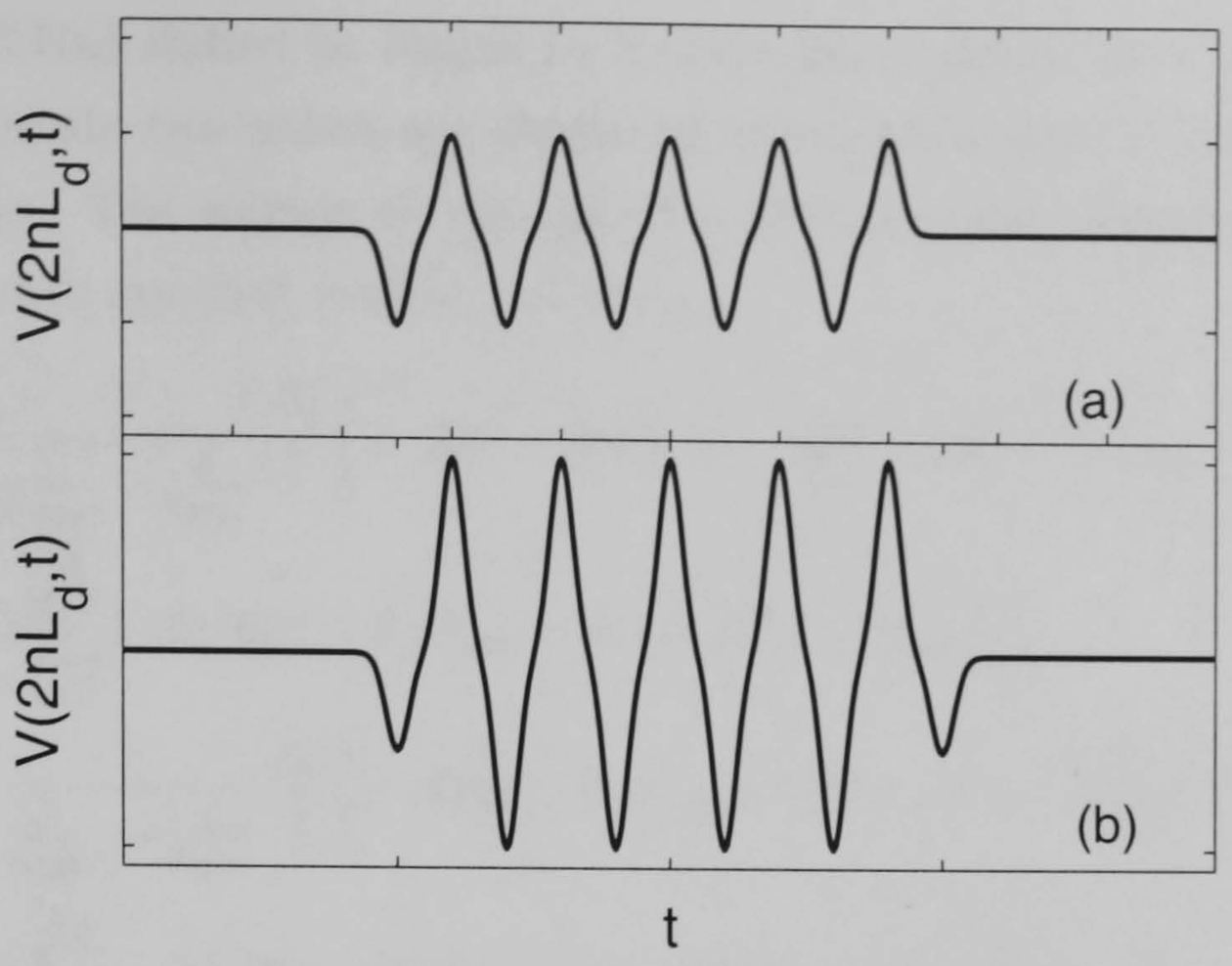

Figure 3.9: Schematic of generated voltage $V(2nL_\mathrm{d}, t)$ (n=5) at the end of transmission line with modulated source, walk-off and domain length are matched corresponding to eq. (3.27), only the dynamic part is depicted, (a) domains without source (Fig. 3.7(a)), (b) distributed source with alternating signs (Fig. 3.7(b)).

$$f_\mathrm{mid} = \frac{1}{2L_\mathrm{d}\left|\frac{1}{v_\mathrm{opt}} - \frac{1}{v_\mathrm{mic}}\right|}\,, \tag{3.25}$$

Solutions for the voltages on the transmission line can be obtained from eqs. (3.7), (3.8) and eqs. (3.14), (3.15) by matching the currents and voltages at the respective boundaries $z = iL_\mathrm{d}$. For a transmission line depicted in Fig. 3.7 (a) consisting of $2n$ alternating layers with the same length L_d one obtains for the voltage at $z = 2nL_\mathrm{d}$ (open circuit at $z = 0$, matched load at $z = 2nL_\mathrm{d}$),

$$\begin{aligned} V(2nL_\mathrm{d}, t) = {} & \frac{1}{\frac{1}{v_\mathrm{opt}} - \frac{1}{v_\mathrm{mic}}} \frac{Z_0}{2} \sum_{i=1}^{2n} (-1)^i \, Q[t - 2nT_\mathrm{md} - (i-1)(T_\mathrm{od} - T_\mathrm{md})] \\ & + \frac{1}{\frac{1}{v_\mathrm{opt}} + \frac{1}{v_\mathrm{mic}}} \frac{Z_0}{2} \sum_{i=1}^{2n} (-1)^i \, Q[t - 2nT_\mathrm{md} - (i-1)(T_\mathrm{od} + T_\mathrm{md})]\,, \end{aligned} \tag{3.26}$$

where $T_\mathrm{od} = L_\mathrm{d}/v_\mathrm{opt}$ and $T_\mathrm{md} = L_\mathrm{d}/v_\mathrm{mic}$. As shown schematically in Fig. 3.8, the second term corresponds to small static parts which are reflected at boundaries between domains with and without source. Fig. 3.9 shows schematically the generated train of electrical pulses at the end of the transmission line. For a high conversion efficiency and narrow bandwidth the domain length and the velocity mismatch should be matched to the walk-off length and hence pulse width of the incoming pulse T_FWHM,

$$L_\mathrm{d} = \frac{T_\mathrm{FWHM}}{\left|\frac{1}{v_\mathrm{opt}} - \frac{1}{v_\mathrm{mic}}\right|}\,, \tag{3.27}$$

The basic principle of a structure shown in Fig. 3.7(b) is very similar to the one in Fig. 3.7(a). This can be explained by interpreting the structure as a combination of two networks

as shown in Fig. 3.7(a) shifted by length L_d and having opposite signs of the nonlinearity. Hence, in every domain two pulses are generated which add constructively giving the final voltage distribution. The voltage at the end of a structure with length $2nL_d$ amounts to (open circuit at $z = 0$, matched load at $z = 2nL_d$),

$$\begin{aligned} V(2nL_d, t) = & \frac{1}{\frac{1}{v_{opt}} - \frac{1}{v_{mic}}} \frac{Z_0}{2} \Big\{ - Q(t - 2nT_{md}) - Q[t - (2n+1)T_{md} - 2nT_{od}] \\ & + 2 \sum_{i=2}^{2n} (-1)^i \, Q[t - 2nT_{md} - (i-1)(T_{od} - T_{md})] \Big\} \\ & + \frac{1}{\frac{1}{v_{opt}} + \frac{1}{v_{mic}}} \frac{Z_0}{2} \Big\{ - Q(t - 2nT_{md}) - Q[t - (2n+1)T_{md} - 2nT_{od}] \\ & + 2 \sum_{i=2}^{2n} (-1)^i \, Q[t - 2nT_{md} - (i-1)(T_{od} + T_{md})] \Big\} . \end{aligned} \tag{3.28}$$

Note that at a transition between two domains with alternating sign of the nonlinearity the generated voltage travelling with the velocity v_{mic} is increased by a factor 2 resulting in a higher conversion efficiency. The generated signal is shown schematically in Fig. 3.9(b). Both formulas eqs. (3.25, 3.27) also apply in this case. Not included in the simple model presented here are losses which will lead to a decaying envelope of the generated microwave signal.

The principle of narrow bandwidth THz generation discussed in this Section requires a periodic modulation of the nonlinearity in the structure. However, as will be shown in Section 4.5.2, a similar effect can be achieved by using two optical polarisation components with slight mismatch between the corresponding phase constants.

In conclusion, the aim of this Chapter is a qualitative understanding of the basic mechanisms of OR in a transmission line. The optical source term is interpreted as a displacement current due to an induced charge in the line capacitance proportional to the injected optical power. The formulation includes bidirectional wave propagation and appropriate boundary conditions at the beginning and the end of the line. However, this simple model gives no indications of physical magnitudes involved. Furthermore, for large interaction lengths the optical wave might be subject to depletion, dispersion or phase modulation. A detailed quantitative description including these effects is the subject of the next Chapter.

4 Interaction between Optical Wave and Microwave

4.1 Introduction

In the previous Chapter, a simple transmission line model was introduced to explain the essential mechanisms of optical rectification (OR) in a travelling wave structure. Whereas that approach is purely phenomenological, we will now focus on a more quantitative analysis of the interaction between an optical wave and a microwave in a combined waveguide. In particular, the modal structures of both fields, the crystal orientation and hence polarisation effects, losses, dispersion and the backcoupling of the generated microwave to the optical wave via the electro-optic effect are taken into account.

To give an impression of physical magnitudes, we choose as examples the structures shown in Fig. 4.1. Here a dielectric optical waveguide is combined with typical microwave transmission lines. The optical waveguide consists of a layered structure for vertical guidance and a rib for lateral confinement. The corresponding microwave transmission lines are a coplanar wave guide (CPW) with a signal electrode placed on top of the rib and infinitely extended ground electrodes (Fig. 4.1 (a)), and a coplanar strip (CPS) line with two electrodes of finite width placed adjacent to the rib (Fig. 4.1 (b)). For the substrate, we choose AlGaAs with the usual growth [100] and cleaving [011] directions. AlGaAs is a semiconductor with a zinc-blende (or cubic) symmetry belonging to the class $\bar{4}3m$. The only nonzero second-order susceptibility tensor elements are $\tilde{\chi}^{(2)}_{xyz}(-\omega_3;\omega_1,\omega_2) = \tilde{\chi}^{(2)}_{zxy}(-\omega_3;\omega_1,\omega_2) = \tilde{\chi}^{(2)}_{yzx}(-\omega_3;\omega_1,\omega_2)$ which correspond to the electro-optic coefficients $r_{41} = r_{52} = r_{63}$. A more detailed discussion of the properties of AlGaAs can be found in Appendix D. Whereas the structures shown in Fig. 4.1 are essentially electro-optic modulators, in this thesis we are mainly interested in effects which arise at high optical peak powers. Here the optical wave generates an electrical signal by OR and potentially interacts with the generated microwave via the electro-optic effect.

The transmission line structures have been chosen because they are examples for two essential cases. Whereas for a CPW structure which is symmetric with respect to the x-z-plane only the TE optical mode interacts with the microwave field in x-direction, in the

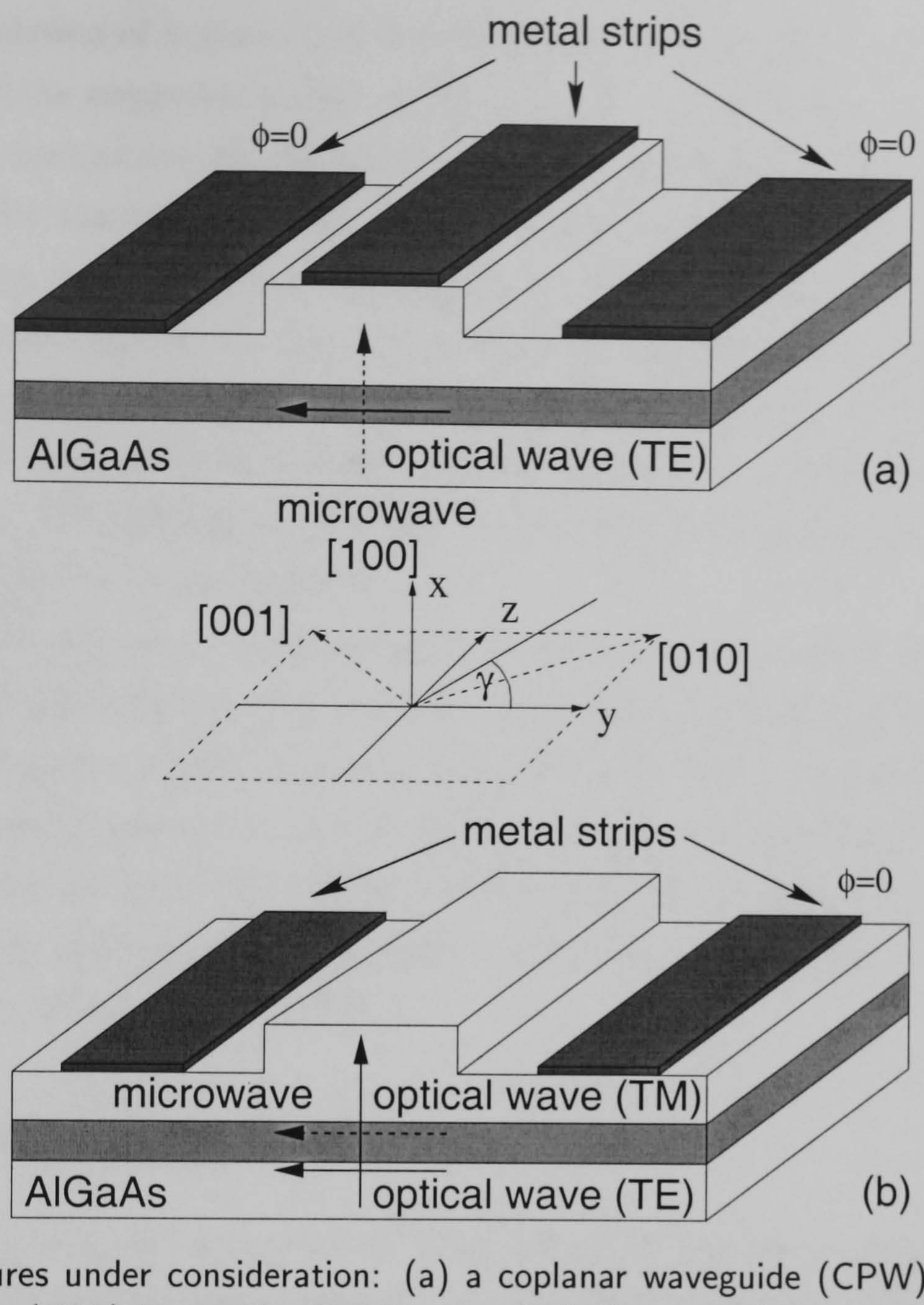

Figure 4.1: Structures under consideration: (a) a coplanar waveguide (CPW) or (b) a coplanar stripline (CPS) is combined with an optical rib waveguide on a substrate of AlGaAs with usual [100] growth and [011] cleaving directions. The dashed arrow indicates the field direction of the microwave interacting with the optical TE and TM mode (solid arrow). An optical pulse is injected into the structure with a polarisation angle γ.

case of a symmetric CPS structure the interaction between both TE and TM optical modes is required for the generation of a microwave signal in y-direction. As will be shown in subsequent Sections, the latter case exhibits very different effects arising from the coupling of two optical modes with slightly different propagation constants.

It should be pointed out that the model used in this Chapter is easily modified to account for other materials, e.g. electro-optic crystals as KTP and $LiNbO_3$. Also, a number of other guiding structures can be considered, provided that the appropriate modes of the microwave transmission line have no cut-off. The equations obtained are similar to a system derived for the interaction of optical waves and electrical signals in bulk material when neglecting the tansverse spatial derivatives [22]. This implies that essential results obtained in this analysis apply to a broad range of configurations.

In Section 4.2, the evolution equations for the mutual interaction of both optical and microwave are derived and basic properties of the system are discussed. A quantitative analysis

requires the calculation of a number of system parameters such as overlap integrals, dispersion and losses of the respective modes in the waveguide. In Section 4.3, the corresponding transmission line parameters are discussed and techniques for their approximate estimation are introduced. For the two example structures shown in Fig. 4.1, we calculate a set of parameters which are used throughout the thesis to give an indication of physical magnitudes involved. The specific geometry and the collection of the respective data can be found in Appendix F. However, it should be noted that the structure is by no means optimized for the observation of effects described in subsequent Chapters, i.e. modulational instability and soliton formation. Nevertheless it is useful to give specific examples to uncover potential difficulties one might face in an experiment.

Section 4.4 gives a short review of the mode of action of electro-optic modulators based on the equations derived in Section 4.2. Section 4.5 is dedicated to the generation of electrical signals from high power optical waves by means of OR. Here, both the single and mixed polarisation case are discussed in detail. Finally, Section 4.6 considers phenomena arising from the interaction of both OR and the electro-optic effect, also called *cascading* effects. One of the resulting mechanisms, a self phase modulation of the optical wave, is essential for effects described in subsequent Chapters.

4.2 Derivation of Equations

In the following the evolution equations are derived for the case of a coupled waveguide where both the optical and microwave modes are confined in the transverse directions. The basic principle is the expansion of fields with induced nonlinear polarisation into the linear modes of the waveguide when no polarisation is present. The transverse fields are taken into account by overlap integrals including the field profiles of the respective modes. The derivation is formulated in the spectral domain, frequency-dependent magnitudes being expanded in a Taylor series followed by a subsequent Fourier transformation back to the time domain. The derivation starts with Maxwell's equations in frequency domain assuming a nonmagnetic and isotropic dielectric in the absence of free charges or external currents,

$$\nabla \times \tilde{\mathbf{E}} = \mathrm{i}\omega\mu_0\tilde{\mathbf{H}} \,, \tag{4.1}$$

$$\nabla \times \tilde{\mathbf{H}} = -\mathrm{i}\omega\varepsilon_0\varepsilon_r\tilde{\mathbf{E}} - \mathrm{i}\omega\tilde{\mathbf{P}}_{\mathrm{NL}} \,, \tag{4.2}$$

where $\tilde{\mathbf{E}}$ and $\tilde{\mathbf{H}}$ are the electric and magnetic fields, respectively. Both quantities depend on the spatial coordinates x, y and z as well as the angular frequency ω. ε_0 and μ_0 are the free space permittivity and permeability respectively. We consider a structure with translational invariance in z-direction. Hence, the dielectric constant $\varepsilon_r(x, y, \omega)$ is a function of frequency and the transverse directions only. The action of the nonlinearity is taken into account by the nonlinear contribution to the polarisation $\tilde{\mathbf{P}}_{\mathrm{NL}}$. Assuming the nonlinear polarisation to

be weak we can expand the fields into the modes of the linear problem (see, for example [35]),

$$\tilde{\mathbf{E}}=\sum_n u_n(z,\omega)\,\mathbf{e}_n(x,y,\omega)\;, \tag{4.3}$$

$$\tilde{\mathbf{H}}=\sum_n u_n(z,\omega)\,\mathbf{h}_n(x,y,\omega)\;. \tag{4.4}$$

Here $\mathbf{e}_n(x,y,\omega)$ and $\mathbf{h}_n(x,y,\omega)$ are the frequency-dependent transverse electric and magnetic field profiles of the respective modes. The calculation of the mode profiles will be considered in Sections 4.3.1 and 4.3.2. The dimensionless coefficients $u_n(z,\omega)$ describe the evolution of the mode amplitude under the influence of the nonlinearity. Inserting the ansatz (4.3, 4.4) into (4.1, 4.2) and using the orthogonality between modes at a particular frequency evolution equations for the coefficients $u_n(z,\omega)$ can be derived as [35],

$$\frac{\partial u_n}{\partial z} - \mathrm{i}\beta_n(\omega)u_n = \frac{\mathrm{i}\omega}{p_n}\iint \mathbf{e}_n^*\cdot\tilde{\mathbf{P}}_{\mathrm{NL}}\,dxdy\;, \tag{4.5}$$

where $\beta_n(\omega)$ is the propagation constant of the n-th mode and p_n is the guided wave power defined as,

$$p_n = 2\mathrm{Re}\iint[\mathbf{e}_n\times\mathbf{h}_n^*]_z\,dxdy\;. \tag{4.6}$$

A detailed derivation of eq. (4.5) can be found in Appendix B. Eq. (4.5) describes in general the coupling between modes in a structure with translational invariance under the presence of a perturbation, assuming back-reflection can be neglected. Here we are interested in the interaction between optical waves and microwaves in a material with a second order nonlinearity.

To get a deeper insight into the physics it is appropriate to transform the evolution equation (4.5) into the time domain. To this end we separate the frequency domain into the optical regime around a carrier frequency ω_{opt} and the microwave domain located around $\omega = 0$. Note that we neglect higher harmonics, in particular frequency doubling, assuming a large phase mismatch between the fundamental and the second harmonic. Additionally, the propagating wave might be influenced by the cubic or higher order nonlinearities of the material. Here we neglect those effects concentrating mainly on OR and the electro-optic effect. Whereas we consider the propagation of both TE and TM optical modes, we assume the microwave transmission line to be single moded.

The frequency dependent propagation constants $\beta_n(\omega)$ are expanded in the respective frequency domains. In the optical range the expansion for $\beta_n(\omega)$ (n=TE,TM) reads as,

$$\beta_n(\omega)\approx\beta_n+\frac{\omega-\omega_{\mathrm{opt}}}{v_n}+\frac{D_n}{2}(\omega-\omega_{\mathrm{opt}})^2\;, \tag{4.7}$$

where β_n, v_n and D_n denote the mean propagation constant, the group velocity and the group velocity dispersion of the optical pulse defined as,

$$\beta_n=\frac{\omega_{\mathrm{opt}}\,n_n}{c}=\beta_n(\omega_{\mathrm{opt}})\quad,\quad\frac{1}{v_n}=\frac{n_n^{\mathrm{gr}}}{c}=\left.\frac{\partial\beta_n}{\partial\omega}\right|_{\omega=\omega_{\mathrm{opt}}}\quad,\quad D_n=\left.\frac{\partial^2\beta_n}{\partial\omega^2}\right|_{\omega=\omega_{\mathrm{opt}}}\;. \tag{4.8}$$

Here n_n is the effective refractive index, n_n^{gr} is the group index and c is the velocity of light in vacuum. The propagation constant β_n and hence n_n can be complex to account for optical losses.

The expansion for the microwave is somewhat different. As we expand around $\omega = 0$, the propagation constant $\beta(\omega)$ obeys the symmetry condition $\beta(-\omega) = -\beta(\omega)^*$. Hence we obtain for the microwave,

$$\beta(\omega) \approx j\alpha_{\mathrm{mic}} + \frac{1}{v_{\mathrm{mic}}}\omega + j\alpha'_{\mathrm{mic}}\omega^2 + \frac{T_{\mathrm{mic}}}{6}\omega^3 \quad , \tag{4.9}$$

where v_{mic} is the group velocity of the microwave, which coincides with the phase velocity. T_{mic} represents the third order dispersion and α_{mic} and α'_{mic} are the frequency-independent and -dependent losses respectively defined as,

$$\alpha_{\mathrm{mic}} = \mathrm{Im}[\beta(0)] \quad , \quad \frac{1}{v_{\mathrm{mic}}} = \frac{n_{\mathrm{mic}}}{c} = \mathrm{Re}\left[\left.\frac{\partial\beta_{\mathrm{mic}}}{\partial\omega}\right|_{\omega=0}\right] ,$$
$$\alpha'_{\mathrm{mic}} = 2\mathrm{Im}\left[\left.\frac{\partial^2\beta_{\mathrm{mic}}}{\partial\omega^2}\right|_{\omega=0}\right] \quad , \quad T_{\mathrm{mic}} = \mathrm{Re}\left[\left.\frac{\partial^3\beta_{\mathrm{mic}}}{\partial\omega^3}\right|_{\omega=0}\right] . \tag{4.10}$$

Note that the expansions (4.7, 4.9) include both mode and material dispersions.

Before moving on a comment has to be made about the power of the guided microwave mode. As we expand around $\omega = 0$, the mode profile is given by the TEM (*transverse electromagnetic*) electric field of the static limit $\omega \to 0$. Hence, eq. (4.6) is not applicable for the guided wave power. Instead, in this limit the guided power can be expressed in terms of the line voltage V and the impedance Z_0 of the transmission line as [36],

$$p_{\mathrm{mic}} = \lim_{\omega\to 0} \mathrm{Re}\iint [\mathbf{e}_{\mathrm{mic}} \times \mathbf{h}^*_{\mathrm{mic}}]_z \, dxdy = \frac{V^2}{Z_0} . \tag{4.11}$$

Inserting the expansions (4.7, 4.9) into the equation for the forward propagating wave (4.5) and performing the backtransformation into the time domain gives,

$$\left[\frac{\partial}{\partial z} + \alpha_{\mathrm{mic}} + \frac{1}{v_{\mathrm{mic}}}\frac{\partial}{\partial t'} - \alpha'_{\mathrm{mic}}\frac{\partial^2}{\partial t'^2} - \frac{T_{\mathrm{mic}}}{6}\frac{\partial^3}{\partial t'^3}\right] u_{\mathrm{mic}} = -\frac{1}{2p_{\mathrm{mic}}}\frac{\partial}{\partial t'}\iint \mathbf{e}^*_{\mathrm{mic}}\cdot\mathbf{P}_{\mathrm{mic}}\, dxdy, \tag{4.12}$$

$$\left[\frac{\partial}{\partial z} - \mathrm{i}\beta_n + \frac{1}{v_n}\frac{\partial}{\partial t'} + \mathrm{i}\frac{D_n}{2}\frac{\partial^2}{\partial t'^2}\right] u_n = \frac{1}{p_n}\left(\mathrm{i}\omega_{\mathrm{opt}} - \frac{\partial}{\partial t'}\right)\iint \mathbf{e}^*_n\cdot\mathbf{P}_{\mathrm{opt}}\, dxdy. \tag{4.13}$$

Note that eq. (4.13) refers to two evolution equations corresponding to the index n=TE/TM. The Fourier backtransformation was performed separately around the relevant frequency ranges $\omega = \omega_{\mathrm{opt}}$ and $\omega = 0$. Correspondingly the time dependent electric fields are written as,

$$\begin{aligned}\mathbf{E}(x,y,z,t') =& [u_{\mathrm{TE}}(z,t')\exp[-\mathrm{i}\omega_{\mathrm{opt}}t']\,\mathbf{e}_{\mathrm{TE}}(\omega_{\mathrm{opt}}) + c.c.] \\ &+ [u_{\mathrm{TM}}(z,t')\exp[-\mathrm{i}\omega_{\mathrm{opt}}t']\,\mathbf{e}_{\mathrm{TM}}(\omega_{\mathrm{opt}}) + c.c.] + u_{\mathrm{mic}}(z,t')\,\mathbf{e}_{\mathrm{mic}}(0) ,\end{aligned} \tag{4.14}$$

where *c.c.* denotes the complex conjugate. The transverse mode profiles are assumed to be frequency independent so that we end up with $\mathbf{e}_{\mathrm{mic}}(0)$ being the TEM mode of the static problem and $\mathbf{e}_{\mathrm{TE/TM}}(\omega_{\mathrm{opt}})$ the optical mode at the carrier frequency ω_{opt}. Further we assume the optical losses to be moderate so that only the real parts of the optical mode profiles are taken into account in further calculations. Similarly the time dependent polarisation can be constructed as,

$$\mathbf{P}_{\mathrm{NL}}(x,y,z,t') = \mathbf{P}_{\mathrm{opt}}(x,y,z,t')\exp[-\mathrm{i}\omega_{\mathrm{opt}}t'] + c.c. + \mathbf{P}_{\mathrm{mic}}(x,y,z,t')\,. \tag{4.15}$$

Until now only the relevant frequency domains have been chosen and the number of modes allowed to propagate have been fixed. The order of the nonlinearity as well as the crystal orientation comes in at this stage. As indicated in the introduction of this Chapter, we choose as an example a cubic material, i.e. GaAs, with the crystal orientation indicated in Fig. 4.1. According to the fcc lattice the only nonzero element of the susceptibility tensor is then $\chi^{(2)}_{123}$. The electric field and polarisation in time domain are related to each other by a convolution integral. As discussed in Appendix D, we assume the susceptibilities corresponding to OR, electro-optic effect and microwave self-interaction defined in Chapter 2 to be equal,

$$\chi^{(2)} = \tilde{\chi}^{(2)}_{ijk}(0;0,0) = \tilde{\chi}^{(2)}_{ijk}(-\omega;\omega,0) = \tilde{\chi}^{(2)}_{ijk}(0;\omega,-\omega)\,. \tag{4.16}$$

The convolution integral then simplifies to simple multiplication. A modification of the equations to account for varying susceptibilities is straightforward. Furthermore, the method can be easily adapted to other material systems by introducing the respective susceptibility tensor. However, the majority of results obtained here should apply in other material systems as well.

For the AlGaAs-system we obtain for the relevant vector components of the polarisation,

$$\begin{aligned}[\mathbf{P}_{\mathrm{NL}}]_x &= -\frac{\varepsilon_0\chi^{(2)}}{2}[\mathbf{E}]_y^2\,,\\ [\mathbf{P}_{\mathrm{NL}}]_y &= -\varepsilon_0\chi^{(2)}[\mathbf{E}]_x[\mathbf{E}]_y\,.\end{aligned} \tag{4.17}$$

As the field profiles in propagation direction are zero for the TEM microwave field profile and small for the optical modes, the polarisation component in z-direction can be neglected. Further we consider the weak-guiding limit where only y-components of the TE mode and x-components of the TM mode are significant. In contrast the microwave has large field components in x- and y-direction which have to be considered in the calculation of the polarisation. The microwave components of the polarisation can now be obtained by inserting eq. (4.14) into eqs. (4.17) and we get,

$$\begin{aligned}[\mathbf{P}_{\mathrm{mic}}]_x &= -\frac{\varepsilon_0\chi^{(2)}}{2}\left([\mathbf{e}_{\mathrm{mic}}]_y^2u_{\mathrm{mic}}^2 + 2[\mathbf{e}_{\mathrm{TE}}]_y^2|u_{\mathrm{TE}}|^2\right)\,,\\ [\mathbf{P}_{\mathrm{mic}}]_y &= -\varepsilon_0\chi^{(2)}\left[[\mathbf{e}_{\mathrm{mic}}]_y[\mathbf{e}_{\mathrm{mic}}]_xu_{\mathrm{mic}}^2 + 2\mathrm{Re}([\mathbf{e}_{\mathrm{TE}}]_y[\mathbf{e}_{\mathrm{TM}}]_xu_{\mathrm{TE}}u_{\mathrm{TM}}^*)\right]\,,\end{aligned} \tag{4.18}$$

where we included the microwave self-interaction terms for completeness. For the optical polarisation we obtain,

$$\begin{aligned}
[\mathbf{P}_{\text{opt}}]_x &= -\varepsilon_0 \chi^{(2)} [\mathbf{e}_{\text{TE}}]_y [\mathbf{e}_{\text{mic}}]_y u_{\text{TE}} u_{\text{mic}} \,, \\
[\mathbf{P}_{\text{opt}}]_y &= -\varepsilon_0 \chi^{(2)} \left([\mathbf{e}_{\text{TE}}]_y [\mathbf{e}_{\text{mic}}]_x u_{\text{TE}} u_{\text{mic}} + [\mathbf{e}_{\text{TM}}]_x [\mathbf{e}_{\text{mic}}]_y u_{\text{TM}} u_{\text{mic}} \right) \,.
\end{aligned} \tag{4.19}$$

Inserting the polarisation components eqs. (4.18, 4.19) into eqs. (4.12, 4.13) we can derive the final system of equations. Before doing so we move the reference frame with the group velocity of the TE-mode $t = t' - z/v_{\text{TE}}$. Further we scale the amplitudes in terms of guided wave power and remove fast varying terms as,

$$\begin{aligned}
U_{\text{mic}} &= u_{\text{mic}} \sqrt{p_{\text{mic}}} \,, \\
U_{\text{TE}} &= u_{\text{TE}} \sqrt{p_{\text{TE}}} \exp[-\mathrm{i}\beta_{\text{TE}} z] \,, \\
U_{\text{TM}} &= u_{\text{TM}} \sqrt{p_{\text{TM}}} \exp[-\mathrm{i}\beta_{\text{TE}} z] \,.
\end{aligned} \tag{4.20}$$

The final system of equations is then given by [36, 37],

$$\begin{aligned}
&\left[\frac{\partial}{\partial z} + \alpha_{\text{mic}} + \frac{\Delta n}{c} \frac{\partial}{\partial t} - \alpha'_{\text{mic}} \frac{\partial^2}{\partial t^2} - \frac{T_{\text{mic}}}{6} \frac{\partial^3}{\partial t^3} \right] U_{\text{mic}} = \\
&\qquad \frac{\chi_{\text{eff1}}}{2} \frac{\partial}{\partial t} |U_{\text{TE}}|^2 + \frac{\chi_{\text{eff2}}}{2} \frac{\partial}{\partial t} [U_{\text{TE}} U^*_{\text{TM}} + U^*_{\text{TE}} U_{\text{TM}}] + \chi_{\text{eff3}} \frac{\partial}{\partial t} U^2_{\text{mic}} \,,
\end{aligned} \tag{4.21}$$

$$\left[\mathrm{i} \frac{\partial}{\partial z} - \frac{D_{\text{TE}}}{2} \frac{\partial^2}{\partial t^2} \right] U_{\text{TE}} = \chi_{\text{eff1}} [\omega_{\text{opt}} + \mathrm{i} \frac{\partial}{\partial t}] [U_{\text{TE}} U_{\text{mic}}] + \chi_{\text{eff2}} [\omega_{\text{opt}} + \mathrm{i} \frac{\partial}{\partial t}] [U_{\text{TM}} U_{\text{mic}}] \,, \tag{4.22}$$

$$\left[\mathrm{i} \frac{\partial}{\partial z} - \Delta\beta - \mathrm{i}\delta_{\text{vopt}} \frac{\partial}{\partial t} - \frac{D_{\text{TM}}}{2} \frac{\partial^2}{\partial t^2} \right] U_{\text{TM}} = \chi_{\text{eff2}} [\omega_{\text{opt}} + \mathrm{i} \frac{\partial}{\partial t}] [U_{\text{TE}} U_{\text{mic}}] \,, \tag{4.23}$$

where $\Delta n/c = (n_{\text{mic}} - n^{\text{gr}}_{\text{TE}})/c$ is the group velocity mismatch between microwave and TE optical mode, whereas $\Delta\beta = 2\pi\Delta n_{\text{opt}}/\lambda = 2\pi(n_{\text{TE}} - n_{\text{TM}})/\lambda$ and $\delta_{\text{vopt}} = (n^{\text{gr}}_{\text{TE}} - n^{\text{gr}}_{\text{TM}})/c$ represent phase-mismatch and walk-off between both optical waves, respectively. Here λ denotes the wavelength of the optical wave. The overlap integrals are given by,

$$\chi_{\text{eff1}} = \varepsilon_0 \frac{\iint \chi^{(2)}(x,y) \, [\mathbf{e}_{\text{mic}}]_x \, [\mathbf{e}_{\text{TE}}]_y^2 \, dxdy}{p_{\text{mic}}^{1/2} \, p_{\text{TE}}} \,, \tag{4.24}$$

$$\chi_{\text{eff2}} = \varepsilon_0 \frac{\iint \chi^{(2)}(x,y) \, [\mathbf{e}_{\text{mic}}]_y \, [\mathbf{e}_{\text{TE}}]_y \, [\mathbf{e}_{\text{TM}}]_x \, dxdy}{[p_{\text{mic}} \, p_{\text{TE}} \, p_{\text{TM}}]^{1/2}} \,, \tag{4.25}$$

$$\chi_{\text{eff3}} = \frac{3\varepsilon_0}{4} \frac{\iint \chi^{(2)}(x,y) \, [\mathbf{e}_{\text{mic}}]_x \, [\mathbf{e}_{\text{mic}}]_y^2 \, dxdy}{p_{\text{mic}}^{3/2}} \,. \tag{4.26}$$

The system of equations (4.21-4.23) is the starting point for a discussion of a wide range of phenomena related to the interplay of OR and the electro-optic effect in a travelling wave structure. Due to the first derivative in z-direction only forward propagating waves are considered. Separate evolution equations could be derived for the backward propagating wave using eq. (B.17) in Appendix B. The resulting evolution equation for the microwave is similar to eq. (4.12) apart from changing signs in front of the z-derivative and the nonlinearity.

However, the excitation of a backward travelling microwave due to a forward propagating optical wave is almost negligible [36].

The excitation terms of the microwave are given by the first derivative of the optical power distribution. The phase of the optical wave hence has no influence on the evolution of the microwave. This is somewhat in contrast to second harmonic generation, where both fundamental and second harmonic are described by an envelope function with an underlying modulation frequency and therefore the phase influences the evolution considerably. Whereas the sole action of the TE mode can act as a source for the microwave, the action of the effective nonlinearity eq. (4.25) requires the presence of both TE and TM mode. In the following both scenarios are referred to as the single polarisation and mixed polarisation case, respectively. Under absence of an optical field eq. (4.21) has the form of the Korteweg de Vries equation, which will be discussed more in detail in Chapter 5. It is convenient to express the amplitude of the microwave in terms of voltage rather then in terms of power. Therefore in most of the following calculations we give the electrical signal in voltage as $V_{\mathrm{mic}}(z,t) = U_{\mathrm{mic}}(z,t)\sqrt{Z_0}$.

It should be noted that the coplanar structure in Fig. 4.1(a) supports always two modes. However, setting both ground electrodes to the same potential suppresses the asymmetric mode and the assumption of a single mode microwave guide is justified. Provided the structures in Fig. 4.1(a) and (b) are symmetric with respect to the x-z-plane, for the given growth direction of the fcc lattice χ_{eff2} is zero for the coplanar line whereas χ_{eff1} is zero for the stripline. We hence can treat both cases separately.

The action of the microwave on the TE optical mode due to the electro-optic effect is mainly described by the term proportional to $\omega_{\mathrm{opt}}\chi_{\mathrm{eff1}}$. This term affects only the phase of the optical wave but does not give rise to an energy exchange. Similarly, the TE and TM modes are coupled to each other by an electric field via the nonlinearity χ_{eff2}. Energy conservation is ensured by the time derivative of the remaining nonlinear term. This implies a high conversion of optical energy into microwave energy for very short pulses. Neglecting losses in all waves, it can be easily shown that the system conserves energy,

$$\frac{\partial}{\partial z}\int_{-\infty}^{\infty}\left(U_{\mathrm{mic}}^2 + |U_{\mathrm{TE}}|^2 + |U_{\mathrm{TM}}|^2\right)\,dt = 0\,. \tag{4.27}$$

We should compare the evolution equation for the microwave eq. (4.21) with eq. (3.5) in Chapter 3. Eq. (3.5) can be rewritten as,

$$\left(\frac{\partial}{\partial z} - \frac{1}{v_{\mathrm{mic}}}\frac{\partial}{\partial t}\right)\left(\frac{\partial}{\partial z} + \frac{1}{v_{\mathrm{mic}}}\frac{\partial}{\partial t}\right)V = L'\frac{\partial^2 Q}{\partial t^2}\,. \tag{4.28}$$

Assuming the excitation to be a small perturbation, in first order we can approximate for a forward propagating wave $\partial_z \cong -1/v_{\mathrm{mic}}\,\partial_t$ giving,

$$\left(\frac{\partial}{\partial z} + \frac{1}{v_{\mathrm{mic}}}\frac{\partial}{\partial t}\right)V = -2Z_0\frac{\partial Q}{\partial t}\,. \tag{4.29}$$

Neglecting losses, dispersion and microwave self-interaction, eq. (4.29) has essentially the same structure as eq. (4.21). As was shown in Chapter 3, bidirectional wave propagation and different boundary conditions have an influence on the small static part of the solution for the generated microwave only. Here we concentrate on the dynamically evolving signals on the transmission line, which do not depend on the boundary conditions applied. In what follows we assume the voltage at $z = 0$ to be fixed. In most cases it is set to zero at the input facet, which can be achieved by a short circuit between the electrodes. The optical wave is assumed to enter the waveguide without reflection at the input facet. Further, backreflections of both optical wave and microwave at the output are neglected.

Equations (4.21-4.23) are a system of partial differential equations (PDE's). In particular in this Chapter main emphasis is laid on analytical solutions which give insight into the physics. However, the complete set of equations can be solved numerically by means of standard methods, for example a Crank Nicholson scheme or a split step procedure. A discussion of both methods can be found, for example, in [38].

4.3 Characterisation of Travelling Wave Structure

Before discussing eqs. (4.21-4.23) in detail, we will elaborate more on the properties of the structures shown in Fig. 4.4. This provides a basis for a quantitative estimation of relevant parameters and gives hence an indication of physical magnitudes one should expect in an experiment. Sections 4.3.1 and 4.3.2 are devoted to the calculation of both optical and microwave modes. The field profiles allow the calculation of the effective nonlinearities eq. (4.24-4.26) considered in Section 4.3.3. Section 4.3.4 discusses losses and dispersion of both optical and microwave mode. As indicated in the last Chapter, the velocity mismatch between optical and microwave is a crucial parameter for the interaction between both fields. In Section 4.3.5 we will briefly discuss how the velocity of the microwave can be tuned to obtain velocity matching or a defined mismatch between both waves.

4.3.1 Optical Waveguide

For the numerical computation of modes in dielectric waveguides, a number of suitable techniques are available. Methods which have been used in the past are, for example, finite differences [39, 40], finite elements [41] or mode matching [42, 43]. A recent review is given in [44]. In this work, the finite difference method has been chosen because of its flexibility and easy implementation.

The basic principle is the numerical solution of the wave equation by expressing the transverse spatial derivatives with finite differences. This procedure leads to an eigenvalue problem which can then be solved by suitable techniques. Here the eigenvalue provides the propagation constant whereas the transverse field profiles of the optical mode are obtained

from the corresponding eigensolution.

There are a number of different possibilities for the formulation of the finite difference scheme. For example, the transverse or longitudinal electric or magnetic fields can be used in the formulation [44]. The scheme implemented here is similar to the one in [39, 45] and uses the transverse electric fields with meshpoints lying between the boundaries of the different dielectrics. We assume the dielectric waveguide to consist of a linear, isotropic, charge free and non-magnetic material. Maxwell's equation in frequency domain then read as,

$$\nabla \times \tilde{\mathbf{E}} = \mathrm{i}\omega\mu_0\tilde{\mathbf{H}} \,, \tag{4.30}$$

$$\nabla \times \tilde{\mathbf{H}} = -\mathrm{i}\omega\varepsilon_0\varepsilon_r\tilde{\mathbf{E}} \,, \tag{4.31}$$

where the notation follows the one in Section 4.2. The dielectric constant $\varepsilon_r(x, y)$ is a function of the transverse directions x and y only. Taking the curl of eq. (4.30) and introducing eq. (4.31) we obtain,

$$\nabla \times \nabla \times \tilde{\mathbf{E}} - \frac{\omega^2}{c^2}\varepsilon_r\tilde{\mathbf{E}} = 0 \,, \tag{4.32}$$

where $c = 1/\sqrt{\varepsilon_0\mu_0}$ is the velocity of light in free space. Using the vector identity $\nabla\times\nabla\times\tilde{\mathbf{E}} = -\nabla^2\tilde{\mathbf{E}} + \nabla(\nabla\cdot\tilde{\mathbf{E}})$, we can derive the vector wave equation,

$$\nabla^2\tilde{\mathbf{E}} - \nabla(\nabla\cdot\tilde{\mathbf{E}}) + \frac{\omega^2}{c^2}\varepsilon_r\tilde{\mathbf{E}} = 0 \,. \tag{4.33}$$

The longitudinal component $\tilde{E}_z$ can be removed from the first two components of (4.33) by rewriting the term $\nabla\cdot\tilde{\mathbf{E}}$ using Gauss's law,

$$\begin{aligned} & \nabla\cdot\mathbf{D} = 0 \,, \\ \Rightarrow \quad & \nabla\cdot(\varepsilon_0\varepsilon_r\tilde{\mathbf{E}}) = \varepsilon_0(\tilde{\mathbf{E}}\cdot\nabla\varepsilon_r + \varepsilon_r\nabla\cdot\tilde{\mathbf{E}}) = 0 \,, \\ \Rightarrow \quad & \nabla\cdot\tilde{\mathbf{E}} = -\frac{1}{\varepsilon_r}\tilde{\mathbf{E}}\cdot\nabla\varepsilon_r \,. \end{aligned} \tag{4.34}$$

With this substitution, one overcomes also the problem of spurious modes [46] being unphysical solutions for which the divergence relation is not fulfilled. The reformulated equation now reads as,

$$\nabla^2\tilde{\mathbf{E}} + \nabla[\varepsilon_r^{-1}\tilde{\mathbf{E}}\cdot\nabla\varepsilon_r] + \frac{\omega^2}{c^2}\varepsilon_r\tilde{\mathbf{E}} = 0 \,. \tag{4.35}$$

The z-dependence of all field vectors can be written as $e^{\mathrm{i}\beta z}$. Replacing the z-derivatives of the fields with $\mathrm{i}\beta$ and bearing in mind that ε_r does not change in longitudinal direction, the transverse components of the electric field are described by,

$$\nabla_t^2\tilde{\mathbf{E}}^t + \nabla_t[\varepsilon_r^{-1}\tilde{\mathbf{E}}^t\cdot\nabla_t\,\varepsilon_r] + \frac{\omega^2}{c^2}\varepsilon_r\tilde{\mathbf{E}}^t - \beta^2\tilde{\mathbf{E}}^t = 0 \,, \tag{4.36}$$

where $\nabla_t = [\partial_x, \partial_y]^{\mathrm{T}}$ and $\tilde{\mathbf{E}}^t = [\tilde{E}_x, \tilde{E}_y]^{\mathrm{T}}$. To obtain the finite difference form of eq. (4.36) the transverse plane of the waveguide is discretized and the derivatives are expressed by finite

differences. This procedure leads to the eigenvalue problem,

$$\mathbf{A} \cdot \tilde{\mathbf{E}}_D^t - \beta^2 \tilde{\mathbf{E}}_D^t = \begin{bmatrix} \mathbf{A}_{xx}\, \mathbf{A}_{xy} \\ \mathbf{A}_{yx}\, \mathbf{A}_{yy} \end{bmatrix} \cdot \begin{bmatrix} \tilde{\mathbf{E}}_D^x \\ \tilde{\mathbf{E}}_D^y \end{bmatrix} - \beta^2 \begin{bmatrix} \tilde{\mathbf{E}}_D^x \\ \tilde{\mathbf{E}}_D^y \end{bmatrix} = 0\,. \tag{4.37}$$

The full set of equations and the discretisation scheme used is discussed in Appendix C. The vectors $\tilde{\mathbf{E}}_D^x$ and $\tilde{\mathbf{E}}_D^y$ represent the discrete set of field components $\tilde{E}_x$ and $\tilde{E}_y$ at the respective meshpoints. The submatrix $\mathbf{A}_{xx}$ contains the coefficients which link the neighboring $\tilde{E}_x$-values, analogously the submatrix $\mathbf{A}_{yy}$ links the $\tilde{E}_y$-values. $\tilde{E}_x$ and $\tilde{E}_y$ are coupled only at plane dielectric interfaces by the elements of $\mathbf{A}_{xy}$ and $\mathbf{A}_{yx}$. If both matrices $\mathbf{A}_{xy}$ and $\mathbf{A}_{yx}$ are neglected, the equations reduce to a scalar finite difference scheme with fields in only one direction similar to the one considered in [47].

Modelling of dielectric wave guide structures requires the restriction to a finite computational domain. In order not to perturb the field profile the computation domain has to be chosen large enough so that the fields at the boundaries are negligible. The fields at the boundaries or their derivatives can then be set to zero. For symmetric waveguides the computing and storage requirements can be reduced by introduction of electric and magnetic walls at lines of symmetry. The corresponding boundary condition for an electric wall are,

$$\partial_\perp D_\perp = 0\,,\ \tilde{E}_{||} = 0\,, \tag{4.38}$$

and for a magnetic wall,

$$\partial_\perp \tilde{E}_{||} = 0\,,\ \tilde{E}_\perp = 0\,, \tag{4.39}$$

where $\partial_\perp$ is the derivative normal to the surface and $\tilde{E}_{||}(D_{||})$ and $\tilde{E}_\perp$ is the electric field (displacement) parallel and perpendicular to the wall, respectively. All cases are easily implemented by a special treatment of points near the boundary.

According to the required discretisation of the waveguide the matrix $\mathbf{A}$ is large but sparsely populated. Direct solvers are consequently not suited for the calculation of the eigenvalue β^2 and the eigenvector. The solution scheme is therefore based on a Gauss-Seidel iterative solver in conjunction with a Rayleigh quotient formula [48]. The convergence of the Gauss-Seidel scheme can be accelerated by application of successive overrelaxation [48]. In the implemented code the waveguide is first solved scalar by neglecting the matrices $\mathbf{A}_{xy}$ and $\mathbf{A}_{yx}$ respectively. The scalar calculated TE or TM-mode is then used as an initial guess in the full vectorial scheme.

To validate the method, the HE_{00} mode of a ridge waveguide with large refractive index step was calculated at a wavelength $\lambda = 1.55\,\mu$m (shown in Fig. 4.2). The waveguide has been analyzed by several authors using different methods [40]. The calculated HE_{00} and EH_{00} modes are shown in Fig. 4.3 and 4.4 respectively. Tab. 4.1 lists the effective indices $n_{\text{eff}} = \beta/\beta_0 = \beta\lambda/2\pi$ of the HE_{00} mode for different discretisations and computation windows. As the first decimal digits of the effective index are not significant in a comparison, the

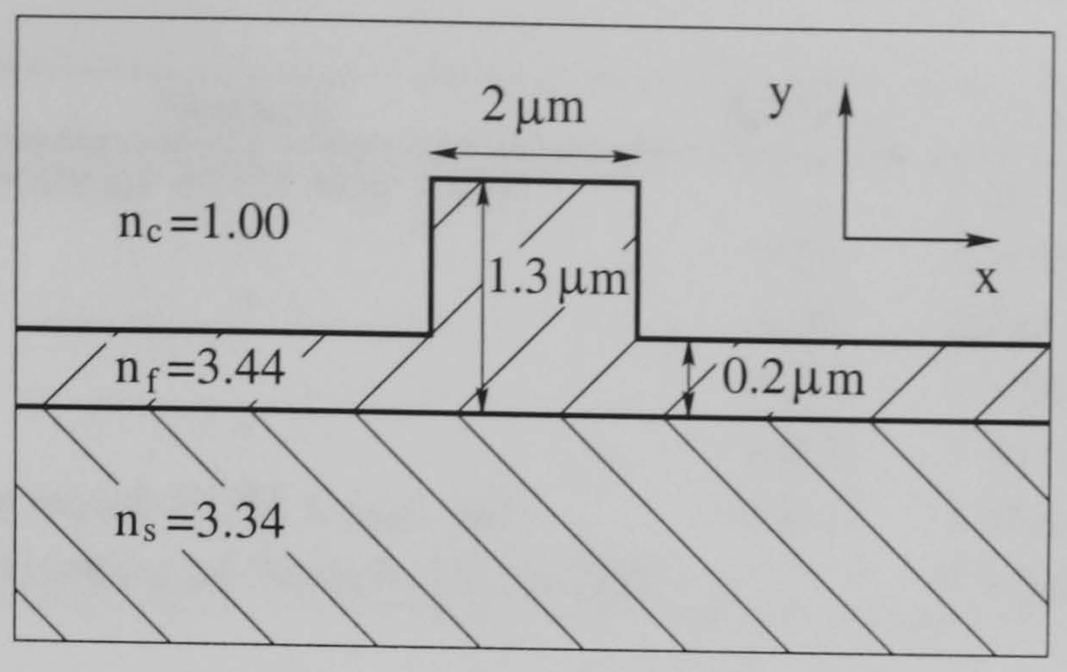

Figure 4.2: Cross-section of the test rib waveguide with large refractive index step.

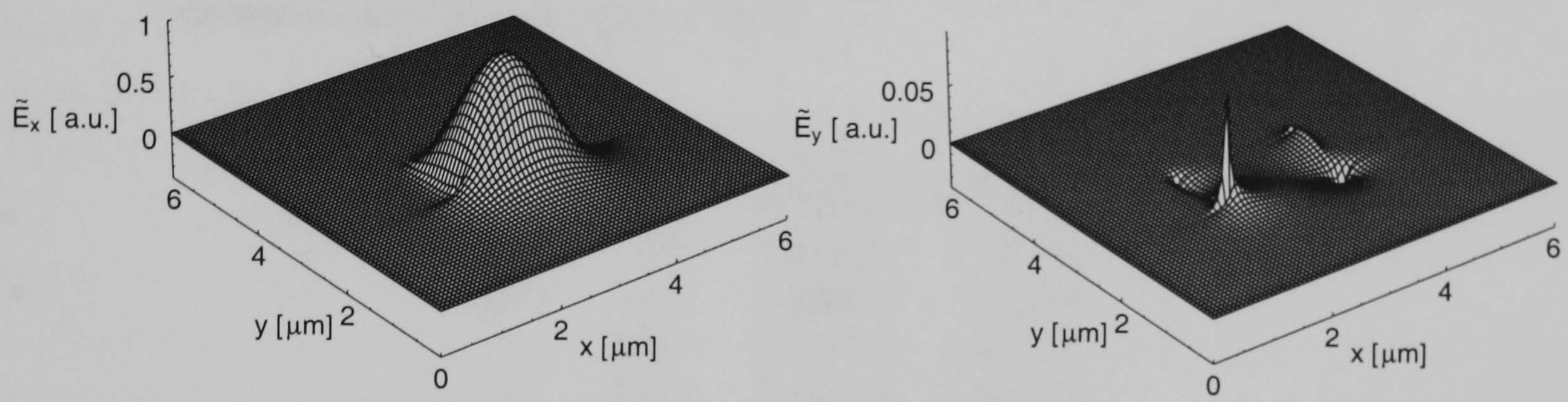

Figure 4.3: Transverse electric fields of the HE_{00} mode of the test waveguide depicted in Fig. 4.2.

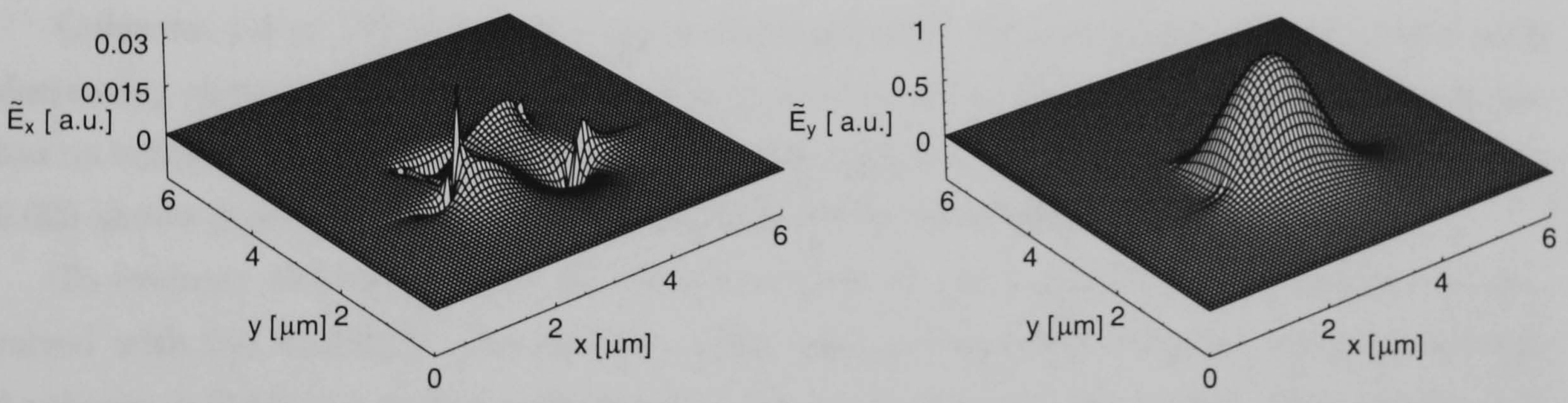

Figure 4.4: Transverse electric fields of the EH_{00} mode of the test waveguide depicted in Fig. 4.2.

normalized propagation constant $B = (n_{\mathrm{eff}}^2 - n_{\mathrm{f}}^2)/(n_{\mathrm{s}}^2 - n_{\mathrm{f}}^2)$ is also given. n_{s} and n_{f} are the effective indices of the substrate and the core layer, respectively (see Fig. 4.2). The calculated values are compared with [40], where a non-uniform finite difference scheme based on transverse magnetic fields was used. Further the effective index calculated in [49] with a mode matching technique including special functions for the treatment of edge singularities is given.

	Method	$\Delta x/\mu$m	β/β_0	B
1	vectorial FDM this work	0.1	3.389461	0.490925
2(a)	"	0.05	3.388894	0.485252
2(b)	"	0.05	3.388894	0.485252
3	"	0.033	3.388784	0.484153
4	"	0.025	3.388745	0.483769
6	vectorial FDM Lüsse [40]	0.013	3.388687	0.483185
7	mode matching technique Rozzi [49]	-	3.388690	0.483215

Table 4.1: Effective index $n_{\text{eff}} = \beta/\beta_0$ and normalized propagation constant $B = (n_{\text{eff}}^2 - n_{\text{f}}^2)/(n_{\text{s}}^2 - n_{\text{f}}^2)$ of the HE_{00} mode for the test rib waveguide computed with different discretisations $\Delta x = \Delta y$. The matrix is solved with a Gauss Seidel iterative scheme. Columns 1, 2(a), 3, and 4 are calculated with a computation window $8\mu\text{m} \times 8\mu\text{m}$, column 2(b) is calculated with an area $16\mu\text{m} \times 16\mu\text{m}$.

	$\Delta x/\mu$m	β/β_0	B
1	0.1	3.389461	0.490924
2(a)	0.05	3.388894	0.485251
2(b)	0.05	3.388894	0.485252
3	0.033	3.388784	0.484156
4	0.025	3.388746	0.483775

Table 4.2: Effective index of the HE_{00} mode for the test rib waveguide computed with ARPACK which uses an implicitly restarted Arnoldi method. The columns correspond to the first 5 cases in Tab. 4.1.

Columns 1-4 of Table 4.1 show good convergence of the calculated effective index with decreasing meshsize. Columns 2(a) and 2(b) indicate that the computation window chosen has no influence on the result. The effective index calculated with a discretisation of $\Delta x/\mu\text{m} = 0.025$ shows good agreement with values obtained by Lüsse [40] and Rozzi [49].

To evaluate the influence of the iterative solver on the final result, the matrix was also solved with the ARPACK package [50], which uses an implicitly restarted Arnoldi method. As shown in Table 4.2, there is very good agreement between both schemes. This implies that the main error is due to discretisation, i.e. replacing the differential equations by difference equations.

4.3.2 Microwave Transmission Line

The derivation of the evolution equation for the microwave is based on an expansion around zero frequency. The transverse electric field of the microwave mode in the stationary limit $\omega \to 0$ is then given by the TEM field distribution of the static problem [51]. In this limit, the microwave fields can be calculated by solving Laplaces equation with a finite difference

scheme [52]. After solving for the potential, the respective transverse fields can be calculated and transmission line parameters, e.g. the impedance Z_0 and the effective microwave index n_{mic}, can be extracted.

In the static limit, the electric field is curl-free and can be written in terms of a scalar potential Φ as,

$$\mathbf{E} = -\nabla\Phi \,. \tag{4.40}$$

Application of Gauss law and the assumption of a charge free region gives the Laplace equation,

$$\nabla \cdot (\varepsilon \nabla\Phi) = 0 \,. \tag{4.41}$$

To solve for the transverse potential of a microwave transmission line, the potential at the electrodes of the transmission line is fixed, i.e. the potential is kept constant Φ=V at the center conductor and set to zero Φ=0 at the ground electrodes (see Fig. 4.5). Discretisation of eq. (4.41), i.e. expressing the derivatives by finite differences, leads to a system of linear equations which can be solved by a Gauss Seidel scheme similar to the one used in Section 4.3.1. The discretisation scheme and the full set of equations can be found in [52] and will not reproduced here.

Once the potential is solved for, the electric field and the displacement vector $\mathbf{D} = \varepsilon\mathbf{E}$ can be calculated from eq. (4.40). As already discussed in Chapter 3, the impedance of the transmission line Z_0 and the effective index n_{mic} can be expressed by a capacitance C' and inductance L' per unit length as,

$$Z_0 = \sqrt{\frac{L'}{C'}} \,, \quad n_{\text{mic}} = c\,\sqrt{L'C'} \,. \tag{4.42}$$

The charge Q' per unit length on the guiding strip and hence the capacitance $C' = Q'/V$ is obtained by integrating the normal component of $\mathbf{D}$ on an integration path around the strip,

$$Q' = \oint\limits_{\text{strip}} \mathbf{D}\cdot\mathbf{n}\,ds \,, \tag{4.43}$$

where $\mathbf{n}$ is a unit vector normal to the integration path s. Z_0 and n_{mic} are calculated in two steps. First, the capacitance C'_0 is calculated for a structure with all dielectrics removed. As for this case the effective refractive index is $n_{\text{mic}} = 1$ and the inductance of a transmission line on a non-magnetic substrate does not depend on the dielectric constant ε_r, L' can be obtained from eq. (4.42). In a second step the charge C' on the actual transmission line is calculated. The effective microwave index is then given by,

$$n_{\text{mic}} = \sqrt{\frac{C'}{C'_0}} \,. \tag{4.44}$$

Similarly, the impedance of the line amounts to,

$$Z_0 = \frac{1}{c}\sqrt{\frac{1}{C'C'_0}} \,. \tag{4.45}$$

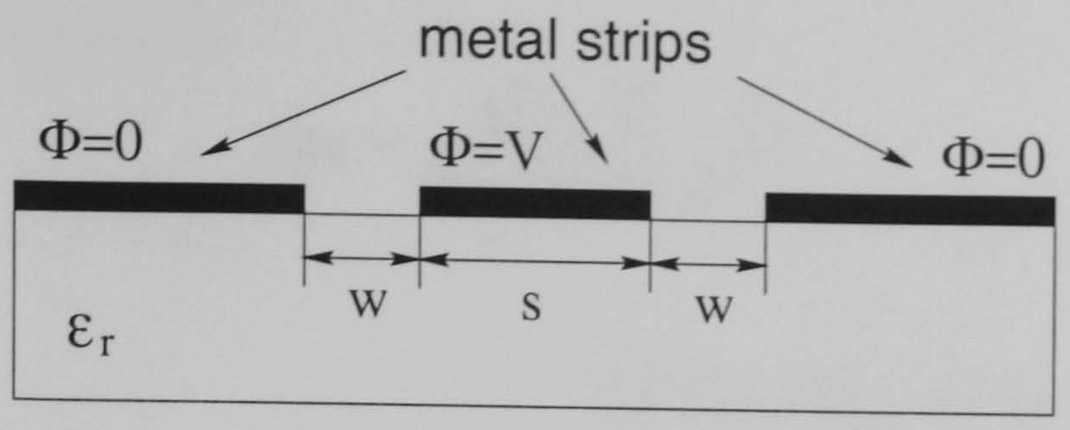

Figure 4.5: Cross-sectional view of coplanar waveguide.

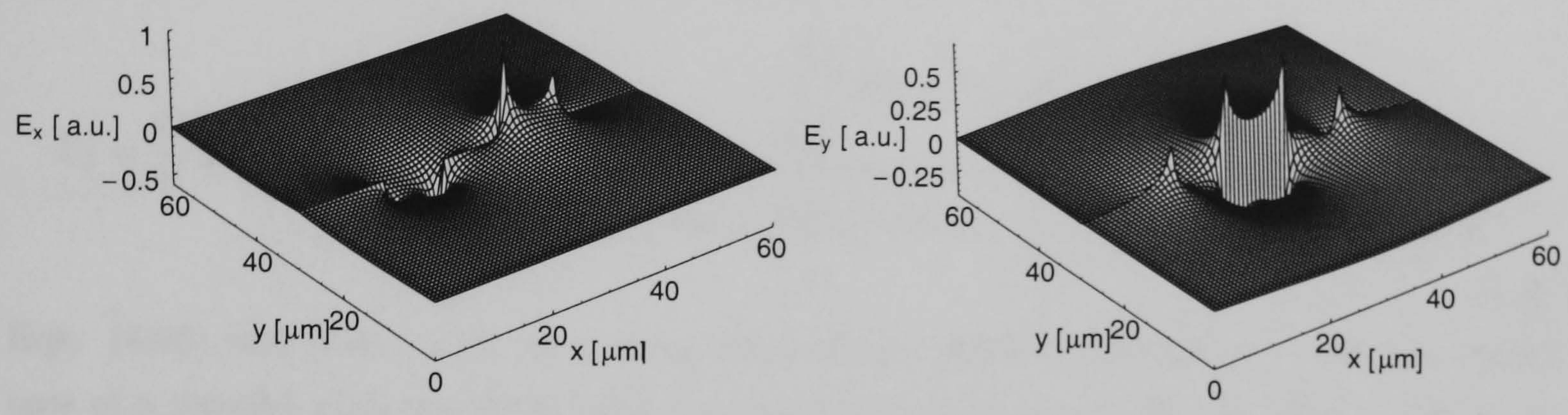

Figure 4.6: Transverse electric fields of the coplanar waveguide depicted in Fig 4.5 ($\varepsilon_r = 12.9, w = s = 10\ \mu$m, infinitely thin perfect conductors are assumed).

As an example, Fig. 4.6 shows the field profile of the fundamental even mode of the coplanar waveguide depicted in Fig. 4.5. The calculated effective index of $n_{\text{mic}} = 2.6363$ is in very good agreement with a value $n_{\text{mic}} = 2.6363$ obtained by a semiempirical formula after [53] (see also Appendix E).

4.3.3 Overlap Integrals

The efficiency of the nonlinear coupling between optical wave and microwave is characterised by the effective nonlinearities defined in Section 4.2. Having introduced schemes for the calculation of the transverse field profiles in the two previous Sections, we can now analyze the dependence of the corresponding overlap integrals on the parameters of the coupled waveguide. Also in this Section, some comments will be made about the effective nonlinearity eq. (4.26) which leads to a nonlinear self-interaction of the microwave.

Overlap between Optical and Microwave Component

For a discussion of the effective nonlinearities representing the coupling between optical and microwave it is convenient to rewrite eqs. (4.24, 4.25). Following the notation used in the literature on electro-optic modulators [54], χ_{eff1} and χ_{eff2} are reformulated as,

$$\chi_{\text{eff1}} = \frac{\chi^{(2)}\sqrt{Z_0}}{2c\, n_{\text{TE}}}\,\frac{\Gamma_1}{G}\,, \tag{4.46}$$

and,

$$\chi_{\text{eff2}} = \frac{\chi^{(2)}\sqrt{Z_0}}{2c\sqrt{n_{\text{TE}}n_{\text{TM}}}}\,\frac{\Gamma_2}{G}\,, \tag{4.47}$$

where we defined,

$$\Gamma_1 = \frac{G}{V}\,I_1\,, \quad \text{with} \quad I_1 = \frac{\iint\limits_{A_{\text{NL}}} E_{\text{mic}x}E_{\text{TE}x}^2\,dx\,dy}{\iint \left[E_{\text{TE}x}^2 + E_{\text{TE}y}^2\right]\,dx\,dy}\,, \tag{4.48}$$

and,

$$\Gamma_2 = \frac{G}{V}\,I_2\,, \quad \text{with} \quad I_2 = \frac{\iint\limits_{A_{\text{NL}}} E_{\text{mic}y}E_{\text{TE}x}E_{\text{TM}y}\,dx\,dy}{\sqrt{\iint \left[E_{\text{TE}x}^2 + E_{\text{TE}y}^2\right]\,dx\,dy}\cdot\sqrt{\iint \left[E_{\text{TM}x}^2 + E_{\text{TM}y}^2\right]\,dx\,dy}}\,. \tag{4.49}$$

Eqs. (4.46) and (4.47) refer to a comparison of the effective nonlinearity with the simple case of a parallel plate capacitor with uniform field distributions. The correction factors for a structure with nonuniform fields are then given by the overlap integrals Γ_1 and Γ_2. Here we introduced the interelectrode gap G, which is defined as the spacing between signal and ground electrodes. V refers to the difference between the potentials applied at the respective electrodes when calculating the microwave mode field $E_{\text{mic}}(x, y)$ (see Section 4.3.2). For a given nonlinearity one tries to optimize the factor $\Gamma_{1,2}/G$. This suggests that G and hence the structures should be as small as possible. However, as will be discussed below, microwave losses increase considerably with decreasing electrode size, so that the structures cannot be made arbitrarily small.

Figs. 4.7-4.9 show the results of calculations of overlap integrals and effective nonlinearities. The transverse field of the respective modes are computed with the methods introduced in the previous Sections. Subsequently, the overlaps are calculated by integrating over the area A_{NL} where a nonlinear polarisation is present. All calculations are based on the example structures described in Appendix F, the dimensions are defined in Fig. F.1. We assume the optical waveguide, i.e. substrate and dimensions of the rib, to be fixed and restrict ourselves to a discussion of the electrode structures. For the CPS structure, the interelectrode gap G can easily be defined as the spacing between the conducting strips $G = 2s + w_1$. In case of a CPW structure with a center strip located on top of the rib, we approximate $G = s + (w_1 - w_2)/2$ and hence neglect its height. For the structure shown in the inset of Fig. 4.8, i.e. with a center electrode covering the rib, G is similarly defined as for the CPS structure. In all Figures circles and crosses refer to calculated values whereas the dashed lines correspond to a spline interpolation.

Fig. 4.7 shows the dependence of the effective nonlinearity and the overlap integral of the CPW structure on the spacing between ground electrode and signal electrodes, here located

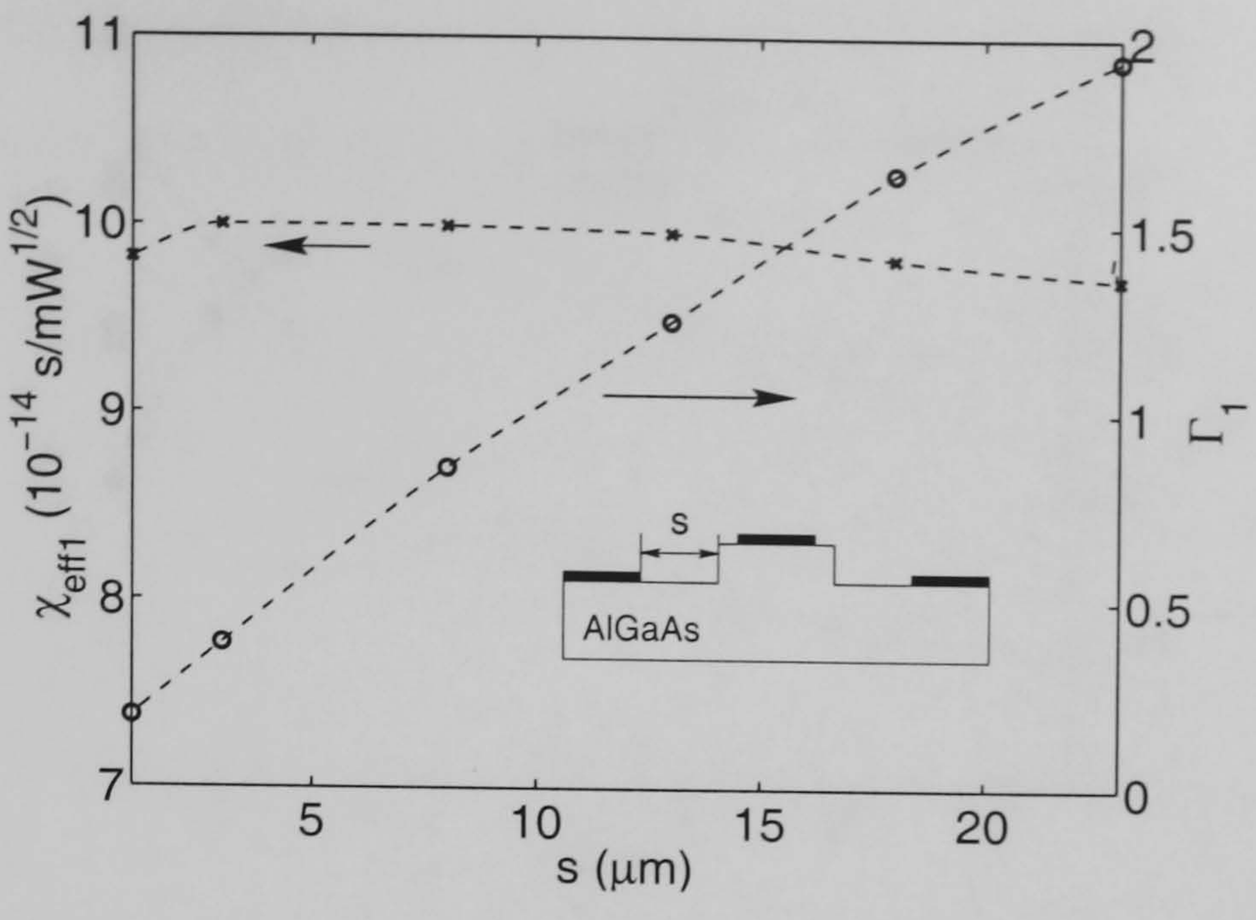

Figure 4.7: Effective nonlinearity and overlap integral of CPW structure vs. electrode spacing s (all other parameters as in Appendix F). The interelectrode gap is defined as $G = s + (w_1 - w_2)/2$.

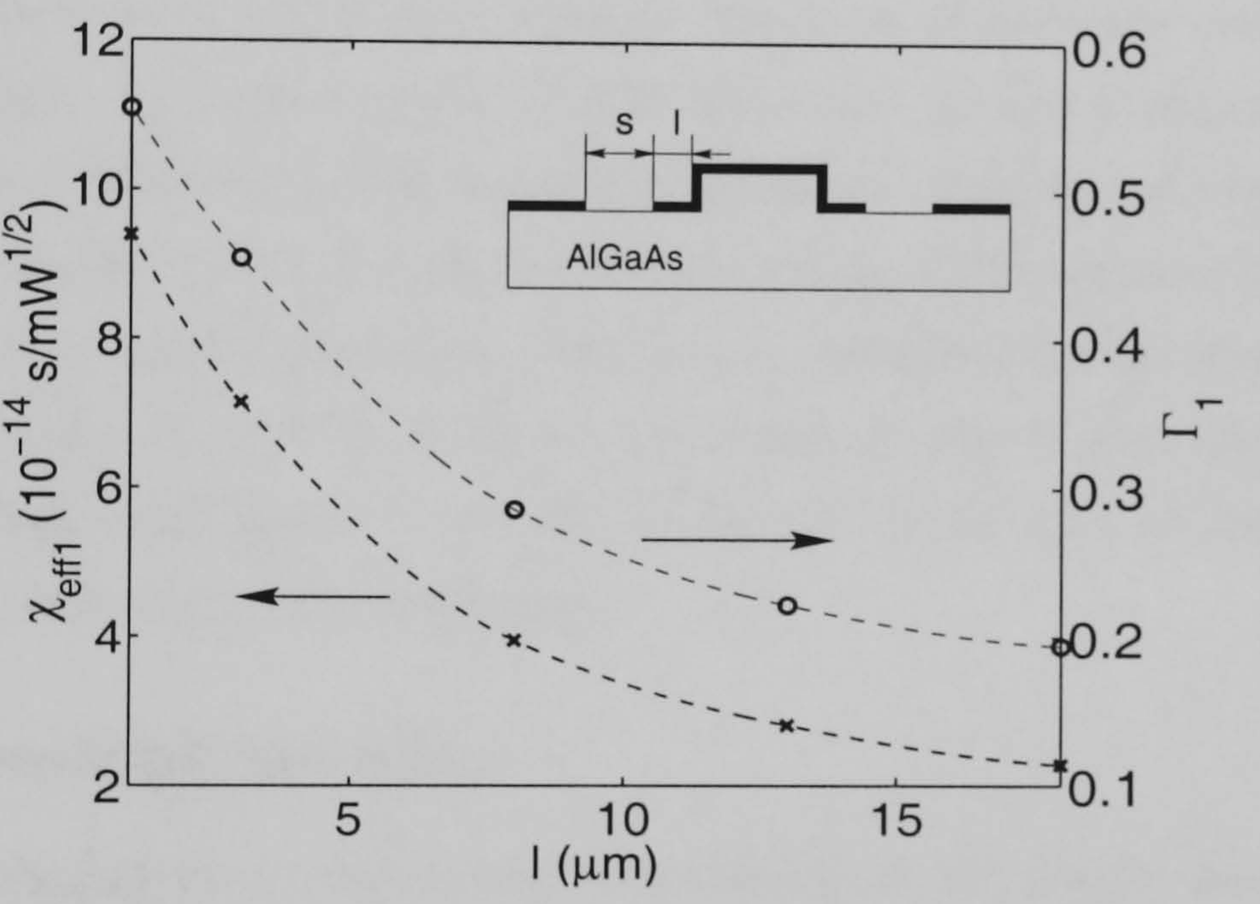

Figure 4.8: Effective nonlinearity and overlap integral of CPW structure vs. width of center electrode covering the rib and adjacent area ($s = 5\,\mu$m, all other parameters as in Appendix F). The interelectrode gap is defined as $G = s$.

on the rib. In the range of parameters considered here, for a constant width of the center electrode the effective nonlinearity depends only marginally on the gap between signal and ground electrodes. However, as shown in Fig. 4.8, the overlap between both fields drops off rapidly for a larger width of the center electrode. As the electric field of the microwave mode is mainly located in the gap between center and ground electrode, both overlap and effective nonlinearity decrease for a broader center strip. This represents the main problem in this configuration: a high nonlinearity requires a small center conductor which in return introduces higher losses.

The influence on the spacing between both electrodes in a CPS structure is shown in Fig. 4.9. For a symmetric configuration, the overlaps between both fields do not vary considerably

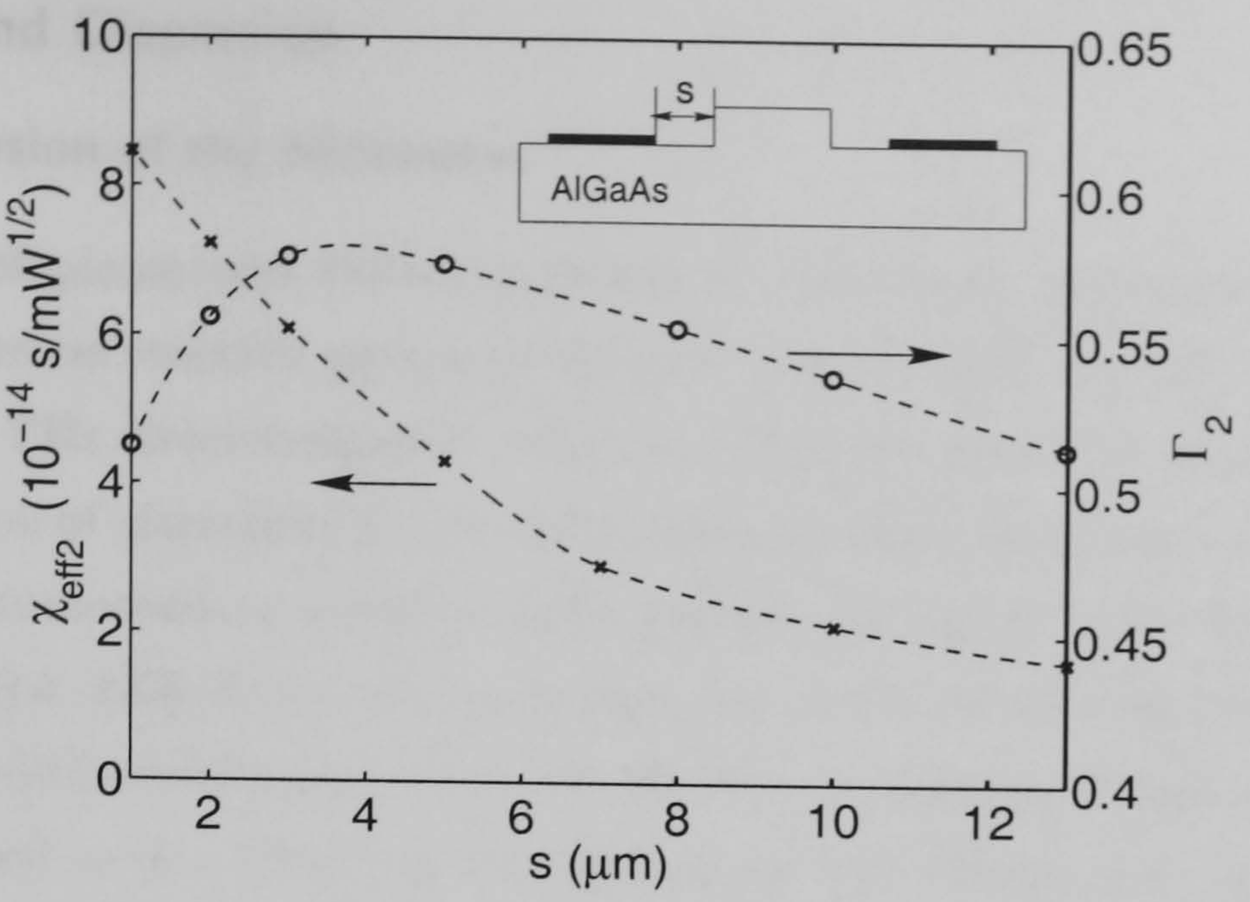

Figure 4.9: Effective nonlinearity and overlap integral for CPS structure vs. electrode spacing (all other parameters as in Appendix F).

when the gap between both electrodes changes. Thus, as G becomes smaller, the effective nonlinearity increases. As in the case of a CPW structure, a narrow electrode configuration is necessary for a high efficiency of the respective structure. Further calculations showed that the width of the strip has only a marginal influence on the effective nonlinearities.

For highly efficient optical-microwave interaction, small electrode dimensions are hence necessary. Whereas for the CPW structure the width of the center conductor should be similar to the modesize and hence to the size of the rib, in the case of the CPS structure a small gap between both strip lines is essential.

Overlap for Microwave Self-Interaction

In eq. (4.21) we included also a microwave self-interaction term with an effective nonlinear coefficient χ_{eff3}. For the given crystal orientation, the interaction of both E_x and E_y field components is required for a nonlinear self-interaction of the microwave signal. From symmetry consideration follows further that the effective nonlinearity for the CPS structure is zero. Calculations showed that the magnitude of χ_{eff3} can be comparable to those of the effective nonlinearities of χ_{eff1} or χ_{eff2}. As an example, for the CPW structure in Appendix F it amounts to $\chi_{\text{eff3}} = 1.5 \times 10^{-14}\text{s/mW}^{1/2}$. However, as will be shown later, the conversion efficiency in OR is small so that the power of the optical wave is magnitudes larger then the power of the generated microwave. As a result, the microwave self-interaction term in eq. (4.21) is small in comparison to the optical excitation term and can usually be neglected. Nevertheless, we will discuss the presence of this term for the case of microwave propagation without interaction with an optical field in Chapter 5.

4.3.4 Losses and Dispersion

Losses and Dispersion of the Microwave

The propagation of picosecond electrical pulses on microwave transmission lines has been addressed by numerous research groups in the past (for a review, see [27]). In comparison to freely propagating THz electromagnetic radiation, there are a number of problems associated with the propagation of ultrashort pulses on lithographically defined planar transmission lines. In particular for picosecond or subpicosecond pulses, the signals were found to be severely distorted within a few millimeters of propagation due to frequency-dependent losses and high dispersion at submillimeter frequencies [3, 55, 56, 57]. As these problems are essential for the structures considered in this thesis, in this Section we will discuss their origins and mention some approaches which have been made in the past to circumvent them.

To give an impression of the evolution of both losses and dispersion in the frequency domain, a coplanar waveguide on a GaAs substrate was modeled using approximate formulas from the literature [3, 51, 57]. We assume the signal to propagate as,

$$V(f,z) = V(f,0)\,\exp\{[\mathrm{i}\beta_0(f)\,n_{\mathrm{mic}}(f) - \alpha(f)]z\}\,, \tag{4.50}$$

where $V(f,z)$ is the Fourier transform of the voltage on the transmission line at frequency f and distance z. $\alpha(f)$ are frequency dependent losses, whereas $\beta_0(f) = 2\pi f/c$ and $n_{\mathrm{mic}}(f)$ denote the propagation constant in free space and the effective microwave index, respectively. The formulas used can be found in Appendix E. A similar analysis for CPS structures was experimentally shown to give reasonable results even at very high frequencies [3]. As both CPW and CPS lines behave similarly, those results are not reproduced here.

The main sources for loss in a transmission line are radiation loss, metallic losses and dielectric loss. It was shown by Grischkowsky *et al.* that radiation loss can be interpreted in terms of electromagnetic shockwaves similar to Cherenkov radiation [58, 59]. Cherenkov radiation describes the radiation of electromagnetic waves from electrons which move faster than the phase velocity of electromagnetic waves in the material. Interestingly, it was shown by Auston and Kleinmann [9, 60] in the context of OR that the propagation of dipoles leads to a similar radiation. As the microwave index of the transmission lines considered here is a mixture between the indices of substrate and superstrate [51], the propagation of electrical pulses can be interpreted as travelling dipoles moving with a velocity greater than the phase velocity of electromagnetic waves in the substrate. As a consequence, the pulse radiates a considerable amount of energy into the substrate. In a good approximation, the corresponding loss scales as $\sim f^3$ [61]. It was later shown by Frankel *et al.* [57] that this dependence is altered at high frequencies due to the frequency dependence of the effective microwave index.

Metallic losses are due to the finite conductivity of the metal electrodes. As a result, the strips absorb real power proportional to the real part of a surface impedance as the microwave

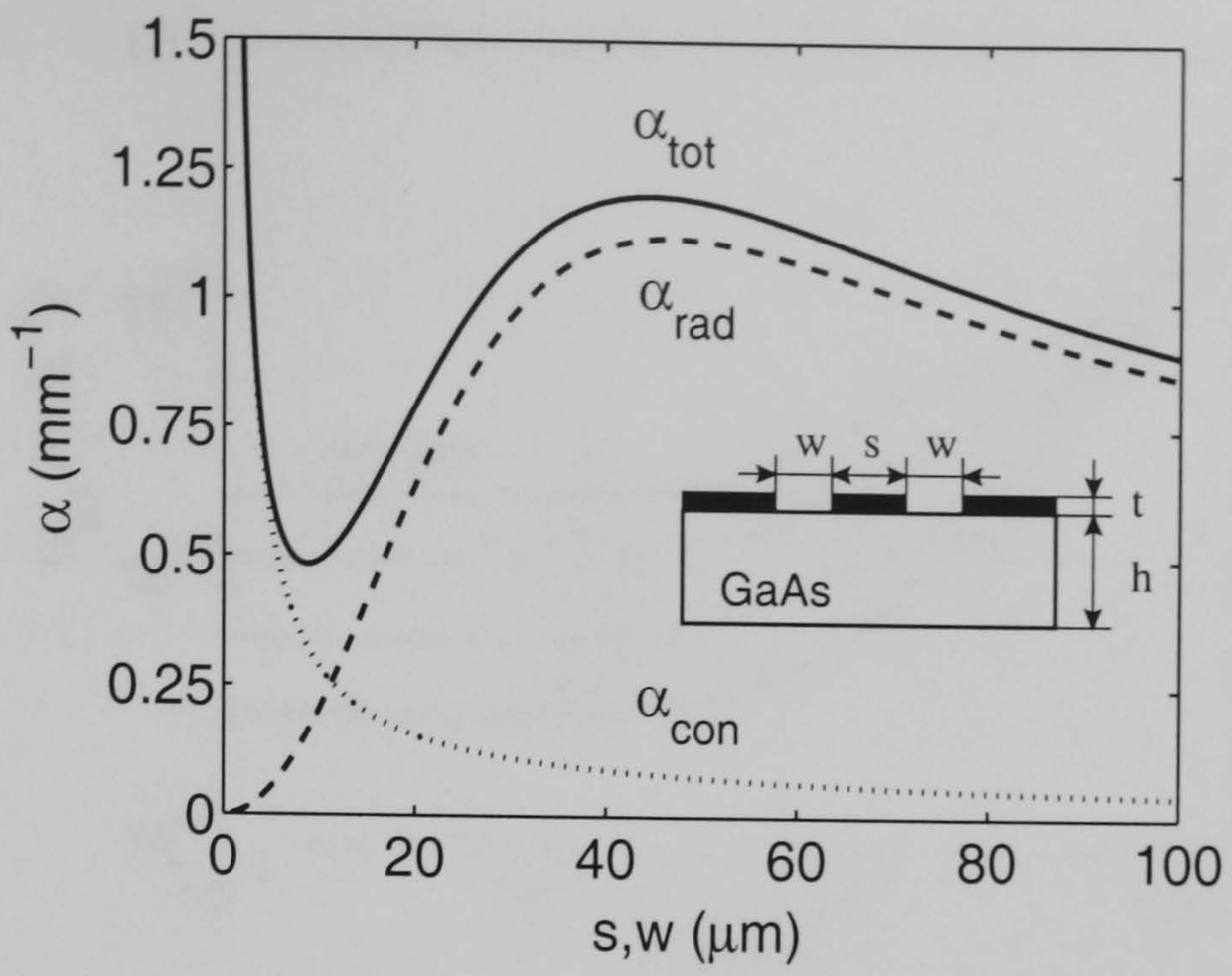

Figure 4.10: Contributions of conductor loss α_{con} and radiation loss α_{rad} to the total loss α_{tot} vs. conductor width w and spacing s for CPW line at f=500 GHz ($\varepsilon_r = 12.9$, $h = 500\,\mu\mathrm{m}$, $t = 0.5\,\mu\mathrm{m}$, gold electrodes $\sigma = 4.5 \times 10^{-7}\,\Omega^{-1}\mathrm{m}^{-1}$, $w = s$).

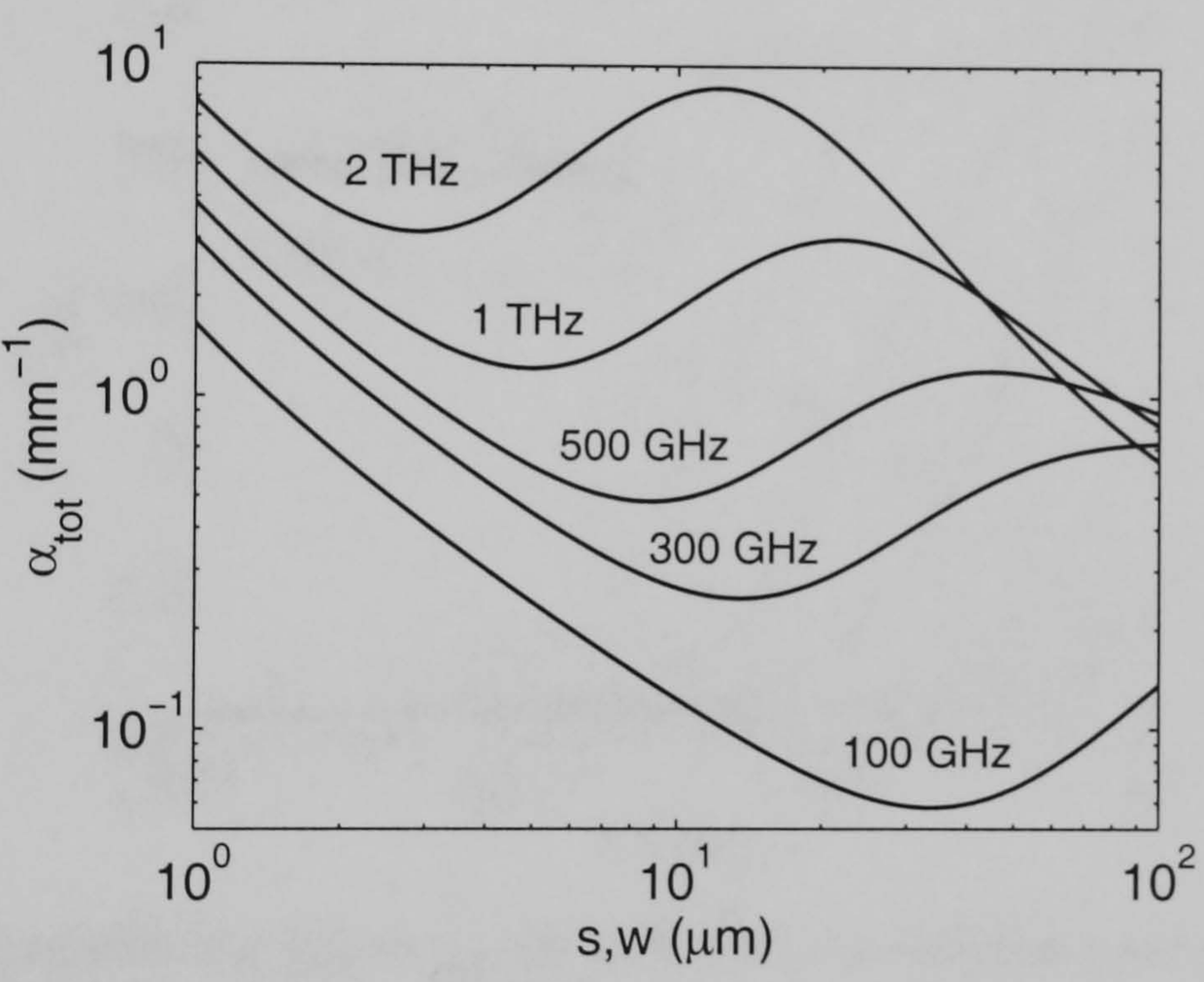

Figure 4.11: Total loss α_{tot} of CPW line vs. conductor width w and spacing s (w=s) for different frequencies, all other parameters as in Fig. 4.10.

mode travels along the transmission line [51]. Additionally, the imaginary part of the surface impedance influences the phase of the microwave leading to dispersion of the propagating pulse. The surface impedance and hence metallic losses scale approximately as $\sim f^{1/2}$ [61].

Fig. 4.10 shows the contributions of conductor loss and radiation loss to the total loss in a CPW line vs. the dimensions of the transmission lines at a fixed frequency. Whereas for structures with moderate size the absorption is dominated by radiation loss, metallic losses increase significantly as the dimensions of the strip lines become smaller. This leads to an optimum size for the corresponding geometry. However, as shown in Fig. 4.11, this optimum

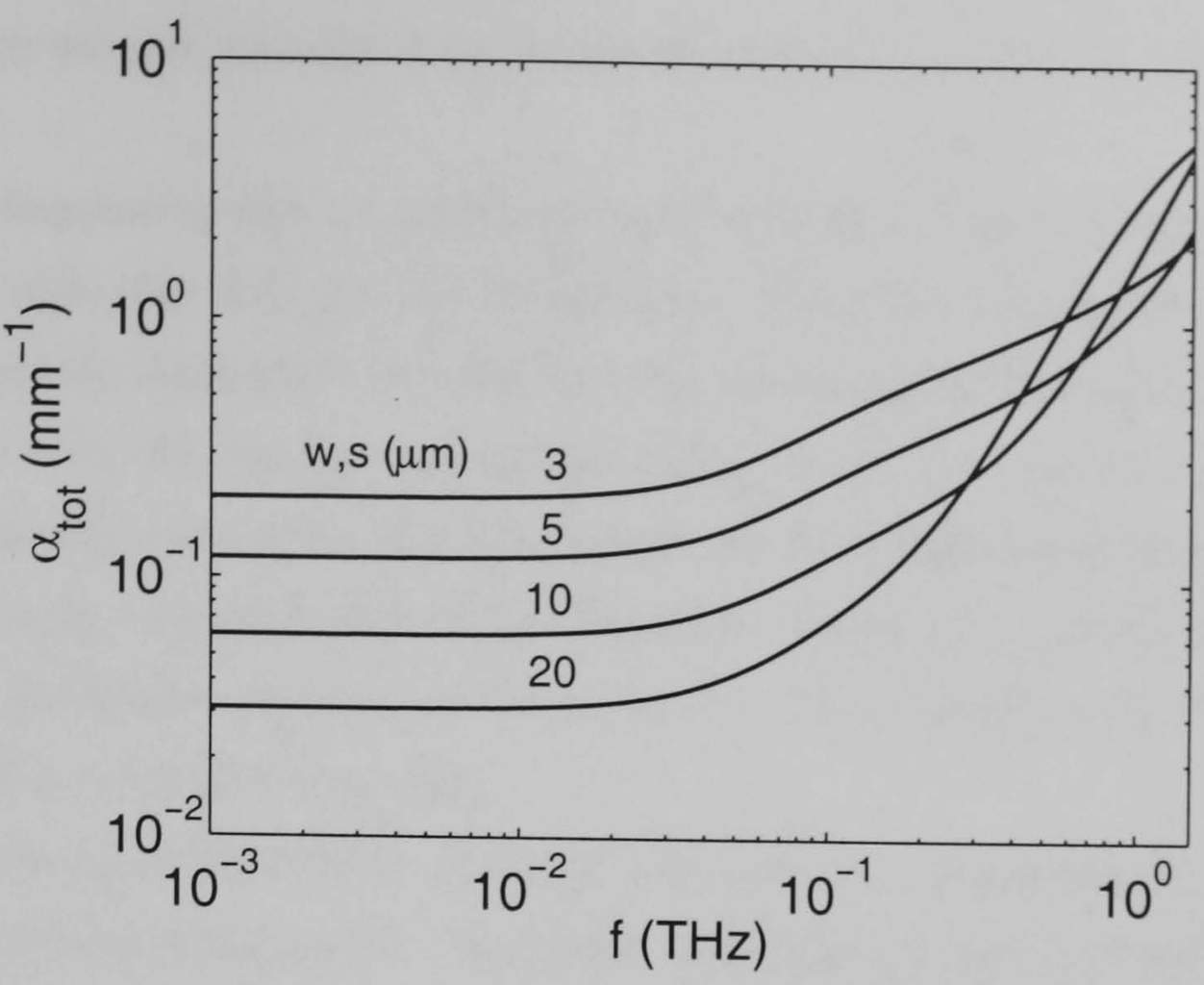

Figure 4.12: Total loss $\alpha_{\rm tot}$ of CPW line vs. frequency for different line parameters, all other parameters as in Fig. 4.10.

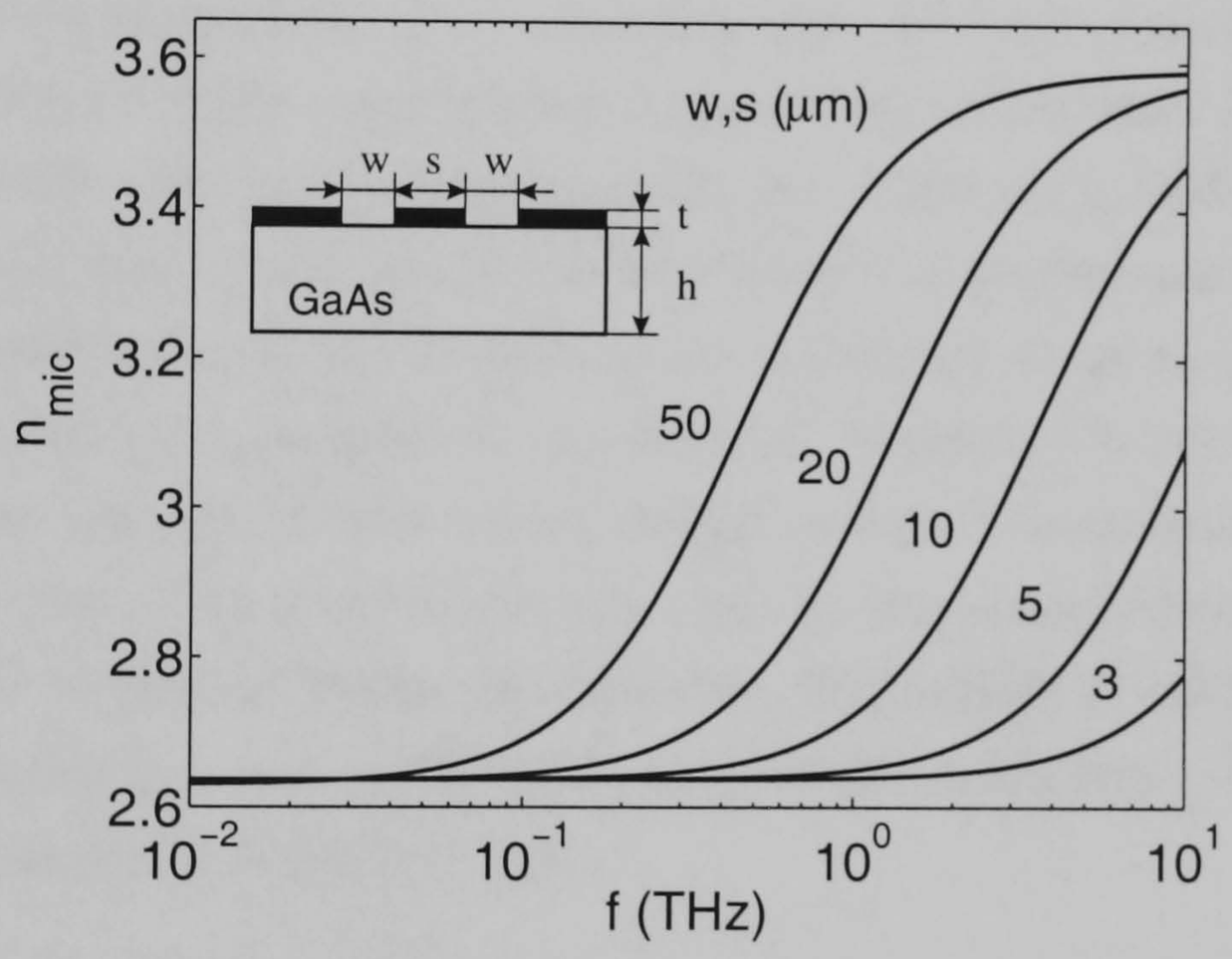

Figure 4.13: Calculated effective index $n_{\rm mic}$ for a CPW line on a GaAs substrate for different line parameters s and w ($\varepsilon_r = 12.9$, $h = 500\,\mu$m, $w = s$, $t = 0$), only mode dispersion is taken into account (after [53]).

point shifts considerably with the frequency under consideration. In general, as shown in Fig. 4.12, losses increase dramatically in the frequency range corresponding to picosecond and subpicosecond pulses.

Not included in Figs. 4.10-4.12 are dielectric losses. In particular near dielectric resonances, both loss and dispersion can strongly influence the propagation of short pulses [62]. In GaAs, the dielectric constant has a TO phonon resonance around 8.0 THz [63]. As will be shown in subsequent Sections, optical pulses in the picosecond range generate electrical pulses in the frequency range around 1 THz. This implies that the main source of loss in

the frequency range we are interested in is due to the finite conductivity of electrodes and radiation losses.

In addition to dispersion due to the finite conductivity of metal strips, modal dispersion can play a considerable role [53]. At low frequencies the microwave mode corresponds to the TEM mode of the static limit with the effective microwave index having a value between that of the dielectric and air. As the wavelength becomes comparable to the line dimensions, the mode profile changes and hence the effective index. At very high frequencies, the electric field of the mode is strongly concentrated in the dielectric leading to an effective index equal to the corresponding dielectric constant of the substrate. This results in a S-shaped dispersion curve as shown in Fig 4.13 (see also [53]).

A number of attempts have been made in the past to circumvent the effects explained above (see [27] and references therein). Cherenkov radiation can be avoided by using transmission lines with no mismatch between the dielectric constants of the substrate and superstrate. As an example, coplanar air transmission lines where the underlying substrate is partially removed should be mentioned [3]. As discussed earlier, for very small structures metallic losses dominate. This led to the investigation of transmission lines based on superconductors with a high superconducting transition temperature like $YBa_2Cu_3O_x$ (YBCO) [64]. However, until now those transmission lines have not demonstrated superiority over conventional lines.

In conclusion, dispersion as well as losses in the microwave range can be considerable as one goes to millimeter and submillimeter wavelengths. Furthermore, all effects are strongly frequency dependent. In what follows we are mainly interested in analytical solutions of the system (4.21-4.23). This often requires the restriction to frequency-independent losses in the expansion eq. (4.9). As this is a strong simplification, in a number of calculated examples we will give solutions with first order attenuation as a variable parameter to give an indication of the influence of frequency-dependent losses.

Losses and Dispersion of Optical Wave

The sources for optical losses in the rib waveguide can in general be classified as losses due to absorption, scattering, and leakage [65]. In this work, we are interested in wavelengths much longer than the corresponding band edge of the material, i.e. ≈ 870 nm for GaAs. An important loss mechanism in this domain is free carrier absorption requiring a reduction of the residual carrier concentration in the material. Furthermore, losses due to the metallic electrodes on the structure, in particular in the TM mode, can play a considerable role. This can be overcome by a thin layer of low index material, e.g. SiO_2, between substrate and electrode. Scattering losses arise mainly from rough surfaces both between the epilayer substrates and the etched rib surfaces. Finally, when the guiding layers are grown on a substrate with a refractive index comparable to the core index, leakage of guided light into the substrate might occur.

For a rib waveguide shown in Fig. F.1 with gold electrodes of thickness 450 nm separated from the substrate by a 200 nm film SiO_2, typical losses are in the range of 2..4 dB/cm [66] for both TE and TM mode. In comparison to microwave losses in the corresponding transmission line, optical losses are therefore moderate. For this reason, in the following calculations attenuation of the optical mode in the waveguide will be neglected.

The dispersion in the optical waveguide is composed of material dispersion and mode dispersion. However, for a weakly guiding structure as shown in Fig. F.1, the dispersion is only slightly influenced by mode dispersion. The dispersion coefficients for both the TE and TM modes can be calculated with the techniques described in Section 4.3.1.

4.3.5 Structures for Tuning of Velocity Mismatch

In Chapter 3 first indications were given that a high conversion efficiency can be reached in the case of velocity matching between optical and microwave, leading potentially to a linear growth of the generated microwave signal. Velocity matching is also necessary for high frequency modulation of optical waves in travelling wave optical modulators. As will be shown in subsequent Sections, for some effects arising from the interaction between OR and the electro-optic effect it can further be desirable to have a well-defined mismatch between both waves. In general, it seems to be rather difficult to change the group velocity of the optical wave. However, for a tuning of the effective index of the microwave, techniques have been demonstrated in the past in the context of travelling wave optical modulators which will be reviewed in this Section.

The most common material systems for travelling wave electro-optic modulators are $LiNbO_3$ [67] and the AlGaAs system [68, 69]. For a structure based on $LiNbO_3$ operating at 1.5μm the effective microwave index for a strip line is around 4.2 whereas a typical effective index of the guided optical mode is 2.14 [70]. To match both velocities, fast wave structures have been designed and demonstrated in such a way that a significant part of the microwave field travels in a material with lower refractive index [67].

However, in this thesis we chose as an example the AlGaAs-system. Here, the microwave travels significantly faster than the optical wave. For the example structure given in Appendix F, the microwave index of the CPW structure amounts to $n_{\mathrm{mic}} = 2.4$ whereas the group index of the optical modes is around 3.42. This high mismatch is due to the fact that the microwave index for both CPS and CPW structures is approximately given by [51],

$$n_{\mathrm{mic}} = \sqrt{\frac{\varepsilon_{\mathrm{s}} + \varepsilon_{\mathrm{c}}}{2}}\,, \tag{4.51}$$

which corresponds to a mixture of the indices of both substrate ε_{s} and superstrate ε_{c}, respectively. To circumvent this high mismatch between both waves periodically loaded slow wave structures have been designed and fabricated for both CPW and CPS structures which allow a tuning of the microwave velocity in a wide range of parameters [25, 71].

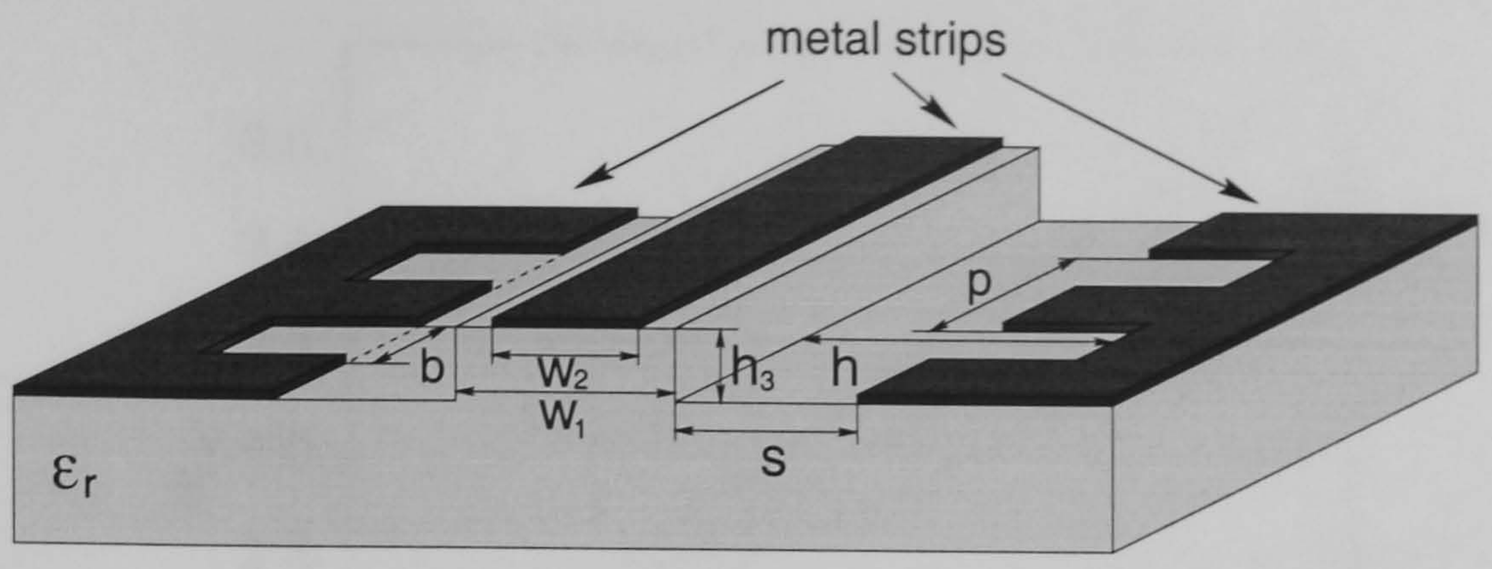

Figure 4.14: Schematic picture of a CPW slow wave structure with periodic slots cut into the ground electrodes.

A schematic picture demonstrating the basic principle is shown in Fig. 4.14. Here slots of width b and depth $(h-s)$ are cut periodically into the ground electrodes of a CPW structure. According to transmission line theory, the phase velocity of the microwave is given by,

$$v_{\mathrm{mic}} = \frac{1}{\sqrt{L'C'}} , \tag{4.52}$$

where L' and C' are the inductance and capacitance per length, respectively. The mode of action of slow-wave structures becomes clear when we consider narrow fins, i.e. the ratio b/p is near to 1 and $(h-s) \gg (p-b)$. Due to the presence of fins along the structure the capacitance per unit length is effectively increased. On the other hand, the inductance will only slightly be reduced in comparison to a transmission line without periodic loading resulting in an effective slowing of the microwave. If the structures are much smaller than the corresponding wavelength of the propagating microwave, the dispersion will only slightly increase due to the presence of a periodic grating in the electrodes. This suggests the possibility of tuning the microwave velocity up to frequencies into the hundreds of gigahertz for periods p and slot depths $(h-s)$ around 10 μm.

The propagation characteristics of a periodic microwave structure can be analyzed as follows (for details, see [71, 72]). In a first step, the S-parameter, relating incoming and reflected waves of a microwave two-port, of a unit cell of the periodic structure under consideration are determined by suitable, e.g. numerical, techniques. The S-matrix can be transformed in the transfer matrix, also called ABCD matrix, which relates the current I_{b} and voltage V_{b} at the beginning and the current I_{e} and voltage V_{e} at the end of a section,

$$\begin{bmatrix} V_{\mathrm{b}} \\ I_{\mathrm{b}} \end{bmatrix} = \begin{bmatrix} A\,B \\ C\,D \end{bmatrix} \cdot \begin{bmatrix} V_{\mathrm{e}} \\ I_{\mathrm{e}} \end{bmatrix} . \tag{4.53}$$

The matrix elements A, B, C, and D are in general frequency-dependent. Assuming an infinitely extended series of sections, the line is analyzed using Floquet's theorem. Given the length of a unit cell to be p, it states that a propagating mode after travelling the distance p changes only by a factor $e^{\gamma p}$. The voltages and currents at the beginning and the end of a

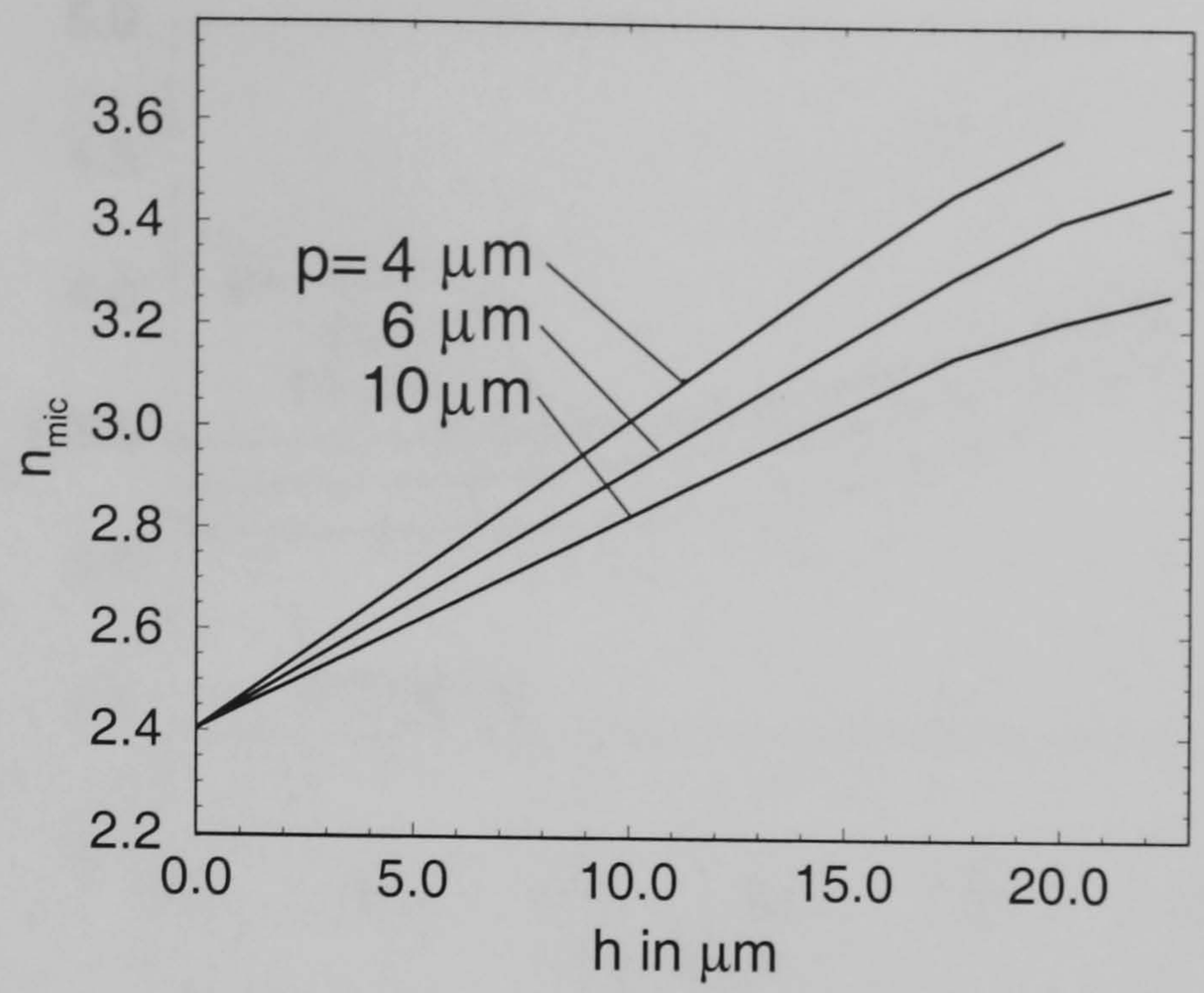

Figure 4.15: Effective index of slow-wave structure depicted in Fig. 4.14, the substrate corresponds to the example structure in Appendix F; $w_1 = 5\,\mu$m, $w_2 = 4\,\mu$m, $b = p/2$, $h_3 = 0.8\,\mu$m, $s = 3\,\mu$m, $f = 100$ GHz.

section are hence related as,

$$\begin{bmatrix} V_\mathrm{b} \\ I_\mathrm{b} \end{bmatrix} = e^{-\gamma p} \begin{bmatrix} V_\mathrm{e} \\ I_\mathrm{e} \end{bmatrix} , \tag{4.54}$$

where γ is composed of the phase constant β and damping constant α as $\gamma = -\alpha + \mathrm{i}\beta$. The combination of eqs. (4.53) and (4.54) leads to an eigenvalue problem which relates the complex propagation constant γ to the matrix parameters. A straightforward calculation gives,

$$\gamma = \frac{1}{p} \ln \left[\frac{A+D}{2} \pm \sqrt{\left(\frac{A+D}{2}\right)^2 - 1} \right] . \tag{4.55}$$

The impedance of the structure can be obtained similarly by relating the respective voltage and current of the eigensolution.

To give an example and an impression of the action of a grating for a CPW structure, the S-parameter of the structure shown in Fig. 4.14 were modeled with the commercial FDTD code EMLAB [73] (finite-difference time-domain, for a detailed treatment of the method, see [74]). In the simulation, the S-parameter were modeled with sections containing 4 grating periods and the propagation constant extracted according to eq. (4.55).

Fig. 4.15 shows the effective microwave index n_mic as a function of the grating depth h for different periods p. With increasing grating depth the microwave is efficiently slowed. The design goal, which is in our case an effective microwave index of $n_\mathrm{mic} = 3.4$, can be reached by application of small periods and a sufficiently high modulation depth. As indicated earlier, structures with dimensions comparable to the wavelength of the propagating microwave might have a large microwave dispersion. This is shown in Fig. 4.16, where the frequency dependence

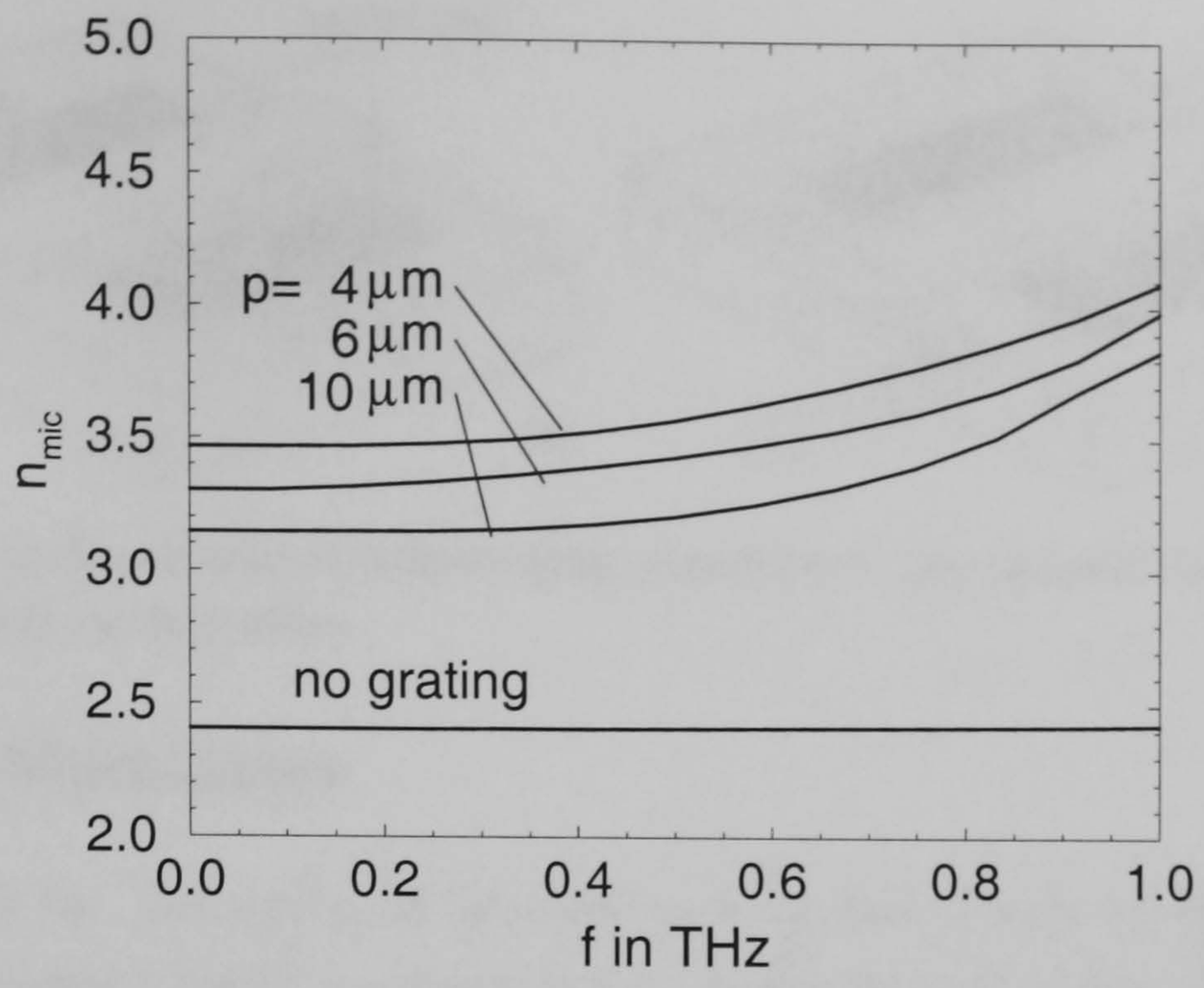

Figure 4.16: Effective index of slow-wave structure depicted in Fig. 4.14 vs. frequency for $h = 17.5\,\mu$m, all other parameters as in Fig. 4.15.

of the effective index is depicted for a grating with depth $h = 17.5\,\mu$m. Here, at frequencies higher than 500 GHz the dispersion is considerably larger than in structures without periodic modulation. It should be noted that in this calculations the electrodes are assumed to be infinitely thin perfect conductors. Losses due to electrodes with finite conductivity and the electrode thickness are not taken into account.

At this stage some comments shall be made about the parameters used for the calculations in the next Sections and Chapters, respectively. For the calculations two structures, the CPW and CPS structures shown in Fig. F.1, with the particular geometry given in Appendix F were chosen. For this geometry the optical parameters (effective index, group index, dispersion) and microwave parameters (effective index, impedance, dispersion) as well as the corresponding overlap integrals and hence effective nonlinearities were estimated with the methods discussed in the preceding Sections. If not stated otherwise, the calculations in the following Chapters use the values given in Tables F.1-F.3. In a number of calculations we assume the velocity of the microwave to be a variable parameter assuming the application of suitable, i.e. slow-wave, structures for tuning the microwave velocity. This might affect the microwave impedance and dispersion as well as overlap integrals. Furthermore, as stated earlier, a number of examples are calculated with first order, i.e. frequency-independent, microwave loss as a variable parameter to give an impression of the influence of higher order terms. The aim is first to discuss a variety of different effects and scenarios, and second to give an idea of physical magnitudes involved rather than modelling the structures in Appendix F rigorously.

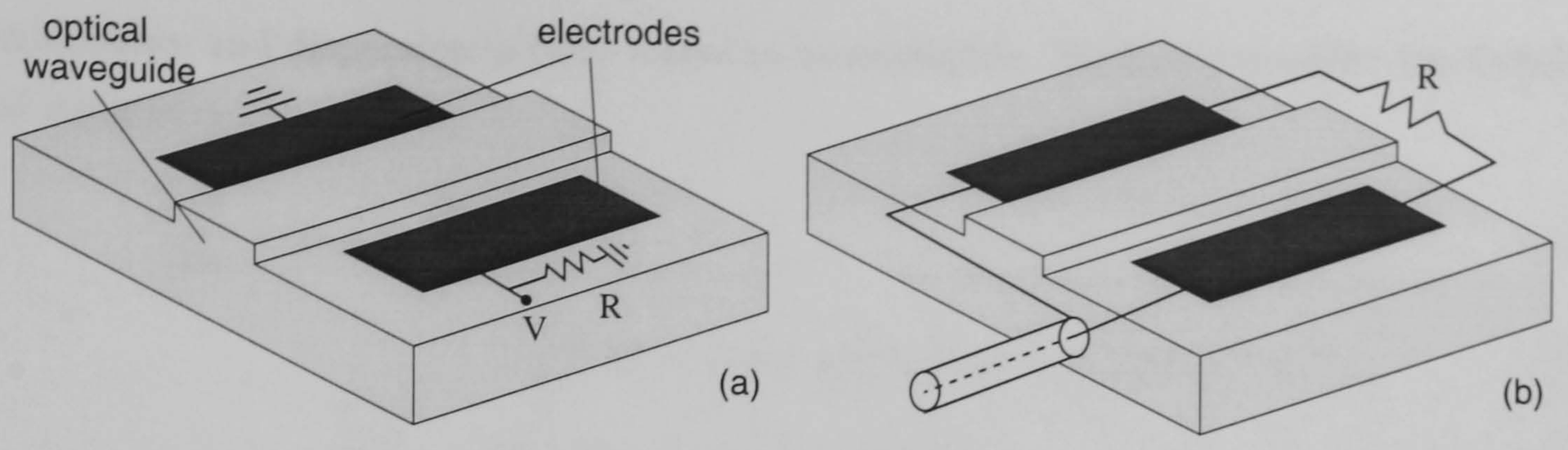

Figure 4.17: Basic configurations of electro-optic modulators: (a) lumped electrodes, (b) travelling wave configuration.

4.4 Optical Modulators

Before we consider the generation of microwaves from high power optical signals by OR, the action of an electrical signal on optical waves with moderate power via the electro-optic effect shall shortly be discussed. The aim here is first to demonstrate that the equations introduced in Section 4.2 describe also travelling wave electro-optic modulators. Furthermore, this Section provides the basis for an understanding of effects arising from the interplay of both optical rectification and electro-optic effect.

There are in general two types of electrode configurations in waveguide modulators, i.e. lumped electrodes and travelling wave configurations [26]. Both modulator types are sketched in Fig. 4.17. The achievable modulation bandwidth of lumped electrode modulators is limited by the time constant of the lumped circuit parameters, in particular electrode charging and decharging times of the capacitance resulting from the electrode configuration. The basic idea of a travelling wave configuration is the modulator as an extension of the microwave transmission line carrying the incoming electrical signal. Here the bandwidth should, at least in principle, only depend on the velocity mismatch between microwave and optical wave rather than by electrode charging times.

As indicated earlier, the structures sketched in Fig. 4.1 are essentially travelling wave electro-optic modulators. However, for the given orientation of the substrate, there are two different modes of action arising from the electro-optic effect. First, the sole action of the effective nonlinearity χ_{eff1} results in a phase change in the optical TE mode. This corresponds to an electrode configuration shown in Fig. 4.1(a) - a symmetric CPW structure. The CPS structure shown in Fig. 4.1(b) provides an effective nonlinearity χ_{eff2} acting on both the TE and TM modes. Here eqs. (4.22, 4.23) are coupled mode equations with a coupling factor depending on the applied voltage. Thus, the device acts as a mode converter.

4.4.1 Phase Modulators

For a low power optical wave the action of the nonlinearity on the microwave in eq. (4.21) can be neglected. For an analytical treatment, we assume further frequency-dependent losses in

the microwave and dispersion in both waves to be negligible. We hence consider the simplified set of equations,

$$\left[\frac{\partial}{\partial z} + \alpha_{\text{mic}} + \frac{\Delta n}{c}\frac{\partial}{\partial t}\right] U_{\text{mic}} = 0 \,, \tag{4.56}$$

$$\mathrm{i}\frac{\partial}{\partial z} U_{\text{TE}} = \chi_{\text{eff1}}\omega_{\text{opt}} U_{\text{TE}} U_{\text{mic}} + \chi_{\text{eff2}}\omega_{\text{opt}} U_{\text{TM}} U_{\text{mic}} \,, \tag{4.57}$$

$$\left[\mathrm{i}\frac{\partial}{\partial z} - \Delta\beta\right] U_{\text{TM}} = \chi_{\text{eff2}}\omega_{\text{opt}} U_{\text{TE}} U_{\text{mic}} \,. \tag{4.58}$$

The sole action of the nonlinearity χ_{eff1} leads to an electro-optically induced phase shift $\Delta\phi$ in the optical TE mode given by,

$$U_{\text{TE}}(z,t) = U_{\text{TE}}(0,t)e^{-\mathrm{i}\Delta\phi} \,, \quad \text{with} \quad \Delta\phi = \chi_{\text{eff1}}\omega_{\text{opt}} \int_0^L U_{\text{mic}}(z,t)dz \,, \tag{4.59}$$

where L is the length of the structure. Assuming the applied voltage to be constant, we can define a π-voltage for which the phase change of the optical wave is $\Delta\phi = \pi$ after a propagation length of $L = 1$ cm,

$$V_\pi = \frac{\pi}{\chi_{\text{eff1}}\omega_{\text{opt}} L\sqrt{Z_0}} \,. \tag{4.60}$$

For the example structure given in Appendix F, the corresponding voltage amounts to $V_\pi =$ 21 V. However, the actual aim of a travelling wave structure is a high modulation bandwidth. Let us therefore write the voltage along the electrodes as a travelling wave (which is a solution of eq. (4.56)),

$$U_{\text{mic}}(z,t) = U^0_{\text{mic}} e^{-\alpha_{\text{mic}} z} \cos\left[2\pi f_{\text{m}}\left(\frac{\Delta n}{c}z - t\right)\right] \,, \tag{4.61}$$

where f_{m} is the microwave frequency. The induced phase shift $\Delta\phi$ can then be calculated analytically,

$$\Delta\phi = \chi_{\text{eff1}}\omega_{\text{opt}} U^0_{\text{mic}} L \sqrt{\frac{(e^{-\alpha_{\text{mic}}L} - 1)^2 + 4e^{-\alpha_{\text{mic}}L}\sin^2(u)}{(\alpha_{\text{mic}}L)^2 + (2u)^2}} \sin(\Theta - 2\pi f_{\text{m}} t) \,, \tag{4.62}$$

where,

$$\Theta = \arctan\left(\frac{e^{-\alpha_{\text{mic}}L}\sin(2u)}{e^{-\alpha_{\text{mic}}L}\cos(2u) - 1}\right) - \arctan\left(\frac{\alpha_{\text{mic}}L}{2u}\right) \,, \tag{4.63}$$

and we defined,

$$u = \frac{\pi f_{\text{m}}}{f_0} \quad \text{, with} \quad f_0 = \frac{c}{L\Delta n} \,. \tag{4.64}$$

As eq. (4.62) is quite involved, it is convenient to discuss velocity mismatch and losses separately. To this aim we first ignore the effects of losses, i.e. $\alpha_{\text{mic}} = 0$. The induced phase shift reduces then to,

$$\Delta\phi = \chi_{\text{eff1}}\omega_{\text{opt}} U^0_{\text{mic}} L \frac{\sin(u)}{u} \cos(u - 2\pi f_{\text{m}} t) \,. \tag{4.65}$$

Thus, walk-off between microwave and optical wave leads to a decrease of the effective modulation depth corresponding to the $\sin(u)/u$ term. As a figure of merit, it is common to define an optical 3-dB bandwidth $\Delta f \approx 0.603 f_0$ which corresponds to the microwave frequency for which $\Delta\phi$ drops to half of its value at zero frequency.

Eq. (4.65) suggests that for perfect velocity mismatch the bandwidth is unlimited and a sufficiently long structure will lead to very small drive voltages. However, a lossy transmission line will finally lead to an attenuation of the travelling microwave. Assuming perfect velocity mismatch but including losses we obtain,

$$\Delta\phi = \chi_{\mathrm{eff1}}\omega_{\mathrm{opt}}U^0_{\mathrm{mic}}\frac{1-e^{-\alpha_{\mathrm{mic}}L}}{\alpha_{\mathrm{mic}}}\cos(2\pi f_{\mathrm{m}}t)\ . \tag{4.66}$$

Note that the presence of losses reduces the modulation depth. Keeping in mind that losses increase with increasing frequency (see also Section 4.3.4), it becomes clear that attenuation also limits the achievable bandwidth.

In a practical structure, phase modulators are usually integrated in devices like directional couplers or Mach-Zehnder interferometers to convert the induced phase shift into an intensity modulation. However, a further discussion is beyond the scope of this thesis and can be found in the literature [54, 26].

4.4.2 Mode Converters

For the CPS structure shown in Fig. 4.1(b), eqs. (4.57, 4.58) correspond to coupled-mode equations. This implies mode conversion from TE to TM and vice versa depending on the phase mismatch $\Delta\beta$ and the coupling factor $\chi_{\mathrm{eff2}}\omega_{\mathrm{opt}}$. For simplification, we assume a constant microwave signal U_{mic} along the transmission line. Both TE and TM polarisation in the waveguide then evolve as,

$$\begin{aligned} U_{\mathrm{TE}}(z,t) &= e^{-\mathrm{i}\Delta\beta z}\left[U_{\mathrm{TE}}(0,t)\cos(C_{\mathrm{I}}z) - \mathrm{i}\frac{2C_{\mathrm{II}}U_{\mathrm{TM}}(0,t)-\Delta\beta U_{\mathrm{TE}}(0,t)}{2C_{\mathrm{I}}}\sin(C_{\mathrm{I}}z)\right]\ , \\ U_{\mathrm{TM}}(z,t) &= e^{-\mathrm{i}\Delta\beta z}\left[U_{\mathrm{TM}}(0,t)\cos(C_{\mathrm{I}}z) - \mathrm{i}\frac{2C_{\mathrm{II}}U_{\mathrm{TE}}(0,t)+\Delta\beta U_{\mathrm{TM}}(0,t)}{2C_{\mathrm{I}}}\sin(C_{\mathrm{I}}z)\right]\ , \end{aligned} \tag{4.67}$$

where,

$$C_{\mathrm{I}} = \frac{\sqrt{(2C_{\mathrm{II}})^2+\Delta\beta^2}}{2}\ , \quad C_{\mathrm{II}} = \chi_{\mathrm{eff2}}\omega_{\mathrm{opt}}U_{\mathrm{mic}}\ . \tag{4.68}$$

For vanishing phase mismatch between both TE and TM modes, complete mode conversion occurs for a voltage,

$$V_{\mathrm{c}} = \frac{\pi}{2\chi_{\mathrm{eff2}}\omega_{\mathrm{opt}}L\sqrt{Z_0}}\ . \tag{4.69}$$

Note that the voltage V_{c} is half of the π-voltage of the corresponding phasemodulator given that the overlap integrals of both structures are equal. However, as shown in Fig. 4.18, the difference in phase velocities between both TE and TM mode leads to a rather complex conversion scenario shifting the required switching voltages to much higher values. This has been experimentally shown for example in [69].

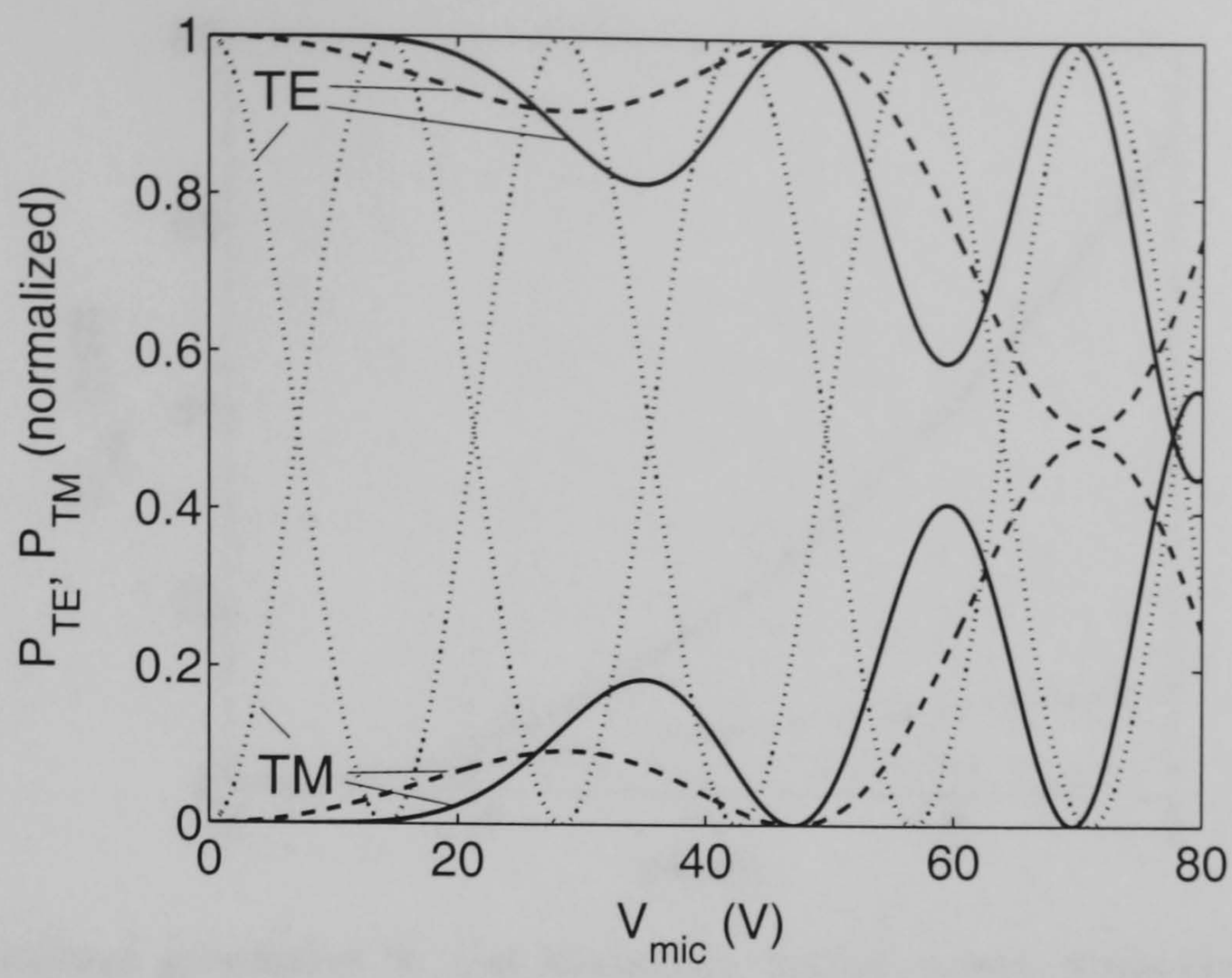

Figure 4.18: Conversion of power in TE mode P_{TE} into power of TM mode P_{TM} vs. applied voltage in the CPS structure shown in Fig. F.1 (b), solid and dotted line after propagation length $L = 1\,\mathrm{cm}$, dashed line propagation length $L = 2\,\mathrm{cm}$. All parameters as in Appendix F except dotted line without phase velocity mismatch $\Delta\beta = 0$.

4.5 Generation of Microwaves

We now turn or attention to the case of large optical power. Here the source terms in eq. (4.21) should lead to the generation of a microwave signal with considerable magnitude. For the time being we assume that the microwave is still small enough not to affect the optical pump wave. Further we neglect dispersion and frequency-independent losses. As a result, the optical wave is assumed to propagate without any changes and we have to deal with eq. (4.21) only. As will be shown, single polarisation case and mixed polarisation case can lead to very different effects depending on the phase velocity mismatch between TE and TM mode. We start the discussion with the single polarisation case, i.e. we concentrate on the case of a CPW structure where $\chi_{\mathrm{eff}2} = 0$.

4.5.1 Single Polarisation

Two Optical Frequencies

Within the approximation that the microwave at the beginning of the line is zero, there is no real power conversion for an optical CW input wave. Therefore, as a first example, we consider the simple nonstationary case of an optical input wave with two frequency components of equal amplitude which are slightly detuned from the midfrequency as $\omega_{\mathrm{opt}} \pm \Delta\omega$. The optical source term can then be written as,

$$U_{\mathrm{TE}}(z,t) = U_{\mathrm{o}} \cos(\Delta\omega t)\,, \tag{4.70}$$

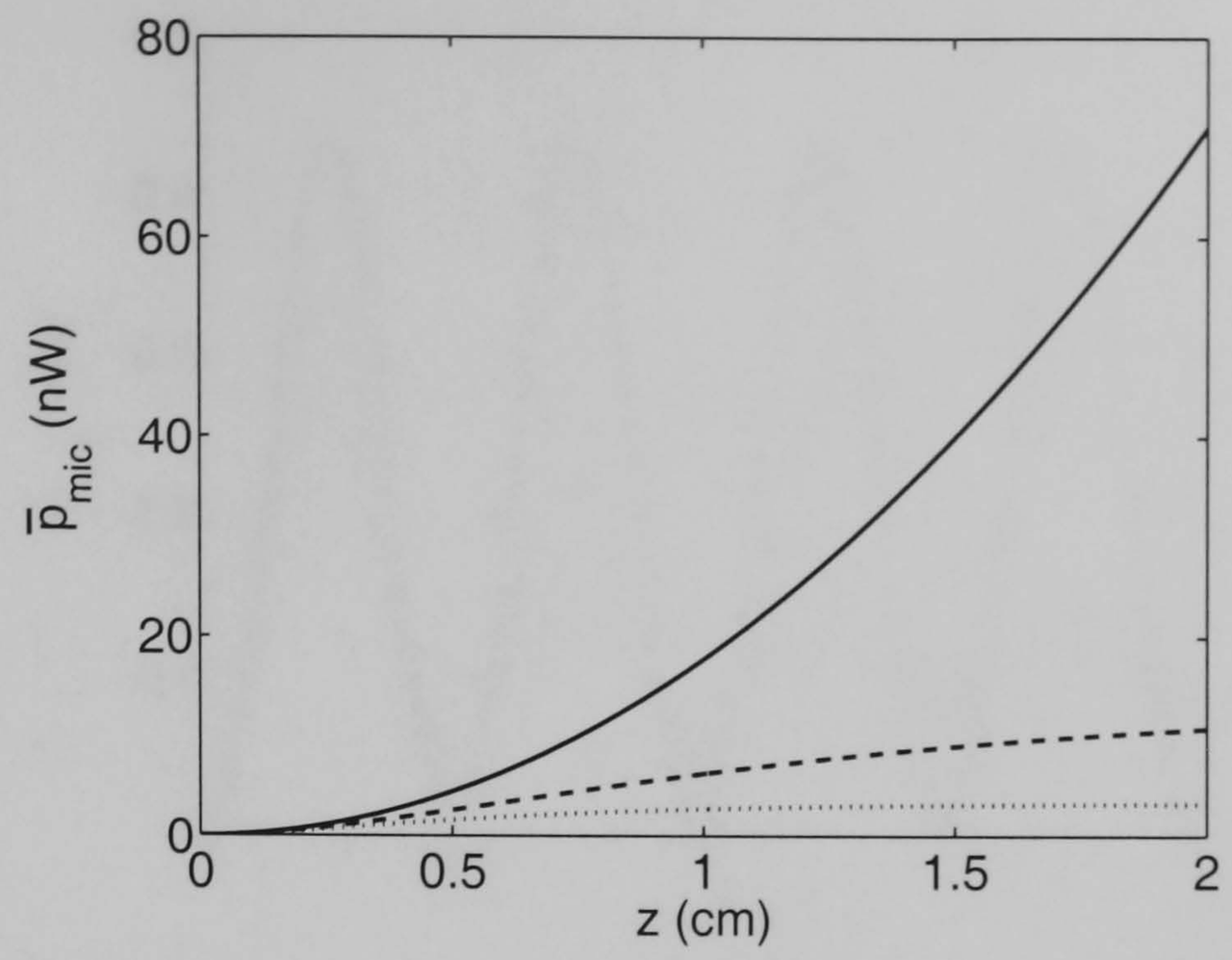

Figure 4.19: Microwave generation by two interacting optical waves, dispersion and frequency-dependent losses neglected, velocity matched case ($\Delta n = 0$); solid line no losses, dashed line $\alpha_{\mathrm{mic}} = 10\,\mathrm{dB/cm}$, dotted line $\alpha_{\mathrm{mic}} = 20\,\mathrm{dB/cm}$; input power of optical waves $\overline{P}_{\mathrm{o}} = U_{\mathrm{o}}^2/2 = 1\,\mathrm{W}$, difference frequency $\Delta\omega/2\pi = 30\,\mathrm{GHz}$, effective nonlinearity as in Appendix F.

where $U_{\mathrm{o}}/2$ is the amplitude of the optical CW waves. Neglecting dispersion and frequency-dependent losses, the evolution of the microwave is then obtained by solving eq. (4.21),

$$U_{\mathrm{mic}}(z,t) = \frac{\chi_{\mathrm{eff1}}|U_{\mathrm{o}}|^2\Delta\omega\, c\left[F(t) - \exp(-\alpha_{\mathrm{mic}}z)F\left(t - \frac{\Delta n}{c}z\right)\right]}{2(\alpha_{\mathrm{mic}}^2 c^2 + 4\Delta n^2\Delta\omega^2)}\,, \tag{4.71}$$

where,

$$F(x) = 2\Delta n\Delta\omega\cos(2\Delta\omega x) - \alpha_{\mathrm{mic}}c\sin(2\Delta\omega x)\,. \tag{4.72}$$

The generated microwave signal corresponds to a travelling wave oscillating at the difference frequency $2\Delta\omega$. It is convenient to write the generated microwave signal in terms of the average power on the transmission line as,

$$\overline{p}_{\mathrm{mic}}(z) = \frac{\chi_{\mathrm{eff1}}^2|U_{\mathrm{o}}|^4\Delta\omega^2\, c^2}{4(\alpha_{\mathrm{mic}}^2 c^2 + 4\Delta n^2\Delta\omega^2)}\exp(-\alpha_{\mathrm{mic}}z)\left[\cosh(\alpha_{\mathrm{mic}}z) - \cos\left(\frac{2\Delta n\Delta\omega}{c}z\right)\right]\,. \tag{4.73}$$

As shown in Fig. 4.19, in a lossless velocity matched structure the microwave power grows with the square of the length. If microwave losses are present, the generated power will finally saturate due to a balance between generation and attenuation.

In a structure with velocity mismatch (see Fig. 4.20), we find an oscillation of the generated microwave power along the transmission line. The alternating up- and down-conversion can be understood by interpreting the standing wave pattern due to the beating optical waves as a train of optical pulses. As discussed in Section 3.3, in case of velocity mismatch we obtain two sets of microwave pulses, one train travelling with the velocity of the optical

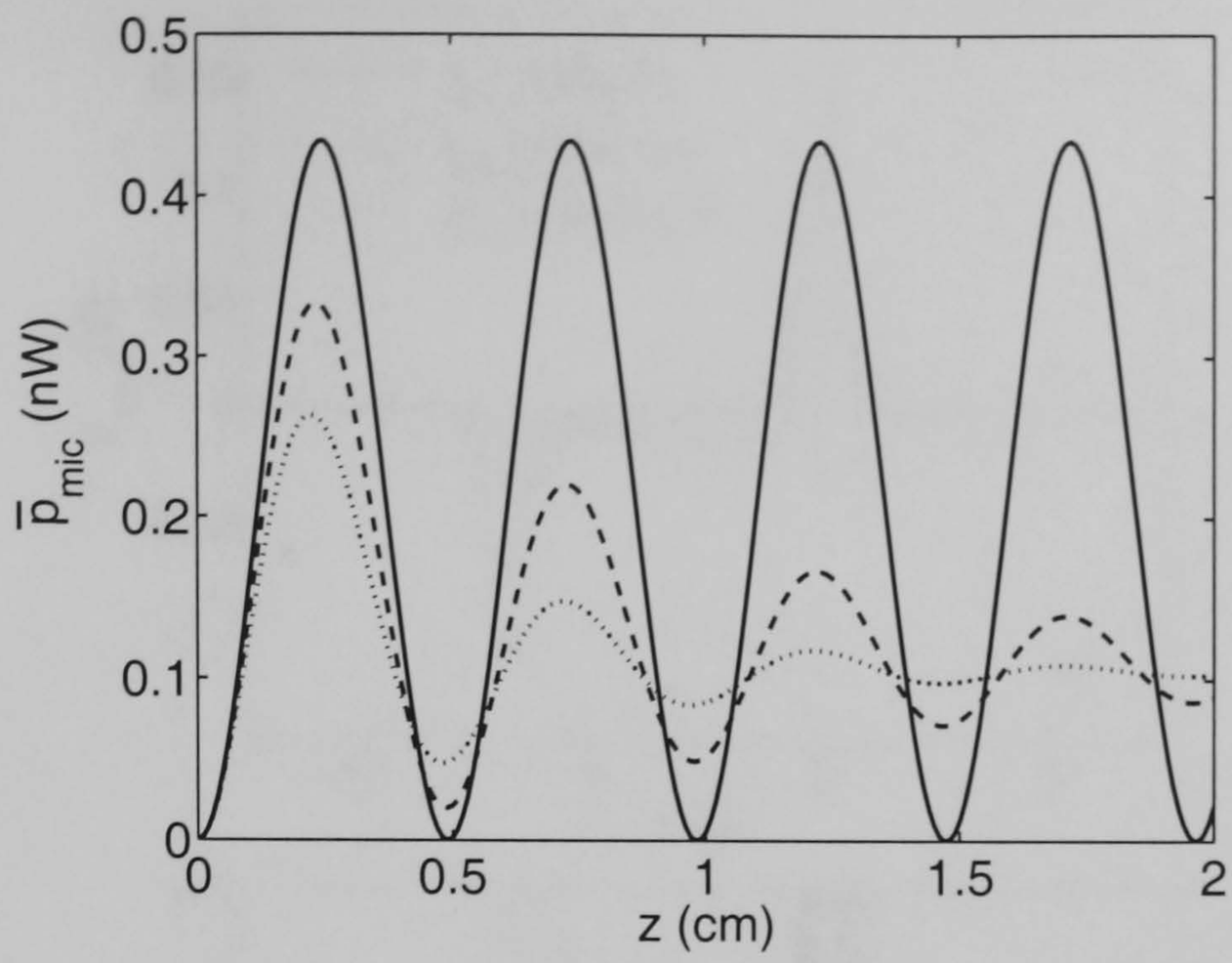

Figure 4.20: Microwave generation by two interacting optical waves, velocity mismatched case, all parameters as in Fig. 4.19 but velocity mismatch as in Appendix F.

wave and one travelling with the velocity of the microwave. The constructive and destructive interference of both trains as they travel along the line leads finally to the oscillating pattern shown in Fig. 4.20. In the presence of microwave losses the oscillations are damped and a stationary state is approached. The maximum generated power can be as much as four times as high as the finally approached value in the stationary limit. The length of a device for the generation of microwaves by mixing of two optical frequencies should therefore be chosen carefully to obtain optimum results.

Pulsed Pump Fields in a Non-Velocity Matched Geometry

Higher conversion efficiency than in the case of mixing of two CW optical waves can be expected from high power pulsed pump fields. As indicated earlier, transmission lines based on GaAs will have a velocity mismatch between microwave and optical group velocity if no special care is taken. Therefore, the case of a non-velocity matched geometry is considered first. To obtain analytical solutions, we neglect dispersive effects and further take into account only frequency-independent losses in the microwave.

Assuming the optical beam to have a pulse shape $U_{\mathrm{TE}}(t)$, the generated microwave is given by,

$$U_{\mathrm{mic}}(z,t) = \frac{c\chi_{\mathrm{eff1}}}{2\Delta n}[|U_{\mathrm{TE}}|^2(t) - |U_{\mathrm{TE}}|^2(t - \Delta n/cz)\exp(-\alpha_{\mathrm{mic}}z) - \alpha_{\mathrm{mic}}\int_0^z \exp(\alpha_{\mathrm{mic}}z)|U_{\mathrm{TE}}|^2(t - \Delta n/c(z-z'))dz']\,. \tag{4.74}$$

As shown in Fig. 4.21, the generated microwave signal consists of two pulses, one travelling with the optical wave and one travelling with the velocity of the microwave. For negligible

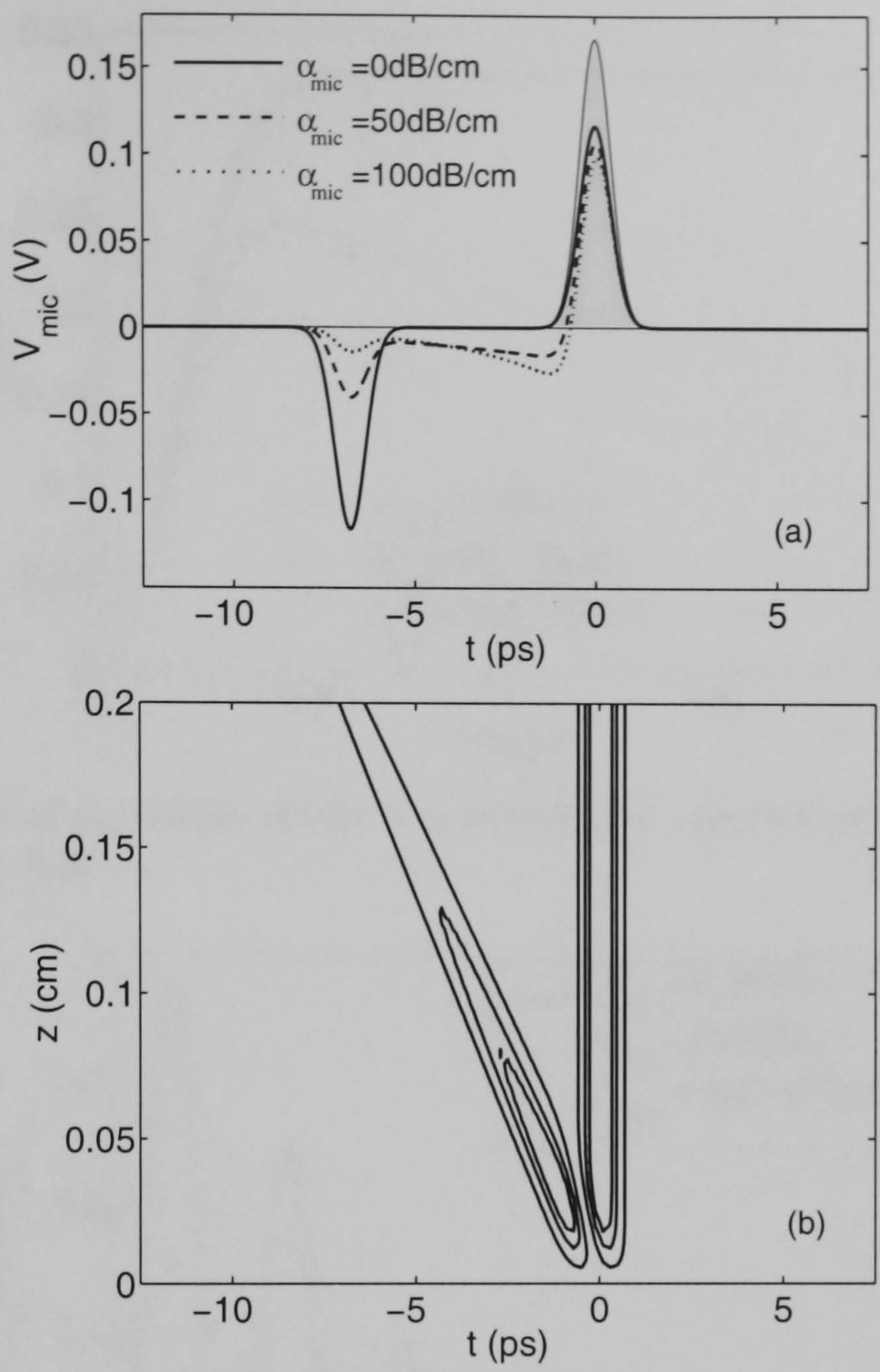

Figure 4.21: Evolution of microwave in a non-velocity matched geometry for varying microwave losses. An optical pulse (Gaussian, peak power $P_{\mathrm{opt}} = 1\,\mathrm{kW}$, $T_{\mathrm{FWHM}} = 1\,\mathrm{ps}$) is injected at $z = 0$. All parameters as in Appendix (F), but dispersion and frequency-dependent losses neglected. (a) Voltage after propagation length $L = 2\,\mathrm{mm}$, also indicated injected optical pulse at $z = 0$ (shaded). (b) Contour plot of microwave for $\alpha_{\mathrm{mic}} = 50\,\mathrm{dB/cm}$.

losses these pulses are an exact image of the optical power distribution. No further growth of the microwave field occurs when the pulses have walked off from each other. As a figure of merit, we can define a walk-off length L_{wo} as,

$$L_{\mathrm{wo}} = \frac{T_{\mathrm{FWHM}}\, c}{\Delta n}\,, \tag{4.75}$$

where T_{FWHM} is the pulse duration of the optical pulse. For an optical peak power $P_{\mathrm{opt}} = 1\,\mathrm{kW}$ and a pulse width $T_{\mathrm{FWHM}} = 1\,\mathrm{ps}$, for the example structure given in Appendix F the peak voltage amounts to $V_{\mathrm{mic}} = 0.12\,\mathrm{V}$ after a walk-off length of $L = 0.29\,\mathrm{mm}$ in the lossless case. A microwave signal which has left the optical pulse is subject to losses (see Fig. 4.21). An absorption length L_{abs} can be defined as,

$$L_{\mathrm{abs}} = \frac{1}{\alpha_{\mathrm{mic}}}\,, \tag{4.76}$$

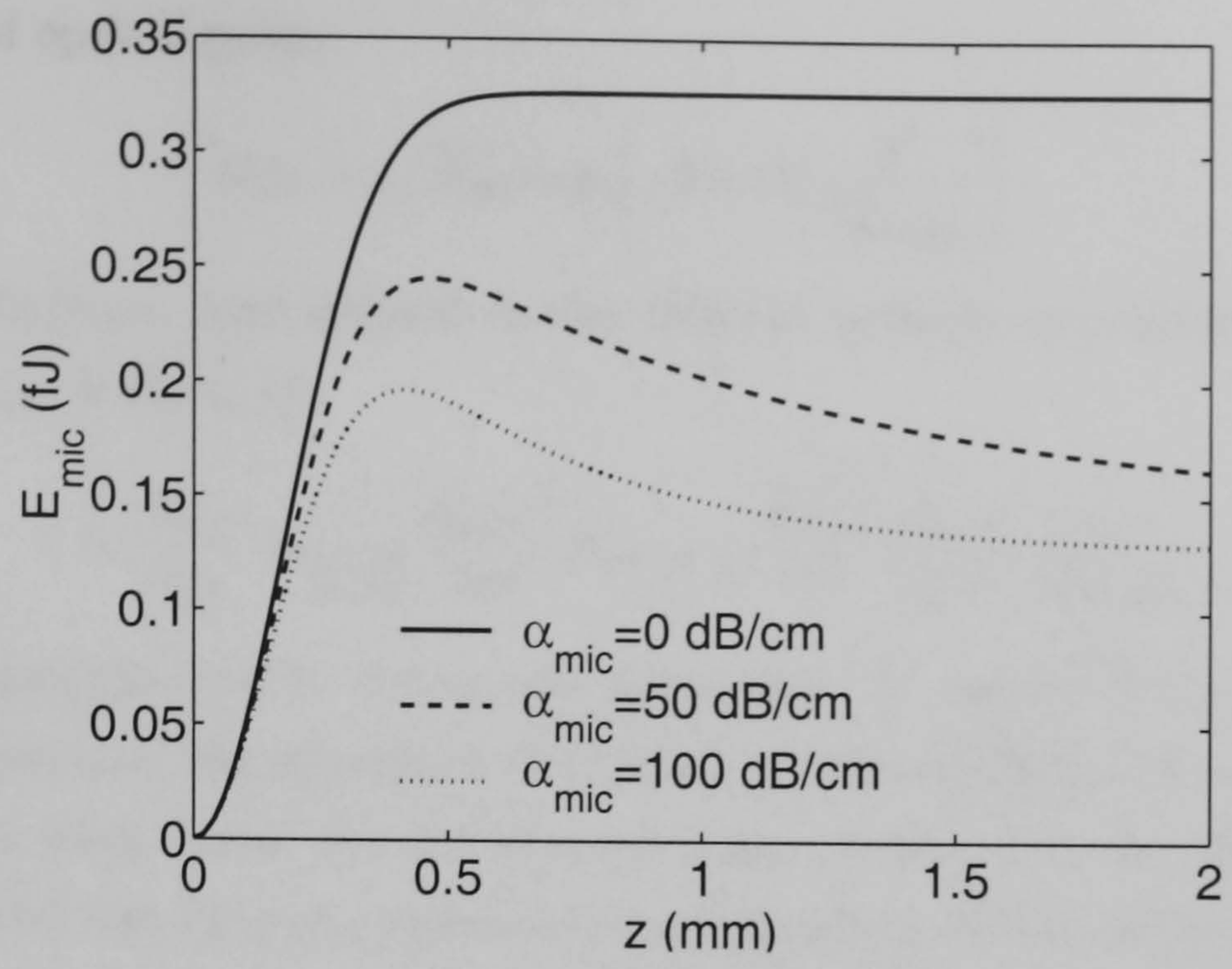

Figure 4.22: Evolution of microwave energy in a non-velocity matched geometry. All parameters as in Fig. 4.21.

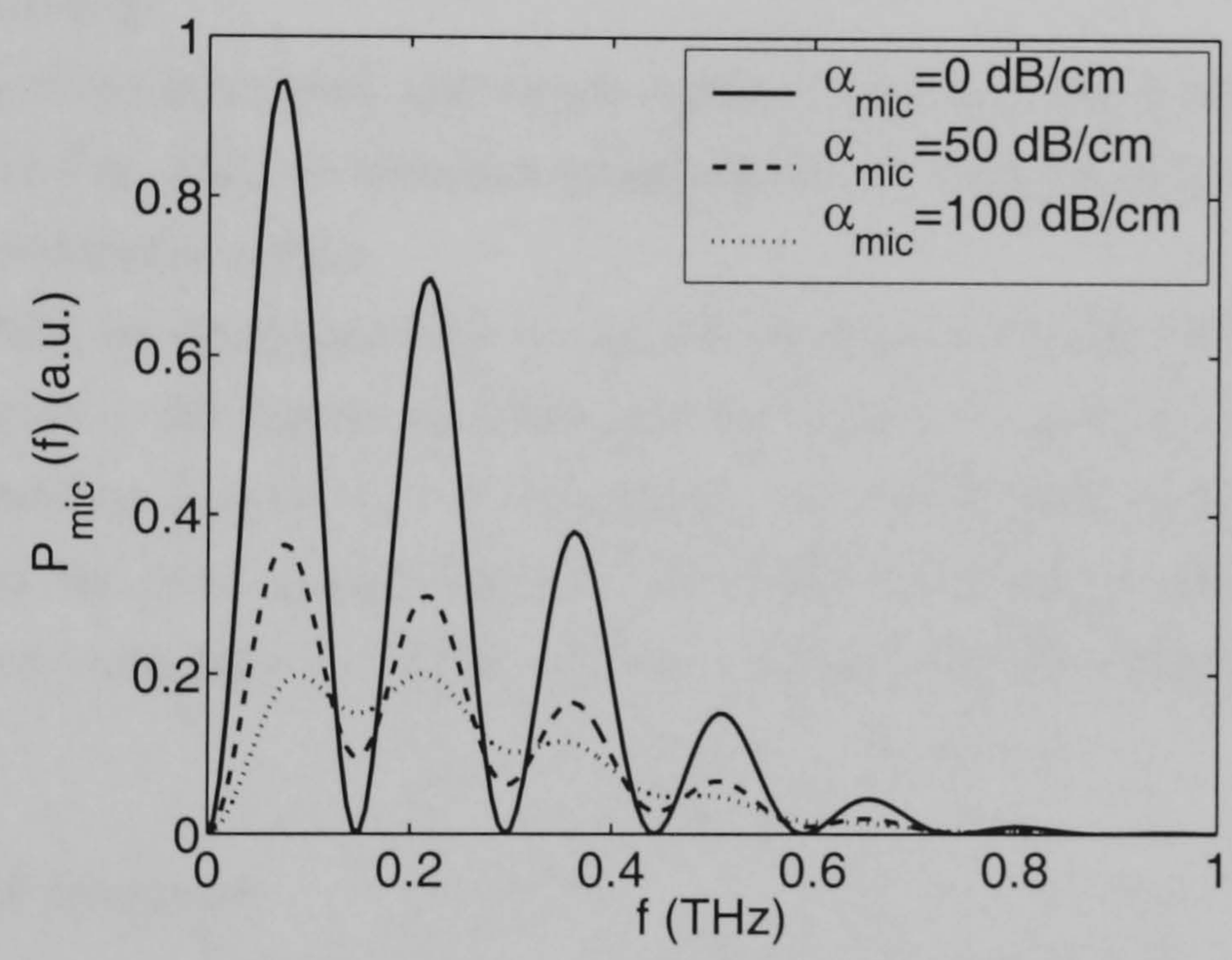

Figure 4.23: Power spectrum of microwave in non-velocity matched structure after propagation length $L = 2\,\text{mm}$. All parameters as in Fig. 4.21.

after which only the pulse travelling with the optical wave remains. This pulse is constantly pumped by the nonlinear polarisation, i.e. the optical wave acting as a source. Losses do not result in its extinction but in a change of its shape according to eq. (4.74).

The evolution of microwave energy along the transmission line is shown in Fig. 4.22. The generated microwave energy reaches a maximum when both pulses have separated. As the pulse travelling with the microwave velocity is absorbed, it drops finally to about half its value. For the lossless case, the conversion efficiency can be calculated analytically. Assuming

a gaussian shaped optical pulse,

$$U_{\mathrm{TE}} = \sqrt{P_{\mathrm{opt}}} \exp\left[-2\ln(2)\frac{t^2}{T_{\mathrm{FWHM}}^2}\right] , \tag{4.77}$$

the conversion efficiency, here defined as the relation between microwave energy E_{mic} and optical energy E_{opt}, is given by,

$$\eta = \frac{E_{\mathrm{mic}}}{E_{\mathrm{opt}}} = \frac{1}{2\sqrt{2}}\frac{\chi_{\mathrm{eff1}}^2 c^2}{\Delta n^2} P_{\mathrm{opt}} = \sqrt{\frac{\ln(2)}{2\pi}}\frac{\chi_{\mathrm{eff1}}^2 c^2}{\Delta n^2}\frac{E_{\mathrm{opt}}}{T_{\mathrm{FHWM}}} . \tag{4.78}$$

The efficiency is proportional to the optical power and the square of the effective nonlinear coefficient. Furthermore, the generated microwave energy depends critically on the velocity mismatch between both waves. For the example shown in Fig. 4.22 the efficiency amounts to $\eta = 3.1 \times 10^{-7}$. The fact that the optical wave essentially propagates through a transparent medium could be the basis for an ultrafast photodetector. Here one would further use that in the case of OR transient effects do not limit the achievable resolution but nonlinearities act near-instantaneously.

The spectrum of the generated microwave signal is related to the spectrum of the optical pulse. As shown in Fig. 4.23, we obtain a broad spectrum with interference patterns due to the time shifted microwave pulses.

Eq. (4.74) should be compared with eq. (3.19) obtained from the bidirectional approach presented in Chapter 3. As indicated earlier, the unidirectional system considered here with the boundary condition $U_{\mathrm{mic}}(0,t) = 0$ suppresses the small static part which is instantaneously induced at the facet of the structure. However, emphasis in this Chapter is laid on the dynamically evolving part eq. (4.74), which coincides with the solution eq. (3.19) in the lossless case.

Velocity Matched Structure

As was shown in the previous Section, for a velocity mismatch between microwave and optical wave the conversion efficiency is rather low. We will now focus on the case of perfect velocity matching, i.e. the group velocity of the optical wave is equal to the velocity of the microwave. Here $\Delta n = 0$, and the solution eq. (4.74) is no longer valid. Under the same assumptions as have been made in deriving eq. (4.74), the microwave then evolves as,

$$U_{\mathrm{mic}} = \frac{\chi_{\mathrm{eff1}}}{2}\frac{1-\exp(-\alpha_{\mathrm{mic}} z)}{\alpha_{\mathrm{mic}}}\frac{\partial |U_{\mathrm{TE}}|^2}{\partial t} . \tag{4.79}$$

As shown in Fig. 4.24, the signal form of the microwave changed to the first derivative of the optical power distribution. Here, both optical and microwave travel with the same velocity resulting in a constant amplification of the microwave signal generated at both slopes of the optical pulse. For vanishing losses, we hence obtain a linear growth of the generated voltage. However, for microwave losses present in the transmission line, part of the generated

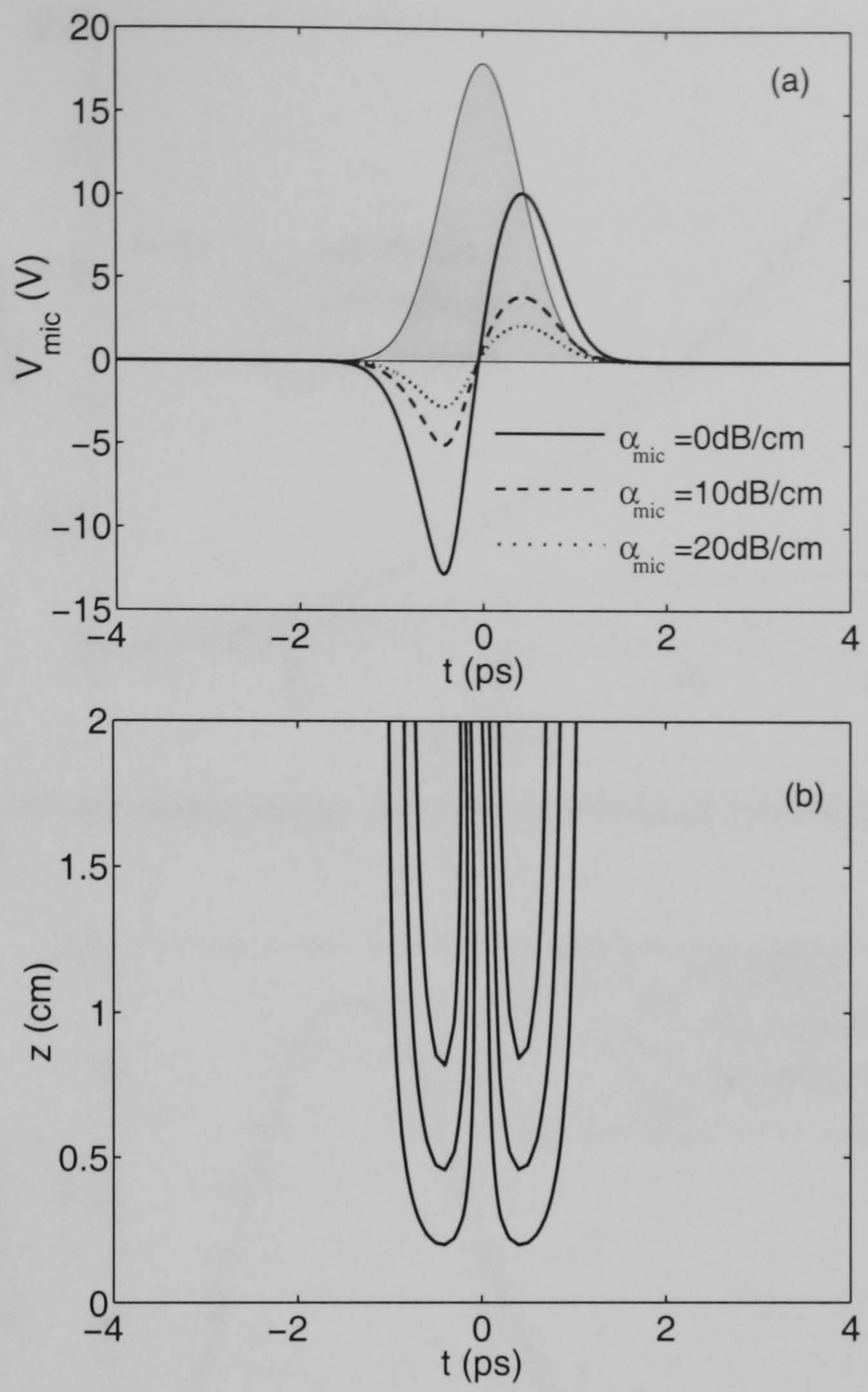

Figure 4.24: Evolution of microwave in a velocity matched structure for varying microwave losses. An optical pulse (Gaussian, peak power $P_{\mathrm{opt}} = 1\,\mathrm{kW}$, $T_{\mathrm{FWHM}} = 1\,\mathrm{ps}$) is injected at $z = 0$. All parameters as in Appendix (F), but $\Delta n = 0$; dispersion and frequency-dependent losses are neglected. (a) Voltage after propagation length $L = 2\,\mathrm{cm}$, also indicated injected optical pulse at $z = 0$ (shaded). (b) Contour plot of evolving microwave signal for $\alpha_{\mathrm{mic}} = 20\,\mathrm{dB/cm}$.

microwave is damped leading to a saturation of the obtainable microwave energy (see Fig. 4.25).

In the case of excitation with an optical pulse with width T_{FWHM}, the electrical signal can be seen as a single cycle microwave pulse with a broad spectrum located around a midfrequency f_{mid} given as,

$$f_{\mathrm{mid}} = \frac{1}{2T_{\mathrm{FWHM}}} \,. \tag{4.80}$$

This is illustrated in Fig. 4.26. The midfrequency can be tuned by optical pulse broadening or narrowing. As the generated microwave signal is insensitive against the phase of the optical wave, this could simply be realized by dispersive broadening or chirp-induced narrowing of the respective pulse.

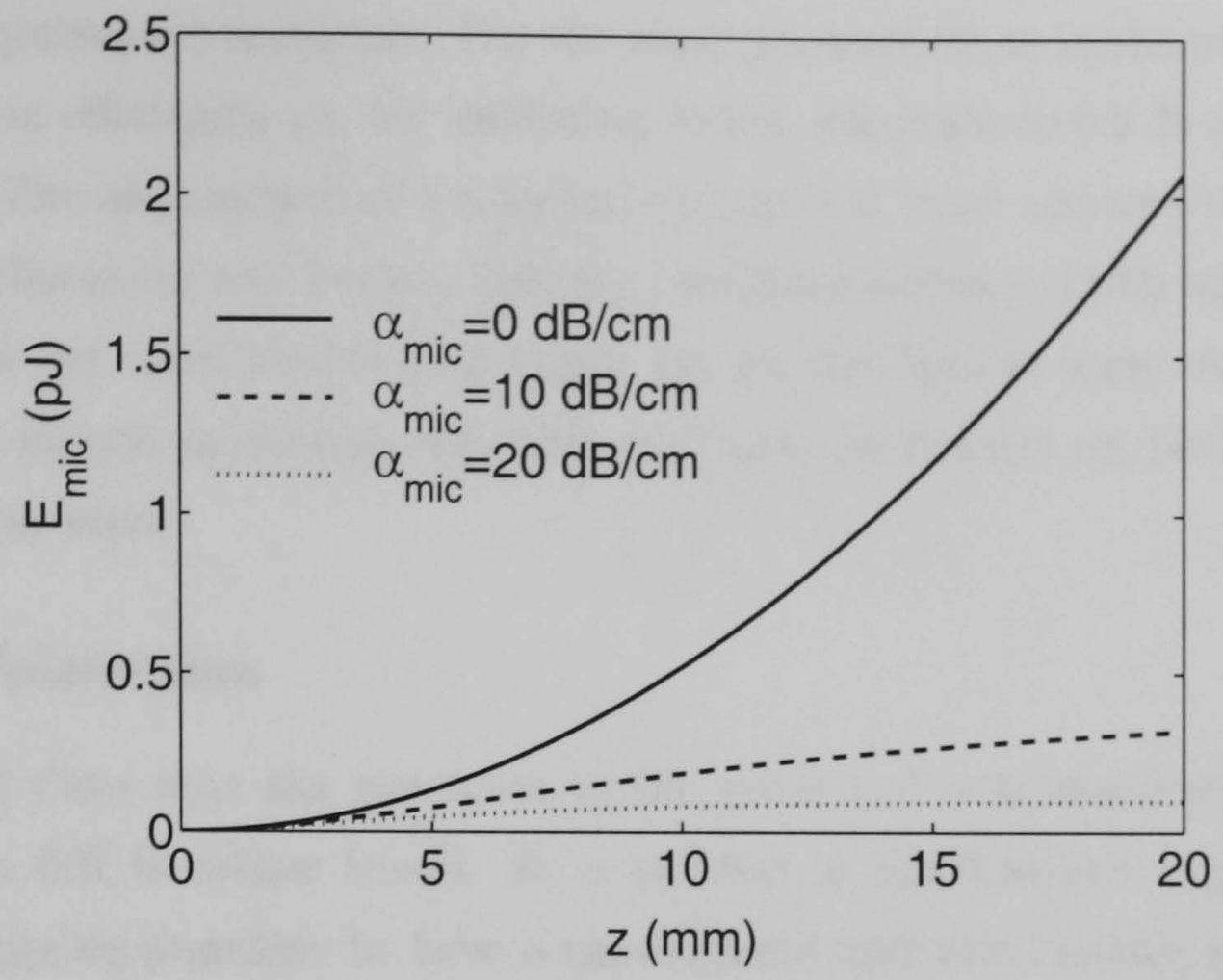

Figure 4.25: Evolution of microwave energy in a velocity matched geometry. All parameters as in Fig. 4.24.

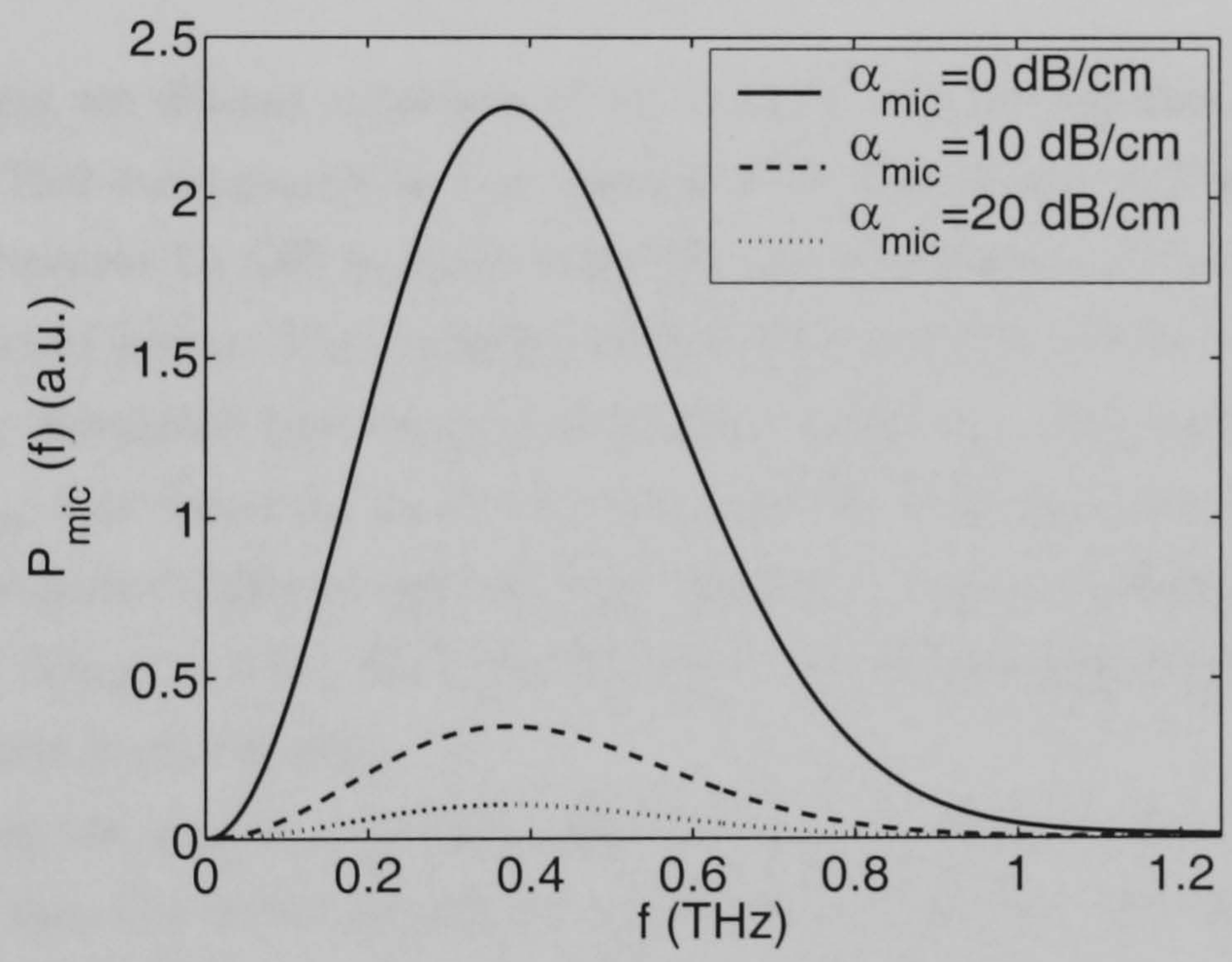

Figure 4.26: Power spectrum of microwave in a velocity matched structure after propagation length $L = 2\,\mathrm{cm}$. All parameters as in Fig. 4.24.

As in the case of velocity mismatch the conversion efficiency can be calculated analytically for a gaussian input pulse. Assuming an optical pulse corresponding to eq. (4.77), we obtain,

$$\begin{aligned}\eta(z) = \frac{E_{\mathrm{mic}}}{E_{\mathrm{opt}}} &= \frac{\ln(2)}{\sqrt{2}}\chi^2_{\mathrm{eff1}}\left[\frac{1-\exp(-\alpha_{\mathrm{mic}}z)}{\alpha_{\mathrm{mic}}}\right]^2 \frac{P_{\mathrm{opt}}}{T^2_{\mathrm{FWHM}}}\,, \\ &= \frac{2\ln(2)^{3/2}}{\sqrt{2}\pi}\chi^2_{\mathrm{eff1}}\left[\frac{1-\exp(-\alpha_{\mathrm{mic}}z)}{\alpha_{\mathrm{mic}}}\right]^2 \frac{E_{\mathrm{opt}}}{T^3_{\mathrm{FWHM}}}\,.\end{aligned} \tag{4.81}$$

For vanishing losses, the efficiency is proportional to the square of the propagated distance. In comparison to the non-velocity matched case the optical pulse width has an even stronger influence on the conversion efficiency. Hence, to generate high energy microwave signals

ultrashort optical pulses are necessary. For the same parameters as in the previous Section the optimum conversion efficiency, i.e. for vanishing losses, amounts to 0.2 % after a propagation length $L = 2\,\mathrm{cm}$. The assumption of a nondepleted optical wave appears to be valid even for long propagation distances and perfect velocity matching between both waves. However, the generated voltages are considerable and might act on the optical wave via the electro-optic effect. As will be shown in Section 4.6, this can have an impact on both phase and pulse shape of the optical wave.

4.5.2 Mixed Polarisation

Fig. 4.23 and 4.26 show that the spectrum of the generated microwave signal in the case of single polarisation OR is rather broad. In a number of applications, e.g. millimeter wave spectroscopy, it may be desirable to have a narrowband and also tunable source. A first step in this direction was discussed in Section 3.5, i.e. the modulation of the nonlinearity in the structure. However, in this Section we will show that mixed polarisation OR leads to similar effects.

In the following we discuss solutions of eq. (4.21) with an effective nonlinearity χ_{eff2} only ($\chi_{\mathrm{eff1}} = 0$). This corresponds to the example CPS line shown in Fig. 4.1(b). Here the excitation of microwaves by OR requires both TE and TM modes to be present. We again assume a nondepleted pump. The evolution of both TE and TM modes is then governed by the phase velocity mismatch and the group velocity mismatch. The walk-off between both optical waves δ_{vopt} was found to be in the range of 10 fs/cm and can be neglected when considering optical pulse widths in the ps-range. However, beating between both modes with a typical value of $\Delta n_{\mathrm{opt}} = 2.5 \times 10^{-4}$ corresponds to a beat length of $\pi/\Delta\beta = 0.62$ cm at $\lambda = 1.6\mu$m and plays a crucial role.

In the following we assume a linearly polarized optical pulse with a power distribution $|U_{\mathrm{o}}(t)|^2$ injected into the structure with a polarisation angle γ. The source term for the microwave is then given by,

$$S_{\mathrm{OR}} = \sin(2\gamma)\cos(\Delta\beta z)\frac{\chi_{\mathrm{eff2}}}{2}\,\frac{\partial|U_{\mathrm{o}}(t)|^2}{\partial t}\,, \tag{4.82}$$

We end up with an effective modulation of the nonlinearity depending on the phase velocity mismatch between both TE and TM. This is not too different from the case discussed in Section 3.5, where the nonlinearity changes its sign in adjacent sections of the transmission line. Here, the period of the modulation is determined entirely by the phase velocity mismatch between both TE and TM modes.

Velocity Matched Structure

Neglecting dispersion, higher order attenuation, walk-off between both optical waves and assuming a non-depleted pump we derive for the evolution of the generated microwave U_{mic}

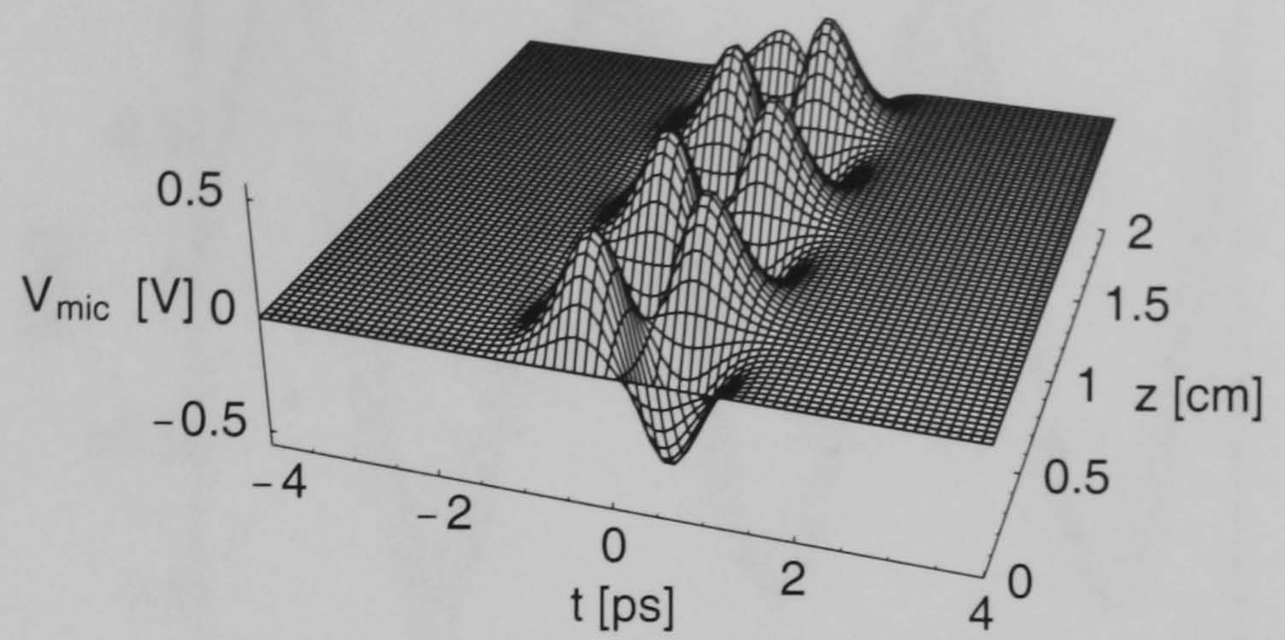

Figure 4.27: Evolution of microwave signal in stripline for velocity matching ($\Delta n = 0$, all other parameters as in Appendix F). The optical pulse with a peak power $P_{\mathrm{opt}} = 1\,\mathrm{kW}$ and width $T_{\mathrm{FWHM}} = 1\,\mathrm{ps}$ is injected at $z = 0$ with an angle $\gamma = 45^{\mathrm{o}}$. Walk-off, dispersion and attenuation are neglected.

in a velocity matched structure ($\Delta n = 0$),

$$U_{\mathrm{mic}}(z,t) = M(z)\frac{\chi_{\mathrm{eff2}}\sin(2\gamma)}{2}\frac{\partial}{\partial t}|U_{\mathrm{o}}(\,t\,)|^2 \quad , \tag{4.83}$$

with

$$M(z) = \frac{\Delta\beta\sin(\Delta\beta z) + \alpha_{\mathrm{mic}}[\cos(\Delta\beta z) - \exp(-\alpha_{\mathrm{mic}} z)]}{\Delta\beta^2 + \alpha_{\mathrm{mic}}^2} \; . \tag{4.84}$$

Similar to the single polarisation case, the generated microwave signal follows the temporal derivative of the optical power distribution. This corresponds to a single cycle pulse with a broad frequency spectrum around a carrier frequency depending on the optical pulse width. However, beating between both optical modes leads to a modulation of the microwave in propagation direction. Fig. 4.27 shows the evolution of the generated microwave signal.

Optimum conversion efficiency with $M = 1/\Delta\beta$ is obtained at length $z = (\mathrm{n}\pi)/(2\Delta\beta)$, $(\mathrm{n} = 1, 3, ...)$ for the lossless case. As shown in Fig. 4.28, high microwave losses can lead to a decrease in maximum voltage and further modify the optimum propagation length. The effective modulation of the nonlinearity in a CPS structure with moderate losses results hence in a decreased efficiency in comparison to the single polarisation case, where we end up with a linearly growing amplitude of the generated microwave.

Structure with Velocity Mismatch

For the velocity mismatched case ($\Delta n \neq 0$) we derive under the same assumptions,

$$\begin{aligned} U_{\mathrm{mic}}(z,t) =& \frac{\chi_{\mathrm{eff2}}\sin(2\gamma)c}{2\Delta n} \\ &\times \left[|U_{\mathrm{o}}(t)|^2\cos(\Delta\beta z) - |U_{\mathrm{o}}(t - \Delta n/cz)|^2\exp(-\alpha_{\mathrm{mic}} z) + U_{\mathrm{thz}}(z,t)\right] \; , \end{aligned} \tag{4.85}$$

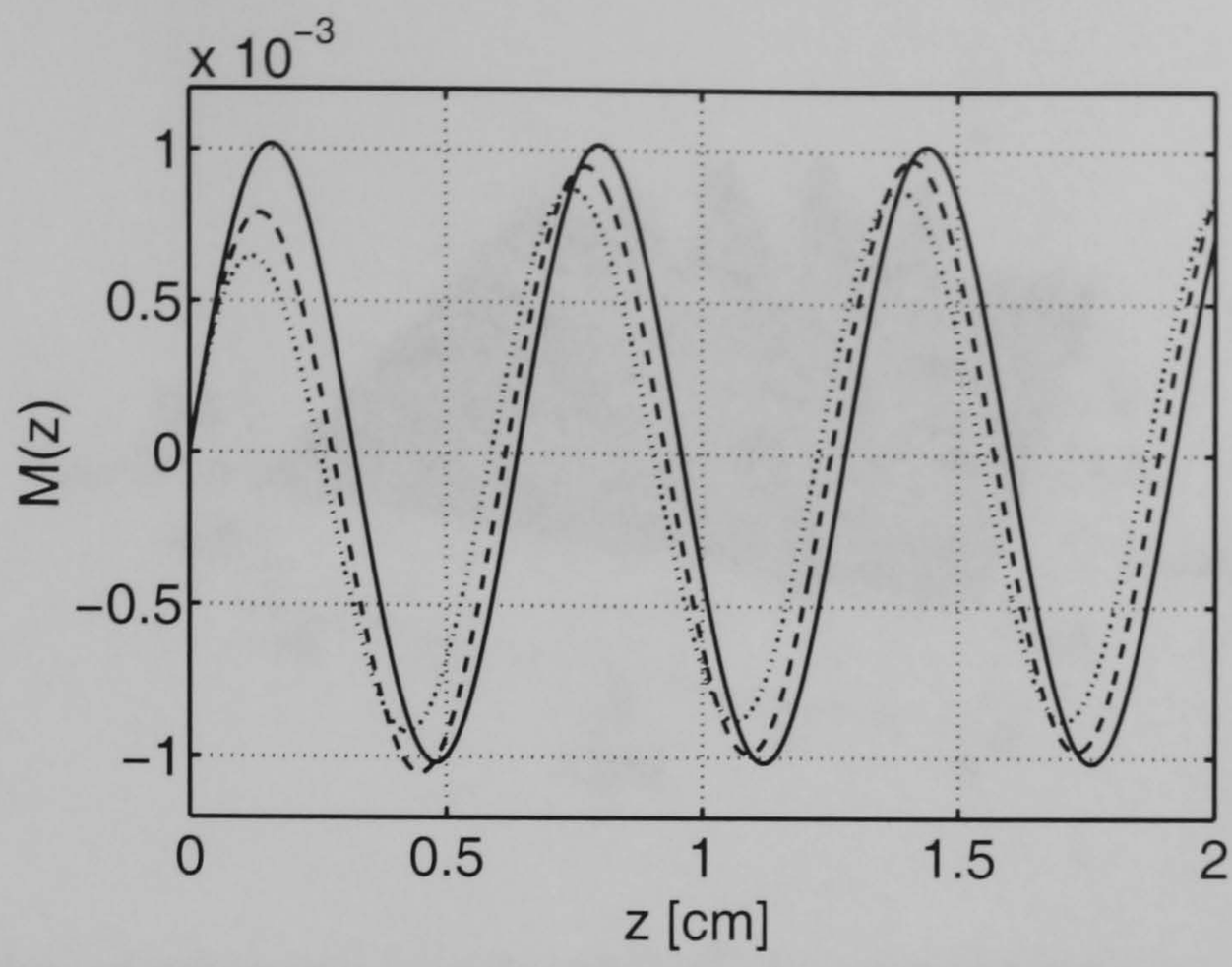

Figure 4.28: Evolution of factor M(z) in eq. (4.83) for different losses. Solid line $\alpha_{\mathrm{mic}} = 0$; dashed line $\alpha_{\mathrm{mic}} = 25\,\mathrm{dB/cm}$; dotted line $\alpha_{\mathrm{mic}} = 50\,\mathrm{dB/cm}$.

with,

$$U_{\mathrm{thz}}(z,t) = -\exp(-\alpha_{\mathrm{mic}} z) \times \int_0^z \exp(\alpha_{\mathrm{mic}} z') \left[\alpha_{\mathrm{mic}} \cos(\Delta\beta z') - \Delta\beta \sin(\Delta\beta z')\right] |U_{\mathrm{o}}[t - \Delta n/c(z - z')]|^2 \mathrm{d}z' \,. \tag{4.86}$$

Similar to the single polarisation case we obtain two pulses following the optical power distribution, one travelling with the optical wave and one travelling with the velocity of the microwave which is subject to losses. Both pulses are separated approximately after the walk-off length $L_{\mathrm{wo}} = \Delta T c/|\Delta n|$ where ΔT is the pulse width of the optical pulse. As in the velocity matched case we have an additional modulation of the pulse travelling with the optical wave depending on the phase mismatch between TE and TM modes. However, as shown in Fig. 4.29, the third term $U_{\mathrm{thz}}(z,t)$ gives rise to the generation of a periodic microwave signal evolving between the two pulses. The beating between TE and TM modes in the waveguide can hence be exploited for narrow bandwidth THz generation. To study the action of the term eq. (4.86), we neglect losses and, as a first approximation, use a rectangular pulse for the optical power distribution,

$$|U_{\mathrm{o}}(t)|^2 = \begin{cases} P_0 & : \quad -\Delta T/2 \le t \le \Delta T/2 \,, \\ 0 & : \quad \text{otherwise} \,. \end{cases} \tag{4.87}$$

For a propagation length longer than the walk-off length $z > L_{\mathrm{wo}}$, the generated microwave in the time interval $\Delta T/2 < t < z\Delta n/c - \Delta T/2$ for $\Delta n > 0$ or $\Delta T/2 - z|\Delta n|/c < t < -\Delta T/2$ for $\Delta n < 0$ respectively is then given by,

$$U_{\mathrm{thz}}(z,t) = 2P_0 \sin\left(\frac{\Delta\beta\Delta T c}{2\Delta n}\right) \sin\left[\Delta\beta\left(z - \frac{c}{\Delta n}t\right)\right] \,. \tag{4.88}$$

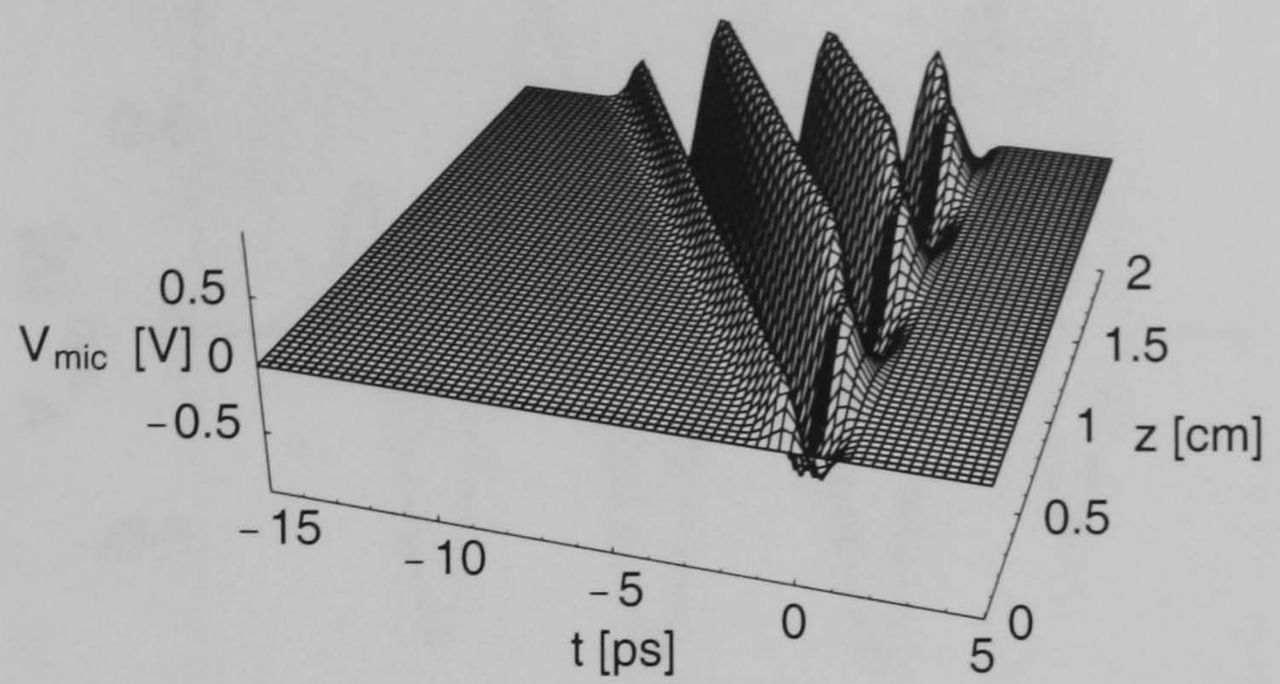

Figure 4.29: Evolution of microwave signal with velocity mismatch ($\Delta n = -0.17$, all other parameters as in Appendix F). The optical pulse with a peak power $P_{\text{opt}} = 1\,\text{kW}$ and width $T_{\text{FWHM}} = 1\,\text{ps}$ is injected at $z = 0$ with an angle $\gamma = 45^{\text{o}}$. Walk-off, dispersion and attenuation are neglected.

We end up with a sinusoidal signal with a mid frequency determined by beat length and velocity mismatch as,

$$f_{\text{mic}} = \frac{c\Delta n_{\text{opt}}}{\lambda \Delta n} \,. \tag{4.89}$$

It follows further from eq. (4.88), that for maximum amplitude the walk-off length should be matched to the phase velocity difference between both optical waves as,

$$L_{\text{wo}} = \frac{\lambda}{2\Delta n_{\text{opt}}} \,. \tag{4.90}$$

In this case the amplitude of the generated signal can be as twice as high as the amplitude of the pulses travelling with the optical or microwave velocity, respectively.

Changing the optical pulse shape does not change the mid-frequency and only modifies the pre-factor in eq. (4.88). For example, approximating the optical pulse with a raised cosine,

$$|U_{\text{o}}(t)|^2 = \begin{cases} \frac{P_0}{2}\left(\cos\left[\frac{\pi t}{\Delta T}\right] + 1\right) & : \quad -\Delta T \leq t \leq \Delta T \,, \\ 0 & : \quad \text{otherwise} \,, \end{cases} \tag{4.91}$$

gives a generated microwave for a propagation length longer than $z > 2L_{\text{wo}}$ (in the corresponding time interval $\Delta T < t < z\Delta n/c - \Delta T$ for $\Delta n > 0$ or $\Delta T - z|\Delta n|/c < t < -\Delta T$ for $\Delta n < 0$ respectively),

$$U_{\text{thz}}(z,t) = P_0 \frac{\sin(x)}{1-(x/\pi)^2} \sin\left[\Delta\beta\left(z - \frac{c}{\Delta n}t\right)\right] \,, \text{ with } x = \frac{\Delta\beta\Delta T c}{\Delta n} \,. \tag{4.92}$$

The maximum amplitude is now given by $P_0 * 1.636$ under the matching condition,

$$L_{\text{wo}} = \frac{\lambda}{2\Delta n_{\text{opt}}} * 0.837 \,. \tag{4.93}$$

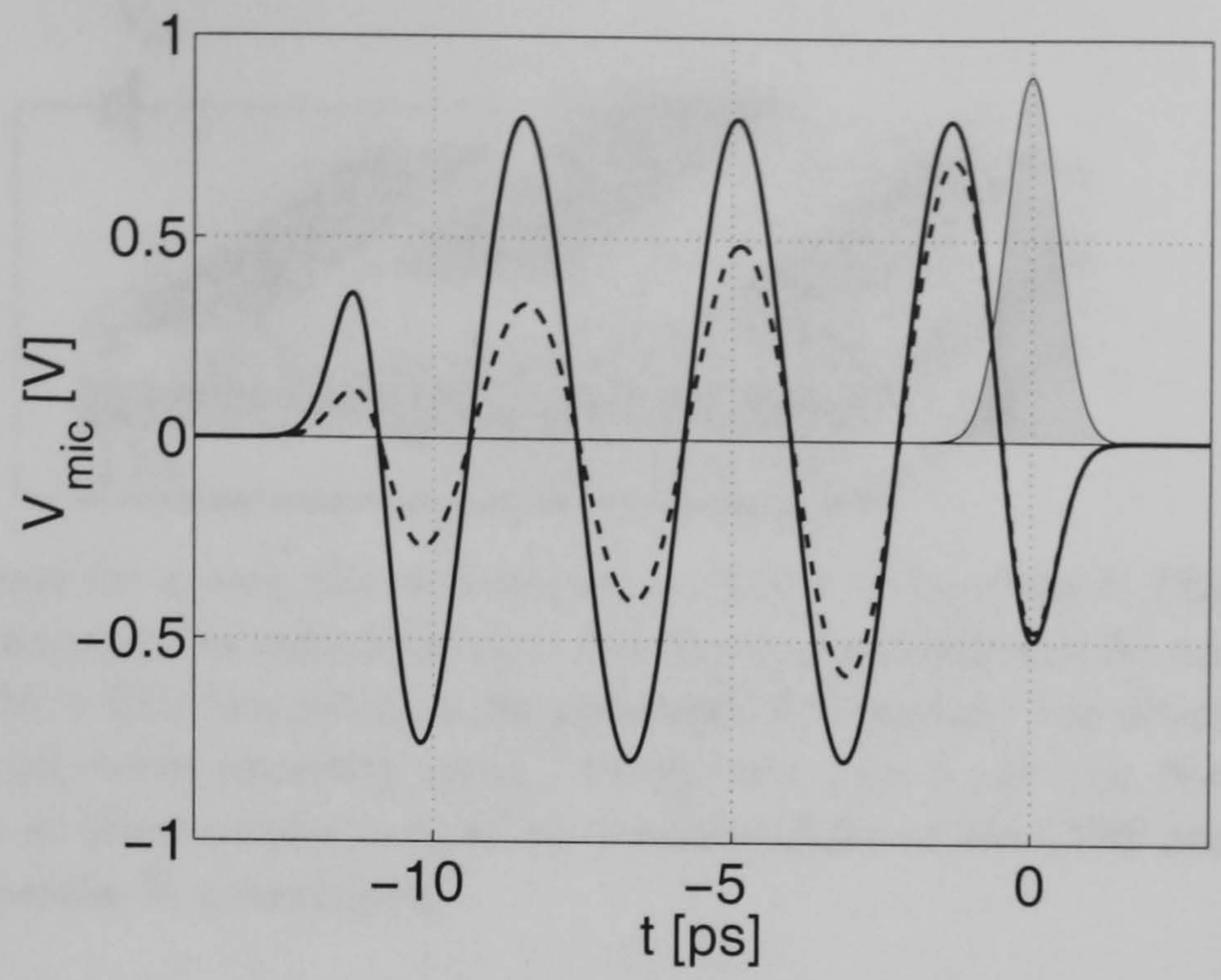

Figure 4.30: Generated microwave signal in Fig. 4.29 after propagation length $z = 2\,\mathrm{cm}$, also indicated injected optical pulse at $t = 0$ (shaded). Solid line $\alpha_{\mathrm{mic}} = 0$; dashed line with microwave loss $\alpha_{\mathrm{mic}} = 5\,\mathrm{dB/cm}$.

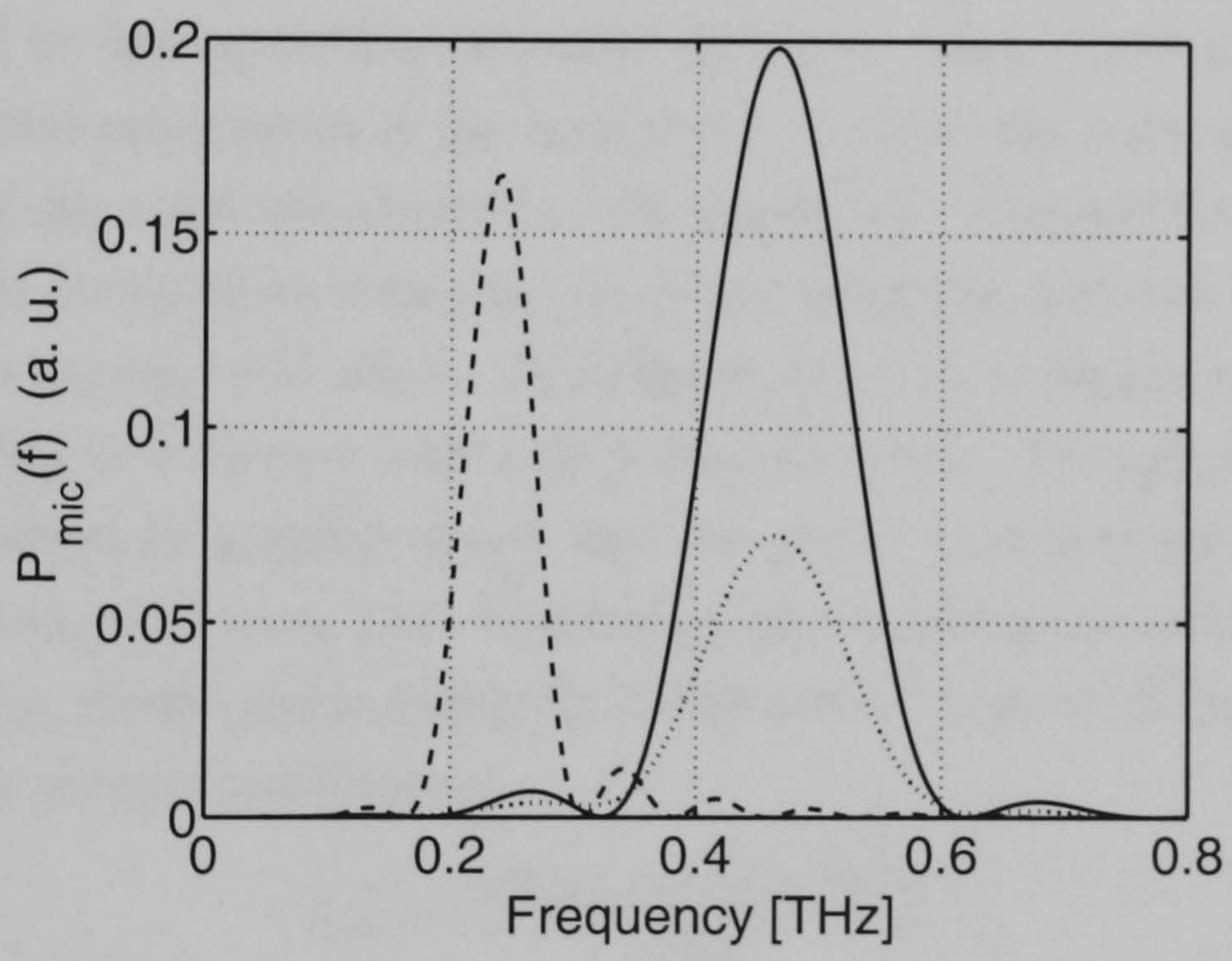

Figure 4.31: Amplitude spectra of generated microwave signals with velocity mismatch (all parameters as in Fig. 4.29 apart from losses and mismatch). Solid line Δn=-0.1, $\alpha_{\mathrm{mic}} = 0$; dotted line Δn=-0.1, $\alpha_{\mathrm{mic}} = 5\,\mathrm{dB/cm}$; dashed line Δn=-0.2, $\alpha_{\mathrm{mic}} = 0$.

Numerical calculations showed that the essential results hold also for more realistic pulse shapes, e.g. a Gaussian.

The number of cycles and hence the bandwidth of the generated signal is determined by the length of the structure. However, the microwave is subject to losses resulting in a decaying envelope of the generated signal as shown in Fig. 4.30. As indicated in Fig. 4.31, the bandwidth of the generated signal depends on the interplay between walk-off length, phase velocity mismatch and finally losses in the structure.

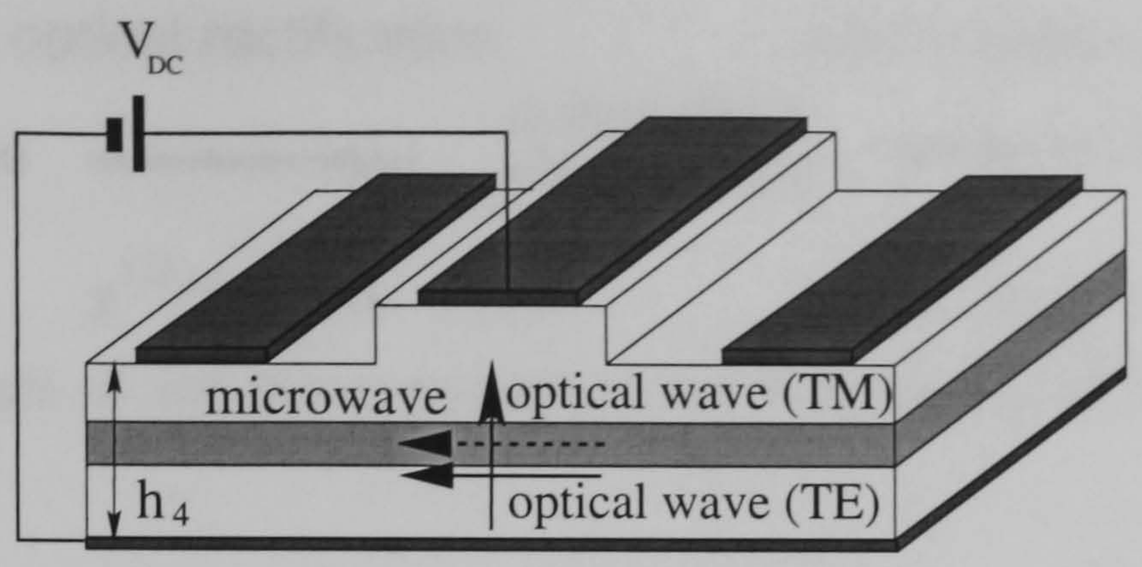

Figure 4.32: Structure for tuning the mid-frequency of narrow bandwidth THz generation. A DC voltage across the microstrip structure tunes the phase velocity mismatch between TE and TM, a CPS line extracts the generated THz signal. The effective nonlinearity has been calculated assuming perfect conductors with h=20 μm, the strip configuration on top of the structure is equal to the dimensions of the CPW and the CPS structure in Appendix F, respectively.

The results obtained here should be compared with the principle of modulating the nonlinear susceptibility for the generation of microwave signals discussed in Section 3.5. In case of modulating the nonlinearity, the period of domain reversal is matched to the walk off length determined by the material properties. However, using mixed polarisations in OR we obtain an effective modulation of the nonlinearity without the necessity of manipulating the nonlinearity of the substrate material of the waveguide. The mid-frequency of the generated signal could be tuned by changing the phase mismatch between the optical modes, for example by the electro-optic effect. An example structure is depicted in Fig. 4.32. Here a microwave stripline is combined with a microstrip structure. The ground electrode of the latter could be realized by a highly doped layer or simply by contacting the bottom of the substrate. Neglecting dispersion and the small energy conservation term in eq. (4.22), an applied DC field V_{DC} gives a phase change in the optical TE wave of $\Delta\phi_{\mathrm{TE}} = -\chi_{\mathrm{eff1}}\omega_{\mathrm{opt}}V_{\mathrm{DC}}$. The mid-frequency is hence modified as,

$$f_{\mathrm{mic}} = \frac{c(\Delta n_{\mathrm{opt}} - c\chi_{\mathrm{eff1}}V_{\mathrm{DC}})}{\lambda\Delta n}. \tag{4.94}$$

To give an example, assuming the ground electrode of the structure in Fig. 4.32 to be a perfect conductor the effective nonlinearity amounts to $\chi_{\mathrm{eff1}} = 9.6 \times 10^{-14}\mathrm{s/m}\sqrt{\mathrm{W}}$. This corresponds to a shift of the mid-frequency of $\Delta f_{\mathrm{mic}} = 0.27$ THz by application of $V_{\mathrm{DC}} = 5V$ at $\lambda = 1.6\mu$m for $\Delta n = -0.1$.

4.6 Cascading Effects

As was shown in the preceding Section, even for a velocity matched structure the conversion efficiency remains rather low. However, at high optical powers, the generated electrical signals can reach voltages which are comparable to the π-voltage of the corresponding electro-optic modulator. Although the power of the optical wave does not change significantly, we should

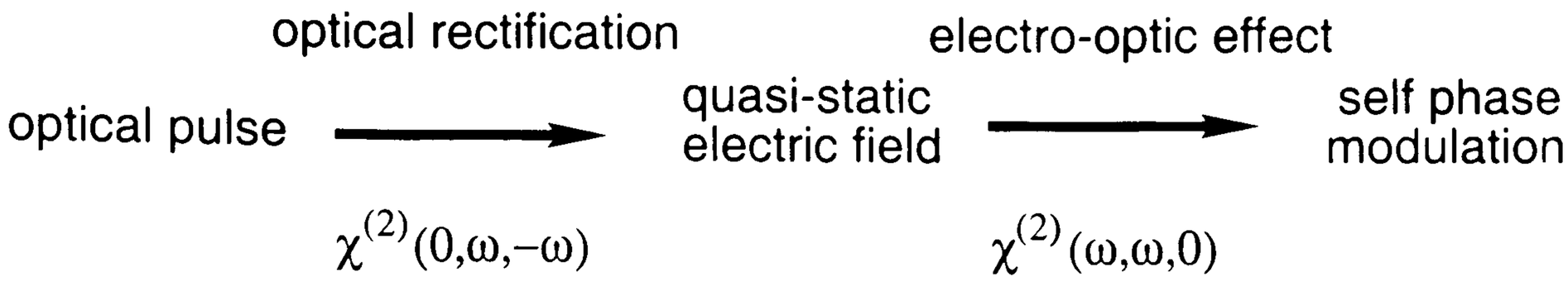

Figure 4.33: Principle of self phase modulation due to cascading of OR and the electro-optic effect.

therefore expect an effect on the phase of the optical wave. The basic principle of this cascaded process is shown in Fig. 4.33. The optical wave generates an electric field by OR, and the generated electrical signal couples back to the optical wave via the electro-optic effect giving rise to a self phase modulation (SPM). The resulting phase shift is proportional to the power of the optical wave.

This effect is well known from media with third order nonlinearities, where the refractive index and hence phase of the optical wave is strongly intensity dependent [75]. The fact that media with a second order nonlinearity can also show an effective cubic nonlinearity due to cascading effects is well known from second harmonic generation (SHG) [14]. Here the phase modulation arises as a consequence of the interaction of a fundamental field with its second harmonic. The effect of SPM due to SHG has been described numerically [76] and analytically [77] and was demonstrated experimentally, for example, in [78]. It is therefore interesting to investigate if similar effects could be exploited by the corresponding cascading mechanism via OR.

The self modulation of picosecond pulses due to a rectified field was predicted for the first time by Gustafson *et al.* in 1970 [16]. More recent theoretical studies include the investigation of cascaded phase shifts in planar slab waveguides [19] or the consequent electro-optical effect for propagating pulses [18]. Recently Bosshardt *et al.* demonstrated cascading of OR and the electro-optic effect for the first time in $KNbO_3$ [17], where a dominant contribution of the rectification induced cubic nonlinearity to the nonlinear refractive index was shown for certain crystal orientations.

Before moving, on some fundamental differences between SHG and OR cascading in the case of a continuous fundamental wave (CW) should be mentioned. First, the phase modulation due to SHG is always strongly dependent on the phase mismatch between fundamental and second harmonic. In contrast, OR cascading in the CW case is always phasematched since the rectified signal is a purely static electric field. Interesting in this respect is that the fundamental can interact potentially with DC electric fields in longitudinal direction. Furthermore, the attenuation of the fundamental wave in OR is much lower than in the case of SHG, which can be an advantage if one is interested merely in self phase modulation. However, in this work we are mainly interested in transient effects where the velocity mismatch plays an inherent role for the interaction of optical pulse and microwave. Some of these effects

will be discussed in the following.

4.6.1 Single Polarisation

In a structure with velocity mismatch, the accumulation of an additional phase in the optical wave for structures much longer than the walk-off length is mainly determined by the microwave pulse travelling with the optical pulse, in the lossless case given by,

$$U_{\mathrm{mic}}(z,t) = \frac{\chi_{\mathrm{eff1}} c}{2\Delta n} |U_{\mathrm{TE}}(t)|^2 \,. \tag{4.95}$$

In the following we will refer to eq. (4.95) as the stationary limit $\partial_z U_{\mathrm{mic}} = 0$. Inserting eq. (4.95) into the evolution equation for the TE mode eq. (4.22) gives,

$$\left[\mathrm{i}\frac{\partial}{\partial z} - \frac{D_{\mathrm{TE}}}{2}\frac{\partial^2}{\partial t^2} - \frac{\omega_{\mathrm{opt}}\chi_{\mathrm{eff1}}^2 c}{2\Delta n}|U_{\mathrm{TE}}|^2\right] U_{\mathrm{TE}} = \mathrm{i}\frac{\chi_{\mathrm{eff1}}^2 c}{2\Delta n}\frac{\partial}{\partial t}|U_{\mathrm{TE}}|^2 U_{\mathrm{TE}} \,. \tag{4.96}$$

For moderate optical pulse widths the term on the right hand side, which corresponds to self steepening of the optical wave, can be neglected. Eq. (4.96) is then the nonlinear Schroedinger (NLS) equation which is well known in nonlinear wave propagation. Solutions of the nonlinear Schroedinger equation include solitons, i.e. pulses where dispersion and nonlinearity counterbalance each other leading to distortion-free propagation. Soliton propagation due to cascading of OR and the electro-optic effect will be considered in detail in Chapter 5. An effective cubic nonlinearity can be defined as,

$$\gamma_{\mathrm{c}} = \frac{\omega_{\mathrm{opt}}\chi_{\mathrm{eff1}}^2 c}{2\Delta n} \,. \tag{4.97}$$

The effective cubic nonlinearity is proportional to the square of the OR-induced nonlinearity. Note that the sign and the magnitude of the effective cubic nonlinearity depend critically on the velocity mismatch between optical wave and microwave and hence can be tuned in a large range of parameters by application of slow wave structures. In the case of negligible dispersion, the induced phase follows mainly the optical power distribution while the pulse shape remains unchanged,

$$U_{\mathrm{TE}}(z,t) = U_{\mathrm{TE}}(0,t)e^{\mathrm{i}\Delta\phi} \quad \text{with} \quad \Delta\phi = -\gamma_{\mathrm{c}}|U_{\mathrm{TE}}(0,t)|^2 z \,, \tag{4.98}$$

Assuming a velocity mismatch of $\Delta n = -0.1$, the effective nonlinearity γ_{c} for the example CPW structure amounts to $-1.8 \times 10^{-2}\mathrm{m}^{-1}\mathrm{W}^{-1}$. Injecting a symmetric optical pulse with a peak power $P_{\mathrm{o}} = 1\,\mathrm{kW}$, after a propagation length of $L = 2\,\mathrm{cm}$ the maximum phase shift at the pulse center is $\Delta\phi_{\mathrm{max}} = -0.35\,\mathrm{rad}$.

Higher phase shifts are expected for velocity matched structures. For bulk material this case has been discussed by Gustafson *et al.* in [16]. The generated microwave power acting on the optical wave is then given by eq. (4.79). If we neglect dispersion, the induced phase shift due to OR cascading amounts to,

$$U_{\mathrm{TE}}(z,t) = U_{\mathrm{TE}}(0,t)e^{\mathrm{i}\Delta\phi} \quad \text{with} \quad \Delta\phi = -\frac{\chi_{\mathrm{eff1}}^2\omega_{\mathrm{opt}}}{2}\frac{\alpha z - 1 + \exp(-\alpha z)}{\alpha^2}\frac{\partial}{\partial t}|U_{\mathrm{TE}}|^2 \,. \tag{4.99}$$

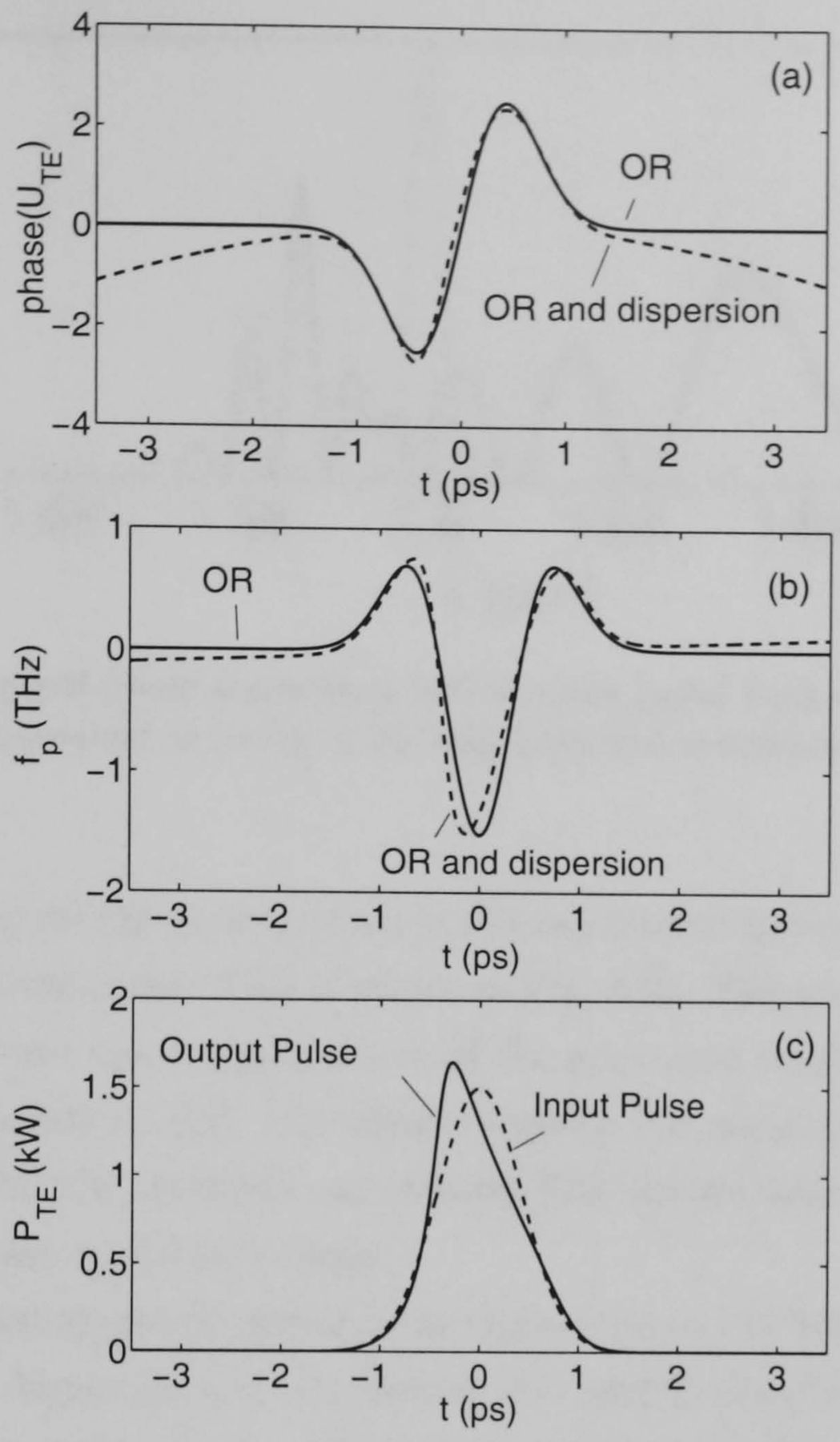

Figure 4.34: (a) Phase of optical pulse after self phase modulation due to OR and the electro-optic effect (CPW structure, $\Delta n = 0$, losses and dispersion of microwave neglected, all other parameters as in Appendix F), input power $P_0 = 1.5\,\mathrm{kW}$, width $T_{\mathrm{FWHM}} = 1\,\mathrm{ps}$ (Gaussian), propagation length $L = 2\,\mathrm{cm}$; (b) instantaneous frequency shift, (c) pulse shape at the output for both SPM and dispersion.

Note that, in contrast to a Kerr nonlinearity the induced phase follows the derivative of the optical power distribution. The phase profile is shown in Fig. 4.34 (a). Maximum phase shifts are hence obtained for very short high power optical pulses, provided the walk-off length is maintained. In case of vanishing losses, the phase shift due to SPM grows quadratically with the propagation distance. High microwave losses modify the required propagation length for a certain phase shift whereas the form of the phase profile is maintained. The instantaneous frequency shift along the optical pulse is given by,

$$f_{\mathrm{p}} = -\frac{1}{2\pi}\frac{\partial \Delta\phi}{\partial t}\,. \tag{4.100}$$

As shown in Fig. 4.34 (b) the wings of the optical pulse are upshifted whereas the the central part is downshifted. This is somehow in contrast to the case of a Kerr nonlinearity, where one obtains frequency shifts at both edges of the pulse with alternating sign. For very high power

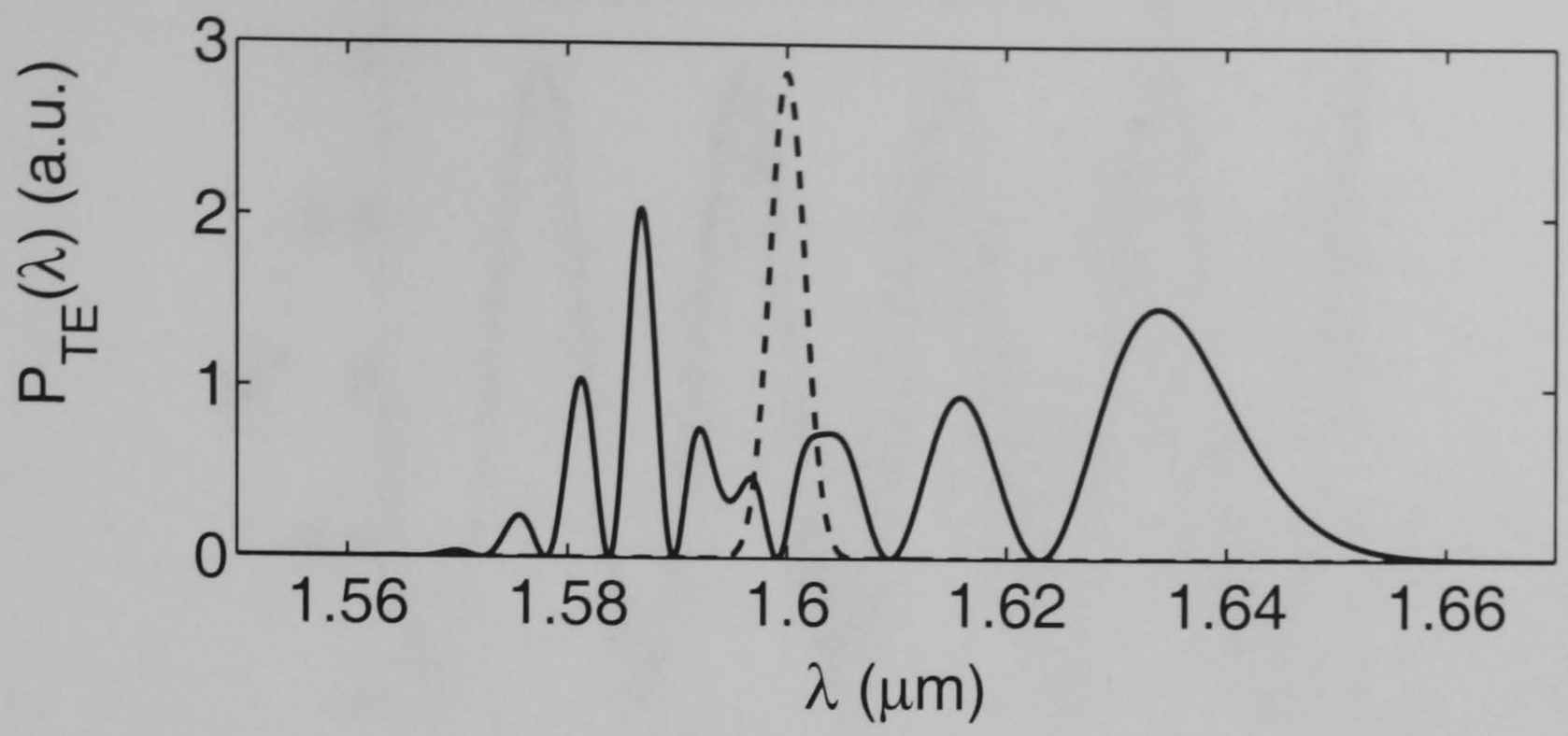

Figure 4.35: Spectrum of self phase modulated optical pulse (solid line), input power $P_0 = 5\,\mathrm{kW}$, all other parameters as in Fig. 4.34, also indicated spectrum of injected optical pulse (dashed).

pulses, the generation of new frequency components can lead to a considerable broadening of the spectrum of the optical pulse. This is shown in Fig. 4.35. The spectrum is characterized by an oscillatory structure due to interference of the generated frequency components [79]. As was pointed out already in [16], one obtains mainly two structures, an overall pattern due to interference within the upshifted and downshifted regions and a finer structure due to cross interference between upshifted regions.

Fig. 4.34(c) shows a propagated optical pulse under influence of both SPM and dispersion. The interplay between dispersion and nonlinearity can lead to considerable narrowing of the optical pulse. The discussion of further effects arising from both dispersion and nonlinearity will be discussed in the next Chapter.

4.6.2 Mixed Polarisation

As a first example for effects arising from the presence of power in both modes we consider the effect on the polarisation state in the structure. Here we assume the injection of an optical pulse into the CPW structure which excites both TE and TM mode ($\gamma = 45°$). The cascading between OR and electro-optic effect gives rise to a phase modulation in the optical TE mode, whereas the phase of the TM mode is unaffected by cascading effects.

The influence on the polarisation dynamics is shown in Fig. 4.36. As a measure for circular polarisation the parameter $m_c = S_3/I$ is plotted with S_3 being the Stokes parameter defined as,

$$S_3 = \langle \mathrm{i}(U_{\mathrm{TE}} U_{\mathrm{TM}}^* - U_{\mathrm{TE}}^* U_{\mathrm{TM}}) \rangle \,, \tag{4.101}$$

and the irradiance I,

$$I = \langle |U_{\mathrm{TE}}|^2 + |U_{\mathrm{TM}}|^2 \rangle \,, \tag{4.102}$$

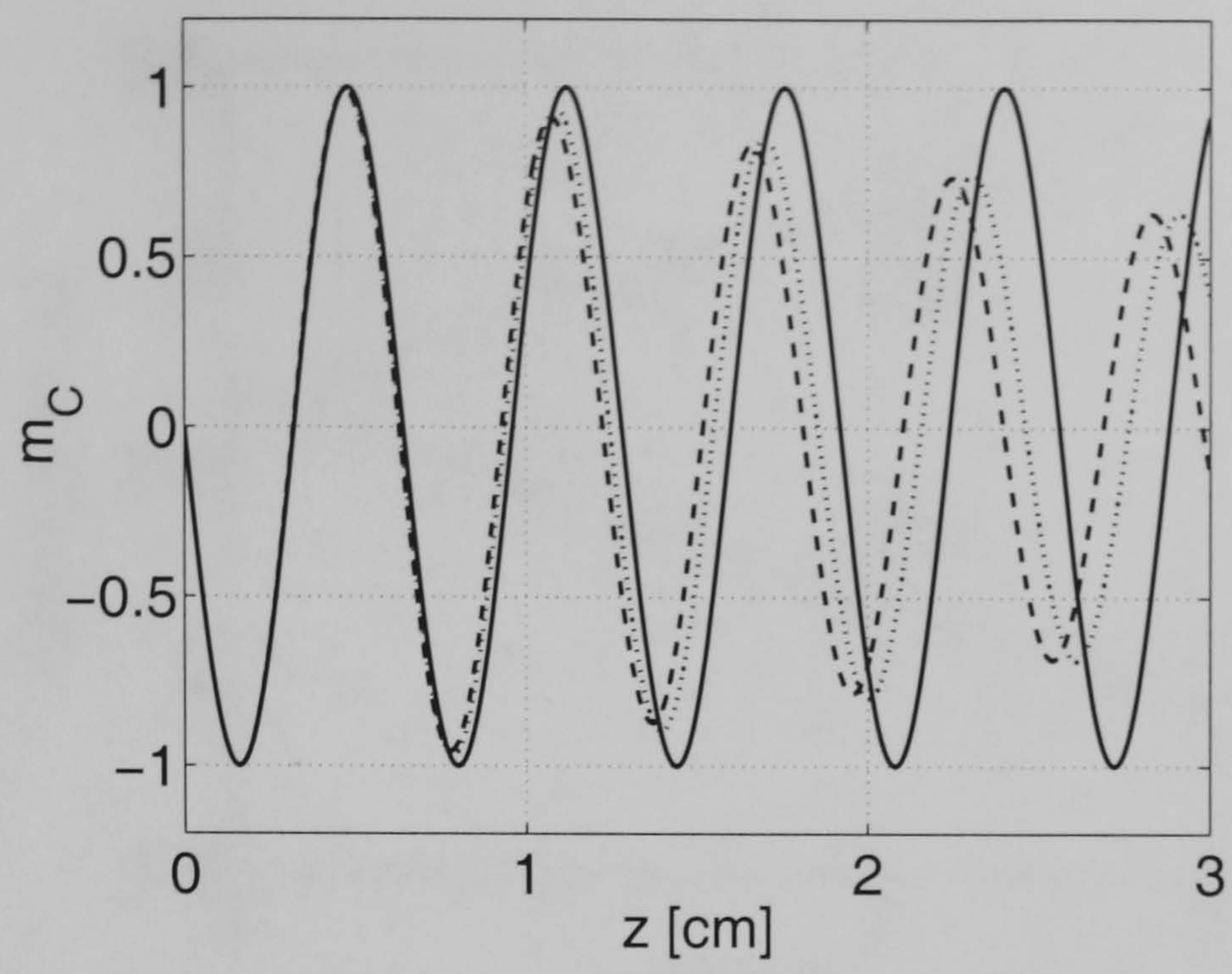

Figure 4.36: Evolution of circular polarisation due to nonlinear phase modulation in TE mode in CPW structure, optical pulse width $T_{\mathrm{FWHM}} = 1\,\mathrm{ps}$. Solid line low power; dashed line optical peak power $P_{\mathrm{o}} = 5\,\mathrm{kW}$, $\alpha_{\mathrm{mic}} = 0$; dotted line $P_{\mathrm{o}} = 5\,\mathrm{kW}$, $\alpha_{\mathrm{mic}} = 10\,\mathrm{dB/cm}$. All parameters as in Appendix F but $\Delta n = -0.038$.

where $\langle * \rangle$ denotes the time average. At low powers the change of polarisation state is governed by the different phase velocities of both optical modes resulting in periodic changes between linear and circular polarisation. At high optical powers we have an additional phase modulation of the TE mode due to the influence of the generated microwave signal. As a result, we can observe an effective change of the beat length in the structure at high optical powers. Note that the additional nonlinear contribution to the phase $\phi_{\mathrm{TE}}(t, z)$ due to cascading results in a rather complicated time varying polarisation state demonstrated by the decreasing envelope of the time-averaged parameter m_c. The change of polarisation in Fig. 4.36 has been calculated for a slight mismatch between optical and microwave. Here the phase modulation is mainly determined by the microwave pulse travelling with the optical pulse leading to an accumulation of the nonlinear phase $\phi_{\mathrm{TE}}(t, z)$ which is proportional to the optical power distribution. In the velocity matched case the generated microwave and hence the induced phase follows the first derivative of the optical pulse. As a result there is no effective change of beat length due to cancellation effects.

As a further example we consider the effective nonlinearity χ_{eff2}. Here both modes generate a microwave signal corresponding to eq. (4.85), which couples the optical modes according to eq. (4.22, 4.23). Similarly to the discussion in Section 4.4.2, this implies the possibility of self-induced mode conversion in the structure. Again a linearly polarized optical pulse is injected with an angle $\gamma = 45°$, i.e. TE and TM are excited with the same pulse shape and phase. For this symmetric initial conditions an asymmetry is required for mode conversion to occur. This asymmetry is provided by the velocity mismatch $\Delta\beta$. As a result, we observe self-induced mode conversion in the waveguide (see Fig. 4.37). As the combination of both

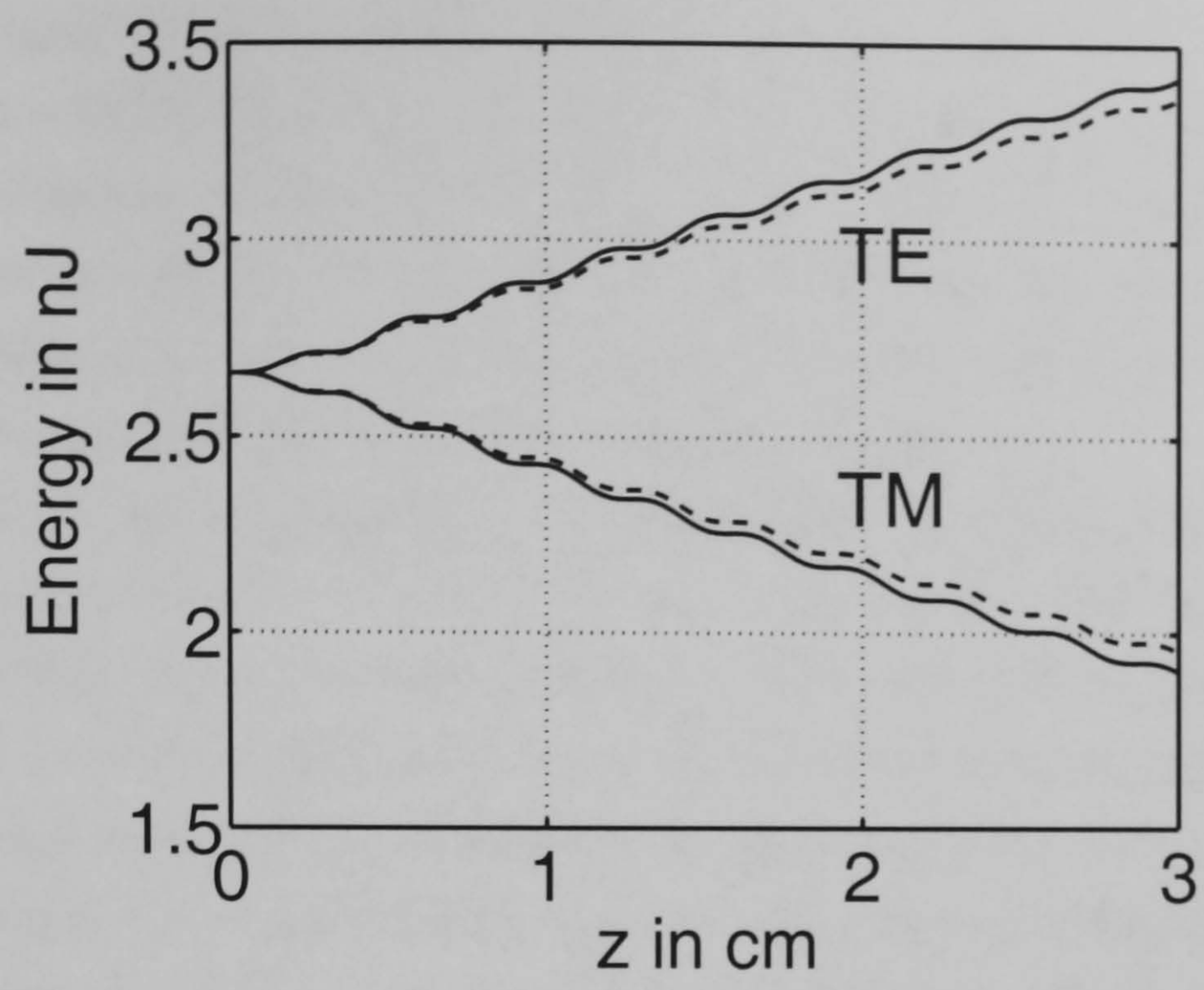

Figure 4.37: Self-induced mode conversion due to cascading of OR and electro-optic effect in CPS structure. Optical peak power $P_o = 5\,\mathrm{kW}$, solid line no losses, dashed line $\alpha_{\mathrm{mic}} = 5\,\mathrm{dB/cm}$. All parameters as in Appendix F but $\Delta n = -0.17$.

modes delivers the source term for the microwave, the amplitude of the generated microwave will finally decrease and so will the conversion of energy. In the case of velocity matching we did not observe an effective mode conversion due to the modulation of the generated microwave signal in propagation direction.

4.7 Conclusions

In this Chapter we considered the interaction of an optical wave with a microwave due to the action of a second order nonlinearity in a travelling wave structure. Evolution equations are derived based on a coupled mode formalism assuming the modes of the respective fields only slightly perturbed. The perturbation manifests itself in an induced polarisation due to the second order nonlinearity. Transverse fields are accounted for by overlap integrals. Included are two optical modes, namely the fundamental TE and TM-like modes interacting with one microwave mode. Dispersion and attenuation are taken into account by an expansion of the propagation constant around the respective center-frequencies of the fields. The set of equations can be solved numerically, or analytically under simplifying assumptions.

The basic properties of the structures under consideration are discussed. Here, techniques are introduced for the calculation of the optical mode and the respective microwave mode which allow the estimation of overlap integrals. Dispersion and attenuation properties of both optical and microwave are discussed. In particular microwave losses are found to considerably influence the propagation of microwaves at high, i.e. near THz, frequencies. For an effective coupling between microwave and optical wave, velocity matching is essential. Therefore

possibilities for tuning of the microwave effective index are discussed. For two example structures, namely a CPW and a CPS structure, typical parameters are estimated and used in subsequent calculations to give quantitative results. Whereas structures based on the AlGaAs system are considered, the essential results should apply for other material systems as well. In particular, the model can be easily adjusted by modification of the polarisation terms based on the susceptibility tensor of the respective material.

In the limit of low optical power the structures work essentially as electro-optic modulators. The two essential modes of action, i.e. phase modulation and mode conversion, are explained on the basis of the example structures. For high optical powers, i.e. for peak powers around $P_0 = 1\,\mathrm{kW}$, excitation terms for the microwave become significant. Assuming a nondepleted pump, analytical expressions for the generated microwave are obtained. If no care is taken to match the velocities of both waves, the velocity mismatch for the example structures is approximately $\Delta n \approx -1$. After the walk-off length, which in this case amounts to only tenths of a mm, two pulses are generated which follow the optical power distribution. One is travelling with the velocity of the microwave und is hence subject to microwave losses, and the other is travelling with the optical wave. Even in the case of high microwave losses of around 100 dB/cm, the latter pulse can have a considerable amplitude as it is steadily pumped by the optical wave. However, the conversion efficiency, which is proportional to the optical power, is extremely low and amounts to $\approx 10^{-7}$ for a peak power $P_0 = 1\,\mathrm{kW}$.

For perfect velocity matching, which could be achieved by application of slow-wave structures, the generated microwave follows the derivative of the optical power distribution and is similar to a quasi single cycle electrical signal. The spectrum is located around a carrier frequency determined by the width of the optical pulse. The conversion efficiency is strongly dependent on the optical pulse width suggesting that for highly efficient OR ultrashort laser pulses are necessary. In the ideal case of a lossless structure the conversion efficiency can reach 10^{-3} for optical pulses in the ps-range and a device length in the cm-range. Here the amplitude of the microwave signal grows linearly with distance. However, high microwave losses, as is the case in typical structures, lead to a saturation of the generated electrical signal typically after a couple of mm so that the efficiency can easily be one to two magnitudes lower than in the lossless case. Nevertheless, the predicted voltages can reach the π-voltage of the corresponding modulator so that cascading effects might be observed at very high optical powers.

Depending on the symmetry of the microwave mode and the susceptibility tensor of the nonlinear material under consideration, the action of both TE and TM modes in the waveguide might be necessary to generate a microwave signal. For the AlGaAs-system, this is the case for a symmetric CPS structure. Here, even a slight difference between both propagation constants, typically around $\Delta n_{\mathrm{opt}} = 2.5 \times 10^{-4}$, can lead to a very different behaviour. The changing polarisation state in the waveguide, i.e. a change between linear and circular

polarisation, results in a modulation of the effective nonlinearity. In the case of perfect velocity mismatch, this leads to a periodic up- and down-conversion with propagation distance. Consequently, the length of a device for microwave generation has to be chosen carefully. In case of a slight velocity mismatch between microwave and optical wave, a sinusoidal electric signal evolves between the two pulses travelling with the optical and microwave velocities. By matching the beat length of the two optical modes to the walk-off length one obtains a rather efficient narrow-bandwidth source which can potentially be tuned by adjusting the beat length via the electro-optic effect. The main problem here is the damping of the microwave components which have left the optical pulse resulting in an exponentially decreasing envelope of the microwave signal.

Finally, similar to the case of second harmonic generation, the generated microwave can act back on the optical wave giving rise to a phase shift due to the electro-optic effect. This cascading effect leads essentially to an effective Kerr nonlinearity. In the case of velocity mismatch, after the walk-off length the evolution of the optical wave is approximately governed by a nonlinear Schroedinger equation. The effective cubic nonlinearity is inversely proportional to the velocity mismatch, and its magnitude and sign can potentially be tuned by application of slow-wave structures. For perfect velocity matching, the induced phase is proportional to the derivative of the optical power distribution. The resulting broadened spectrum due to self phase modulation is different in structure than in the case of a Kerr nonlinearity. Some further ideas explored are the change of beat length and hence polarisation state of the optical wave as well as self induced mode conversion from TE to TM due to cascading effects. However, in these cases a very high optical peak power of around $P_0 \approx 5\,\mathrm{kW}$ is required. In all cases we neglected the intrinsic cubic nonlinearity of the material. The competition between both second and third (or higher) order nonlinearities might influence or even dominate the cascading effects considered here. Whereas a modification of the model to higher order nonlinearities is straightforward, the consideration of those effects will be left for future investigation.

5 Solitary Waves due to Cascading of Optical Rectification and the Electro-Optic Effect

5.1 Introduction

Many traditional systems in physics describing the evolution of magnitudes in time and space rely on models which are inherently linear and time-invariant. By linear we mean that the response of a system is proportional to the amplitude at the input. One important phenomenon, among others, of propagation of a pulse in linear transmission systems is dispersion. This means that the different spectral components of the input pulse travel with different velocities leading to a change of the pulseform, e.g. broadening, after a certain propagation distance simply because the different spectral components arrive at different times at the output of the system. A variety of phenomena in nature cannot be considered as linear. Here the response of the system depends strongly on the amplitude of the input signal. As an example, the velocity of the spectral components of a pulse can be intensity dependent. In certain circumstances, i.e. for a certain pulse shape, the nonlinearity in the system can counteract or even cancel the linear dispersion. Such a pulse is called a *solitary wave* or, if some other conditions are fulfilled, a *soliton*. Soliton propagation has been demonstrated in a variety of nonlinear systems and is now a well investigated area of research.

The first documented observation of solitary waves dates back to the year 1834, when John Scott Russell observed a

> "...rounded, smooth and well defined heap of water, which continued its course along the channel apparently without change of form or diminution of speed." [80]

What Mr. Russell observed was indeed a soliton which is a solution of the Korteweg de Vries (KdV) equation. The KdV equation is one of the classical equations describing nonlinear wave phenomena and is suitable to describe the evolution of water waves in shallow water channels (see, for example [81]). In 1965, Zabusky and Kruskal [82] performed numerical experiments with solutions of the KdV equation and observed that solitary wave solutions retained their shape upon collisions with other solitary waves. The discovery that these solutions behave somewhat like particles lead to the name soliton. The fact that solitons

show a behaviour which we would expect for linear equations, e.g. the ability to form a solution under superposition, supposes that nonlinear systems which exhibit soliton solutions exhibit special properties.

This special property is called integrability and implies that the system can be solved analytically by a technique called *Inverse Scattering Transform* [83]. That is, given an initial condition of the system, the solution can, in principle, be explicitly determined for all time. Important examples for integrable and hence analytically solvable nonlinear dynamic systems are the KdV equation or the Nonlinear Schroedinger Equation (NLS) which will be introduced in an upcoming Section. Integrable nonlinear systems show remarkable properties, one of them being that solitons are always stable against small perturbations. However, numerous nonlinear systems in physics are nonintegrable or only integrable under certain approximations. Nevertheless, among their solutions are bound states which show soliton-like, e.g. dispersionless, propagation. These soliton-like pulses can show a rich dynamic behavior, ranging from instability to complicated interaction scenarios. Bound states in integrable systems are traditionally called solitons whereas bound solutions in nonintegrable systems are termed solitary waves. However, following the trend in the literature, in this thesis we neglect this strict distinction and refer to bound states in our system (which is in general nonintegrable) occasionally as solitons.

Research in optical soliton propagation was motivated by the possibility of dispersionless long distance propagation in optical fibers [75]. Proposed in 1973 by Hasegawa and Tappert [84], the first experimental observation of optical solitons was demonstrated by Mollenauer *et al.* in 1980 [85]. The origin of the nonlinearity in an optical fiber is the cubic or Kerr nonlinearity resulting in an intensity dependent phase shift in the optical wave which can counterbalance dispersion or diffraction of the respective pulse. However, optical soliton formation is not restricted to cubic media. In fact, it was shown a quarter of a century ago by Karamzin and Sukhorukov [86] that the interaction of a fundamental with its second harmonic in a medium with quadratic nonlinearity can also lead to solitary waves. The extensive theoretical investigation of this effect, in the following also called SHG cascading, has been carried out only in the last decade [14, 15, 77, 78]. Spatial formation of diffractionless beams due to SHG cascading was demonstrated experimentally in [87, 88].

In this Chapter we will demonstrate that the interaction of an optical wave with a microwave in a quadratic material also offers the possibility of soliton formation. As was already discussed in Section 4.6, here an effective cubic nonlinearity arises from a cascaded process of optical rectification (OR) and the electro-optic effect. First attempts to exploit this cascading effect for soliton formation were the prediction of diffractionless beams in the continuous wave limit [20] and the formation of a new type of Bragg grating solitons [21]. In both cases the appearance of a pure DC field does not require a separate evolution equation and the

final expression corresponds to a simple cubic nonlinearity. However, in this work we are interested in transient effects, where the temporal evolution of the microwave signal plays a significant role. This kind of interaction was considered by Kalocsai and Haus in [22], where the mutual interaction of an optical pulse with a quasi-static field in a bulk medium was investigated. Neglecting the transverse spatial derivatives, the equations come close to the case of a waveguiding structure considered here. Also in this work analytical soliton solutions were suggested.

Before moving on to temporal solitons via OR and the electro-optic effect, we will briefly introduce two important nonlinear wave equations, the KdV equation and the NLS equation, which are somehow the building blocks of the system we are interested in - the long wave short wave interaction.

5.2 Relevant Soliton Equations

5.2.1 The Korteweg de Vries Equation

There are a number of principal types of equations describing nonlinear wave propagation in physical systems. Characteristic for a number of those equations is the simultaneous description of propagation, dispersion and nonlinearity. Two important equations which are closely related to the problem considered here are the Korteweg de Vries (KdV) equation and the Nonlinear Schroedinger (NLS) equation.

The KdV equation describes the unidirectional propagation of long waves, i.e. with a narrow frequency spectrum around zero, under influence of the lowest order of dispersion and nonlinearity. Originally derived for the propagation of water waves in shallow water channels [89], the equation is a useful approximation for a variety of physical phenomena (see, for example, [90] and references therein). An interesting example related to the work in this thesis is the evolution of electrical signals on nonlinear transmission lines [91], [92]. The KdV equation can be written in the form,

$$\left[\frac{\partial}{\partial z} + (\delta + \alpha u)\frac{\partial}{\partial t} + \beta\frac{\partial^3}{\partial t^3}\right] u = 0 \,, \tag{5.1}$$

where $u(z,t)$ is a real valued function. α and β are parameters determining nonlinearity and dispersion, respectively. The parameter δ is related to the propagation velocity of plane waves.

If the effects of dispersion and nonlinearity are small, the solution of eq. (5.1) is simply a travelling wave which propagates at speed $v = 1/\delta$. From this follows intuitively the action of the nonlinearity: the wave can be thought of having an amplitude dependent velocity $v = 1/(\delta + \alpha u)$. Hence, larger amplitudes travel slower or faster depending on the sign of α and u respectively. This effect can lead to self steepening and finally to the breaking of waves. Neglecting the nonlinearity, the dispersion relation of linear waves $u(z,t) = \sin(\omega t - kz)$ is

given by $k = \delta\omega - \beta\omega^3$. This means, both phase and group velocity are frequency dependent leading to a distortion of the original pulse while propagating. Under certain circumstances both dispersion and nonlinearity can cancel each other leading to soliton propagation. A single soliton solution of eq. (5.1) is given by,

$$u = \eta \operatorname{sech}^2 \left[\sqrt{\frac{\eta\alpha}{12\beta}} (t - dz) \right] \quad \text{with} \quad d = \delta + \frac{1}{3}\alpha\eta \,, \tag{5.2}$$

where η is a parameter relating amplitude, speed and width of the soliton. A pulse with greater height has a faster speed and smaller width. The KdV equation is integrable and can be solved by means of the Inverse Scattering Transform [93].

5.2.2 The Nonlinear Schroedinger Equation

A number of evolving physical quantities can be described by a slowly varying envelope function with a fast changing underlying carrier frequency ω_0,

$$U(z,t) = u(z,t) \exp[-\mathrm{i}\omega_0 t] + c.c. \quad . \tag{5.3}$$

Rather then considering the actual amplitude function $U(z,t)$, it is often convenient to describe the evolution of $U(z,t)$ only with the envelope function $u(z,t)$.

The Nonlinear Schroedinger (NLS) equation describes the evolution of *wave packets*, i.e. the envelope function, under influence of the lowest order of nonlinearity and dispersion. In scaled variables the equation can be written as,

$$\mathrm{i}\frac{\partial u}{\partial z} - \frac{1}{2}\frac{\partial^2 u}{\partial t^2} - |u|^2 u = 0 \,, \tag{5.4}$$

where the second term describes group velocity dispersion (GVD) and the third term the nonlinearity. $u(z,t)$ is in general a complex valued function. Examples for the appearance of the NLS equation are light wave propagation [75] or surface water waves [81].

Whereas the sole action of dispersion leads to broadening of a propagating pulse, the nonlinearity manifests itself in a power dependent phase shift (for details, see for example [75]). As in the case of the KdV equation, both effects can cancel each other giving rise to soliton formation. Indeed a variety of soliton solutions exist [75], the fundamental bright soliton given by,

$$u(z,t) = \eta \operatorname{sech}[\eta(t - \kappa z)] \exp[-\mathrm{i}\kappa t - \mathrm{i}(\eta^2 - \kappa^2)/2\ z]. \tag{5.5}$$

The pulse height η is inversely proportional to the pulse width with a velocity κ being an independent parameter. The NLS equation also belongs to the class of completely integrable systems.

5.2.3 Long Wave Short Wave Interaction

It was early noticed that long waves, i.e. with a narrow frequency spectrum around zero, and short waves, i.e. located around a center frequency and described by an envelope function, can interact with each other [94]. The basic idea in this type of wave interaction is that both long and short waves can become resonant provided the group velocity of the short wave is equal to the phase velocity of the long wave, which is sometimes called the Zakharov-Benney long wave short wave resonance [81]. The long wave short wave (LWSW) system relevant for this thesis can be written in the form,

$$\frac{\partial u_\mathrm{l}}{\partial z} + \delta\frac{\partial u_\mathrm{l}}{\partial t} + \alpha\, u_\mathrm{l}\frac{\partial u_\mathrm{l}}{\partial t} + \beta\,\frac{\partial^3 u_\mathrm{l}}{\partial t^3} - \frac{\partial |u_\mathrm{s}|^2}{\partial t} = 0\,, \tag{5.6}$$

$$\mathrm{i}\frac{\partial u_\mathrm{s}}{\partial z} - \frac{\partial^2 u_\mathrm{s}}{\partial t^2} - u_\mathrm{l} u_\mathrm{s} = 0\,, \tag{5.7}$$

where u_l is the real valued amplitude function of the long wave and u_s is the complex valued envelope function of the short wave. Note that in the case of a negligible short wave, eq. (5.6) reduces to the KdV equation. The evolution equation for the short wave is more similar to the NLS equation. However, the nonlinearity arises from the interaction with the long wave. Interestingly, as will be shown in a subsequent Section, for high velocity mismatch between both waves eq. (5.7) reduces to the NLS equation. Hence, the LWSW system can be seen as a combination of both fundamental nonlinear systems. A fascinating manifestation of this hybrid nature is the occurrence of quasibound internal modes of soliton solutions, which will be discussed in detail in Chapter 6.

The LWSW equations were shown to be integrable for $\alpha = \beta = \delta = 0$. An analysis by means of the inverse scattering transform can be found in [95], [96]. A single soliton solution for this case is given by,

$$u_\mathrm{s} = \mathrm{i}2\eta\sqrt{\kappa}\,\mathrm{sech}[\eta t + 2\kappa\eta z]\exp[\mathrm{i}\kappa t + \mathrm{i}(\kappa^2 - \eta^2)z]\,, \tag{5.8}$$

$$u_\mathrm{l} = 2\eta^2\,\mathrm{sech}^2[\eta t + 2\kappa\eta z]\,, \tag{5.9}$$

where κ and η are arbitrary constants. Note that the solution of the long wave is very similar to the KdV soliton eq. (5.2), whereas the envelope function of the short wave maintains the sech-form of the NLS solution eq. (5.5). However, for nonvanishing dispersion in the long wave $\beta = 1$ the system was shown to be non-integrable [97]. Due to the strong dispersion of microwaves at high frequencies this is given in most cases for the OR system. A discussion of a variety of solitary wave solutions for the resonant ($\delta = 0$) LWSW system can be found in [98], [99].

The system (5.6, 5.7) or its derivatives have been predicted for a number of physical systems, including the coupling of gravity and capillary modes of surface water waves [100] or the co-propagation of electron-plasma with ion-acoustic waves [101]. An example somehow related to the case considered here is propagation of electrical signals on a nonlinear

transmission line (NTL). Depending on the dispersion relation of the respective NTL and the frequency domain considered, both KdV and NLS equations have been derived for the evolution of the voltage on the transmission line [102], and the LWSW resonance has been predicted in [103]. The first derivation of a system similar to eqs. (5.6, 5.7) for the case of optical rectification can be found in [22], where the interaction of an optical pulse with a quasistatic electric field in bulk material was considered neglecting the transverse spatial derivatives. Here, the long wave corresponds to the electrical signal whereas the short wave is given by the optical wave travelling in the structure.

Interestingly, although the LWSW resonance is discussed in a number of publications, we did not find experimental evidence of soliton formation due to this kind of interaction in the literature.

5.3 Normalisation

In the following we concentrate on the interaction of a single polarized optical wave with a microwave in a travelling wave structure. For both the discussion of solitons and modulational instability we will neglect the attenuation in both the microwave and the optical wave. This is obviously a strong simplification of the corresponding model. However, the aim of the following Chapters is to demonstrate the potential occurrence of these effects leaving the design of an actual structure for future investigation. The scalar interaction equations derived in the preceding Chapter are then given by,

$$\begin{aligned}\left[\frac{\partial}{\partial Z}+\frac{\Delta n}{c}\frac{\partial}{\partial T}-\frac{T_{\mathrm{mic}}}{6}\frac{\partial^3}{\partial T^3}\right]U_{\mathrm{m}}-\frac{\chi_{\mathrm{eff1}}}{2}\frac{\partial}{\partial T}|U_{\mathrm{o}}|^2-\chi_{\mathrm{eff3}}\frac{\partial}{\partial T}U_{\mathrm{m}}^2=0\,,\\ \left[\mathrm{i}\frac{\partial}{\partial Z}-\frac{D_{\mathrm{opt}}}{2}\frac{\partial^2}{\partial T^2}-\omega_{\mathrm{o}}\chi_{\mathrm{eff1}}U_{\mathrm{m}}\right]U_{\mathrm{o}}-\mathrm{i}\chi_{\mathrm{eff1}}\frac{\partial}{\partial T}[U_{\mathrm{m}}U_{\mathrm{o}}]=0\,.\end{aligned}\tag{5.10}$$

It is useful to normalize the equations to a dimensionless form. The aim of this procedure is to reduce the number of independent parameters and hence to simplify and generalize the equations. We proceed by introducing the following dimensionless variables,

$$z=\frac{Z}{Z_0}\,,t=\frac{T}{T_0}\,,u_{\mathrm{m}}=\frac{U_{\mathrm{m}}}{A_{\mathrm{mic}}}\,,u_{\mathrm{o}}=\frac{U_{\mathrm{o}}}{A_{\mathrm{opt}}}\,,\sigma_{\mathrm{m}}=\frac{T_{\mathrm{mic}}}{|T_{\mathrm{mic}}|}\,,\sigma_{\mathrm{o}}=\frac{D_{\mathrm{opt}}}{|D_{\mathrm{opt}}|}\,.\tag{5.11}$$

After inserting eq. (5.11) into eqs. (5.10) we obtain,

$$\begin{aligned}\left[\frac{\partial}{\partial z}+\delta\frac{\partial}{\partial t}-\sigma_{\mathrm{m}}\frac{\partial^3}{\partial t^3}\right]u_{\mathrm{m}}-\chi\frac{\partial}{\partial t}u_{\mathrm{m}}^2-\frac{\partial}{\partial t}|u_{\mathrm{o}}|^2=0\,,\\ \left[\mathrm{i}\frac{\partial}{\partial z}-\frac{\sigma_{\mathrm{o}}}{2}\frac{\partial^2}{\partial t^2}-u_{\mathrm{m}}\right]u_{\mathrm{o}}-\mathrm{i}\zeta\frac{\partial}{\partial t}[u_{\mathrm{o}}u_{\mathrm{m}}]=0\,,\end{aligned}\tag{5.12}$$

where we have set,

$$A_{\mathrm{mic}} = \frac{36|D_{\mathrm{opt}}|^3}{\omega_{\mathrm{o}}\chi_{\mathrm{eff1}}|T_{\mathrm{mic}}|^2}\,, \quad A_{\mathrm{opt}} = \frac{12|D_{\mathrm{opt}}|^2}{\chi_{\mathrm{eff1}}|T_{\mathrm{mic}}|}\sqrt{\frac{3|D_{\mathrm{opt}}|}{\omega_{\mathrm{o}}|T_{\mathrm{mic}}|}}\,,$$
$$Z_0 = \frac{|T_{\mathrm{mic}}|^2}{36|D_{\mathrm{opt}}|^3}\,, \quad T_0 = \frac{|T_{\mathrm{mic}}|}{6|D_{\mathrm{opt}}|}\,, \tag{5.13}$$
$$\delta = \frac{|T_{\mathrm{mic}}|\Delta n}{6|D_{\mathrm{opt}}|^2 c}\,, \quad \zeta = \frac{6|D_{\mathrm{opt}}|}{\omega_{\mathrm{o}}|T_{\mathrm{mic}}|}\,, \quad \chi = \frac{6\chi_{\mathrm{effm}}|D_{\mathrm{opt}}|}{\chi_{\mathrm{eff1}}\omega_{\mathrm{o}}|T_{\mathrm{mic}}|}\,.$$

In eqs. (5.12) coefficients in front of terms which are essential for the cascading effects discussed below are fixed. These are terms corresponding to the electro-optic effect, excitation of the microwave as well as both dispersion terms. Note that the dispersion coefficients are $\sigma_{\mathrm{m}} = \pm 1$ and $\sigma_{\mathrm{o}} = \pm 1$ corresponding to normal and anomalous dispersion respectively.

Apart from the energy conservation term with a scaled variable ζ eqs. (5.12) have essentially the same form as eqs. (5.6, 5.7) and are hence another example for long wave short wave interaction in physics. However, the parameter ζ is small and can usually be neglected. For the example structure described in Appendix F, it amounts to $\zeta = 6 \times 10^{-4}$. Similarly, the microwave self-interaction term due to the intrinsic nonlinearity is small. For the example structure it amounts to $\chi = 5 \times 10^{-5}$ and has no significant influence on the evolution dynamics.

The parameter δ is proportional to the velocity mismatch between optical wave and microwave and, as indicated earlier, can be tuned by application of slow wave structures. We chose therefore δ to be a variable system parameter.

Most of the results below are presented in scaled variables. However, where appropriate we will give values of physical magnitudes involved corresponding to the example structure in Appendix F. Whereas this structure is by no means designed for the observation of the effects described here, it gives insight into the problems one might face in an actual experiment. All scaling parameters for the example structure are given in Tab. F.4 in Appendix F.

5.4 Conservation Laws and Hamiltonian Structure

Conservation laws are a useful tool for the explanation of the dynamics of a nonlinear system. As pointed out earlier in Chapter 4, if we neglect dissipative terms, the system of equations (5.10) conserves energy. In the scaled system chosen here the energy conservation relation reads as,

$$\frac{d}{dz}\int_{-\infty}^{\infty}\left(\frac{\zeta}{2}u_{\mathrm{m}}^2 + |u_{\mathrm{o}}|^2\right)\,dt = 0\,. \tag{5.14}$$

As pointed out in Section 5.3, ζ is a small parameter. This corresponds to the fact that most of the energy in OR is located in the optical pulse. We checked that ζ has no qualitative and almost no quantitative effect on the effects described below, e.g. the formation of solitary

waves and modulational instability. Therefore, in this Section we will neglect the parameter ζ leading to a simpler mathematical formulation. The same applies to the microwave self-interaction term described by the parameter χ. In the following we consider the system of equations,

$$\begin{aligned} \left[\frac{\partial}{\partial z} + \delta\frac{\partial}{\partial t} - \sigma_{\mathrm{m}}\frac{\partial^3}{\partial t^3}\right] u_{\mathrm{m}} - \frac{\partial}{\partial t}|u_{\mathrm{o}}|^2 = 0\,, \\ \left[\mathrm{i}\frac{\partial}{\partial z} - \frac{\sigma_{\mathrm{o}}}{2}\frac{\partial^2}{\partial t^2} - u_{\mathrm{m}}\right] u_{\mathrm{o}} = 0\,. \end{aligned} \tag{5.15}$$

The interpretation of nonlinear evolution equations as a Hamiltonian system has become an important aspect in the analysis of nonlinear systems in recent years [83]. As an example, conservation laws can arise from symmetries of the system under consideration. Rather then going into details of the theory we will demonstrate in this Section that the system eqs. (5.15) is Hamiltonian and derive conservation laws which are useful for the interpretation of results in Chapter 6. A detailed discussion of the Hamiltonian formalism and its use in nonlinear dynamics can be found, for example, in [83], [104].

Rewriting the system in terms of a Hamiltonian requires the identification of generalized coordinates $[q(z,t), r(z,t)]$ and momenta $[p(z,t), s(z,t)]$ such that the evolution equations can be written as,

$$\frac{\delta H}{\delta r} = -\frac{\partial s}{\partial z}\,, \quad \frac{\delta H}{\delta s} = \frac{\partial r}{\partial z}\,, \tag{5.16}$$

$$\frac{\delta H}{\delta q} = -\frac{\partial p}{\partial z}\,, \quad \frac{\delta H}{\delta p} = \frac{\partial q}{\partial z}\,, \tag{5.17}$$

where $\delta H/\delta r$ denotes the functional or variational derivative. Defining generalized coordinates r, q and momenta p, s as,

$$r = \mathrm{Re}(u_{\mathrm{o}})\,, \quad s = \mathrm{Im}(u_{\mathrm{o}})\,, \quad p = \frac{u_{\mathrm{m}}}{2}\,, \quad ,\partial_t q = p\,, \tag{5.18}$$

the system of eqs. (5.15) is recovered from eqs. (5.16, 5.17) by defining a Hamiltonian as,

$$H = -\int_{-\infty}^{\infty}\left[\frac{\sigma_{\mathrm{o}}}{4}\left(\frac{\partial r}{\partial t}\right)^2 + \frac{\sigma_{\mathrm{o}}}{4}\left(\frac{\partial s}{\partial t}\right)^2 + \sigma_{\mathrm{m}}\frac{\partial p}{\partial t}\frac{\partial^2 q}{\partial t^2} + \delta p\frac{\partial q}{\partial t} - \frac{1}{2}(r^2+s^2)\left(\frac{\partial q}{\partial t} + p\right)\right] dt\,. \tag{5.19}$$

In the following we will use the Hamiltonian formulation to derive conservation laws of the system eqs. (5.15). Here we use invariances, i.e. transformations under which the system does not change its properties. A corresponding variation of the Hamiltonian reproduces a conservation law of the system. The symmetries of the system eq. (5.15) are as follows:

1. The system is invariant against translations in z. Translational invariance with respect to z corresponds in general to the conservation of the Hamiltonian itself.

2. The system is invariant against translations in t.

3. As the microwave amplitude is proportional to the derivative $\partial_t q$, a constant can be added to q without influencing the dynamics of the system.

4. A constant phase in the optical wave has no influence on the evolution of the microwave.

5. A constant electrical background signal adds only a variable phase to the optical wave,

$$u_\mathrm{m} \to u_\mathrm{m} + a_\mathrm{m}\,, u_\mathrm{o} \to u_\mathrm{o} \exp[\mathrm{i} a_\mathrm{m} z]\,. \tag{5.20}$$

The variations of the Hamiltonian with respect to the symmetries stated above can be written as,

$$\begin{aligned}
H[p(z+z_0), q(z+z_0), r(z+z_0), s(z+z_0)] - H(p,q,r,s) &= 0\,,\\
H[p(t+t_0), q(t+t_0), r(t+t_0), s(t+t_0)] - H(p,q,r,s) &= 0\,,\\
H(p, q+q_0, r, s) - H(p,q,r,s) &= 0\,,\\
H[p, q, r\cos(\alpha_0) + s\sin(\alpha_0), -r\sin(\alpha_0) + s\cos(\alpha_0)] - H(p,q,r,s) &= 0\,,\\
H[p + a_0/2, q + t a_0/2, r\cos(a_0 z) + s\sin(a_0 z), -r\sin(a_0 z) + s\cos(a_0 z)] - H(p,q,r,s) &= 0\,.
\end{aligned} \tag{5.21}$$

Differentiating with respect to the variations (quantities with index 0) in eqs. (5.21) leads to the following conserved quantities,

$$\frac{\partial H}{\partial z} = \frac{\partial}{\partial z} \int_{-\infty}^{\infty} \left[\frac{\sigma_\mathrm{o}}{2} \left| \frac{\partial u_\mathrm{o}}{\partial t} \right|^2 + \frac{\delta}{2} u_\mathrm{m}^2 + \frac{\sigma_\mathrm{m}}{2} \left(\frac{\partial u_\mathrm{m}}{\partial t} \right)^2 - u_\mathrm{m} |u_\mathrm{o}|^2 \right] dt = 0\,, \tag{5.22}$$

$$\frac{\partial}{\partial z} I = \frac{\partial}{\partial z} \int_{-\infty}^{\infty} \left(-\frac{1}{2} u_\mathrm{m}^2 + u_\mathrm{o}^\mathrm{r} \frac{\partial u_\mathrm{o}^\mathrm{i}}{\partial t} - u_\mathrm{o}^\mathrm{i} \frac{\partial u_\mathrm{o}^\mathrm{r}}{\partial t} \right) dt = 0\,, \tag{5.23}$$

$$\frac{\partial}{\partial z} M_\mathrm{m} = \frac{\partial}{\partial z} \int_{-\infty}^{\infty} u_\mathrm{m}\, dt = 0\,, \tag{5.24}$$

$$\frac{\partial}{\partial z} E_\mathrm{opt} = \frac{\partial}{\partial z} \int_{-\infty}^{\infty} |u_\mathrm{o}|^2\, dt = 0\,, \tag{5.25}$$

$$\frac{\partial}{\partial z} S_\mathrm{m} - \delta M_\mathrm{m} + E_\mathrm{opt} = \frac{\partial}{\partial z} \int_{-\infty}^{\infty} t\, u_\mathrm{m}\, dt - \delta \int_{-\infty}^{\infty} u_\mathrm{m}\, dt + \int_{-\infty}^{\infty} |u_\mathrm{o}|^2\, dt = 0\,. \tag{5.26}$$

As pointed out earlier, eq. (5.22) corresponds to the fact that the Hamiltonian itself is a conserved quantity. The conservation law eq. (5.23) relates the impulse of the optical wave to the energy of the microwave. According to eq. (5.24), for the microwave we obtain a conserved quantity M_m similar to an effective mass. Due to the neglect of the small parameter ζ, the energy of the optical wave E_opt is conserved (eq. 5.25). Finally, the conservation law eq. (5.26) states that the center of gravity of the microwave amplitude moves with a constant

velocity depending on velocity mismatch, mass of the microwave and energy of the optical wave. As will be shown later, the last conservation law is useful for the interpretation of some results concerning the stability of soliton solutions.

5.5 Modulational Instability

A simple stationary solution of a variety of nonlinear wave equations are continuous plane waves (CW) with an amplitude not depending on spatial or temporal variables. The interplay between dispersion and nonlinearity in such a system can lead to an exponential grow of small perturbations and finally the break up of the CW solution, a phenomenon usually referred to as Modulational Instability (MI). As this instability can lead to the transformation of a CW solution into well defined patterns or trains of solitons, MI is strongly related to soliton propagation.

In the context of optical wave propagation, MI can occur, for example, in optical fibers, where wave propagation is governed by the nonlinear Schroedinger equation and its derivatives. In the temporal case, MI has been shown to lead to the spontaneous generation of sidebands around the center frequency of a quasi CW optical wave (for a detailed discussion, see [75] and references therein). In the spatial case, the same mechanism manifests itself in the filamentation of high power optical beams.

As for the case of soliton propagation, MI in optical systems is not restricted to media with a Kerr nonlinearity. Recently it was shown that cascading effects between a fundamental and its second harmonic in a system with quadratic nonlinearity can also lead to an instability of stationary CW solutions [105],[106]. It is therefore interesting to investigate if similar effects can be potentially observed due to the interaction of an optical wave with a microwave. The aim of this Section is first to show that this is indeed the case and further to give some indications of physical quantities involved.

Starting point are the scaled scalar interaction equations neglecting the small parameters ζ and χ,

$$\begin{aligned} \left[\frac{\partial}{\partial z} + \delta\frac{\partial}{\partial t} - \sigma_{\mathrm{m}}\frac{\partial^3}{\partial t^3}\right] u_{\mathrm{m}} - \frac{\partial}{\partial t}|u_{\mathrm{o}}|^2 = 0 \,, \\ \left[\mathrm{i}\frac{\partial}{\partial z} - \frac{\sigma_{\mathrm{o}}}{2}\frac{\partial^2}{\partial t^2} - u_{\mathrm{m}}\right] u_{\mathrm{o}} = 0 \,. \end{aligned} \tag{5.27}$$

A simple stationary CW solution of eqs. (5.27) is given by,

$$u_{\mathrm{o}} = a_{\mathrm{o}} \exp[\mathrm{i}(\beta z - \omega t)] \,, \quad u_{\mathrm{m}} = a_{\mathrm{m}} \,, \tag{5.28}$$

with the dispersion relation for the optical wave,

$$\beta = \frac{\sigma_{\mathrm{o}}}{2}\omega^2 - a_{\mathrm{m}} \,. \tag{5.29}$$

Solution (5.28, 5.29) refers to a continuous optical wave with constant amplitude a_o (assumed to be real) which is subject to a phase shift due to the electro-optic effect proportional to a constant DC background field a_m. A solution with a non zero frequency ω corresponds simply to a change of the carrier frequency of the optical wave. As this has no influence on the general behaviour apart from a change of the velocity mismatch between both waves, only the case $\omega = 0$ will be considered.

In the following we are interested in the stability of the CW solution against small perturbations. We hence introduce small changes $\Delta a_o(z,t)$, $\Delta a_m(z,t)$ from the stationary solution as,

$$\begin{aligned} u_o &= [a_o + \Delta a_o(z,t)] \exp[-i a_m z] \,, \\ u_m &= a_m + \Delta a_m(z,t) \,. \end{aligned} \tag{5.30}$$

Inserting the ansatz eqs. (5.30) into eqs. (5.27) and keeping only first order terms in $\Delta a_o(z,t)$ and $\Delta a_m(z,t)$, corresponding to small perturbations, one obtains,

$$\begin{aligned} \left[\frac{\partial}{\partial z} + \delta\frac{\partial}{\partial t} - \sigma_m\frac{\partial^3}{\partial t^3}\right]\Delta a_m - a_o\frac{\partial}{\partial t}(\Delta a_o + \Delta a_o^*) = 0 \,, \\ \left[i\frac{\partial}{\partial z} - \frac{\sigma_o}{2}\frac{\partial^2}{\partial t^2}\right]\Delta a_o - a_o\Delta a_m = 0 \,. \end{aligned} \tag{5.31}$$

The set of equations (5.31) does not contain the constant background field a_m indicating that the optical phase has no influence on the microwave. In what follows we express the perturbations as oscillatory functions,

$$[\Delta a_m, \Delta a_o, \Delta a_o^*]^T = [\epsilon_m(z), \epsilon_o(z), \epsilon_o^*(z)]^T \exp(i\Omega t). \tag{5.32}$$

Note that Δa_o and Δa_o^* denote small perturbations of the optical wave and its complex conjugate and have to be varied independently. Substituting (5.32) into (5.31) leads to the eigenvalue problem,

$$\frac{\partial}{\partial z}[\epsilon] = i\bar{M}[\epsilon] \,, \tag{5.33}$$

where $[\epsilon] = [\epsilon_m, \epsilon_o, \epsilon_o^*]^T$ and the matrix $\bar{M}$ is given by,

$$\bar{M} = \begin{bmatrix} -[\delta\Omega + \sigma_m\Omega^3] & a_o\Omega & a_o\Omega \\ -a_o & \dfrac{\sigma_o\Omega^2}{2} & 0 \\ a_o & 0 & -\dfrac{\sigma_o\Omega^2}{2} \end{bmatrix} . \tag{5.34}$$

Unstable, i.e. growing, frequencies Ω are given by eigenvalues λ of the matrix $\bar{M}$ with negative imaginary part. The eigenvalues are determined by a cubic equation,

$$\lambda^3 + c_1\lambda^2 - c_2\lambda + c_3 - c_1c_2 = 0 \,, \tag{5.35}$$

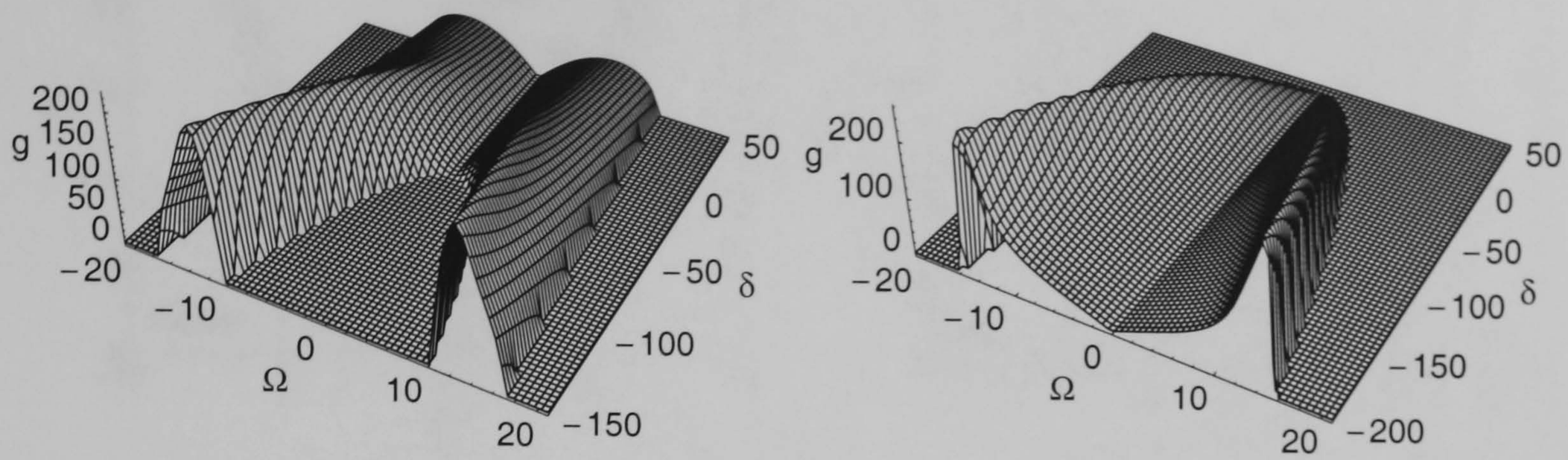

Figure 5.1: Gain g versus frequency detuning Ω and the velocity mismatch δ; amplitude of the optical wave $a_o = 100$. (a) normal dispersion for both waves σ_o=1, σ_m=1, (b) anomalous dispersion for optical wave σ_o=-1, normal dispersion for microwave σ_m=1.

with real valued coefficients $c_1 = \Omega(\delta + \sigma_m\Omega^2)$, $c_2 = \Omega^4/4$, $c_3 = \sigma_o a_o^2\Omega^3$. The solutions of eq. (5.35) are given by,

$$\lambda_1 = u + v - \frac{c_1}{3}\,, \tag{5.36}$$

$$\lambda_{2,3} = -\frac{u+v}{2} - \frac{c_1}{3} \pm \mathrm{i}\frac{\sqrt{3}(u-v)}{2}\,, \tag{5.37}$$

where,

$$\begin{aligned} u &= \sqrt[3]{-q + \sqrt{D}} \quad , \quad v = \frac{p}{u}\,, \\ \text{with} \quad D &= q^2 - p^3 \quad , \quad p = \frac{c_2}{3} + \frac{c_1^2}{9} \quad , \quad q = \frac{1}{3}c_1(\frac{1}{9}c_1^2 - c_2) + \frac{c_3}{2}\,. \end{aligned} \tag{5.38}$$

For $D > 0$ we obtain a pair of complex eigenvalues λ_2, λ_3 and the system is modulationally unstable. $D = 0$ marks hence the boundary to unstable domains. The MI gain for an unstable solution is given by $g = |\mathrm{Im}(\lambda_{2,3})|$. The gain does not depend on the sign of Ω resulting in symmetric sidebands around the carrier frequency of the optical wave. As the MI gain is invariant against the transformation $\sigma_o \to -\sigma_o$, $\sigma_m \to -\sigma_m$, and $\delta \to -\delta$ we can restrict ourselves to the cases of normal dispersion in both waves (σ_o=1, σ_m=1) and anomalous dispersion in the optical wave and normal dispersion in the microwave (σ_o=-1, σ_m=1).

MI is found to exist in a large range of system parameters, i.e. the amplitude of the optical CW solution a_o and the velocity mismatch δ. As shown in Fig. 5.1, a stationary solution can be modulationally unstable in all regimes of dispersion. This is somehow in contrast to MI in Kerr media governed by the nonlinear Schroedinger equation, where MI occurs either for anomalous dispersion (positive nonlinearity) or normal dispersion (negative nonlinearity) [75]. Furthermore, MI exists in domains for which the system exhibits no

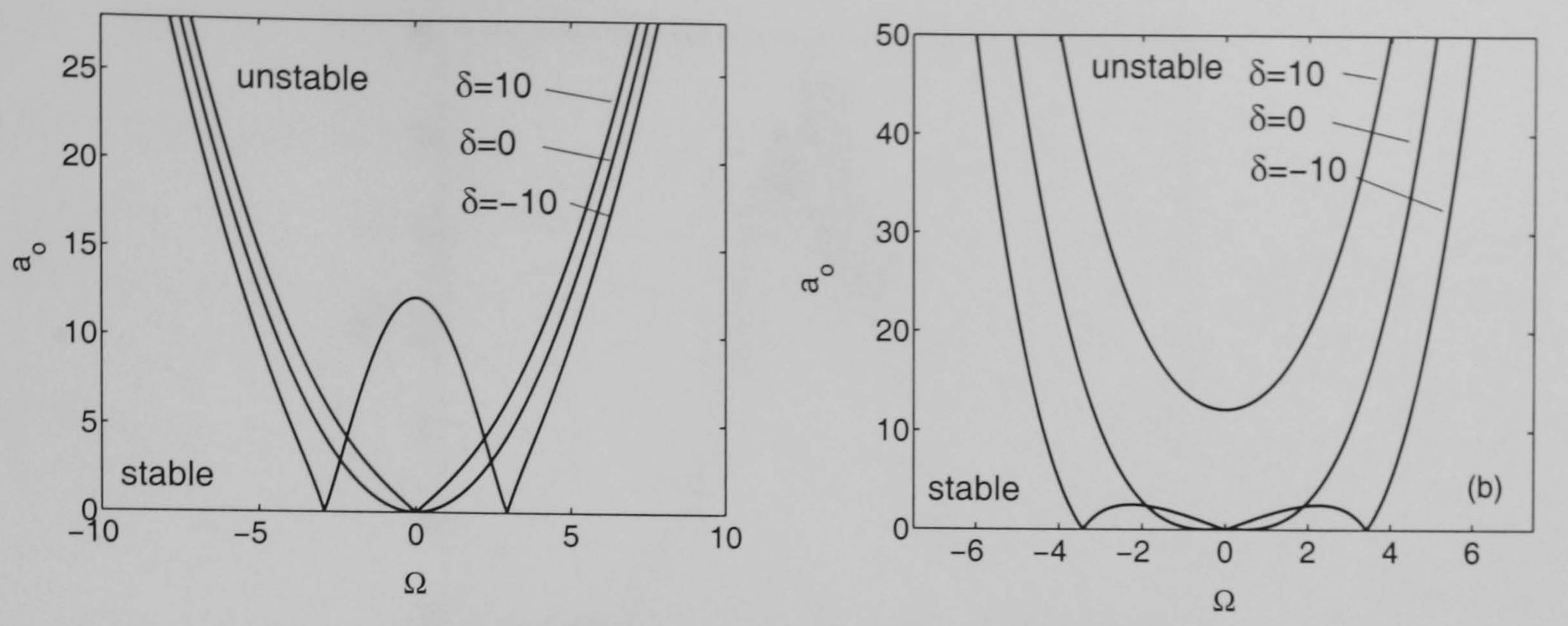

Figure 5.2: Boundary between stable and unstable domains D=0. (a) normal dispersion for both waves σ_o=1, σ_m=1, (b) anomalous dispersion for optical wave σ_o=-1, normal dispersion for microwave σ_m=1.

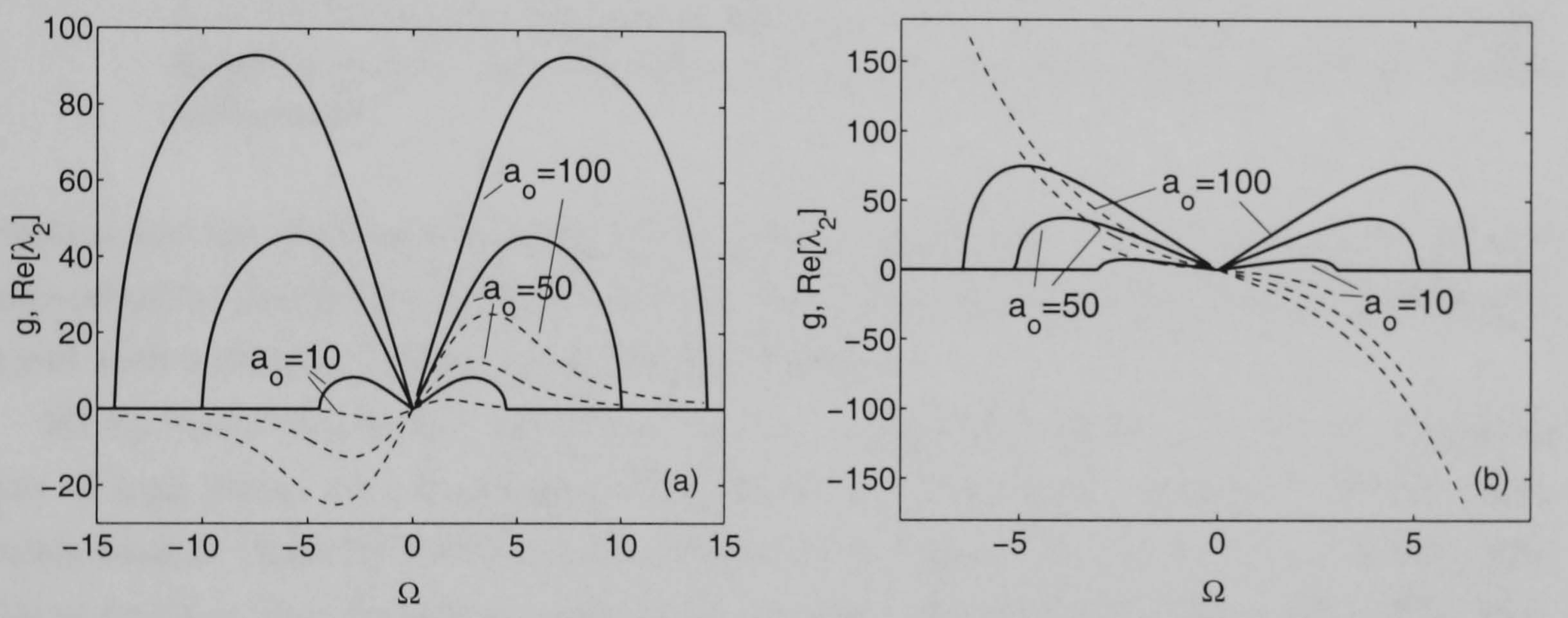

Figure 5.3: MI gain g (solid line) vs. detuning Ω for different amplitudes a_o of CW solution ($\delta = 0$). Also shown real part of eigenvalue Re[λ_2] (dashed line). (a) normal dispersion for both waves σ_o=1, σ_m=1, (b) anomalous dispersion for optical wave σ_o=-1, normal dispersion for microwave σ_m=1.

fundamental bright soliton solutions (see Section 5.6.2). This has also been observed for MI due to SHG cascading [106]. In both dispersion domains the MI gain becomes narrowband and increases with increasing negative velocity mismatch.

In Fig. 5.2 the boundaries between stable and unstable domains $D = 0$ are depicted for both dispersion regions. The bandwidth of unstable frequencies increases with increasing amplitude of the optical wave. For normal dispersion in both waves CW solutions are generally modulational unstable. For normal microwave dispersion and anomalous dispersion in the optical wave a threshold amplitude for the onset of MI exists for positive velocity mismatch $\delta > 0$ given by,

$$a_{oT} = \sqrt{\frac{4\delta^3}{27}} \,. \tag{5.39}$$

As shown in Fig. 5.3, the magnitude of the the MI gain grows with the amplitude of the CW

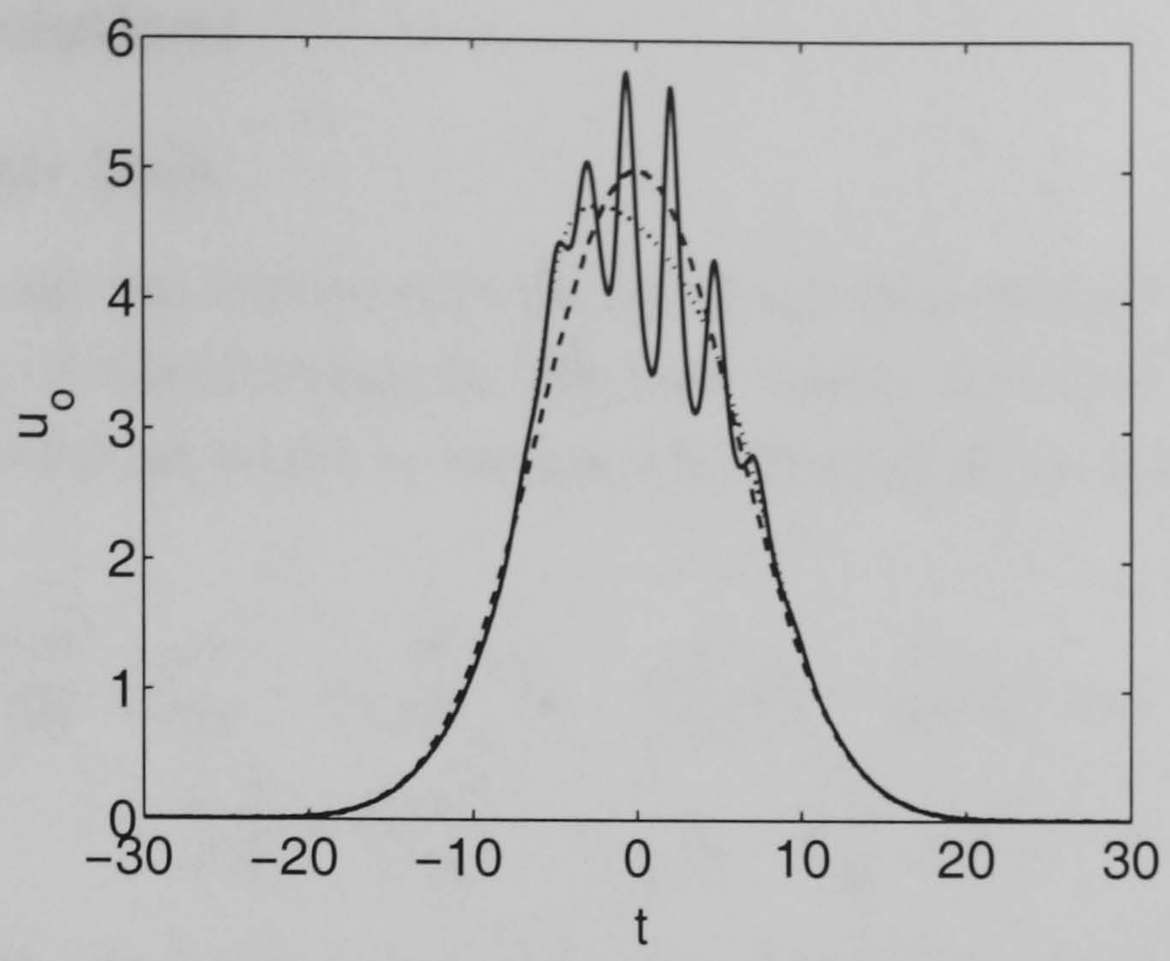

Figure 5.4: Filamentation of an optical pulse due to modulational instability ($u_{\mathrm{m}}(0,t) = 0$), $\delta = -5$, σ_{o}=1, σ_{m}=1), dashed line input pulse at $z = 0$, pulse after propagation length $z = 1.5$: solid line with perturbation (random noise), dotted line without perturbation.

solution and the peak gain detuning shifts to larger frequencies. Further, the eigenvalue corresponding to instability exhibits a real part. This means exponentially growing modulations travel with a velocity different from the optical wave.

MI by interaction with a microwave field may be observed experimentally by filamentation of high power optical pulses propagating in a second order nonlinear material. Here pulses broader than the width corresponding to the sideband frequency with maximum gain $T_{\mathrm{MI}} = 2\pi/\Omega_{\mathrm{max}}$ can develop a spontaneous modulation and finally break up into filaments. Fig. 5.4 shows the outcome of a corresponding numerical experiment obtained from integration of eqs. (5.27). A propagated optical pulse with an initial small perturbation by random noise develops a modulation with a frequency corresponding approximately to the detuning frequency at peak gain $\Omega = 2.57$. This principle could be applied for the generation of trains of ultrashort electrical pulses from high power optical pulses.

Finally, some comments shall be made about the physical magnitudes involved with respect to the example structure in Appendix F. For a peak power of an optical pulse P_{o}=1.5 kW in a structure with a velocity mismatch of $\Delta n = -0.01$, we obtain a scaled peak gain of $g_{\mathrm{max}} \approx 150$ at a detuning frequency $\Omega_{\mathrm{max}} \approx 8.1$. The unscaled gain is then given by $g_r = g/Z_0 \approx 1/\mathrm{cm}$ at a frequency $f = \Omega/(2\pi T_0) \approx 0.9\,\mathrm{THz}$. Keeping in mind that for a spontaneous periodic modulation out of noise the sample length should be a few gain lengths $l_g = 1/g_r$, this value seems not too unrealistic. However, high losses in the microwave might shift the net gain to smaller values and even higher optical peak powers may be necessary.

5.6 Soliton Solutions

5.6.1 Schroedinger Limit

In the following we will demonstrate that the set of equations derived in Chapter 4 indeed offers the possibility of soliton formation. We start with a discussion of the Schroedinger limit, which was already addressed in Section 4.6. Starting point is the scaled system of equations,

$$\begin{aligned}\left[\frac{\partial}{\partial z}+\tilde{\delta}\frac{\partial}{\partial t'}-\sigma_{\mathrm{m}}\frac{\partial^3}{\partial t'^3}\right]\tilde{u}_{\mathrm{m}}-\tilde{\chi}\frac{\partial}{\partial t'}\tilde{u}_{\mathrm{m}}^2-\frac{\partial}{\partial t'}|\tilde{u}_{\mathrm{o}}|^2=0\,,\\ \left[\mathrm{i}\frac{\partial}{\partial z}-\frac{\sigma_{\mathrm{o}}}{2}\frac{\partial^2}{\partial t'^2}-\tilde{u}_{\mathrm{m}}\right]\tilde{u}_{\mathrm{o}}-\mathrm{i}\tilde{\zeta}\frac{\partial}{\partial t'}[\tilde{u}_{\mathrm{o}}\tilde{u}_{\mathrm{m}}]=0\,,\end{aligned} \tag{5.40}$$

where we changed the notation for convenience. For large velocity mismatch between optical wave and microwave $|\tilde{\delta}| \gg 1$, we can neglect the dispersion term and the small parameter $\tilde{\chi}$ in the evolution equation for the microwave. In the stationary limit, an approximate solution for $\tilde{u}_{\mathrm{m}}$ is then given by,

$$\tilde{u}_{\mathrm{m}} \approx \frac{|\tilde{u}_{\mathrm{o}}|^2}{\tilde{\delta}}\,. \tag{5.41}$$

Substituting this approximate solution into the evolution equation for the optical wave and neglecting ζ we derive a nonlinear Schroedinger equation,

$$\mathrm{i}\frac{\partial \tilde{u}_{\mathrm{o}}}{\partial z}-\frac{\sigma_{\mathrm{o}}}{2}\frac{\partial^2 \tilde{u}_{\mathrm{o}}}{\partial t'^2}-\frac{1}{\tilde{\delta}}|\tilde{u}_{\mathrm{o}}^2|\tilde{u}_{\mathrm{o}}=0\,. \tag{5.42}$$

Interestingly, a similar Schroedinger limit exists in the case of second harmonic cascading at large phase mismatch [14].

The sign and the magnitude of the effective cubic nonlinearity $\chi^{(3)}_{\mathrm{eff}} = 1/\tilde{\delta}$ is entirely determined by the velocity mismatch between optical and microwave and can be tuned by changing the phase velocity of the microwave. The fundamental bright soliton solution in the regime of large velocity mismatch for normal dispersion ($\sigma_{\mathrm{o}} = 1$) is given by,

$$\tilde{u}_{\mathrm{ms}} = \eta^2 \mathrm{sech}^2[\eta(t+\kappa z)]\,, \tag{5.43}$$

$$\tilde{u}_{\mathrm{os}} = \eta\sqrt{\tilde{\delta}}\,\mathrm{sech}[\eta(t+\kappa z)]\exp[\mathrm{i}(\kappa t+(\kappa^2-\eta^2)/2\;z)]\,, \tag{5.44}$$

where η and κ are arbitrary constants. Eqs. (5.43, 5.44) corresponds to a two parameter family of solutions, i.e. solutions exist for arbitrary amplitudes and velocities of the optical wave. Note that the solution for the microwave eq. (5.43) comes close to the soliton solution of the KdV equation.

5.6.2 Properties

Having shown that soliton solutions for large velocity mismatch are governed by a nonlinear Schroedinger equation, we are now interested in stationary states far from the Schroedinger

limit. To this end we are looking for solutions of the form,

$$\begin{aligned} \tilde{u}_{\mathrm{m}} &= \tilde{u}_{\mathrm{ms}}(\tilde{t} - vz) \,, \\ \tilde{u}_{\mathrm{o}} &= \tilde{u}_{\mathrm{os}}(\tilde{t} - vz)\exp(\mathrm{i}\tilde{\beta}z) \,. \end{aligned} \tag{5.45}$$

Here we introduced an additional phase $\tilde{\beta}$ in the optical wave. Note that the microwave is a real function and hence exhibits no phase as it is centered around zero frequency. Furthermore we allow the solitary wave to travel with an inverse velocity v unequal to the velocity of linear optical waves or microwaves. After substituting,

$$t = \tilde{t} - vz,\ \tilde{u}_{\mathrm{o}} = \tilde{u}'_{\mathrm{o}}\exp(\mathrm{i}\tilde{\beta}z) \,, \tag{5.46}$$

into eq. (5.40), we obtain the following set of equations,

$$\begin{aligned} &\left[\frac{\partial}{\partial z} + [\tilde{\delta} - v]\frac{\partial}{\partial t} - \sigma_{\mathrm{m}}\frac{\partial^3}{\partial t^3}\right]\tilde{u}_{\mathrm{m}} - \tilde{\chi}\frac{\partial}{\partial t}\tilde{u}_{\mathrm{m}}^2 - \frac{\partial}{\partial t}|\tilde{u}'_{\mathrm{o}}|^2 = 0 \,, \\ &\left[\mathrm{i}\frac{\partial}{\partial z} - \tilde{\beta} - \mathrm{i}v\frac{\partial}{\partial t} - \frac{\sigma_{\mathrm{o}}}{2}\frac{\partial^2}{\partial t^2} - \tilde{u}_{\mathrm{m}}\right]\tilde{u}'_{\mathrm{o}} - \mathrm{i}\tilde{\zeta}\frac{\partial}{\partial t}[\tilde{u}'_{\mathrm{o}}\tilde{u}_{\mathrm{m}}] = 0 \,. \end{aligned} \tag{5.47}$$

The number of relevant parameters $\tilde{\delta}$, v and $\tilde{\beta}$ can be further reduced. To this end we introduce the transformation,

$$u_{\mathrm{m}} = (1 + \sigma_{\mathrm{o}}\tilde{\zeta}v)\,\tilde{u}_{\mathrm{m}} \,, u_{\mathrm{o}} = \sqrt{1 + \sigma_{\mathrm{o}}\tilde{\zeta}v}\exp[-\mathrm{i}\sigma_{\mathrm{o}}v^2 z]\exp[\mathrm{i}\sigma_{\mathrm{o}}vt]\,\tilde{u}'_{\mathrm{o}} \,,$$

$$\beta = \tilde{\beta} + \frac{\sigma_{\mathrm{o}}v^2}{2} \,, \delta = \tilde{\delta} - v \,, \chi = \frac{\tilde{\chi}}{1 + \sigma_{\mathrm{o}}\tilde{\zeta}v} \,, \zeta = \frac{\tilde{\zeta}}{1 + \sigma_{\mathrm{o}}\tilde{\zeta}v} \,, \tag{5.48}$$

and obtain,

$$\left[\frac{\partial}{\partial z} + \delta\frac{\partial}{\partial t} - \sigma_{\mathrm{m}}\frac{\partial^3}{\partial t^3}\right]u_{\mathrm{m}} - \chi\frac{\partial}{\partial t}u_{\mathrm{m}}^2 - \frac{\partial}{\partial t}|u_{\mathrm{o}}|^2 = 0 \,, \tag{5.49}$$

$$\left[\mathrm{i}\frac{\partial}{\partial z} - \beta - \frac{\sigma_{\mathrm{o}}}{2}\frac{\partial^2}{\partial t^2} - u_{\mathrm{m}}\right]u_{\mathrm{o}} - \mathrm{i}\zeta\frac{\partial}{\partial t}[u_{\mathrm{o}}u_{\mathrm{m}}] = 0 \,. \tag{5.50}$$

Apart from the small parameters ζ for energy conservation and χ for microwave self-interaction we end up with two system parameters δ and β determining the soliton solutions. Hence a two parameter family of solitons is obtained. It follows further from the scaling eq. (5.48) that the velocity mismatch $\tilde{\delta}$ and the inverse velocity v have a similar influence on soliton solutions. Note that with transformation eq. (5.48) moving solitons ($v \neq 0$) can be obtained from resting ones ($v = 0$).

Soliton solutions are given by stationary states of the system eqs. (5.49, 5.50). Setting the z-derivatives to zero and integrating eq. (5.49) once with respect to t we obtain the following set of ordinary differential equations,

$$\begin{aligned} \sigma_{\mathrm{m}}\frac{\mathrm{d}^2}{\mathrm{d}t^2}u_{\mathrm{ms}} - \delta u_{\mathrm{ms}} + \chi u_{\mathrm{ms}}^2 + |u_{\mathrm{os}}|^2 = 0 \,, \\ \frac{\sigma_{\mathrm{o}}}{2}\frac{\mathrm{d}^2}{\mathrm{d}t^2}u_{\mathrm{os}} + \beta u_{\mathrm{os}} + u_{\mathrm{ms}}u_{\mathrm{os}} + \mathrm{i}\zeta\frac{\mathrm{d}}{\mathrm{d}t}[u_{\mathrm{ms}}u_{\mathrm{os}}] = 0 \,. \end{aligned} \tag{5.51}$$

Until now we included the small parameter ζ for completeness. However, apart from a small imaginary part in the soliton solution for the optical wave [107] we found the corresponding term to have no quantitative effect. In the following discussion we will therefore neglect ζ. As the parameter χ might describe additional nonlinearities in the microwave transmission line (see also Section 5.8), the parameter is included in the discussion of some analytical soliton solutions in Section 5.6.3. However, neglecting ζ and χ, the system of ODE's eqs. (5.51) is very similar to the one obtained in SHG cascading [15].

In this work we concentrate on bright soliton solutions. Accordingly the solutions have to decay to zero for $|t| \to \infty$. The asymptotic solutions are obtained by equating the nonlinear terms in eqs. (5.51) to zero,

$$u_{\mathrm{ms}} \sim \exp(-\sqrt{\delta\sigma_{\mathrm{m}}}|t|) \,, \tag{5.52}$$

$$u_{\mathrm{os}} \sim \exp(-\sqrt{-2\beta\sigma_{\mathrm{o}}}|t|) \,. \tag{5.53}$$

From the asymptotic form eq. (5.52) it follows that the dispersion of the microwave σ_{m} and the parameter δ have to have the same sign,

$$\sigma_{\mathrm{m}}\delta > 0 \,. \tag{5.54}$$

Linear microwaves, i.e. waves propagating without interaction with an optical wave, of the form $\tilde{u}_{\mathrm{m}} = \sin[\Omega(\tilde{t} - vz)]$ are subject to the dispersion relation $\tilde{\delta} - v = -\sigma_{\mathrm{m}}\Omega^2$. As $\delta = \tilde{\delta} - v$, eq. (5.54) expresses the fact that the speed of the soliton must differ from any velocity of a linear microwave. Similarly, from the asymptotic solution eq. (5.53) it follows that,

$$\beta\sigma_{\mathrm{o}} < 0 \,, \tag{5.55}$$

must hold, which corresponds to $\tilde{\beta}\sigma_{\mathrm{o}} < -v^2/2$. As the dispersion relation of linear optical waves of the form $\tilde{u}_{\mathrm{o}} = \exp[\mathrm{i}\tilde{\beta}z - \Omega\tilde{t}]$ is given by $\tilde{\beta}\sigma_{\mathrm{o}} = \Omega^2/2$, the wave number of the optical wave has to be distinct from that of any other linear wave of the optical spectrum.

Given $\chi = 0$, solutions for $\sigma_{\mathrm{m}} = -1$ can be recovered from solutions for $\sigma_{\mathrm{m}} = 1$ by replacing u_{ms}, δ, β and σ_{o} by $-u_{\mathrm{ms}}$, $-\delta$, $-\beta$ and $-\sigma_{\mathrm{o}}$, respectively. For this reason we restrict ourselves to $\sigma_{\mathrm{m}} = 1$ which corresponds to normal dispersion of the microwave. From a study of points of inflection in eqs. (5.51) in conjunction with the boundary condition eq. (5.52) it follows then that the microwave is always positive. Similarly it can be shown from eqs. (5.51) that for bright soliton solutions the signs of σ_{o} and σ_{m} must coincide. Hence, in what follows, we assume both coefficients to be positive $\sigma_{\mathrm{o}} = \sigma_{\mathrm{m}} = 1$, which corresponds to overall normal dispersion.

5.6.3 Analytical Solutions

The equations (5.51) are ordinary differential equations which, in general, have to be solved numerically. However, besides the soliton solution of the NLS equation (5.42) some analytical solutions exist which will be presented in this Section.

For vanishing optical wave, the system eqs. (5.40) corresponds to the KdV equation which fundamental soliton solution has a sech^2 shape. An analytical solution of eqs. (5.51) for $\chi > 2$ which preserves this shape is given by,

$$\begin{aligned} u_{\mathrm{ms}} &= c_{\mathrm{m}}\,\mathrm{sech}^2(\lambda t)\ , \\ u_{\mathrm{os}} &= c_{\mathrm{o}}\,\mathrm{sech}(\lambda t)\tanh(\lambda t)\ , \end{aligned} \tag{5.56}$$

where the coefficients are defined as,

$$\begin{aligned} \beta &= \frac{\delta}{2(2-3\chi)}\ , \quad \lambda^2 = -\frac{\delta}{2-3\chi}\ , \\ c_{\mathrm{m}} &= -\frac{3\,\delta}{2-3\chi}\ , \quad c_{\mathrm{o}}^2 = \frac{9\,\delta^2\,(\chi-2)}{(2-3\chi)^2}\ . \end{aligned} \tag{5.57}$$

However, as the microwave self-interaction due to the intrinsic nonlinearity is small, a value of $\chi > 2$ would require additional nonlinearities in the transmission line (see also Section 5.8). For the more realistic range $\chi < 2$ a single hump solution can be derived,

$$\begin{aligned} u_{\mathrm{ms}} &= c_{\mathrm{m}}\,\mathrm{sech}^2\left[\lambda t\right]\ , \\ u_{\mathrm{os}} &= c_{\mathrm{o}}\,\mathrm{sech}^2\left[\lambda t\right]\ , \end{aligned} \tag{5.58}$$

with the coefficients,

$$\begin{aligned} \beta &= -\frac{\delta}{2}\ , \quad \lambda^2 = \frac{\delta}{4}\ , \\ c_{\mathrm{m}} &= \frac{3\delta}{4}\ , \quad c_{\mathrm{o}} = \frac{3\delta}{4}\sqrt{2-\chi}\ . \end{aligned} \tag{5.59}$$

A similar solution exists for the case of SHG cascading [86]. The amplitude profile of the soliton eq. (5.58) is depicted in Fig. 5.5 (b). Note that the one parameter family of analytical solutions given above is only a subset of the general case, which is two-parametric with an independent propagation constant β.

5.6.4 Numerical Solutions

For the general case soliton solutions are calculated numerically by means of a shooting technique. Here we use the asymptotic forms eqs. (5.52, 5.53) and their derivatives for numerical integration towards $t = 0$. As we are mainly interested in the fundamental soliton, i.e. an even single hump solution, we look for zeros of the functions $\mathrm{d}u_{\mathrm{ms}}/\mathrm{d}t$ and $\mathrm{d}u_{\mathrm{os}}/\mathrm{d}t$ at $t = 0$. This can be done by minimizing $(\mathrm{d}u_{\mathrm{ms}}/\mathrm{d}t)^2 + (\mathrm{d}u_{\mathrm{os}}/\mathrm{d}t)^2$ at $t = 0$ with respect to the initial parameters chosen for $t \to \infty$.

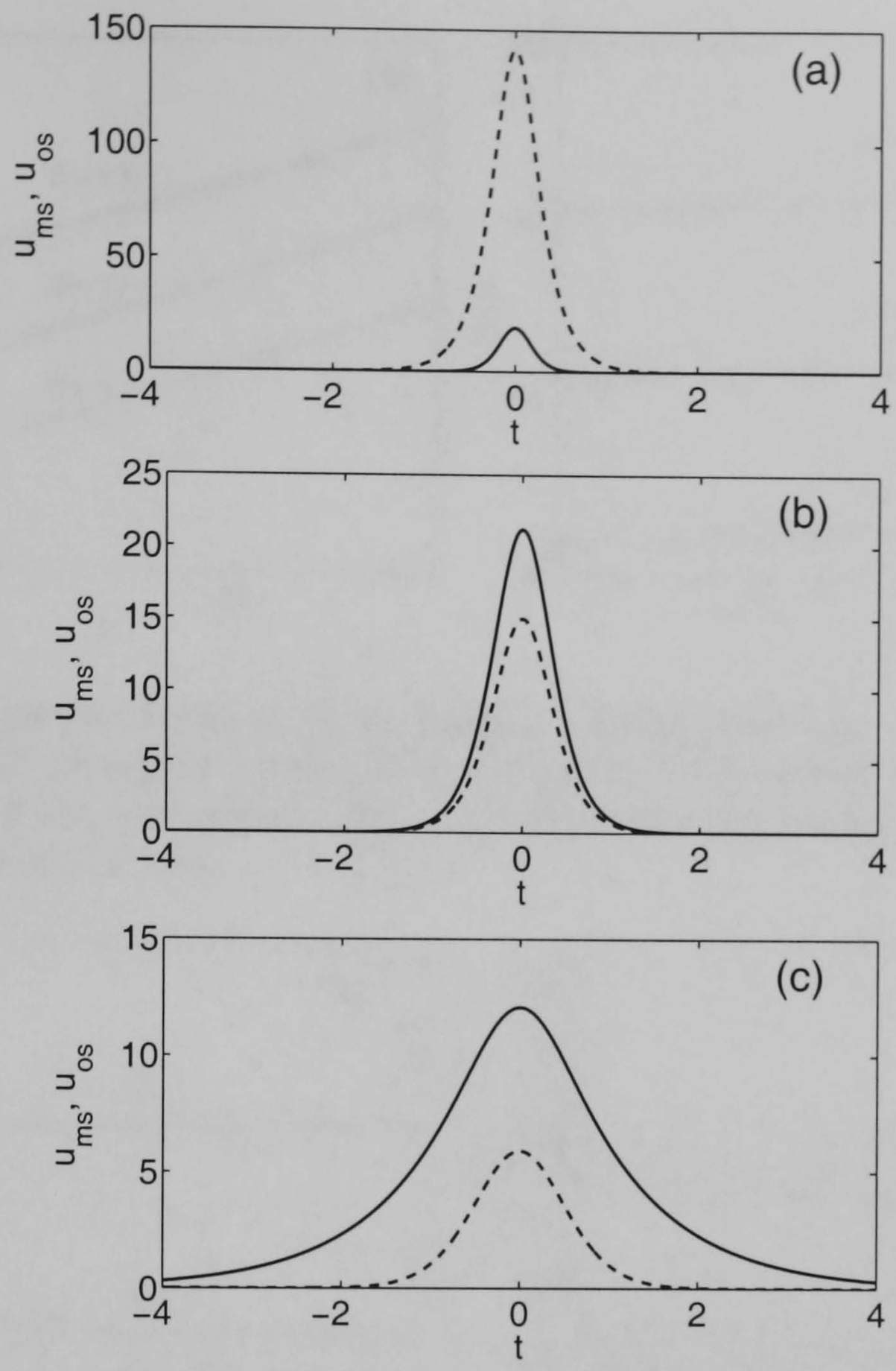

Figure 5.5: Calculated amplitude profiles of soliton solutions with $\beta = -10$ (ζ=0, $\chi = 0$). Solid curve microwave $u_{\rm ms}$; dashed curve optical wave $u_{\rm os}$. (a) Schroedinger limit $\delta = 1000$, (b) analytical solution eq. (5.58), $\delta = 20$, (c) numerical solution $\delta = 1$.

Bright single hump solutions were found for a large range of parameters. Fig. 5.5 shows the calculated amplitude profiles of bright soliton solutions for a varying system parameter δ. Included are an example solution of the Schroedinger limit and the analytical solution eq. (5.58). In the Schroedinger limit, which corresponds to large velocity mismatch between optical wave and microwave, the soliton solution is given by eqs. (5.43, 5.44). As in the case of a Kerr nonlinearity, the optical pulse height is inversely proportional to the pulse width. However, for a constant pulse width the peak power of the optical pulse grows linearly with the velocity mismatch $u_{\rm osp}^2 \propto \delta$. This corresponds to the fact that a higher peak power is necessary to induce a sufficient phase distortion in the optical wave by cascading of OR and the electro-optic effect as δ increases. In contrast, the microwave peak amplitude of the soliton is unaffected by the magnitude of the velocity mismatch and grows quadratically with the inverse pulse width.

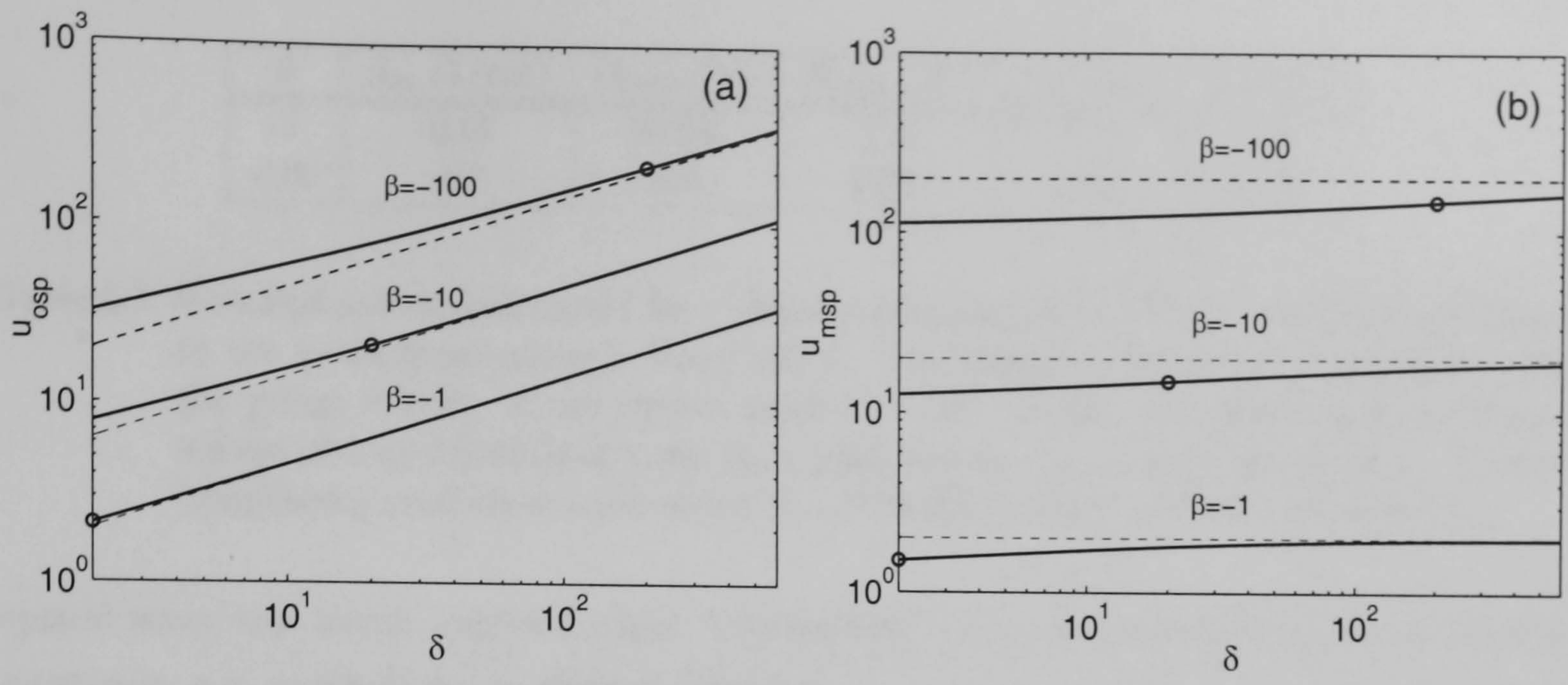

Figure 5.6: Peak amplitude of bright soliton solution: optical wave u_{osp} and microwave u_{msp} vs. system parameter δ (solid line). The dashed lines correspond to the asymptotic solution of the Schroedinger limit. The soliton solution corresponding to eq. (5.58) is marked with a circle.

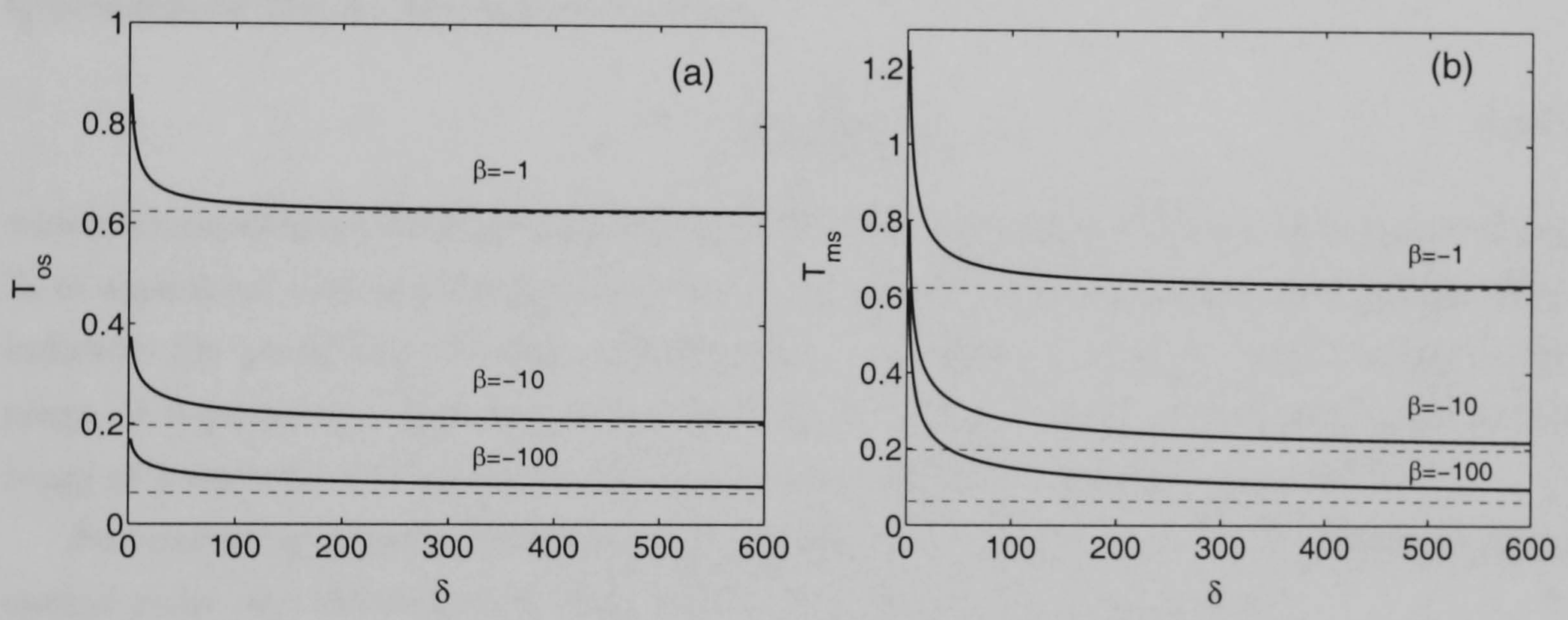

Figure 5.7: Pulse width (full width half maximum) of bright solitary waves: T_{os} corresponds to optical amplitude squared u_{os}^2, T_{ms} corresponds to microwave u_{ms}. Dashed lines as in Fig. 5.6.

Figs. 5.6 and 5.7 show the evolution of pulse amplitudes and widths for varying soliton parameter. Also included are the respective asymptotics of the Schroedinger limit. The amplitude development as discussed above is essentially maintained. However, far from the Schroedinger limit, i.e. for small velocity mismatch, the respective pulses are considerably broader.

Some examples shall be given relating the solution in scaled variables to the physical magnitudes of the example structure in Appendix F. Here the values given in Tab. F.4 are used. If we assume the soliton to propagate with the velocity of the optical wave, a difference in effective indices $\Delta n_{\mathrm{mic}} - \Delta n_{\mathrm{opt}}$=0.01 corresponds to a scaled parameter $\delta = 37$. As the microwave in a coplanar structure based on AlGaAs has a lower effective index than the

β	β_{us} (1/cm)	U_{pmic} (V)	P_{popt} (W)	T_{ms} (ps)	T_{os} (ps)
-1	-0.67	0.084	7.8	1.9	1.8
-100	-67	5.9	1070	0.56	0.29

Table 5.1: Unscaled soliton parameters for a velocity mismatch Δn=0.01 ($\delta = 37$) corresponding to the example structure in Appendix F. The soliton is assumed to propagate with the group velocity of the optical wave ($v = 0$). Values are given for two different soliton phases β (unscaled value β_{us}): peak voltage U_{pmic}, peak power P_{popt}, FWHM (amplitude) microwave pulse width T_{ms}, FWHM (power) optical pulse width T_{os}.

optical wave, this would require a slight "overslowing" of the microwave velocity by suitable structures, e.g. gratings in the ground electrode.

Unscaled peak amplitudes and pulse widths of the respective soliton are given in Tab. 5.1. The required peak amplitudes and pulse widths vary in a wide range of parameters depending on the respective soliton phase. The optical pulse width of the second example in Tab. 5.1 is approximately 290 fs. The dispersion length,

$$L_{\mathrm{D}} = \frac{T_{\mathrm{o}}^2}{4\ln(2)\, D_{\mathrm{opt}}}\,, \tag{5.60}$$

which corresponds to the length for which the FWHM (full width half maximum) pulse width T_{o} of a gaussian optical pulse increases by a factor of $\sqrt{2}$, is then approximately 2.5 cm. This indicates the possibility of soliton observation in modulator structures with a length in the range of centimeters. However, as pointed out in Section 4.3.4, a microwave pulse in the range of hundreds of fs will be subject of excessive losses in conventional structures.

An interesting question remaining is if a soliton can be formed by the sole injection of an optical pulse into the structure. This will be addressed in the next Section.

5.7 Excitation of Solitons

As soliton solutions exist in a broad range of parameters, we will check in the following if an optical pulse can excite a stable dispersionless pulse. To this aim the system eqs. (5.12) was integrated numerically by a Crank-Nicholson-Scheme from the respective boundary condition at $z = 0$. In all examples an optical Gaussian pulse with peak amplitude A and FWHM pulse width T_{o} was used,

$$u_{\mathrm{o}}(0,t) = A\exp[-2\ln(2)t^2/T_{\mathrm{o}}^2]\,, \quad u_{\mathrm{m}}(0,t) = 0\,. \tag{5.61}$$

Fig. 5.8 shows the outcome of a numerical experiment for a peak amplitude A=30 and a pulse width $T_{\mathrm{o}} = 0.4$. A stable solitary wave is excited after a propagation distance of

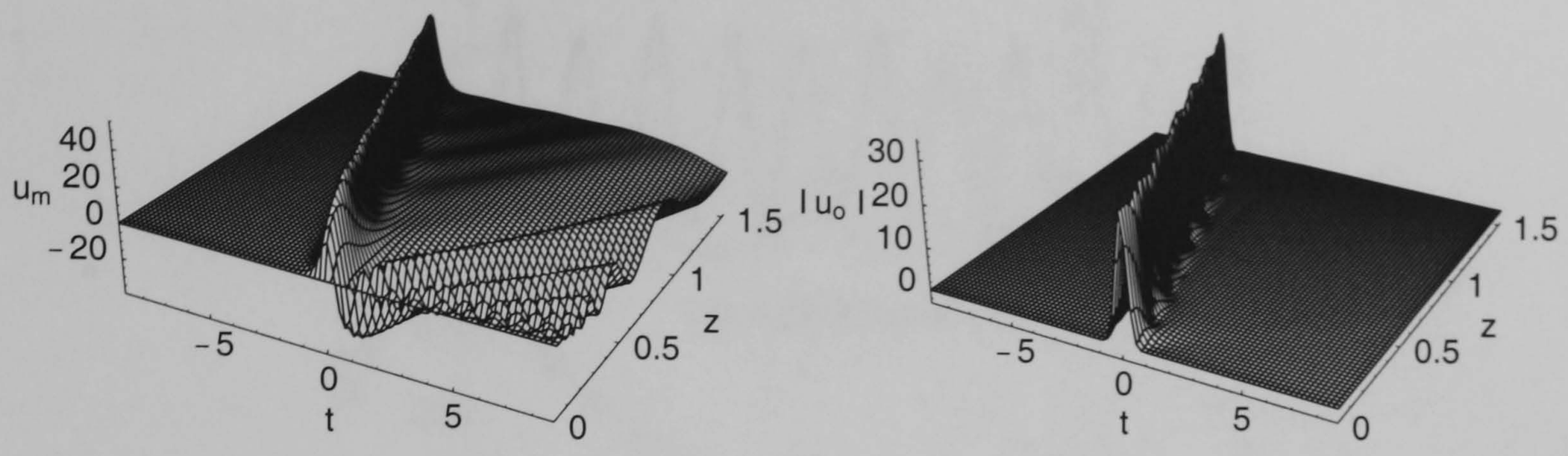

Figure 5.8: Excitation of a solitary wave with an optical input pulse (Gaussian, full width half maximum $T_o = 0.4$, peak amplitude $A = 30$), velocity mismatch $\delta = 5$.

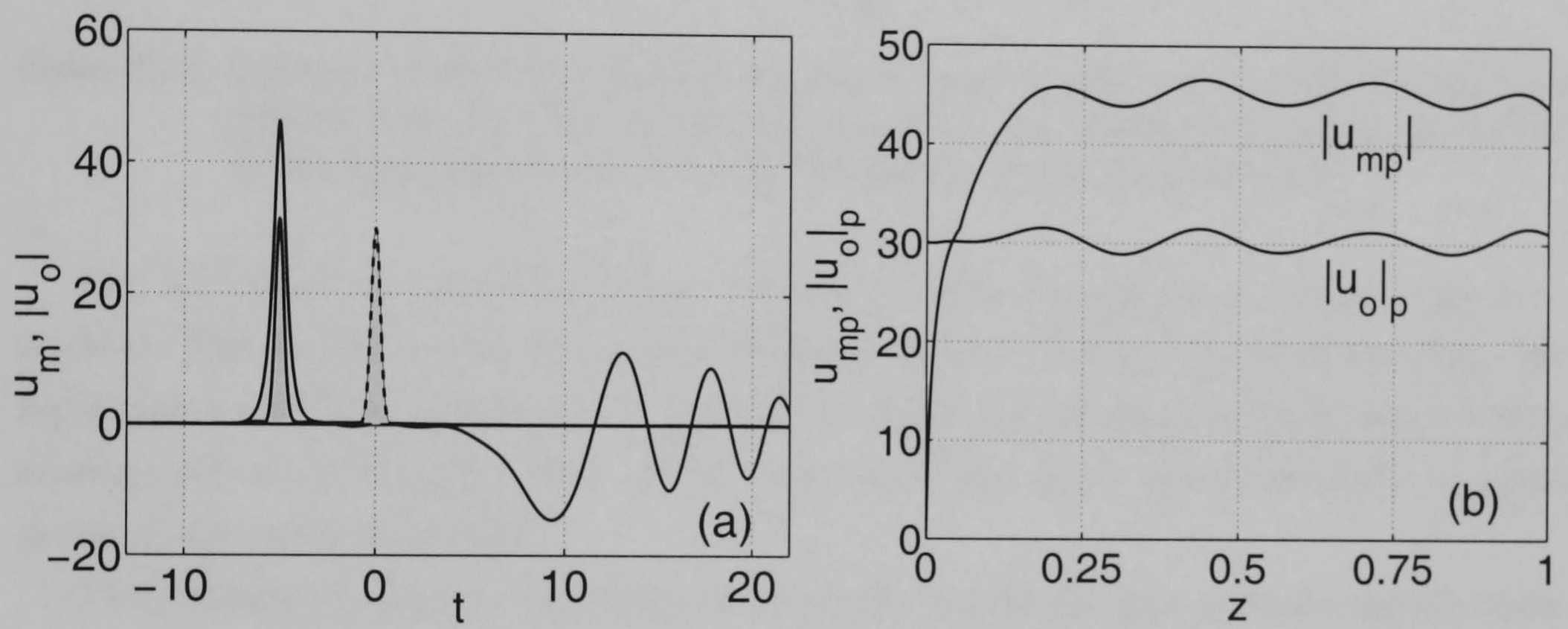

Figure 5.9: Excitation of a solitary wave, same parameters as in Fig. 5.8. (a) Fields at the output: shaded optical pulse, unshaded microwave, also indicated optical input pulse around t=0 (dashed). (b) evolution of peak amplitudes.

approximately $z = 0.2$. Linear microwaves, which are generated during the excitation of the microwave component, are radiated away quickly. The velocity mismatch for this example is $\delta = 5$. As was indicated in Section 5.6.2, the soliton travels faster than allowed velocities for linear microwaves (see also Fig. 5.9). For the peak amplitude and pulse widths chosen in the example, solitons evolved in a velocity mismatch range between $50 < \delta < -10$.

Fig. 5.9 shows the fields at the output and the peak amplitudes of both waves during propagation. After a rather short propagation length, both pulses start to develop regular oscillations around their average field amplitude. This behaviour was also observed in corresponding numerical experiments on the excitation of solitons in SHG cascading [108]. A series of numerical calculations showed that optically excited solitons seem almost always to occur as oscillating states. The reason for these persistent oscillations are internal modes of the generated soliton [109] which will be discussed in detail in Chapter 6.

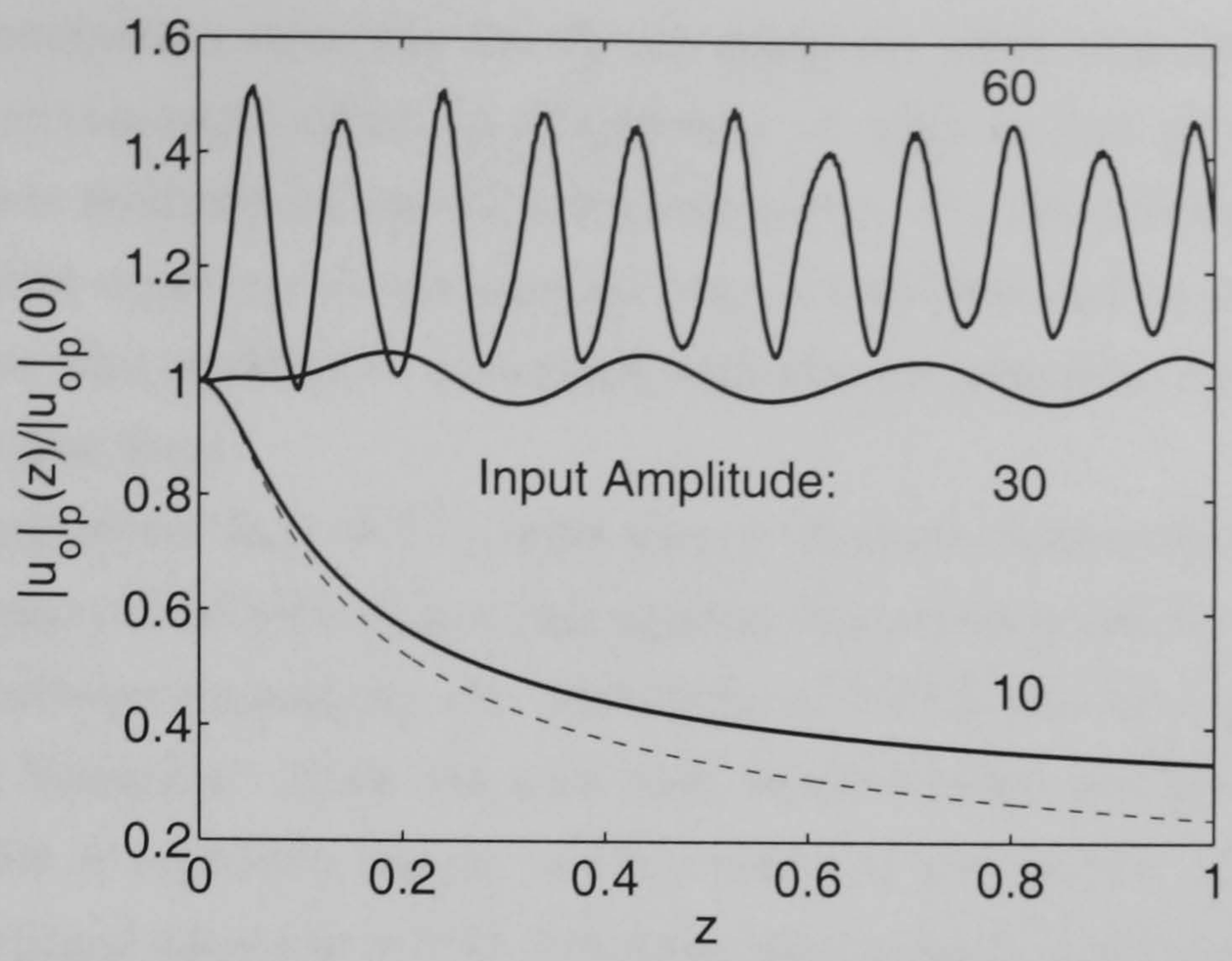

Figure 5.10: Evolution of peak amplitude of the optical wave for different peak amplitudes of the injected pulse (all other parameters as in Fig. 5.8). The peak amplitudes are scaled to the input amplitudes. The dashed curve shows the linear evolution.

Fig. 5.10 shows the evolution of the normalized optical amplitude at different input intensities. The excitation of a bound state seems to require a certain threshold intensity. For input pulses with high amplitudes we observed an initial narrowing of the pulse shape before evolving into an oscillating soliton. Below a threshold, the pulses spread similarly to waves in the absence of nonlinearity.

The propagation distance required to form a soliton becomes shorter for increasing intensity of the input pulse. To give an impression of magnitudes in an experiment, we refer to the second example in Tab. 5.1. Injecting a gaussian pulse with a comparable pulse width and peak amplitude forms a soliton after a propagation distance of approximately $z \approx 0.05$, which corresponds to an unscaled length $L \approx 7.5\,\mathrm{cm}$. Keeping in mind that high microwave losses will increase this propagation length or even prevent the formation of a bound state makes the experimental observation of optically excited solitary waves difficult. However, the propagation distance required to form a soliton becomes shorter for increasing intensity of the input pulse suggesting the requirement of very short pulses with high peak intensities.

5.8 Nonlinear Transmission Lines

Finally, we will discuss the microwave self-interaction term, which leads to the KdV form of the microwave evolution equation in the absence of an optical field. As pointed out earlier, the magnitude of the effective nonlinearities corresponding to the microwave self-interaction $\chi_{\mathrm{eff}3}$ can be comparable to that of the effective nonlinearities corresponding to OR $\chi_{\mathrm{eff}1}$ or $\chi_{\mathrm{eff}2}$ defined in Section 4.2. However, for an efficient optical-microwave interaction the power in the optical wave is several magnitudes larger than the power of the microwave. As

a result, the self-interaction term can usually be neglected when considering effects arising from OR and the electro-optic effect. In this Section we want to give an estimate about the effect of the intrinsic nonlinearity on the sole propagation of a microwave on a transmission line. Here we restrict ourselves to the physical magnitudes involved in soliton propagation. As indicated earlier, this problem is associated with the propagation of electrical signals on nonlinear transmission lines.

Nonlinear transmission lines (NTL) were among the first experimental tools to demonstrate phenomena associated with soliton propagation (for a review, see for example [92],[110], [111]). There are several reasons for the popularity of NTL's for the experimental demonstration of soliton formation. They can offer high nonlinearities, are inexpensive, the measurement equipment is relatively simple and the essential parameters of the line are easily adjusted. The nonlinear effects in a NTL can arise, for example, from a charge in the transmission line which depends nonlinearly on the applied voltage. A simple realisation of such a transmission line is the use of reverse-biased capacitance diodes. The analysis of these structures is based on simple equivalent circuits and can lead to the Boussinesq equation [110], which asymptotically transforms into the KdV equation for long wavelengths [112].

In the case considered here, the nonlinearity arises from the nonlinearity $\chi^{(2)}(0;0,0)$ rather than from the artificial introduction of nonlinear elements. Interestingly, the structure of the resulting equation is essentially the same in both cases. This has been shown earlier in a related publication [113], where the Boussinesq equation was derived directly from Maxwell's equations for microwaves in dispersive, nonlinear dielectrics.

For convenience, we will reproduce the equation for sole, lossless propagation of the microwave derived in Section 4.2,

$$\left[\frac{\partial}{\partial z} + \left(\frac{1}{v_{\mathrm{mic}}} - 2\chi_{\mathrm{eff}} U_{\mathrm{mic}}\right)\frac{\partial}{\partial t} - \frac{T_{\mathrm{mic}}}{6}\frac{\partial^3}{\partial t^3}\right] U_{\mathrm{mic}} = 0\,. \tag{5.62}$$

Eq. (5.62) is basically the KdV equation. The effective nonlinearity depends on the second order nonlinearity $\chi^{(2)}(0;0,0)$ and the overlap of field components of the microwave mode. Corresponding to eq. (4.26), for GaAs with the usual [100] and [011] cleavage direction, modes with field components in both x- and y-direction are necessary. For other crystal orientations, only field components in one direction are required [114]. However, the magnitudes of physical quantities involved for other transmission lines and crystal orientations were found to be comparable. The soliton solution of eq. (5.62) is given by,

$$U_{\mathrm{mic}}(t,z) = A\,\mathrm{sech}^2\left[\sqrt{\frac{\chi_{\mathrm{eff}} A}{T_{\mathrm{mic}}}}\,(t-\eta z)\right]\,, \quad \text{with} \quad \eta = \frac{1}{v_{\mathrm{mic}}} - \frac{2}{3}\chi_{\mathrm{eff}} A \quad , \tag{5.63}$$

where A is an arbitrary amplitude. Note that the peak voltage required grows quadratically with the inverse of the pulse width. This leads to high voltages in particular for short pulses where the dispersion length is comparable to the length of a realistic structure.

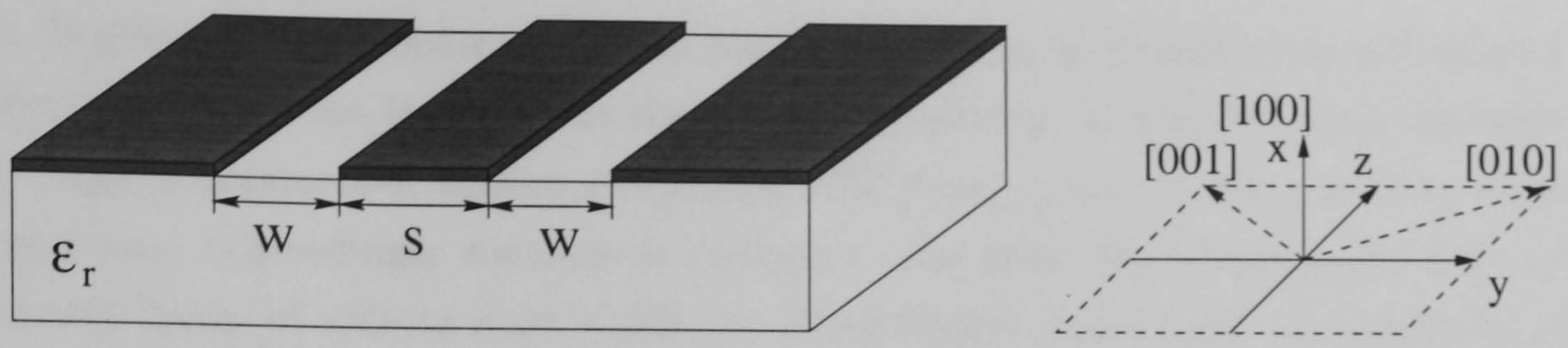

Figure 5.11: Coplanar transmission line on GaAs (ϵ_r=12.9, w=s=4 μm).

χ_{eff3} ($\text{sm}^{-1}\text{W}^{-1/2}$)	T_{mic} (ps^3/m)	Z_0 (Ω)	T_{FWHM} (ps)	V_{mic} (V)
3.4×10^{-14}	8.5	53	100	0.27
			10	27
			1	2.7×10^4

Table 5.2: Calculated parameters for soliton propagation due to the intrinsic nonlinearity $\chi^{(2)}(0;0,0)$ on a microwave transmission line: effective nonlinearity χ_{eff3}, dispersion T_{mic}, impedance Z_0, full width half maximum (amplitude) pulse width T_{FWHM}, peak voltage V_{mic} corresponding to soliton solution (5.63).

Lets consider a simple coplanar transmission line as depicted in Fig. 5.11. The transverse field components are calculated from electrostatics as discussed in Section 4.3.2 by solving the Laplace equation. The dispersion has been estimated by the formulae given in Appendix E. In Tab. 5.2 the corresponding soliton parameters are shown. The dispersion length of a microwave signal can be estimated by,

$$L_{\text{D}} \approx \frac{\Delta t^3}{T_{\text{mic}}}, \tag{5.64}$$

and amounts to centimeters for pulses in the ps range. However, voltages in the order of kV required for this pulse widths seem too high for an experimental observation. Whereas in this example the microwave structure was chosen to be small, the dispersion will increase considerably for structures with larger dimensions. However, the effective nonlinearity decreases for larger dimensions resulting in a smaller nonlinearity acting on the microwave. It should be noted that we did not consider losses for this simple estimate. As discussed in Section 4.3.4, in particular at very short pulse widths losses might influence the evolution of the microwave signal considerably.

5.9 Conclusions

It was shown in this Chapter that the cascading mechanism of OR and the electro-optic effect allows potentially the formation of bound states, i.e. solitary waves. The normalized equations are similar in structure to long wave short wave interaction equations which have been predicted for a number of physical systems, including water waves or nonlinear transmission

lines. Neglecting higher order terms and losses, the system is Hamiltonian and subject to a number of conservation laws. It was shown that the system is modulationally unstable in a wide range of parameters. Similar to the case of SHG cascading, at large velocity mismatch the nonlinear Schroedinger equation is recovered. Far from the Schroedinger limit, a two parameter family of solitons exist which can be calculated numerically. At particular points in parameter space, analytical soliton solutions are obtained similar in structure to analytical soliton solutions in SHG cascading. Dispersionless states can in principle be excited by injection of optical pulses into the structure. Here, large peak powers are necessary to ensure a practical excitation length.

The microwave self-interaction due to the intrinsic nonlinearity $\chi^{(2)}(0;0,0)$ interestingly leads to the same equations as derived in conventional nonlinear transmission lines - the Korteweg de Vries equation. However, the effect was shown to be small and requires very large peak voltages to influence the evolution of the microwave.

6 Stability of Soliton Solutions

6.1 Introduction

In the previous Chapter it was shown that the interaction of optical rectification (OR) and the electro-optic effect can lead to stationary solutions, i.e. solitary waves. We will now investigate how propagating soliton solutions behave under small perturbations. As was pointed out in the introduction of the preceding Chapter, soliton solutions of nonintegrable systems can be unstable, i.e. small perturbations might grow exponentially leading to the eventual decay of the stationary solution. The study of stability is therefore of fundamental importance in the characterisation of solitary waves in such a system.

At this point, some remarks should be made about the term *stability*. In the following we mean by this term the stability with respect to small perturbations which can be expressed by a linearisation of the equations around a stationary solution. In an experiment, additional effects might influence the evolution of bound states which are not considered in the simplified model. In our case, these effects could include higher order dispersion terms or the effect of higher order nonlinearities. Furthermore, as was pointed out in Section 4.3.4, losses can influence the evolution considerably, in particular that of the microwave. However, here we consider only the linear stability of the conservative, i.e. nondissipative system, leaving the discussion of higher order effects and attenuation for future investigation.

A number of effects discussed in this Section have also been observed in other nonintegrable systems. As an important and related example we shall mention solitary waves due to the interaction of a fundamental with its second harmonic in media with a second order nonlinearity (SHG cascading). It was found that for SHG cascading solitary waves exhibit a narrow domain of instability [115]. Associated with the stability of solitary waves is the existence of internal modes, which are the eigensolutions of the linearized problem [109], [116]. Internal modes were found to be the reason for long lived oscillations of perturbed solitons with an oscillation frequency corresponding to the spectrum of the associated eigenvalue problem. The oscillations observed by excitation of solitary waves discussed in Section 5.7 have already indicated the existence of such modes in the system considered here.

Another interesting aspect related to stability is the mutual interaction of solitary waves. It is well known that in integrable systems solitons are resistant against collisions, i.e. they do

not change their shape [82]. In contrast, solitons in nonintegrable systems can show a complex collision behaviour, ranging from nearly interactionless collisions to merged, oscillating states [109].

In this Section we investigate these phenomena for solitary waves due to OR and the electro-optic effect. Here, we restrict ourselves to fundamental bright soliton solutions. Starting with an investigation of the propagation of perturbed solitons in Section 6.2, the observed oscillations are explained by a linear stability analysis and hence the associated internal modes in Section 6.3. The behaviour under collisions is briefly addressed in Section 6.4.

6.2 Behaviour under Perturbation

The starting point are the scaled evolution equations corresponding to (5.49, 5.50) in Section 5.6.2 neglecting the microwave self-interaction parameter χ and the small energy conservation parameter ζ,

$$\begin{aligned} \left[\frac{\partial}{\partial z} + \delta\frac{\partial}{\partial t} - \sigma_\mathrm{m}\frac{\partial^3}{\partial t^3}\right] u_\mathrm{m} - \frac{\partial}{\partial t}|u_\mathrm{o}|^2 = 0 \,, \\ \left[\mathrm{i}\frac{\partial}{\partial z} - \beta - \frac{\sigma_\mathrm{o}}{2}\frac{\partial^2}{\partial t^2} - u_\mathrm{m}\right] u_\mathrm{o} = 0 \,. \end{aligned} \tag{6.1}$$

Because of the symmetry properties discussed in Section 5.6.2, we restrict ourselves to anomalous dispersion in both waves $\sigma_\mathrm{o} = \sigma_\mathrm{m} = 1$, from which follows $\delta > 0$ and $\beta < 0$.

To investigate the behaviour of perturbed solitons, a soliton solution was calculated from eqs. (5.51), perturbed and propagated by integration of eqs. (6.1). The perturbation was performed in a similar manner to [117] using an initial profile for the amplitudes $u_{\mathrm{m,o}}(z,t)$,

$$u_{\mathrm{m,o}}(0,t) = \left[u_{\mathrm{ms,os}}(t)^2 + \xi\frac{u_{\mathrm{ms,os}}^2(0)}{\frac{\mathrm{d}^2}{\mathrm{d}t^2}u_{\mathrm{ms,os}}^2(t)|_{t=0}}\frac{\mathrm{d}^2}{\mathrm{d}t^2}u_{\mathrm{ms,os}}^2(t)\right]^{1/2} , \tag{6.2}$$

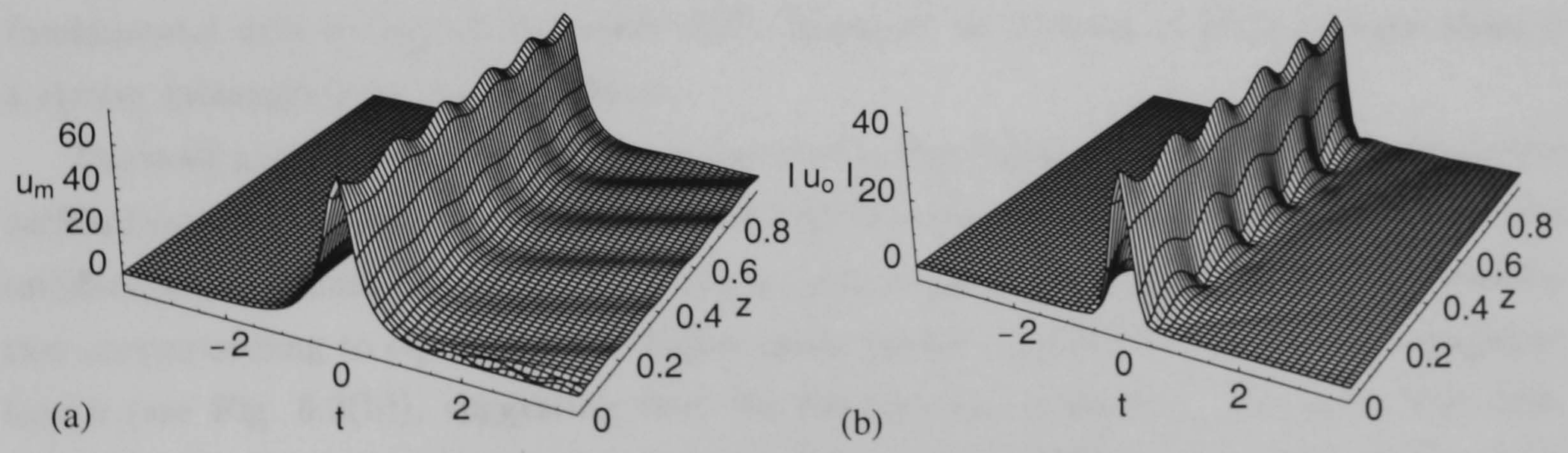

Figure 6.1: Persistent oscillations of perturbed solitary wave solution; $\xi = 0.2$, soliton parameters δ=10, $\beta = -50$. (a) amplitude of the microwave u_m; (b) absolute value of the optical wave $|u_\mathrm{o}|$.

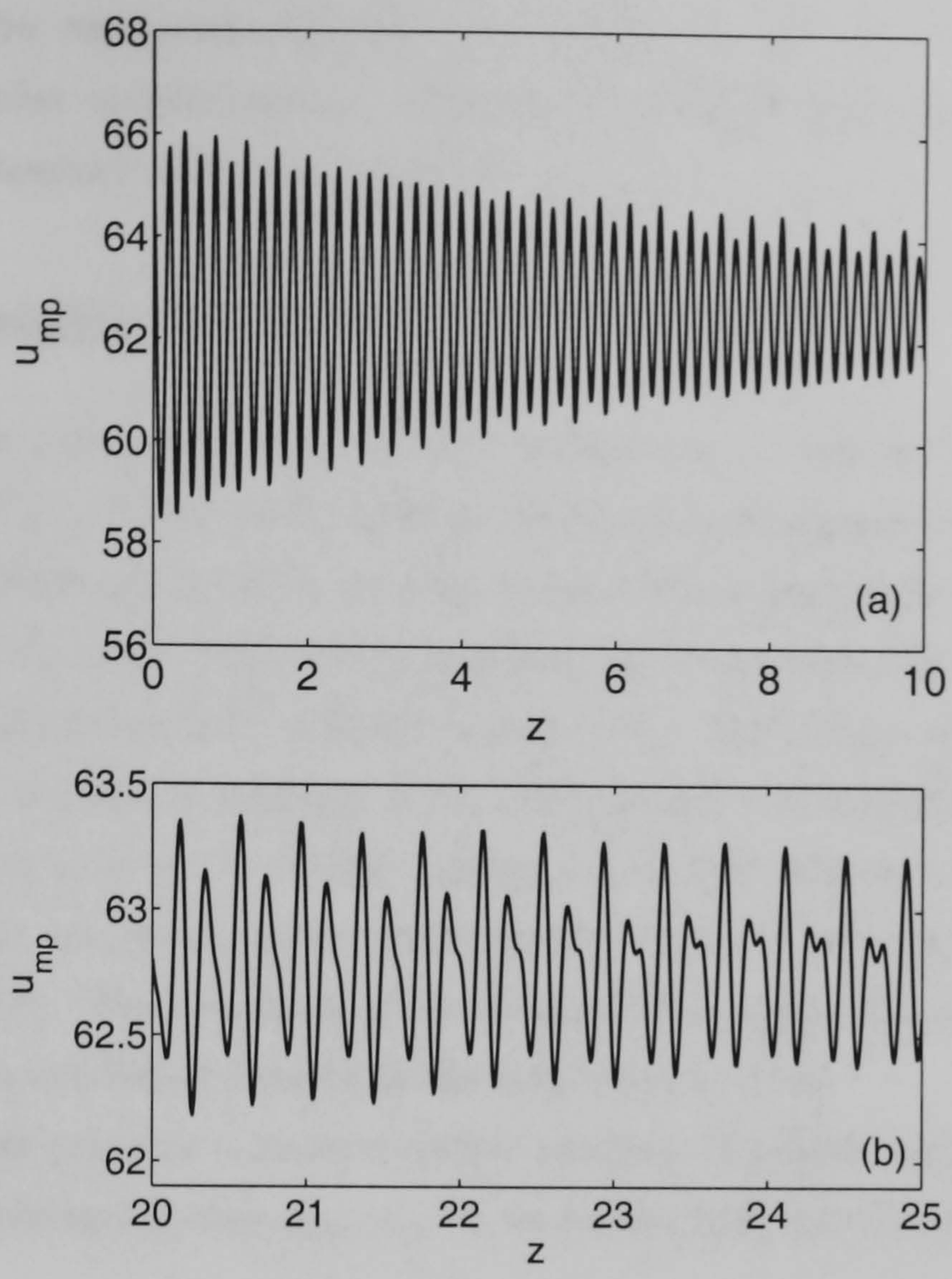

Figure 6.2: Damped oscillation of perturbed soliton: peak amplitude of the microwave u_{mp}; all parameters as in Fig. 6.1. (a) Range $0 < z < 10$, (b) beating between modes in range $20 < z < 25$.

where ξ represents the perturbation amplitude. The symmetric perturbation eq. (6.2) leaves the energy of both optical and microwave unchanged. However, the effects observed for other symmetric perturbations are similar.

Fig. 6.1 shows the outcome of a representative numerical experiment. The perturbed solitary wave shows regular oscillations similarly to solitary waves due to interaction of a fundamental with its second harmonic [117]. However, in contrast to SHG solitons, there is a strong radiation from the microwave.

The peak amplitude of the microwave depicted in Fig. 6.2(a) demonstrates that the soliton oscillations are damped. Further numerical experiments showed that a number of discrete oscillation frequencies can exist depending on soliton parameters β and δ. For a perturbation corresponding to eq. (6.2) these higher order modes emerge after a certain propagation length (see Fig. 6.2(b)), suggesting that the fundamental mode, i.e. the mode with lowest oscillation frequency, is stronger damped than modes of higher order. Propagation with strong perturbation ($\xi = 0.4$) showed stable propagation even for large propagation distances ($z \approx 5000$).

Fig. 6.2 should be compared with Fig. 5.9 in Section 5.7. In both cases, excitation or perturbation, similar oscillations are obtained suggesting that the same mechanism is responsible for the observed evolution dynamics.

6.3 Linear Stability Analysis

It is has been shown that regular, long-lived oscillations in solitary waves correspond to internal eigenmodes [117]. These modes are nontrivial, discrete eigensolutions of the linearized problem. Internal modes are found in a large variety of nonintegrable systems, for example the generalized KdV equation [118], the generalized NLS equation [119, 120] or, as indicated above, the system describing SHG solitary waves [117]. Perturbed solitary waves tend to oscillate around the stationary solution with a frequency corresponding to the eigenvalue associated with the internal mode. These eigenvalues usually depend on system parameters. In particular, they can emerge from the continuous spectrum [116] and further bifurcate into unstable domains [115]. The spectrum of the linearized problem hence provides important information about the soliton dynamics in the respective system.

In the following we perform a linear stability analysis of bright soliton solutions. To this end we assume the soliton solution u_{ms}, u_{os} to be known and introduce small perturbations $\epsilon_{\mathrm{m,o}}(z,t)$,

$$\begin{aligned} u_{\mathrm{m}}(z,t) &= u_{\mathrm{ms}}(t) + \epsilon_{\mathrm{m}}(z,t) \,, \\ u_{\mathrm{o}}(z,t) &= u_{\mathrm{os}}(t) + \epsilon_{\mathrm{o}}(z,t) \,. \end{aligned} \tag{6.3}$$

The ansatz eqs. (6.3) is inserted into eqs. (6.1) and linearized around a soliton solution, i.e. only linear terms in $\epsilon_{\mathrm{m,o}}$ are retained corresponding to small perturbations. We come up the set of equations,

$$\begin{aligned} &\frac{\partial \epsilon_{\mathrm{m}}}{\partial z} + \delta \frac{\partial \epsilon_{\mathrm{m}}}{\partial t} - \frac{\partial^3 \epsilon_{\mathrm{m}}}{\partial t^3} - \frac{\partial}{\partial t}[u_{\mathrm{os}}(\epsilon_{\mathrm{o}}^* + \epsilon_{\mathrm{o}})] = 0 \,, \\ &\frac{\partial \epsilon_{\mathrm{o}}}{\partial z} - \beta \epsilon_{\mathrm{o}} - \frac{1}{2}\frac{\partial^2 \epsilon_{\mathrm{o}}}{\partial t^2} - (u_{\mathrm{os}}\epsilon_{\mathrm{m}} + u_{\mathrm{ms}}\epsilon_{\mathrm{o}}) = 0 \,. \end{aligned} \tag{6.4}$$

The small perturbations are expressed as harmonic functions along z-direction,

$$\begin{aligned} \epsilon_{\mathrm{m}} &= \frac{1}{2} X_{\mathrm{m}}(t) \exp(\mathrm{i}\lambda z) + \frac{1}{2} X_{\mathrm{m}}^*(t) \exp(-\mathrm{i}\lambda^* z) \,, \\ \epsilon_{\mathrm{o}} &= \frac{1}{2}[X_{\mathrm{o}}(t) + Y_{\mathrm{o}}(t)] \exp(\mathrm{i}\lambda z) + \frac{1}{2}[X_{\mathrm{o}}(t) - Y_{\mathrm{o}}(t)]^* \exp(-\mathrm{i}\lambda^* z) \,, \end{aligned} \tag{6.5}$$

where $X_{\mathrm{m,o}}$ and Y_{o} refer to the in-phase and in-quadrature components of the perturbations. Note that the microwave is real and is perturbed by the in-phase component only. We obtain the following eigenvalue problem,

$$\boldsymbol{L}\mathbf{E} = \lambda \mathbf{E} \,, \tag{6.6}$$

where the eigenvector $\mathbf{E}(t) = [X_{\mathrm{m}}(t), X_{\mathrm{o}}(t), Y_{\mathrm{o}}(t)]^{\mathrm{T}}$. The operator L in the present case is given by,

$$L = \begin{pmatrix} -\mathrm{i}\left[\dfrac{\mathrm{d}^3}{\mathrm{d}t^3} - \delta\dfrac{\mathrm{d}}{\mathrm{d}t}\right] & -2\mathrm{i}\left[u_{\mathrm{os}}\dfrac{\mathrm{d}}{\mathrm{d}t} + \dfrac{\mathrm{d}u_{\mathrm{os}}}{\mathrm{d}t}\right] & 0 \\ 0 & 0 & -\dfrac{1}{2}\dfrac{\mathrm{d}^2}{\mathrm{d}t^2} - \beta - u_{\mathrm{ms}} \\ -u_{\mathrm{os}} & -\dfrac{1}{2}\dfrac{\mathrm{d}^2}{\mathrm{d}t^2} - \beta - u_{\mathrm{ms}} & 0 \end{pmatrix} . \tag{6.7}$$

Excitation of eigenvalues with negative imaginary component results in exponential growth and hence in instability of the stationary solution. In contrast, a perturbation with an internal mode with positive imaginary part will finally decay. This is somewhat in contrast to, for example, the SHG system, where due to the λ^2-dependence eigenvalues with an imaginary part will always lead to instability. The eigensystem eq. (6.6, 6.7) has two trivial eigensolutions at $\lambda = 0$,

$$\mathbf{E}_{\mathrm{T}} = \begin{bmatrix} \mathrm{d}u_{\mathrm{ms}}/\mathrm{d}t \\ \mathrm{d}u_{\mathrm{os}}/\mathrm{d}t \\ 0 \end{bmatrix} \quad , \quad \mathbf{E}_{\mathrm{P}} = \begin{bmatrix} 0 \\ 0 \\ \mathrm{i}u_{\mathrm{os}} \end{bmatrix} , \tag{6.8}$$

which corresponds to a temporal shift in both waves and a phase shift in the optical wave, respectively.

For a further discussion, it is useful to consider the asymptotic behaviour of the perturbation functions for $|t| \to \infty$. The asymptotic solutions for $|t| \to \infty$ of the optical perturbation functions X_{o}, Y_{o} are obtained by setting u_{ms} and u_{os} in (6.7) to zero, giving,

$$X_{\mathrm{o}}, Y_{\mathrm{o}} \propto \exp(\pm\Omega_{\mathrm{o}} t) , \tag{6.9}$$

with

$$\Omega_{\mathrm{o}} = \sqrt{2(-\beta \pm \lambda)} , \ (X_{\mathrm{o}} = \mp Y_{\mathrm{o}}) . \tag{6.10}$$

It follows that for $\mathrm{Re}(\lambda) < |\beta|$ bound eigensolutions with evanescent tails exist corresponding to the limit of the continuous spectrum. Similarly we proceed for the microwave perturbation X_{m} resulting in,

$$X_{\mathrm{m}} \propto \exp(\Omega_{\mathrm{m}} t) , \tag{6.11}$$

where Ω_{m} is given by a cubic equation. Hence we obtain three possible solutions for Ω_{m},

$$\Omega_{\mathrm{m}} = \mathrm{i}(p_- - p_+) , \tag{6.12}$$

$$\Omega_{\mathrm{m}} = \pm\frac{\sqrt{3}}{2}(p_+ + p_-) + \frac{1}{2}\mathrm{i}(p_+ - p_-) , \tag{6.13}$$

where

$$p_\pm = \sqrt[3]{\pm\lambda/2 + \sqrt{(\delta/3)^3 + (\lambda/2)^2}} . \tag{6.14}$$

Note that for real λ, p_- and p_+ are always real so that the solution eq. (6.12) results in infinitely extended oscillatory tails. Hence there is no gap in the continuum for the microwave. Solitons with no separation between trivial modes and the continuous spectrum are known from solutions of the perturbed Korteweg de Vries equation [118], a system which comes close to evolution equation of the microwave in our case. Another example for solitons having their intrinsic frequency in the continuum of radiation modes has been found recently in systems with quadratic and cubic nonlinearities [121]. These so-called embedded solitons are characterized by vanishing oscillating tails at discrete frequencies leading to isolated (or zero family) soliton solutions.

Equation (6.12) suggests that for any real λ we find an eigensolution with nonvanishing tails for $t \to \pm\infty$. To explain the appearance of discrete oscillating states as shown in Fig. 6.1, we solve the eigenvalue problem eq. (6.6) numerically. Solutions of eq. (6.6) can be found, for example, by means of the Evans method similar to [122]. The basic idea is that a solution of the eigenvalue problem eq. (6.6) can be written as a linear combination of functions with asymptotics corresponding to eqs. (6.9-6.13).

In the first step, the eigenvalue problem eq. (6.6) is rewritten in terms of a system of ordinary differential equations (ODE's) of first order [123],

$$M\mathbf{E}' = 0\,. \tag{6.15}$$

Here M corresponds to the operator $L - \lambda[I]$ with $[I]$ being the identity operator reduced to a set of first order ODE's. Correspondingly, $\mathbf{E}'$ is a 7 component vector defined as,

$$\mathbf{E}' = [X_\mathrm{m}, X'_\mathrm{m}, X''_\mathrm{m}, X_\mathrm{o}, X'_\mathrm{o}, Y_\mathrm{m}, Y'_\mathrm{m}]^T\,. \tag{6.16}$$

For a chosen eigenvalue λ, the system eq. (6.15) is integrated to $t = 0$ with boundary conditions at $t \to \pm\infty$ corresponding to a particular asymptotic solution. Given n_L non-increasing asymptotic solutions for $t \to -\infty$ and n_R non-increasing asymptotic solutions for $t \to \infty$ we obtain functions $\mathbf{E}'_{Li}$ $(i = 1, \ldots, n_L)$ for $t \leq 0$ and $\mathbf{E}'_{Ri}$ $(i = 1, \ldots, n_R)$ for $t \geq 0$. A solution $\mathbf{E}'$ of eq. (6.15) can be constructed as a linear combination of those functions as,

$$\mathbf{E}' = \begin{cases} t \leq 0 & \sum_{i=1}^{n_L} a_{Li}\mathbf{E}'_{Li}\,, \\ t \geq 0 & \sum_{i=1}^{n_R} a_{Ri}\mathbf{E}'_{Ri}\,, \end{cases} \tag{6.17}$$

with corresponding coefficients a_{Li} and a_{Ri}. At $t = 0$ we hence have to enforce,

$$\sum_{i=1}^{n_L} a_{Li}\mathbf{E}'_{Li}|_{t=0} = \sum_{i=1}^{n_R} a_{Ri}\mathbf{E}'_{Ri}|_{t=0}\,. \tag{6.18}$$

We now construct a matrix $[N]$ as,

$$[N] = \left[\mathbf{E}'_{L1}|_{t=0}, \ldots, \mathbf{E}'_{Ln_L}|_{t=0}, \mathbf{E}'_{R1}|_{t=0}, \ldots, \mathbf{E}'_{Rn_R}|_{t=0}\right]\,. \tag{6.19}$$

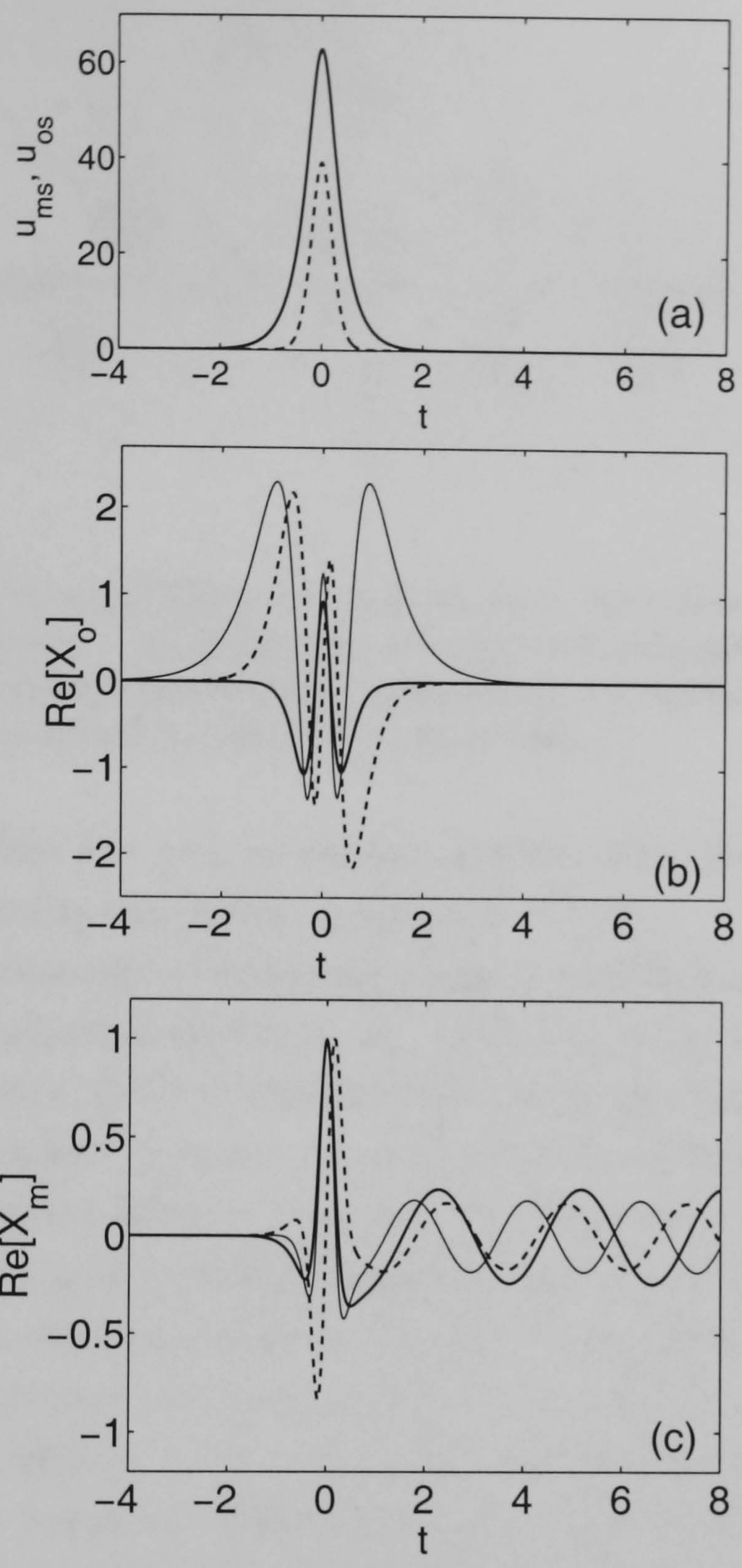

Figure 6.3: Internal one-sided quasibound modes, (a) soliton solution, solid line u_{m}, dashed line u_{o}, (β=-50, δ=10), (b) real part of X_{o} (c) real part of X_{m}. Thick solid line $\lambda = 32.1$, dashed line $\lambda = 43.0$, thin solid line $\lambda = 48.2$.

Note that all elements are functions of the chosen eigenvalue λ. Given the number $n_L + n_R$ equal to the number of vector components of $\mathbf{E}'$, for a solution λ of eq. (6.15) the determinant $|[N]|$ has to be zero. Hence, solutions of the eigensystem can be found by a root finding procedure. For a solution λ, the eigenvector can be obtained by solving for the coefficients a_{Li} and a_{Ri} from eq. (6.18).

For real valued eigenvalues $\lambda < |\beta|$ we obtain 4 decaying solutions for the optical asymptotics according to eq. (6.10). The microwave has 2 decaying solutions corresponding to eq. (6.13) and one oscillating solution eq. (6.12). As we can integrate X_{m} with an oscillating

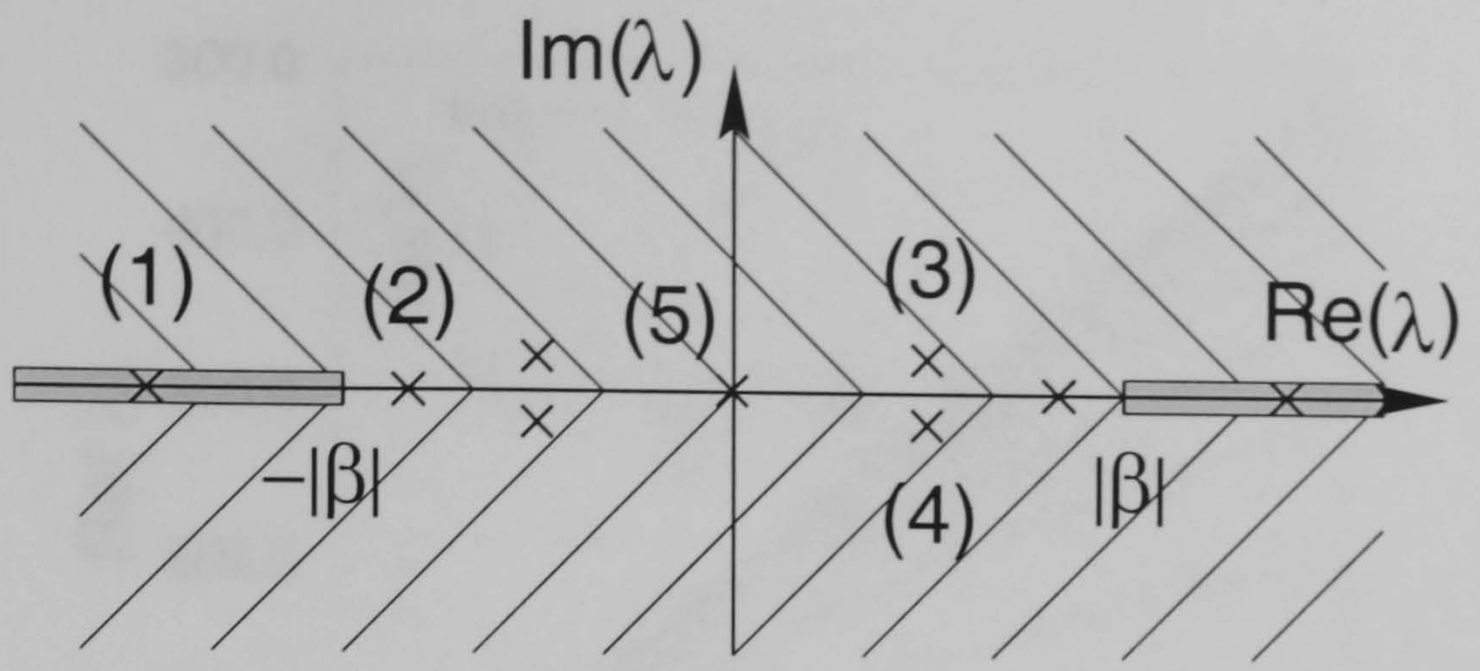

Figure 6.4: Schematic structure of the spectrum of the linear eigenvalue-problem eqs. (6.6, 6.7): (1) both microwave and optical eigenfunctions are unbound, (2) bound optical and unbound microwave eigenfunctions (symmetric), (3) rightsided quasibound modes, (4) leftsided quasibound modes, (5) trivial modes.

asymptotic from both sides $t \to \pm\infty$, we obtain a solution of eq. (6.15) for arbitrary values λ with X_m having oscillating tails in both directions $t \to \pm\infty$.

In addition to this dense band of continuum modes we identified another type of solution. Here we integrate the oscillating asymptotic eq. (6.12) only from one direction and search for zeros of the determinant $|[N]|$. It was found that at discrete values λ eigenmodes exist with vanishing tails for either $t \to \infty$ or $t \to -\infty$ respectively. These asymmetric quasibound modes are depicted in Fig. 6.3. Further, it was found that eigenvalues of modes with radiating tails for $t \to \infty$ showed a small imaginary component $\mathrm{Im}(\lambda) > 0$, which indicates that the discrete modes result in decaying perturbations. Due to the third order derivative in the dispersion term of the microwave evolution equation, for $\delta > 0$ and $\sigma_\mathrm{o} = 1$ linear microwaves can radiate only to the left, i.e. $t > 0$. As a result, only the one-sided quasibound modes can be excited on a zero background explaining the appearance of discrete internal modes of the solitary wave. From the symmetry properties of the eigensystem eq. (6.6) follows that for a solution $\mathbf{E}(t)$ with corresponding eigenvalue λ the vectors $\mathbf{E}^*(t)$, $\mathbf{E}(-t)$ and $\mathbf{E}^*(-t)$ are also solutions with eigenvalues $-\lambda^*$, $-\lambda$ and λ^*, respectively. Hence we also obtain symmetric eigenfunctions with oscillating tails for $t \to -\infty$ and $\mathrm{Im}(\lambda) < 0$. However, these exponentially growing eigenfunctions cannot be excited without an additional external source. From a similar argument it follows that the dense band of symmetric continuum modes with bound optical functions can not be excited on a zero background.

It should be noted that the eigenfunctions responsible for the soliton oscillations found here are somewhat similar to quasibound modes found in the SHG system [117], where the corresponding eigenvalue lies in the gap of the fundamental but in the continuum of the second harmonic. The location of different types of eigenvalues in the complex plane is sketched in Fig. 6.4. In domain (1) we find a dense band of radiation modes with both microwave and optical eigenfunctions are unbound. Domain (2) represents eigenmodes with bound optical

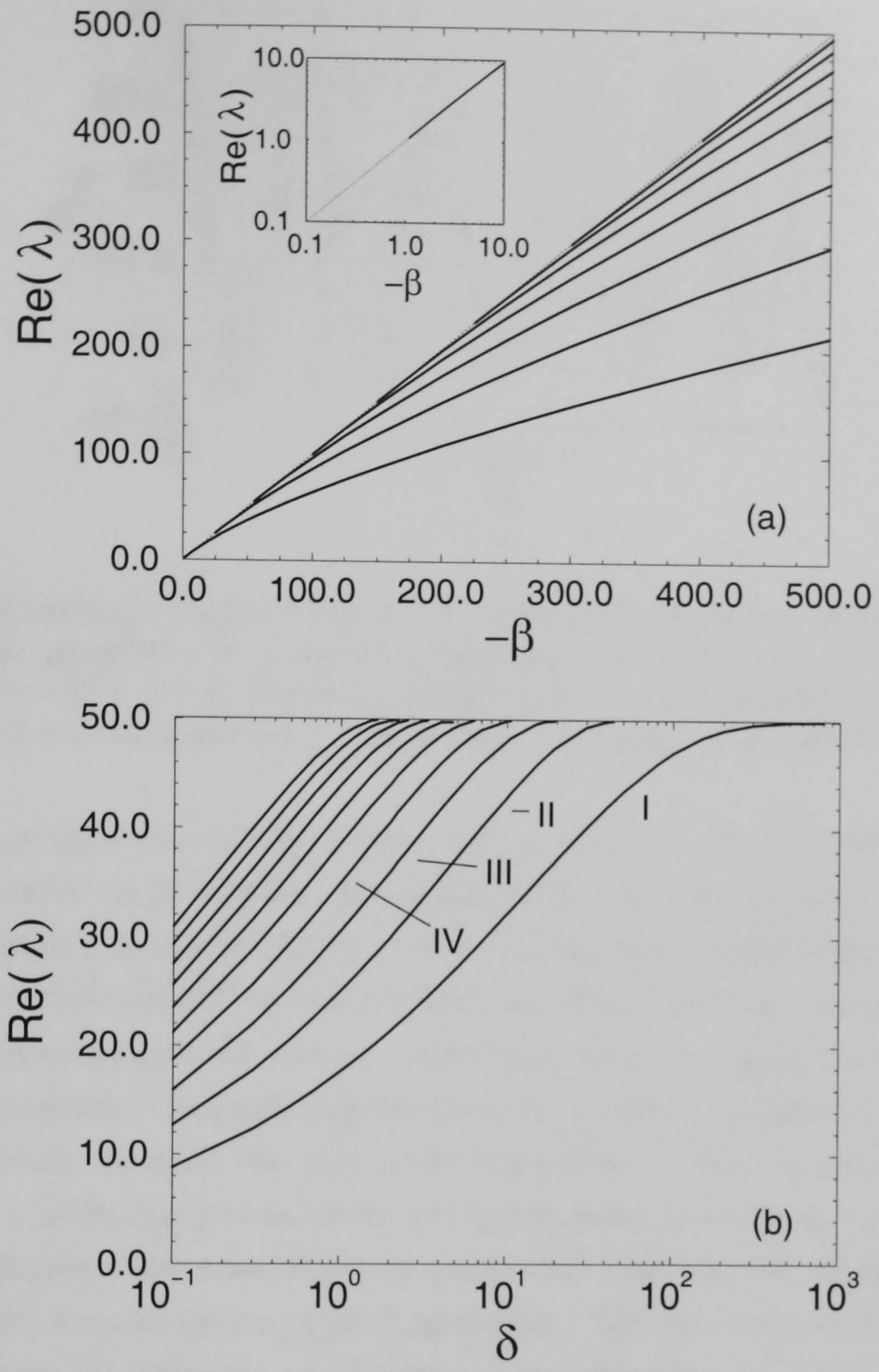

Figure 6.5: Eigenvalues λ of one-sided discrete internal modes as a function of soliton parameters. (a) δ=20, (b) eigenvalues of the first 10 modes with β=-50.

and unbound microwave eigenfunctions. Domain (3) and (4) correspond to discrete rightsided and leftsided asymmetric perturbation functions respectively.

A spectral decomposition of the oscillation depicted in Fig. 6.2 showed a number of discrete frequencies. Numerical calculations confirmed the appearance of multiple discrete asymmetric modes depending on the soliton parameters. Fig. 6.5 shows the calculated eigenvalues λ as a function of the parameters β and δ. For decreasing δ and hence decreasing velocity mismatch a number of eigenvalues emerge from the boundary of the continuous spectrum of the optical wave. Note that in Fig. 6.5(b) only the eigenvalues of the first 10 modes are shown. However,

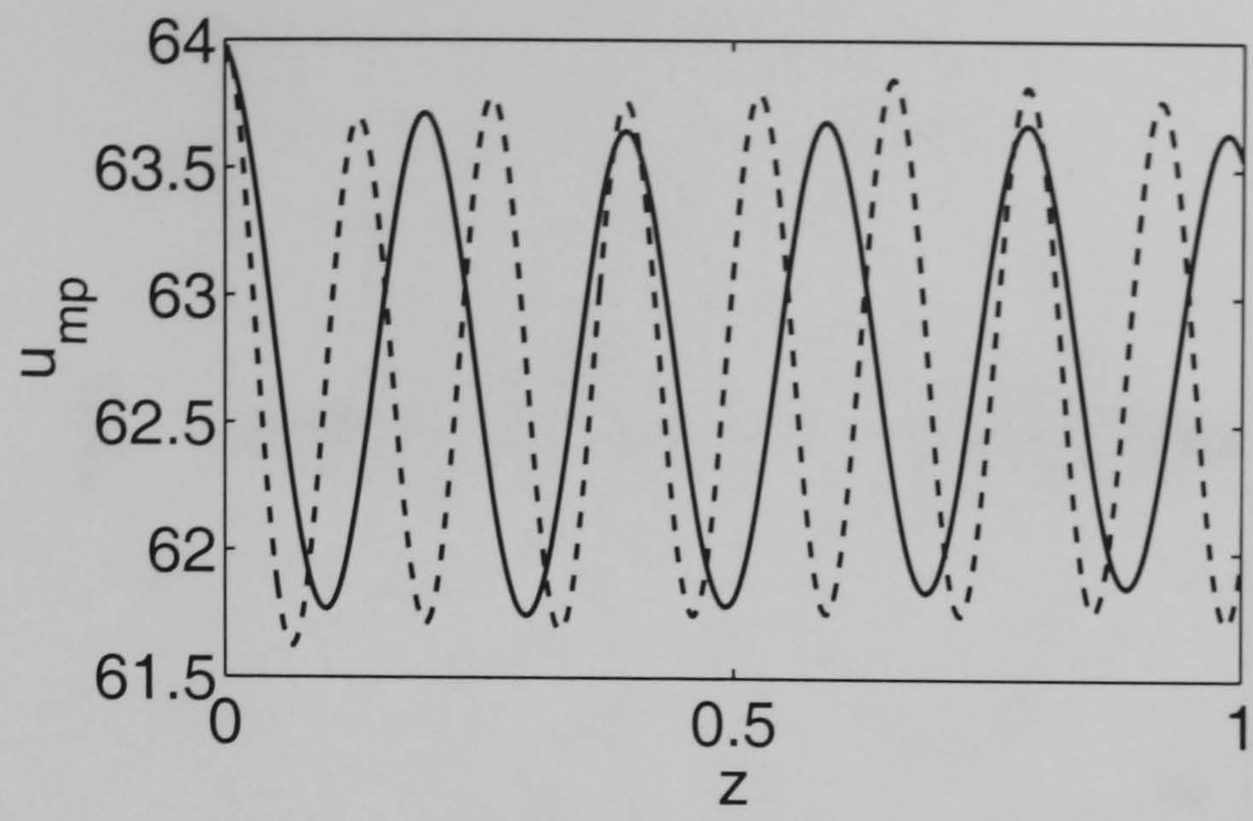

Figure 6.6: Soliton oscillation due to excitation with internal modes, peak amplitude of microwave. Soliton parameters as in Fig. 6.3. Solid line: calculated real part of internal mode $\mathrm{Re}(\lambda) = 32.1$, circular frequency of oscillation $\Omega = 32.0$; dashed line: calculated real part of internal mode $\mathrm{Re}(\lambda) = 48.2$, circular frequency of oscillation $\Omega = 47.8$.

we did not find an upper limit for the number of discrete modes. For large velocity mismatch, i.e. for large δ, there are no internal eigenmodes leading to a threshold for the appearance of soliton oscillations. A similar threshold exists in the case of SHG solitons [116] for the bifurcation of an internal mode from the continuous spectrum, where for large phase mismatch between fundamental and second harmonic the soliton does not support an internal mode.

Numerical simulations confirmed that the frequency of soliton oscillations indeed coincides with the numerically obtained real part of the eigenvalue λ. Here, a soliton solution was perturbed with a particular internal mode and subsequently propagated. As shown in Fig. 6.6, discrete oscillations can indeed be excited separately and both the calculated eigenvalue and the oscillation frequencies are in good agreement. The excitation of an internal mode depends on the overlap between perturbation and eigenfunction. As shown in Fig. 6.2, for the symmetric perturbation eq. (6.2) it is mainly the fundamental mode, i.e. the mode with the smallest $\mathrm{Re}(\lambda)$, which is excited.

As indicated earlier, the eigenvalues of the discrete internal modes exhibit a small imaginary part (see Fig. 6.7(a)). This explains the damping of the oscillations depicted in Fig. 6.2. As shown in Tab. 6.1, the damping rate of internal oscillations is in good agreement with the imaginary part of the discrete eigenvalues $\mathrm{Im}(\lambda)$. Here, the soliton solutions were perturbed with particular modes in a similar manner to Fig. 6.6.

As shown in Fig. 6.7(b), higher order modes are more weakly damped then lower order modes. This coincides with our observation that a symmetric perturbation corresponding to eq. (6.2) leads to an initial strong excitation of the fundamental mode, whereas after a certain propagation length the dynamics is governed by a beating of oscillations with frequencies corresponding to higher order modes.

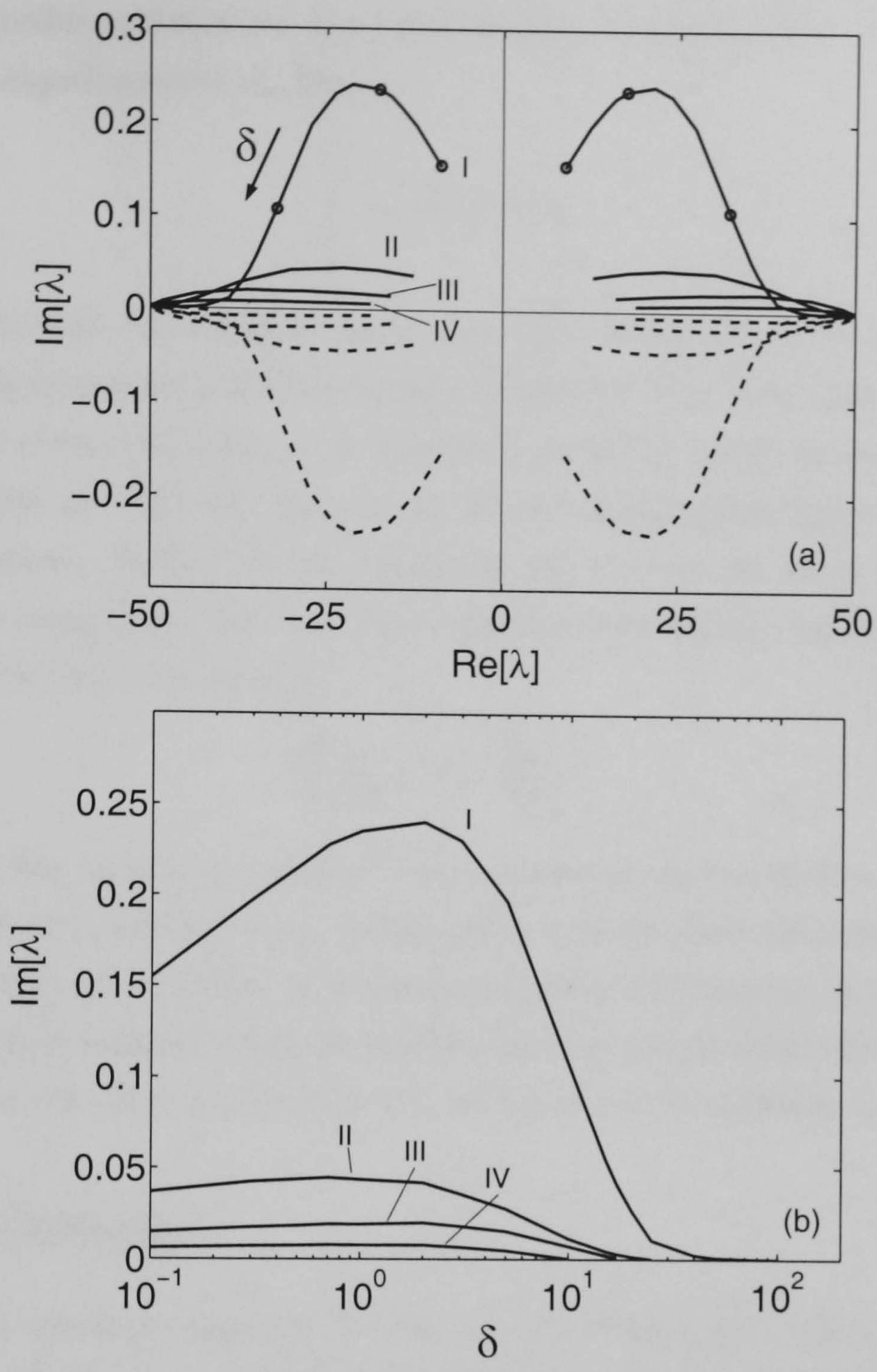

Figure 6.7: Development of eigenvalues λ with varying parameter δ ($\beta = -50$). (a) development in complex plane; solid lines: right-sided quasibound internal modes, dashed line: left-sided quasibound modes. Depicted are the first 4 discrete modes; the numbering corresponds to eigenmodes in Fig. 6.5, circles correspond to excited modes in Tab. 6.1. (b) Imaginary part of eigenvalues λ vs. soliton parameter δ.

δ	$\mathrm{Re}(\lambda)_{\mathrm{calc}}$	$\mathrm{Im}(\lambda)_{\mathrm{calc}}$	$\mathrm{Re}(\lambda)_{\mathrm{prop}}$	$\mathrm{Im}(\lambda)_{\mathrm{prop}}$
0.1	8.83	0.155	8.88	0.141
1	17.6	0.235	17.6	0.238
10	32.1	0.107	32.0	0.128

Table 6.1: Oscillation frequencies and damping constants of perturbed solitary waves, $\beta = -50$. $\mathrm{Re}(\lambda)_{\mathrm{calc}}$ and $\mathrm{Im}(\lambda)_{\mathrm{calc}}$ are real and imaginary part of calculated eigenvalue λ, $\mathrm{Re}(\lambda)_{\mathrm{prop}}$ and $\mathrm{Im}(\lambda)_{\mathrm{prop}}$ correspond to oscillation of soliton perturbed with internal mode.

From the eigenvalue problem eq. (6.6) and taking into account Eq. (5.51) we can derive for bound optical eigenfunctions X_o that,

$$\int_{-\infty}^{\infty} u_{os} X_o \, dt = 0 \, . \tag{6.20}$$

Eq. (6.20) specifies that the internal mode does not add energy to the optical part of the solitary wave. This means that in the process of damping of an internal mode the energy of the optical wave is conserved which is in agreement with the conservation law eq. (5.25).

Note that we did not find any eigenmodes which correspond to decaying and hence unstable soliton solutions. In fact, in the numerical calculations we never observed a soliton to decay even for strong perturbations. This remarkable robustness can be explained by the conservation law derived in Section 5.4,

$$\frac{\partial}{\partial z} S_m = \delta - \frac{E_{opt}}{M_m} \, , \tag{6.21}$$

which states that the center of gravity of the microwave moves with a constant velocity. For a soliton solution according to eq. (5.51) one can easily show that the center of gravity cannot move. A decay of the soliton as a result of small perturbations would result in steady radiation of microwave energy in one particular direction due to dispersion. As a result, the center of gravity would move in this direction, which is in contradiction to eq. (6.21).

6.4 Soliton Collisions

Having shown that solitary waves due to OR and the electro-optic effect are always stable against small perturbations, we will now shortly address the interaction between propagating soliton solutions. Collisions between solitary waves in nonintegrable systems have, for example, been discussed for the SHG system [109]. It was shown that for a high relative velocity difference these solitary waves behave similarly to solitons, i.e. they pass each other nearly unscathed. For a low velocity difference solitary waves were found to merge and form oscillating states or repel each other depending on the phase difference between the optical waves. Rather then investigating the interaction behaviour in detail, the aim of this Section is to show on the basis of examples that a similar collision behaviour can be obtained in the case of OR cascading.

For the unidirectional evolution equations considered in this thesis, the term *collision* corresponds to an interaction between solitons with different relative velocities. Solitons with different velocities can be constructed using the transformation eq. (5.48). Here we calculate a soliton solution according to eq. (5.51) and modify its shape subsequently using eq. (5.48). Note that due to the lack of translational (or Galilean) invariance in the equations solitons with different velocities will in general have different soliton energies. In the numerical

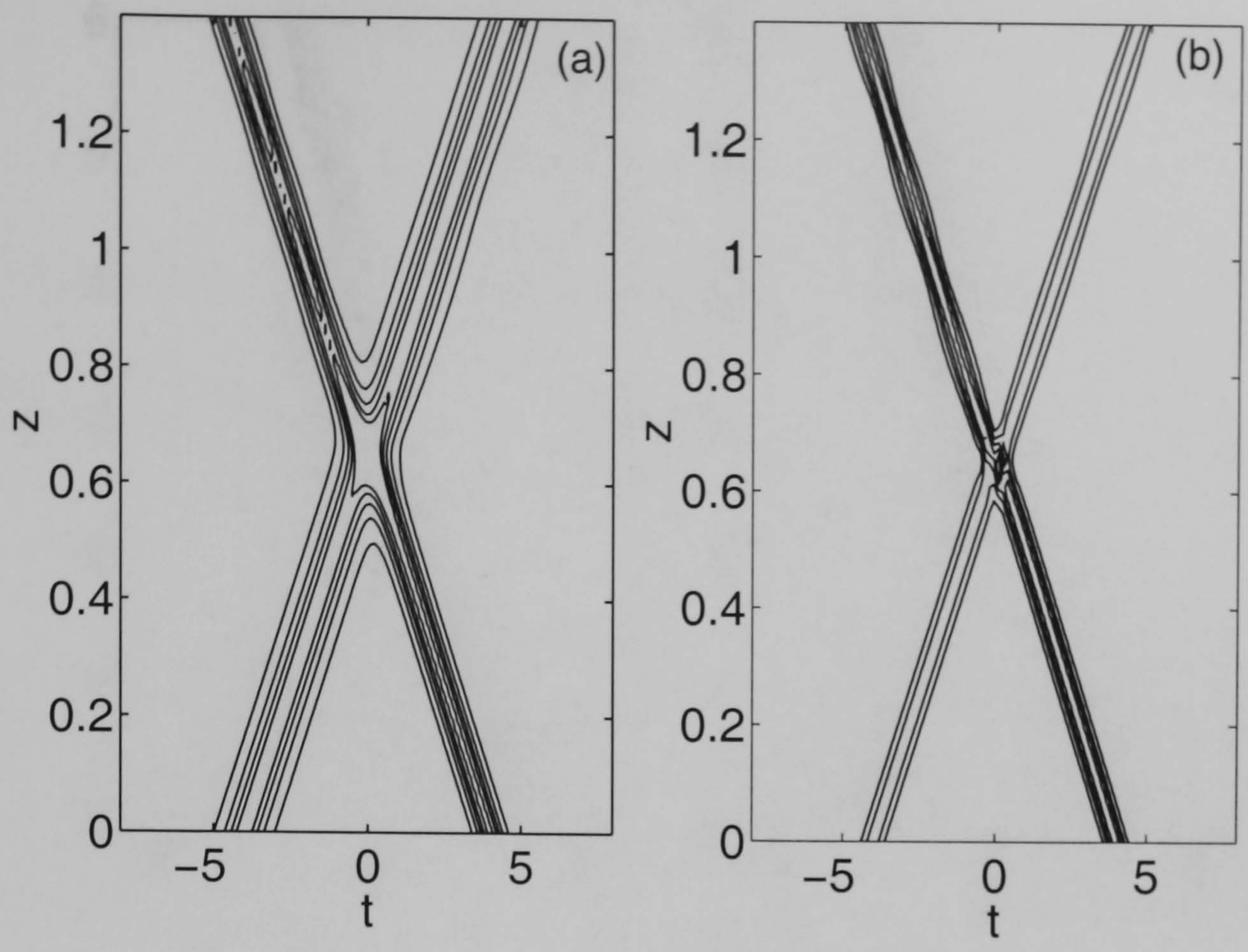

Figure 6.8: Propagation of two solitary waves with different velocities ($v = \pm 6$, $\tilde{\beta} = -50$, $\tilde{\delta} = 10$, $\chi = \zeta = 0$). Contour plot of (a) amplitude of the microwave and (b) modulus of the optical wave.

calculations, solitons were calculated with the same soliton phase and equal but opposite velocities. They are then propagated by integration of eqs. (5.40) by means of a Crank-Nicholson scheme with sufficient separation from each other at $z = 0$.

Fig. 6.8 shows the outcome of a numerical experiment for solitons with large velocity difference. The solitary waves pass each other nearly unperturbed with retention of their original velocities. The solitary waves behave hence similarly to true solitons. However, a closer inspection of the numerical result shows some radiation and a weak excitation of internal modes of the respective solitons.

The collision behaviour is completely different at lower velocity differences and hence longer interaction lengths. As shown in Fig. 6.9, the solitary waves merge and propagate with a velocity different from the initial velocities. Furthermore, both microwave and optical wave radiate a considerable amount of energy into radiation. However, even this strong perturbation of the solitary waves does not lead to a complete decay of the soliton solutions but to a bound state between both waves. As in the case of strong perturbations of solitons, we never observed a soliton to completely decay during a collision.

The results are hence similar to effects observed in other nonintegrable systems. Whereas for large velocity difference solitary waves behave like true solitons, for small velocity difference

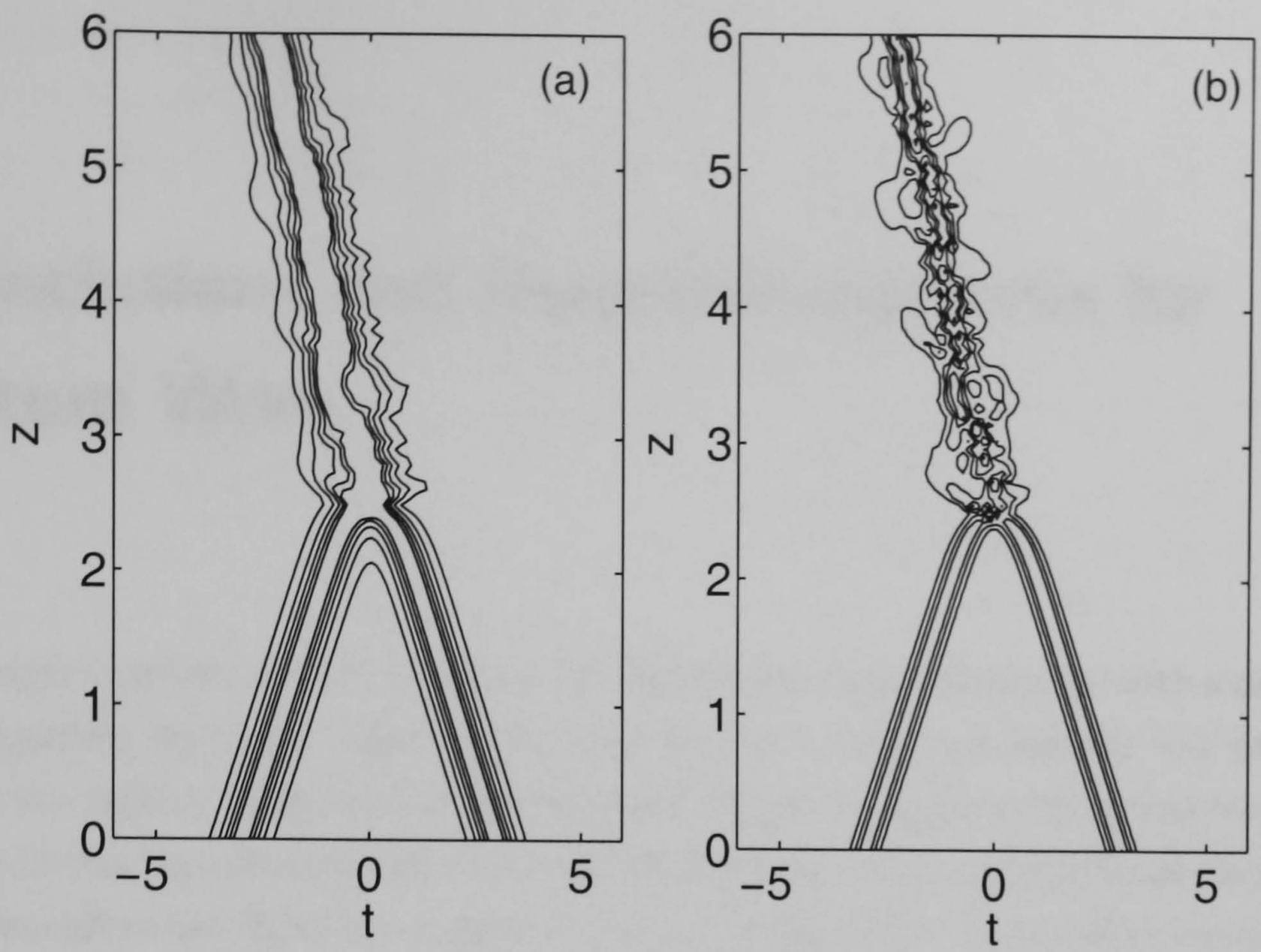

Figure 6.9: Propagation of two solitary waves with different velocities ($v = \pm 1$, $\tilde{\beta} = -50$, $\tilde{\delta} = 10$, $\chi = \zeta = 0$). Contour plot of (a) amplitude of the microwave and (b) modulus of the optical wave.

and hence longer interaction length we find a complex dynamical behaviour which is very different from that expected in integrable systems.

6.5 Conclusions

In this Chapter we considered the linear stability of solitons due to the interaction of a microwave with an optical wave. Perturbed solitons show persistent oscillations with strong radiation from the microwave. These oscillations stem from eigenmodes of the linearized problem. It is found that the solitary waves are always located in the continuum of the microwave. Apart from the dense band of continuum modes, discrete asymmetric modes with complex eigenvalues exist. As the microwave radiates in one direction only, these modes are excited leading to regular, damped oscillations. Although for large mismatch none of these states exist, a number of discrete eigenvalues bifurcate from the border of the continuous spectrum of the optical wave with decreasing velocity mismatch. Eigenvalues corresponding to soliton instability were not found. Collisions between solitons with different velocities showed a complex dynamical behaviour. Whereas for large relative velocity difference the solitons propagate nearly unperturbed, below a critical velocity difference solitons can merge but still maintain a bound propagation.

7 Conclusions and Recommendations for Future Work

In this thesis, a theoretical framework for the interaction of an optical wave with a microwave in a waveguiding structure linked together by a second order nonlinearity was developed. Emphasis was laid on the generation of ultrashort electrical transients by optical rectification (OR) and further on cascading effects due to the interplay of OR and the linear electro-optic effect. Throughout the thesis it was tried not only to describe the various effects qualitatively but also to give an indication of physical magnitudes involved. This Chapter will review the major findings of this work. Some suggestions and indications for future work are presented in the final Section of this Chapter.

7.1 Generation of Electrical Signals

As a first tool for the understanding of OR in a travelling wave structure, a simple transmission line model was introduced. The external optical induction of a polarisation in a transmission line is interpreted as an additional displacement current in the line capacitance. The consideration of bidirectional wave propagation and appropriate boundary conditions were found to be essential for the correct description of the instantaneously generated voltage at the beginning of the line and the charge development on the line for a continuous wave excitation.

For a qualitative description of the dynamically evolving part of the generated electrical signal, which is not dependent on the boundary conditions, a set of evolution equations was developed based on a coupled mode formalism. The model is fairly general as it allows the extension to higher order modes and, in principle, higher order nonlinearities. However, the expansion of the microwave propagation constant around zero frequency restricts the model to microwave guides without a low frequency cut-off.

Techniques for the estimation of relevant parameters were discussed. For example structures based on the AlGaAs-system typical parameters are estimated and used in subsequent calculations to give quantitative results. It was shown that the phase velocity of the microwave can be tuned in a large range by the application of slow wave structures.

Two essential scenarios for the generation of electrical transients were identified. These are the single polarisation case, where one optical mode copropagates with one microwave mode, and the mixed polarisation case, i.e. both TE and TM modes are necessary to generate the microwave.

In the single polarisation case, it was shown that velocity matching between the group velocity of the optical wave and the phase velocity of the microwave is important and can potentially lead to a linear growth of the generated single cycle microwave signal. For a high conversion efficiency, ultrashort high power optical pulses are essential. Whereas conversion efficiencies up to 10^{-3} are calculated for an ideal structure, high microwave losses lead to a saturation of the induced voltage after typically a few millimeters. Nevertheless the amplitude of the electrical signal is predicted to reach the range of Volts. Whereas the energy of the optical pulse remains nearly unchanged, the generated microwave can have a considerable impact on the phase of the optical pulse. The corresponding self phase modulation (SPM) can result in spectral broadening for very high peak powers (around 5 kW for the example structure). Compared to SPM due to a Kerr nonlinearity, the power spectrum was shown to be different in structure due to a phase modulation proportional to the first derivative of the optical power.

In a non-velocity matched structure, there is no further generation of microwave energy after a certain walk-off length. Two pulses are generated, one travelling with the optical wave and one travelling with the microwave velocity. Interestingly, even for very high microwave losses the generated peak voltage can reach hundreds of mV as the optical wave acts as a steady source for the microwave.

The concept of generation of microwave signals via OR in a travelling wave structure considered here should be compared with the injection of electrical transients in transmission lines by photoconductive switching. Here, the amplitude of the generated microwave signal is mainly determined by the bias voltage applied. However, there are fundamental limitations in the frequency response associated with their natural time constants for carrier dynamics [1]. The shortest pulses reported on transmission lines generated by photoconductive switching have a width of 0.45 ps [64]. However, the injection of 180 fs pulses in a microwave transmission line by OR reported recently [28] shows the potential of ultrafast electro-optic processes. A substantial improvement in amplitude can be expected from the approach discussed in this thesis - a travelling wave arrangement.

For mixed polarisation OR, i.e. both the TE and TM modes interact to generate the microwave, beating between both modes leads to effects which are very different from the single polarisation case. In particular, the mismatch between the phase velocities of the TE and TM modes leads to an effective modulation of the nonlinearity. Whereas perfect velocity matching between the optical wave and the microwave results in alternating up- and downconversion, a slight mismatch gives rise to the generation of a sinusoidal signal

evolving between the pulses travelling with the optical wave and the velocity of the microwave, respectively. This could be exploited as a basis for an integrated, on-chip, narrow-bandwidth, tunable THz-source. It was also demonstrated that for very high optical powers self-induced mode conversion might occur.

7.2 Soliton Formation

The second main topic considered in this thesis was soliton formation due to cascading of OR and the electro-optic effect and related aspects. It was found that a number of phenomena discovered for cascading between a fundamental and its second harmonic (SHG cascading) can also occur for the case of OR. The equations derived for the interaction between microwave and optical wave were shown to be similar to the system of long wave short wave interaction which can be found in a variety of other physical systems.

The conservative system was shown to be Hamiltonian and subject to a number of conservation laws. Continuous wave solutions of the system are modulationally unstable in all dispersion domains. Similarly to the case of SHG cascading, the evolution equations reduce to the nonlinear Schroedinger equation for large velocity mismatch between both waves. For small mismatch, a two parameter family of soliton solutions is obtained numerically. Analytical solutions exist for special cases. The excitation of solitons by injection of a sole optical pulse was shown to be possible but required a long excitation length.

Another interesting aspect considered in this thesis was the sole propagation of a microwave governed by a Korteweg de Vries equation which implies the possibility of soliton formation due to the nonlinear microwave self-interaction. However, the effect was shown to be small and certainly difficult to observe in an experiment.

Finally, the linear stability of bright soliton solutions was investigated. It was shown that perturbed solitons exhibit persistent oscillations with strong radiation from the microwave. The origin of the discrete oscillations were found to be quasi-bound internal eigenmodes of the linearized problem. Whereas for large mismatch none of these states exist, a number of discrete eigenvalues bifurcate from the border of the continuous spectrum of the optical wave with decreasing velocity mismatch. Interestingly, there seems to be no upper limit for the number of discrete internal modes. The solitons were always found to be linearly stable.

It should be noted that for all the effects reviewed in this Section, the conservative, i.e. lossless, system was considered. This is certainly a strong simplification. For most of the effects described in this thesis, excessive frequency-dependent microwave losses and dispersion at THz frequencies are the main problem for applications or even for a potential experimental observation. Whereas research is underway [27], the problem of high loss and dispersion of lithographically defined coplanar transmission lines has not been resolved yet. The search for alternative wide-band transmission channels with low loss and dispersion is an area of active

research with a number of papers published only recently [124, 125, 126, 127]. Propagation in circular and metallic waveguides as well as single-crystal sapphire fibers has demonstrated large bandwidth with one-tenth the loss compared to coplanar transmission lines. However, a disadvantage of these waveguides might be the broadband excitation of multiple modes and their extreme group velocity dispersion near cut-off frequencies.

7.3 Future Work

Although an attempt was made to deliver a certain degree of completeness in this thesis, the topic of OR in a travelling wave structure is far from being exhausted and a number of interesting problems could be considered in the future:

- Any optical material with a $\chi^{(2)}$-nonlinearity also exhibits a $\chi^{(3)}$-nonlinearity, or even higher order nonlinearities. In this thesis, the influence of the $\chi^{(3)}$-nonlinearity was neglected. In semiconductors like GaAs, in particular when considering cascading effects, higher order nonlinearities might compete with or even dominate the $\chi^{(2)}$-nonlinearity. For a complete description it would therefore be necessary to include the $\chi^{(3)}$-nonlinearity in the model and investigate its influence.

- All aspects of soliton formation discussed in this thesis considered only the conservative, i.e. lossless system. As was indicated earlier, in particular high microwave losses can have a considerable impact on the nonlinear dynamics. As the overall energy of the system is nearly exclusively determined by the energy of the optical wave which constantly pumps the microwave, even high microwave losses might not necessarily result in the decay of a stationary solution. However, the influence of dissipative effects remains to be determined.

- The conversion efficiency of OR is rather low even for perfect velocity matching. For the enhancement of the efficiency an attractive implementation would be a resonator structure where the optical wave and the microwave travel forwards and backwards exchanging energy in every roundtrip. Furthermore, the device could be integrated in a modelocked laser cavity using ultrashort, high peak power, circulating optical pulses for an efficient conversion of energy.

- A number of results obtained in this thesis should also be applicable to the case of bulk material when the transverse spatial derivatives are neglected, i.e. when considering plane propagating waves. However, an investigation of the effects discussed in this thesis for bulk material including transverse effects would be interesting, in particular from an experimental point of view. Evolution equations for this kind of problem have been published recently [24].

- The recent progress in novel, e.g. dielectric, THz waveguides [127] suggests the use of alternative waveguiding structures instead of coplanar transmission lines. Here, the application of structures with low frequency cut-off would require a modification of the dynamic model presented in this thesis.

Most importantly, an experimental verification of the effects predicted and described in this thesis with sophisticated time-resolving measurement techniques would be an interesting and challenging task.

Appendix

A Forced Hyperbolic Wave Equation

We consider the forced hyperbolic wave equation,

$$\frac{\partial^2 V}{\partial z^2} - \frac{1}{c^2}\frac{\partial^2 V}{\partial t^2} = L'\frac{\partial^2 Q}{\partial t^2} \,, \tag{A.1}$$

where $V(z,t)$ and $f(z,t) = L'\partial^2 Q/\partial t^2$ are defined in the domain $0 \le z \le L$ and $t \ge 0$. The complementary function of eq. (A.1) is given by forward and backward propagating waves,

$$V_{\rm c}(z,t) = V^+(t - z/c) + V^-(t + z/c) \,. \tag{A.2}$$

To find a particular integral $V_{\rm p}(z,t)$, eq. (A.1) is integrated over the area $A = A_{\rm I} \cup A_{\rm II}$ depicted in Fig. A.1. Here the integration paths $s_{\rm I}$ and $s_{\rm II}$ are given by,

$$s_{\rm I} \to t = t_0 - (z_0 - z)/c \,, \quad s_{\rm II} \to t = t_0 + (z_0 - z)/c \,. \tag{A.3}$$

Further we set $V_{\rm p}(z,t) = 0$ at the boundaries $t = 0$, $z = 0$, and $z = L$. Integrating eq. (A.1), one obtains,

$$\iint\limits_A \left(\frac{\partial^2 V_{\rm p}}{\partial z^2} - \frac{1}{c^2}\frac{\partial^2 V_{\rm p}}{\partial t^2}\right) dA = \iint\limits_A f(z,t)\, dA \,. \tag{A.4}$$

Applying Green's Theorem,

$$\iint (\partial_z\, a - \partial_t\, b)\, dtdz = \oint (a\, dt + b\, dz) \,, \tag{A.5}$$

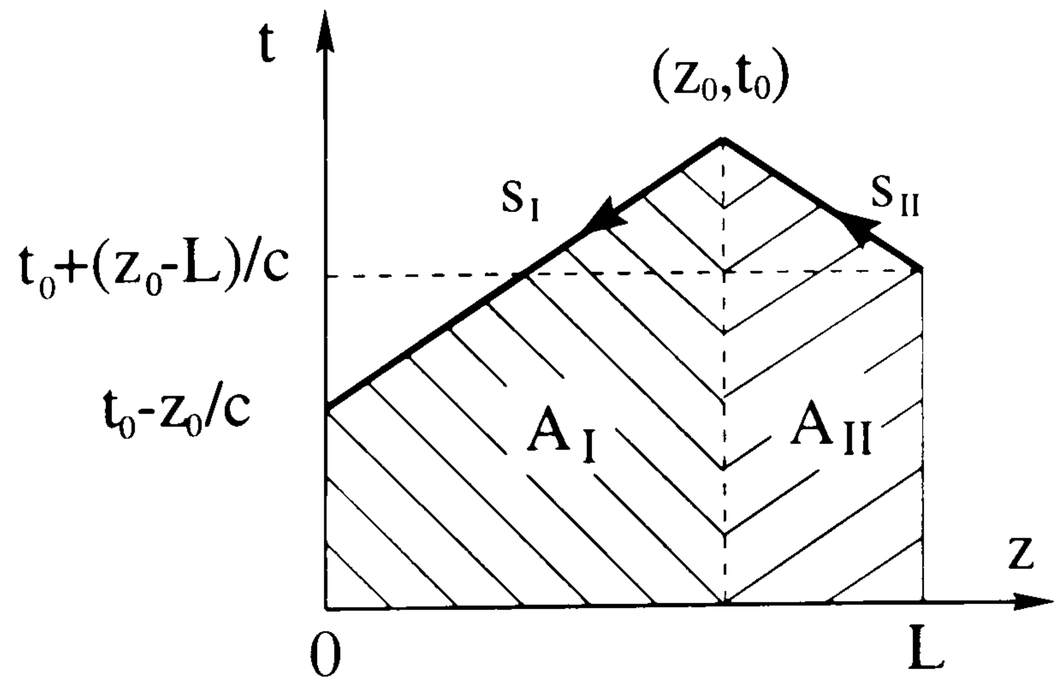

Figure A.1: Schematic of integration domain for solving the forced hyperbolic wave equation, the integration path $s_{\rm I}$ is defined by $t = t_0 - (z_0 - z)/c$, similarly the path $s_{\rm II}$ is given by $t = t_0 + (z_0 - z)/c$.

where the line integral on the boundary has to be taken counterclockwise, one can simplify the left hand side of eq. (A.4) as,

$$\begin{aligned}\iint\limits_A \left(\frac{\partial^2 V_\mathrm{p}}{\partial z^2} - \frac{1}{c^2}\frac{\partial^2 V_\mathrm{p}}{\partial t^2}\right) dA &= \oint \left(\frac{\partial V_\mathrm{p}}{\partial z}\,dt + \frac{1}{c^2}\frac{\partial V_\mathrm{p}}{\partial t}\,dz\right) , \\ &= \int\limits_{s_\mathrm{I}} \left(\frac{\partial V_\mathrm{p}}{\partial z}\,dt + \frac{1}{c^2}\frac{\partial V_\mathrm{p}}{\partial t}\,dz\right) + \int\limits_{s_\mathrm{II}} \left(\frac{\partial V_\mathrm{p}}{\partial z}\,dt + \frac{1}{c^2}\frac{\partial V_\mathrm{p}}{\partial t}\,dz\right) , \\ &= \frac{1}{c}\int\limits_{s_\mathrm{I}} \left(\frac{\partial V_\mathrm{p}}{\partial z}\,dz + \frac{\partial V_\mathrm{p}}{\partial t}\,dt\right) - \frac{1}{c}\int\limits_{s_\mathrm{II}} \left(\frac{\partial V_\mathrm{p}}{\partial z}\,dz + \frac{\partial V_\mathrm{p}}{\partial t}\,dt\right) , \\ &= -\frac{2}{c}\,V_\mathrm{p}(z_0, t_0) . \end{aligned} \tag{A.6}$$

Here we used that along the integration path $s_\mathrm{I} \rightarrow dt = dz/c$ and along $s_\mathrm{II} \rightarrow dt = -dz/c$. The right hand side of eq. (A.4) gives,

$$\iint\limits_A f(z,t)\,dA = \iint\limits_{A_\mathrm{I}} f(z,t)\,dA + \iint\limits_{A_\mathrm{II}} f(z,t)\,dA , \tag{A.7}$$

$$= \int\limits_0^{z_0} \int\limits_0^{t_0-(z_0-z)/c} f(z,t)\,dt dz + \int\limits_{z_0}^{L} \int\limits_0^{t_0-(z-z_0)/c} f(z,t)\,dt dz . \tag{A.8}$$

For $f(z,t) = L'\partial^2 Q/\partial t^2$ and $\partial Q/\partial t\,|_{t=0} = 0$ the integral eq. (A.8) can be further simplified as,

$$\iint\limits_A f(z,t)\,dA = L' \int\limits_0^{z_0} \frac{\partial}{\partial t} Q[z, t_0 - (z_0 - z)/c]\,dz + L' \int\limits_{z_0}^{L} \frac{\partial}{\partial t} Q[z, t_0 - (z - z_0)/c]\,dz . \tag{A.9}$$

From eqs. (A.6, A.9) we can derive a particular integral of eq. (A.1),

$$V_\mathrm{p}(z,t) = -\frac{L'c}{2}\int\limits_0^{z} \frac{\partial}{\partial t} Q[z', t - (z - z')/c]\,dz' - \frac{L'c}{2}\int\limits_z^{L} \frac{\partial}{\partial t} Q[z', t - (z' - z)/c]\,dz' , \tag{A.10}$$

where we changed $t_0 \rightarrow t$, $z_0 \rightarrow z$, $z \rightarrow z'$ for convenience. The solution of the forced hyperbolic wave equation (A.1) is hence given by,

$$\begin{aligned} V(z,t) &= V^+(t - z/c) + V^-(t + z/c) \\ &\quad - \frac{L'c}{2}\int\limits_0^{z} \frac{\partial}{\partial t} Q[z', t - (z - z')/c]\,dz' - \frac{L'c}{2}\int\limits_z^{L} \frac{\partial}{\partial t} Q[z', t - (z' - z)/c]\,dz' . \end{aligned} \tag{A.11}$$

The wave equation for the current on the transmission line eq. (3.6) can be solved similarly.

B Coupled Mode Formalism

The coupled mode formalism used to derive eqs. (4.21-4.23) can in general be applied when considering the coupling between modes in a guiding structure under presence of a perturbation which can be expressed in terms of a polarisation. The treatment here follows closely the one in [128]. The starting point is Maxwell's equations in the frequency domain for an isotropic, nonmagnetic dielectric in the absence of free charges or external currents,

$$\nabla \times \tilde{\mathbf{E}} = \mathrm{i}\omega\mu_0\tilde{\mathbf{H}} \,, \tag{B.1}$$

$$\nabla \times \tilde{\mathbf{H}} = -\mathrm{i}\omega\epsilon_0\epsilon_r\tilde{\mathbf{E}} - \mathrm{i}\omega\tilde{\mathbf{P}}_{\mathrm{NL}} \,. \tag{B.2}$$

The notation corresponds to the one used in Section 4.2. Assuming the nonlinear polarisation to be weak we consider the linear problem first and expand the fields of the problem with nonlinear polarisation present into the modes of the unperturbed problem. The unperturbed fields $\tilde{\mathbf{E}}_0$ and $\tilde{\mathbf{H}}_0$ are then governed by,

$$\nabla \times \tilde{\mathbf{E}}_0 = \mathrm{i}\omega\mu_0\tilde{\mathbf{H}}_0 \,, \tag{B.3}$$

$$\nabla \times \tilde{\mathbf{H}}_0 = -\mathrm{i}\omega\epsilon_0\epsilon_r\tilde{\mathbf{E}}_0 \,. \tag{B.4}$$

The solutions of eqs. (B.3, B.4) in a structure with translational invariance in z-direction are the respective modes [35],

$$\tilde{\mathbf{E}}_0 = \sum_n \left[u^+_{n0}(\omega)\, e^{\mathrm{i}\beta_n(\omega)z} + u^-_{n0}(\omega)\, e^{-\mathrm{i}\beta_n(\omega)z}\right] \mathbf{e}_n(\omega, x, y) \,, \tag{B.5}$$

$$\tilde{\mathbf{H}}_0 = \sum_n \left[u^+_{n0}(\omega)\, e^{\mathrm{i}\beta_n(\omega)z} - u^-_{n0}(\omega)\, e^{-\mathrm{i}\beta_n(\omega)z}\right] \mathbf{h}_n(\omega, x, y) \,, \tag{B.6}$$

where $u^+_{n0}(\omega)$ and $u^-_{n0}(\omega)$ are the frequency dependent coefficients of forward and backward propagating modes in the structure. $\mathbf{e}_n(\omega, x, y)$ and $\mathbf{h}_n(\omega, x, y)$ denote the transverse field profiles of guided modes in the structure. For weak nonlinearities we assume the transverse field structures not to be perturbed by the induced polarisation. The fields $\tilde{\mathbf{E}}$ and $\tilde{\mathbf{H}}$ can hence be expanded into the modes of the unperturbed problem as,

$$\tilde{\mathbf{E}} = \sum_n \left[u^+_n(\omega, z) + u^-_n(\omega, z)\right] \mathbf{e}_n(\omega, x, y) \,, \tag{B.7}$$

$$\tilde{\mathbf{H}} = \sum_n \left[u^+_n(\omega, z) - u^-_n(\omega, z)\right] \mathbf{h}_n(\omega, x, y) \,. \tag{B.8}$$

The aim of the following procedure is the determination of the coefficients u_n^+ and u_n^-. To this end we mix the perturbed and unperturbed fields. The combination of the scalar products of eq. (B.1) with $\tilde{\mathbf{H}}_0^*$, eq. (B.2) with $\tilde{\mathbf{E}}_0^*$, the complex conjugate of eq. (B.3) with $\tilde{\mathbf{H}}$ and the complex conjugate of (B.4) with $\tilde{\mathbf{E}}$ gives,

$$\nabla \cdot [\tilde{\mathbf{E}} \times \tilde{\mathbf{H}}_0^* + \tilde{\mathbf{E}}_0^* \times \tilde{\mathbf{H}}] = \mathrm{i}\omega \tilde{\mathbf{P}}_{\mathrm{NL}} \cdot \tilde{\mathbf{E}}_0^* \,, \tag{B.9}$$

where we used $\nabla \cdot [\mathbf{A} \times \mathbf{B}] = \mathbf{B} \cdot \nabla \times \mathbf{A} - \mathbf{A} \cdot \nabla \times \mathbf{B}$. After integrating eq. (B.9) over the transverse plane one obtains,

$$\frac{\partial}{\partial z} \iint [\tilde{\mathbf{E}} \times \tilde{\mathbf{H}}_0^* + \tilde{\mathbf{E}}_0^* \times \tilde{\mathbf{H}}]_z \, dxdy = \mathrm{i}\omega \iint \tilde{\mathbf{P}}_{\mathrm{NL}} \cdot \tilde{\mathbf{E}}_0^* \, dxdy \,, \tag{B.10}$$

where we assumed exponentially decaying fields in transverse directions towards infinity. To derive evolution equations for forward and backward propagating waves we insert particular solutions of the linear problem into eq. (B.10). Here we use that the linear modes are orthogonal to each other. To extract an equation for a forward propagating wave $u_m^+(\omega, z)$ the fields $\tilde{\mathbf{E}}_0$ and $\tilde{\mathbf{H}}_0$ are chosen as,

$$\tilde{\mathbf{E}}_0 = e^{\mathrm{i}\beta_m z} \, \mathbf{e}_m \,, \quad \tilde{\mathbf{H}}_0 = e^{\mathrm{i}\beta_m z} \, \mathbf{h}_m \,. \tag{B.11}$$

Inserting (B.11) and eqs. (B.7, B.8) into (B.10) gives,

$$\begin{aligned} \frac{\partial}{\partial z} \iint e^{-\mathrm{i}\beta_m z} \left[\left(\sum_n (u_n^+ + u_n^-) \, \mathbf{e}_n \right) \times \mathbf{h}_m^* + \mathbf{e}_m^* \times \left(\sum_n (u_n^+ - u_n^-) \, \mathbf{h}_n \right) \right]_z dxdy \\ = e^{-\mathrm{i}\beta_m z} \, \mathrm{i}\omega \iint \mathbf{e}_m^* \cdot \tilde{\mathbf{P}}_{\mathrm{NL}} \, dxdy \,. \end{aligned} \tag{B.12}$$

This expression can be further simplified by using the orthogonality relation,

$$\iint [\mathbf{e}_n \times \mathbf{h}_m^*]_z \, dxdy = 0 \quad \text{for} \quad m \neq n \,. \tag{B.13}$$

One finally obtains an evolution equation for the m-th forward propagating mode in the waveguide under influence of a polarisation,

$$\frac{\partial u_m^+}{\partial z} - \mathrm{i}\beta_m u_m^+ = \frac{\mathrm{i}\omega}{p_m} \iint \mathbf{e}_m^* \cdot \tilde{\mathbf{P}}_{\mathrm{NL}} \, dxdy \,, \tag{B.14}$$

where we defined,

$$p_m = 2\mathrm{Re} \iint [\mathbf{e}_m \times \mathbf{h}_m^*]_z \, dxdy \,. \tag{B.15}$$

In a similar manner we derive the propagation equations for the backward propagating wave by choosing,

$$\tilde{\mathbf{E}}_0 = e^{-\mathrm{i}\beta_m z} \, \mathbf{e}_m \,, \quad \tilde{\mathbf{H}}_0 = -e^{-\mathrm{i}\beta_m z} \, \mathbf{h}_m \,, \tag{B.16}$$

from which follows similarly,

$$\frac{\partial u_m^-}{\partial z} + \mathrm{i}\beta_m u_m^- = \frac{\mathrm{i}\omega}{p_m} \iint \mathbf{e}_m^* \cdot \tilde{\mathbf{P}}_{\mathrm{NL}} \, dxdy \,. \tag{B.17}$$

Eqs. (B.14, B.17) describe in general the coupling between modes in a translationally invariant structure under presence of a nonlinear polarisation.

C Discretisation Scheme for Optical Mode Solver

The wave equation for the transverse electric fields eq. (4.36) can be written in the form,

$$\partial_x[\varepsilon_r^{-1}\partial_x(\varepsilon_r\tilde{E}_x)+\varepsilon_r^{-1}\partial_y(\varepsilon_r\tilde{E}_y)]+\partial_y(\partial_y\tilde{E}_x-\partial_x\tilde{E}_y)+\tilde{E}_x(\omega^2\varepsilon_r/c^2-\beta^2)=0\,, \quad \text{(C.1)}$$

$$\partial_y[\varepsilon_r^{-1}\partial_x(\varepsilon_r\tilde{E}_x)+\varepsilon_r^{-1}\partial_y(\varepsilon_r\tilde{E}_y)]+\partial_x(\partial_x\tilde{E}_y-\partial_y\tilde{E}_x)+\tilde{E}_y(\omega^2\varepsilon_r/c^2-\beta^2)=0\,. \quad \text{(C.2)}$$

For a discretisation of eqs. (C.1, C.2), we introduce the notation,

$$\tilde{E}_{x,y}^{[i,j]}=\tilde{E}_{x,y}(i\Delta x,j\Delta y)\,, \quad \epsilon_r^{[i,j]}=\epsilon_r(i\Delta x,j\Delta y)\,, \quad \text{(C.3)}$$

where Δx and Δy are the increments in x- and y-direction respectively. The derivatives are replaced by central finite difference formulas as,

$$\partial_x\tilde{E}_{x,y}^{[i,k]}=\frac{\tilde{E}_{x,y}^{[i+1/2,j]}-\tilde{E}_{x,y}^{[i-1/2,j]}}{\Delta x}\,. \quad \text{(C.4)}$$

The y-derivatives are expressed analogously. The discretized form of the equation for the x-component of the electric field (C.1) is then given by,

$$\begin{aligned}
&\tilde{E}_x^{[i+1/2,j]}\left(\frac{\omega^2}{c^2}\varepsilon_r^{[i+1/2,j]}-\frac{1}{\Delta x^2}\frac{\varepsilon_r^{[i+1/2,j]}}{\varepsilon_r^{[i,j]}}-\frac{1}{\Delta x^2}\underbrace{\frac{\varepsilon_r^{[i+1/2,j]}}{\varepsilon_r^{[i+1,j]}}}_{\mathrm{T}_{x1}}-\frac{2}{\Delta y^2}\right)\\
&+\frac{\tilde{E}_x^{[i+3/2,j]}}{\Delta x^2}\frac{\varepsilon_r^{[i+3/2,j]}}{\varepsilon_r^{[i+1,j]}}+\frac{\tilde{E}_x^{[i-1/2,j]}}{\Delta x^2}\underbrace{\frac{\varepsilon_r^{[i-1/2,j]}}{\varepsilon_r^{[i,j]}}}_{\mathrm{T}_{x2}}+\frac{\tilde{E}_x^{[i+1/2,j+1]}}{\Delta y^2}+\frac{\tilde{E}_x^{[i+1/2,j-1]}}{\Delta y^2}\\
&+\frac{\tilde{E}_y^{[i+1,j+1/2]}}{\Delta x\Delta y}\left(\frac{\varepsilon_r^{[i+1,j+1/2]}}{\varepsilon_r^{[i+1,j]}}-1\right)-\frac{\tilde{E}_y^{[i+1,j-1/2]}}{\Delta x\Delta y}\underbrace{\left(\frac{\varepsilon_r^{[i+1,j-1/2]}}{\varepsilon_r^{[i+1,j]}}-1\right)}_{\mathrm{T}_{x3}}\\
&-\frac{\tilde{E}_y^{[i,j+1/2]}}{\Delta x\Delta y}\left(\frac{\varepsilon_r^{[i,j+1/2]}}{\varepsilon_r^{[i,j]}}-1\right)+\frac{\tilde{E}_y^{[i,j-1/2]}}{\Delta x\Delta y}\underbrace{\left(\frac{\varepsilon_r^{[i,j-1/2]}}{\varepsilon_r^{[i,j]}}-1\right)}_{\mathrm{T}_{x4}}\\
&=\beta^2\tilde{E}_x^{[i+1/2,j]}\,. \qquad \text{(C.5)}
\end{aligned}$$

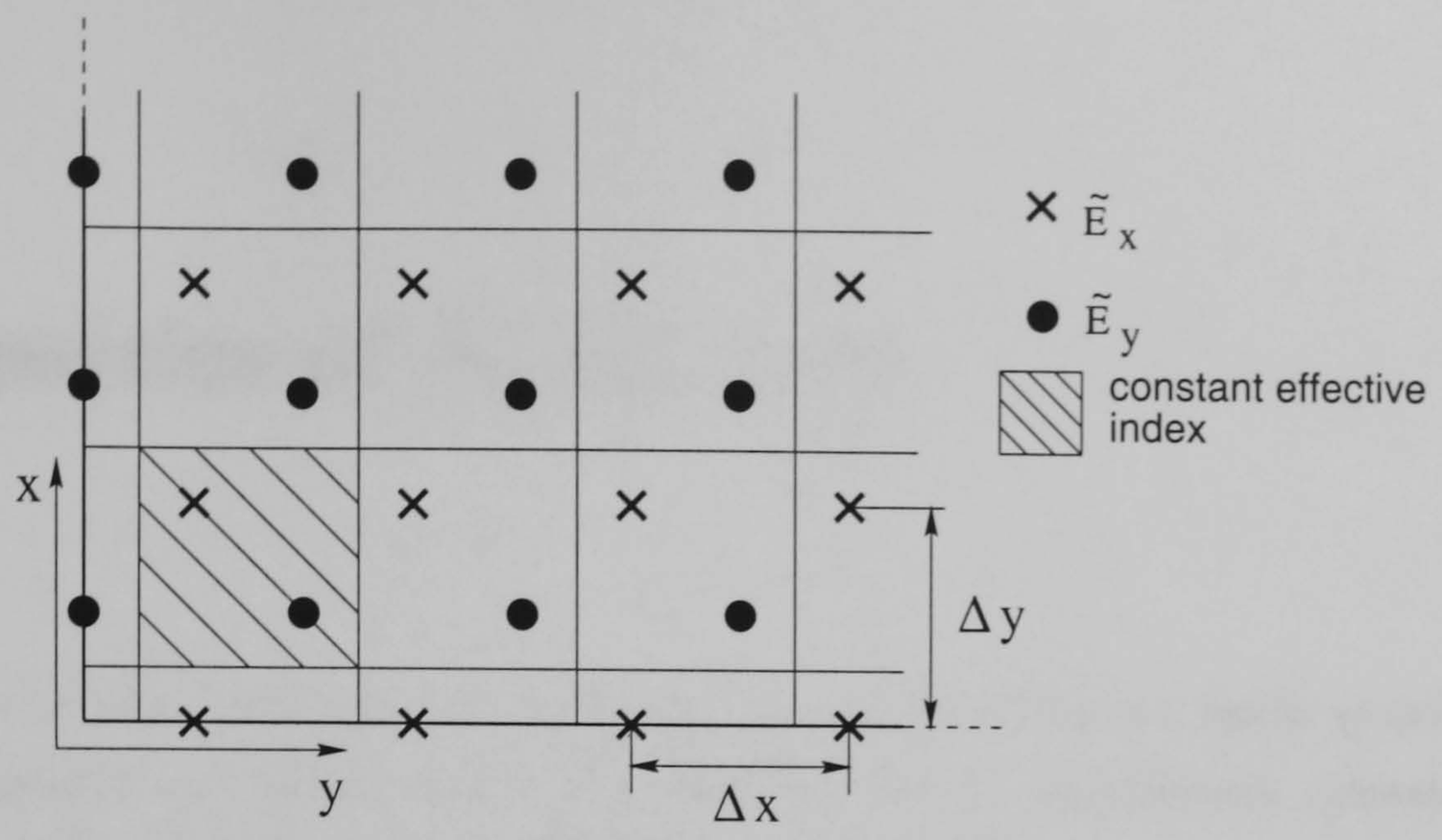

Figure C.1: Discretisation scheme of the waveguide cross-section.

Similarly one obtains a discretized equation for the y-component of the electric field,

$$\begin{aligned}
&\tilde{E}_y^{[i,j+1/2]} \left(\frac{\omega^2}{c^2} \varepsilon_r^{[i,j+1/2]} - \frac{1}{\Delta y^2} \frac{\varepsilon_r^{[i,j+1/2]}}{\varepsilon_r^{[i,j]}} - \frac{1}{\Delta y^2} \underbrace{\frac{\varepsilon_r^{[i,j+1/2]}}{\varepsilon_r^{[i,j+1]}}}_{\mathrm{T}_{y1}} - \frac{2}{\Delta x^2} \right) \\
&+ \frac{\tilde{E}_y^{[i,j+3/2]}}{\Delta y^2} \frac{\varepsilon_r^{[i,j+3/2]}}{\varepsilon_r^{[i,j+1]}} + \frac{\tilde{E}_y^{[i,j-1/2]}}{\Delta y^2} \underbrace{\frac{\varepsilon_r^{[i,j-1/2]}}{\varepsilon_r^{[i,j]}}}_{\mathrm{T}_{y2}} + \frac{\tilde{E}_y^{[i+1,j+1/2]}}{\Delta x^2} + \frac{\tilde{E}_y^{[i-1,j+1/2]}}{\Delta x^2} \\
&+ \frac{\tilde{E}_x^{[i+1/2,j+1]}}{\Delta x \Delta y} \left(\frac{\varepsilon_r^{[i+1/2,j+1]}}{\varepsilon_r^{[i,j+1]}} - 1 \right) - \frac{\tilde{E}_x^{[i-1/2,j+1]}}{\Delta x \Delta y} \underbrace{\left(\frac{\varepsilon_r^{[i-1/2,j+1]}}{\varepsilon_r^{[i,j+1]}} - 1 \right)}_{\mathrm{T}_{y3}} \\
&- \frac{\tilde{E}_x^{[i+1/2,j]}}{\Delta x \Delta y} \left(\frac{\varepsilon_r^{[i+1/2,j]}}{\varepsilon_r^{[i,j]}} - 1 \right) + \frac{\tilde{E}_x^{[i-1/2,j]}}{\Delta x \Delta y} \underbrace{\left(\frac{\varepsilon_r^{[i-1/2,j]}}{\varepsilon_r^{[i,j]}} - 1 \right)}_{\mathrm{T}_{y4}} \\
&= \beta^2 \tilde{E}_y^{[i,j+1/2]} \, . \qquad \text{(C.6)}
\end{aligned}$$

Fig. C.1 shows a sketch of the discretisation scheme. Both $\tilde{E}_x$ and $\tilde{E}_y$ field points are shifted by $\Delta x/2$ and $\Delta y/2$ respectively. Rectangular sections with constant refractive index are defined as shown in Fig. C.1. As a result, the quotients T_{x1}, T_{y1}, T_{x2}, T_{y2} and T_{x3}, T_{y3}, T_{x4}, T_{y4} in eqs. (C.5, C.6) simplify to,

$$T_{x1} = T_{y1} = T_{x2} = T_{y2} = 1 \, , \quad T_{x3} = T_{y3} = T_{x4} = T_{y4} = 0 \, . \qquad \text{(C.7)}$$

The boundaries between areas with the same refractive index profile are located between gridpoints. It can be shown that with the above scheme the boundary conditions between different dielectrics are fulfilled automatically [39]. The discretisation of the cross-section of the dielectric waveguide corresponding to eqs. (C.5, C.6) results in an eigenvalue problem which can then be solved by a sparse matrix solver.

D Properties of $Al_xGa_{1-x}As$

Whereas most of the results presented in this thesis should have a fairly general character, example structures are chosen which are based on the GaAs/AlGaAs system. The basic properties of AlGaAs will shortly be discussed in this Section.

Gallium Arsenide is a semiconductor with a zinc-blende (or cubic) symmetry belonging to the class $\bar{4}3m$. It does not exhibit birefringence, i.e. all dielectric coefficients ε_{ii} are equal. In the optical range we are interested in, i.e. $\lambda \sim 1.6\,\mu$m, $Al_xGa_{1-x}As$ exhibits normal dispersion. The optical index of refraction used in the calculations is based on the model introduced by Afromowitz in [129].

The low frequency dielectric constant of GaAs can be written as [130],

$$\varepsilon_r = \varepsilon_\infty + \frac{f_{\mathrm{TO}}^2(\varepsilon_s - \varepsilon_\infty)}{f_{\mathrm{TO}}^2 - f^2 + \mathrm{i}\gamma_p f}\,, \tag{D.1}$$

where ε_s is the static dielectric constant and ε_∞ the high frequency dielectric constant for frequencies well above the long wavelength TO phonon frequency f_{TO} but below the optical absorption edge. γ_p is a damping coefficient. For GaAs, values given in the literature are $\varepsilon_s = 12.9$, $\varepsilon_\infty = 10.9$, $f_{\mathrm{TO}} = 8.032\,\mathrm{THz}$ and $\gamma_p = 60.48\,\mathrm{GHz}$ [130]. For frequencies near the phonon resonance around 8 THz, material dispersion and losses will increase considerably. However, in this thesis we are mainly interested in the frequency range around 1 THz and hence will neglect these effects. The general behaviour of AlAs is identical to eq. (D.1) with values similar to that of GaAs. The dielectric constant of their alloy can be estimated by a linear interpolation scheme using the dielectric constants $\varepsilon_{r\mathrm{GaAs}} = 12.9$ and $\varepsilon_{r\mathrm{AlAs}} = 10.0$ [63].

From symmetry properties of the $\bar{4}3m$ class it can be shown that the second order susceptibility $\tilde{\chi}^{(2)}_{ijk}(-\omega_3;\omega_1,\omega_2)$ is only nonzero if all indices i, j and k are different and further that [31],

$$\tilde{\chi}^{(2)}_{123}(-\omega_3;\omega_1,\omega_2) = \tilde{\chi}^{(2)}_{231}(-\omega_3;\omega_1,\omega_2) = \tilde{\chi}^{(2)}_{312}(-\omega_3;\omega_1,\omega_2)\,. \tag{D.2}$$

In this thesis, a wavelength of the optical wave is chosen which is far from the band edge $\lambda_b \approx 870\,\mathrm{nm}$. From overall permutation symmetry and the reality condition it can then be shown that the coefficients describing optical rectification and the electro-optic effect are

equal,

$$\begin{aligned}\tilde{\chi}^{(2)}_{123}(0;\omega,-\omega) = \tilde{\chi}^{(2)}_{231}(0;\omega,-\omega) = \tilde{\chi}^{(2)}_{312}(0;\omega,-\omega)\\ =\tilde{\chi}^{(2)}_{123}(-\omega;\omega,0) = \tilde{\chi}^{(2)}_{231}(-\omega;\omega,0) = \tilde{\chi}^{(2)}_{312}(-\omega;\omega,0)\ .\end{aligned} \tag{D.3}$$

In contracted notation, the d-tensor is hence given by,

$$d_{ij} = \begin{pmatrix} 0 & 0 & 0 & d_{14} & 0 & 0 \\ 0 & 0 & 0 & 0 & d_{14} & 0 \\ 0 & 0 & 0 & 0 & 0 & d_{14} \end{pmatrix}\ . \tag{D.4}$$

The susceptibilities might depend on the composition of $Al_xGa_{1-x}As$. For the coefficient corresponding to second harmonic generation it was shown that its value changes only slightly for mole fractions of Al up to $x = 0.3$ at a fundamental wavelength $\lambda = 1.064\,\mu$m [131]. However, in the calculations we use the value of the electro-optic coefficient of GaAs $r_{41} = -1.53\,$pm/V at 1.5 μm given in [130].

At the wavelength of interest in this thesis, Kleinmann symmetry cannot be assumed. That means the susceptibility for the microwave self-interaction $\tilde{\chi}^{(2)}_{ijk}(0;0,0)$ will not necessarily coincide with the coefficients describing rectification and the electro-optic effect. However, due to the lack of appropriate values in the literature, we will use for calculations $\tilde{\chi}^{(2)}_{ijk}(0;0,0) = \tilde{\chi}^{(2)}_{ijk}(-\omega;\omega,0) = \tilde{\chi}^{(2)}_{ijk}(0;\omega,-\omega)$ which gives an indication of physical magnitudes involved.

E Attenuation and Dispersion of Coplanar Transmission Lines

In the following formulas are reviewed which describe dispersion and attenuation of coplanar microwave transmission lines (after [3, 51, 57]). For high frequencies ($f > 100\,\mathrm{GHz}$) the main mechanisms are metal electrode attenuation, radiation loss and mode dispersion. We consider coplanar waveguides and coplanar striplines on a substrate with a dielectric constant ε_r surrounded by air. The corresponding geometries are shown in Fig. E.1.

E.1 Dispersion

The dispersive characteristics of coplanar transmission lines at high frequencies are mainly determined by modal dispersion and dispersion due to the finite conductivity of metallic electrodes. The effective index is hence given by,

$$n_{\mathrm{mic}}(f) = n_{\mathrm{mod}}(f) + n_{\mathrm{cond}}(f)\ . \tag{E.1}$$

An approximate expression for mode dispersion has been derived by curve fitting to results from a full wave analysis in [53],

$$n_{\mathrm{mod}}(f) = \sqrt{\varepsilon_q} + \frac{\sqrt{\varepsilon_r} - \sqrt{\varepsilon_q}}{1 + a\left(\dfrac{f}{f_{\mathrm{te}}}\right)^{-1.8}}\ . \tag{E.2}$$

Here ε_q is the quasi-static permittivity and f_{te} is the surface wave TE_1 mode cutoff frequency,

$$\begin{aligned} \varepsilon_q &= \frac{\varepsilon_r + 1}{2}\ , \\ f_{\mathrm{te}} &= \frac{c}{4d\sqrt{\varepsilon_r - 1}}\ . \end{aligned} \tag{E.3}$$

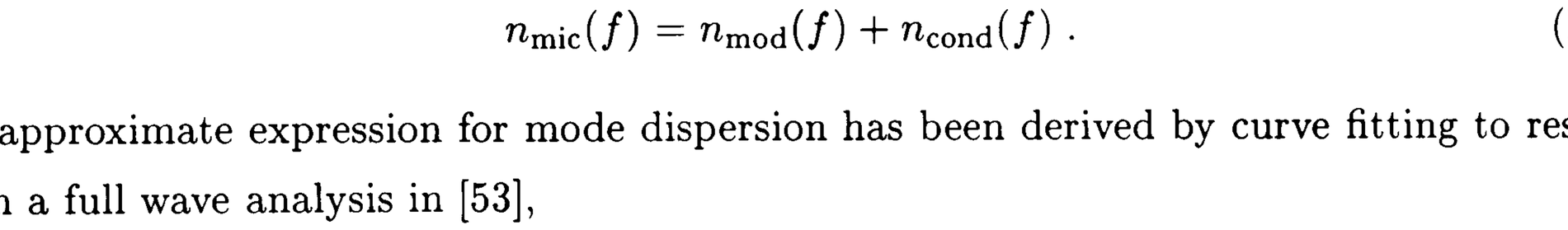

Figure E.1: Cross-sectional view of (a) coplanar waveguide (CPW) and (b) coplanar strip line (CPS) consisting of metal strips on a dielectric substrate surrounded by air.

The parameter a is a factor related to the geometry of the transmission line and given by,

$$\begin{aligned} \log(a) &\sim u \log(s/w) + v \,, \\ u &= 0.54 - 0.64q + 0.015q^2 \,, \\ v &= 0.43 - 0.86q + 0.54q^2 \,, \\ q &= \log(s/d) \,. \end{aligned} \tag{E.4}$$

If the electrode width is comparable to the thickness t, correction factors for s and w should be introduced [3]. Corresponding formulas can be found, for example, in [51].

The contribution due to conductor losses for the CPW line is given by,

$$n_{\mathrm{cpwcond}}(f) = \frac{c}{2\pi f} \frac{\ln 10}{20} \operatorname{Im}\left[Z_s(f) Z_{\mathrm{cpw}}(f)\right] g_{\mathrm{cpw}} \,. \tag{E.5}$$

Here c is the velocity of light in free space and $Z_{\mathrm{cpw}}(f)$ is the characteristic impedance of the line,

$$Z_{\mathrm{cpw}} = \frac{120\pi}{n_{\mathrm{mod}}(f)} \frac{K(\sqrt{1-k^2})}{4K(k)} \,, \tag{E.6}$$

where $k = s/(s+w)$ and $K(k)$ is the complete elliptic integral of the first kind. The surface impedance $Z_s(f)$ and the geometrical factor g_{cpw} are given below. The contribution of conductor losses to the dispersion for the CPS line is similarly given by,

$$n_{\mathrm{cpscond}}(f) = \frac{c}{2\pi f} \frac{\ln 10}{20} \operatorname{Im}\left[\frac{Z_s(f)}{Z_{\mathrm{cps}}(f)}\right] g_{\mathrm{cps}} \,, \tag{E.7}$$

with

$$Z_{\mathrm{cps}} = \frac{120\pi}{n_{\mathrm{mod}}(f)} \frac{K(k)}{K(\sqrt{1-k^2})} \,. \tag{E.8}$$

E.2 Attenuation

The attenuation at high frequencies is determined by radiation loss and a contribution due to the finite conductivity of the electrodes,

$$\alpha(f) = \alpha_{\mathrm{cond}}(f) + \alpha_{\mathrm{rad}}(f) \,. \tag{E.9}$$

The attenuation due to electrode losses for the CPW line amounts to,

$$\alpha_{\mathrm{cpwcond}}(f) = \frac{\ln 10}{20} \operatorname{Re}\left[Z_s(f) Z_{\mathrm{cpw}}(f)\right] g_{\mathrm{cpw}} \,, \tag{E.10}$$

and for the CPS line,

$$\alpha_{\mathrm{cpscond}}(f) = \frac{\ln 10}{20} \operatorname{Re}\left[\frac{Z_s(f)}{Z_{\mathrm{cps}}(f)}\right] g_{\mathrm{cps}} \,, \tag{E.11}$$

The surface impedance Z_s is given by,

$$\begin{aligned} Z_s(f) &= \frac{1+\mathrm{i}}{\sigma\delta} \coth[(1+\mathrm{i})t/\delta] \,, \\ \delta &= \frac{1}{\sqrt{f\mu_0\sigma\pi}} \,, \end{aligned} \tag{E.12}$$

where δ is the skin depth and σ is the conductivity of the metal electrodes. g is a parameter taking into account the geometry of the structure and amounts to [51],

$$g_{\mathrm{cpw}} = 4.88 \times 10^{-4} n_{\mathrm{mod}}^2(f) \frac{P'}{\pi w} \left(1 + \frac{s}{w}\right) \frac{\frac{1.25}{\pi} \ln\left(\frac{4\pi s}{t}\right) + 1 + \frac{1.25t}{\pi s}}{\left\{2 + \frac{s}{w} - \frac{1.25t}{\pi w}\left[1 + \ln\left(\frac{4\pi s}{t}\right)\right]\right\}^2} , \tag{E.13}$$

for the CPW line and,

$$g_{\mathrm{cps}} = 17.34 \frac{P'}{\pi s} \left(1 + \frac{w}{s}\right) \frac{\frac{1.25}{\pi} \ln\left(\frac{4\pi w}{t}\right) + 1 + \frac{1.25t}{\pi w}}{\left\{1 + \frac{2w}{s} + \frac{1.25t}{\pi s}\left[1 + \ln\left(\frac{4\pi w}{t}\right)\right]\right\}^2} , \tag{E.14}$$

for the CPS line. Finally P' is given by,

$$P' = \begin{cases} k \dfrac{[K(k)/K(\sqrt{1-k^2})]^2}{(1-\sqrt{1-k^2})(1-k^2)^{3/4}} & \text{for } 0 \le k \le 0.707 , \\ \dfrac{1}{(1-k)\sqrt{k}} & \text{for } 0.707 \le k \le 1.0 . \end{cases} \tag{E.15}$$

The radiation loss for a CPW line has been calculated by Rutledge *et al.* in [61]. Later work by Frankel *et al.* [57] showed that the quasi static approximation should be modified by including the frequency dependent effective index of the structure. For the radiation loss of a coplanar structure one obtains,

$$\alpha_{\mathrm{cpwrad}} = \left(\frac{\pi}{2}\right)^5 2 \frac{\sqrt{\varepsilon_r}}{n_{\mathrm{mod}}(f)} \left[1 - \frac{n_{\mathrm{mod}}^2(f)}{\varepsilon_r}\right]^2 \frac{(s+2w)^2 \varepsilon_r^{3/2}}{c^3 K(k) K(\sqrt{1-k^2})} f^3 , \tag{E.16}$$

and similarly for the CPS line,

$$\alpha_{\mathrm{cpsrad}} = \pi^5 \frac{3-\sqrt{8}}{2} \frac{n_{\mathrm{mod}}(f)}{\sqrt{\varepsilon_r}} \left[1 - \frac{n_{\mathrm{mod}}^2(f)}{\varepsilon_r}\right]^2 \frac{(s+2w)^2 \varepsilon_r^{3/2}}{c^3 K(k) K(\sqrt{1-k^2})} f^3 . \tag{E.17}$$

These equations should be valid for geometries with $0.1 < s/w < 10$ and $d > 3w$ and for wavelengths $\lambda > s + 2w$.

F Dimensions and Parameters of Example Structures

The example structures are shown in Fig. F.1. An optical rib waveguide is combined with transmission line structures on an AlGaAs substrate. The substrate has the usual growth [100] and cleaving [011] directions and consists of the following layers: an infinitely extended substrate $Al_{0.24}Ga_{0.76}As$ (n_1), a 1.5 μm core layer of $Al_{0.18}Ga_{0.82}As$ (n_2), and a 1.0 μm $Al_{0.24}Ga_{0.76}As$ (n_1) cladding layer.

The values of the dielectric constants used in the calculations can be found in Tab. F.1. Furthermore, the geometry of the rib waveguide is specified. The optical index of refraction

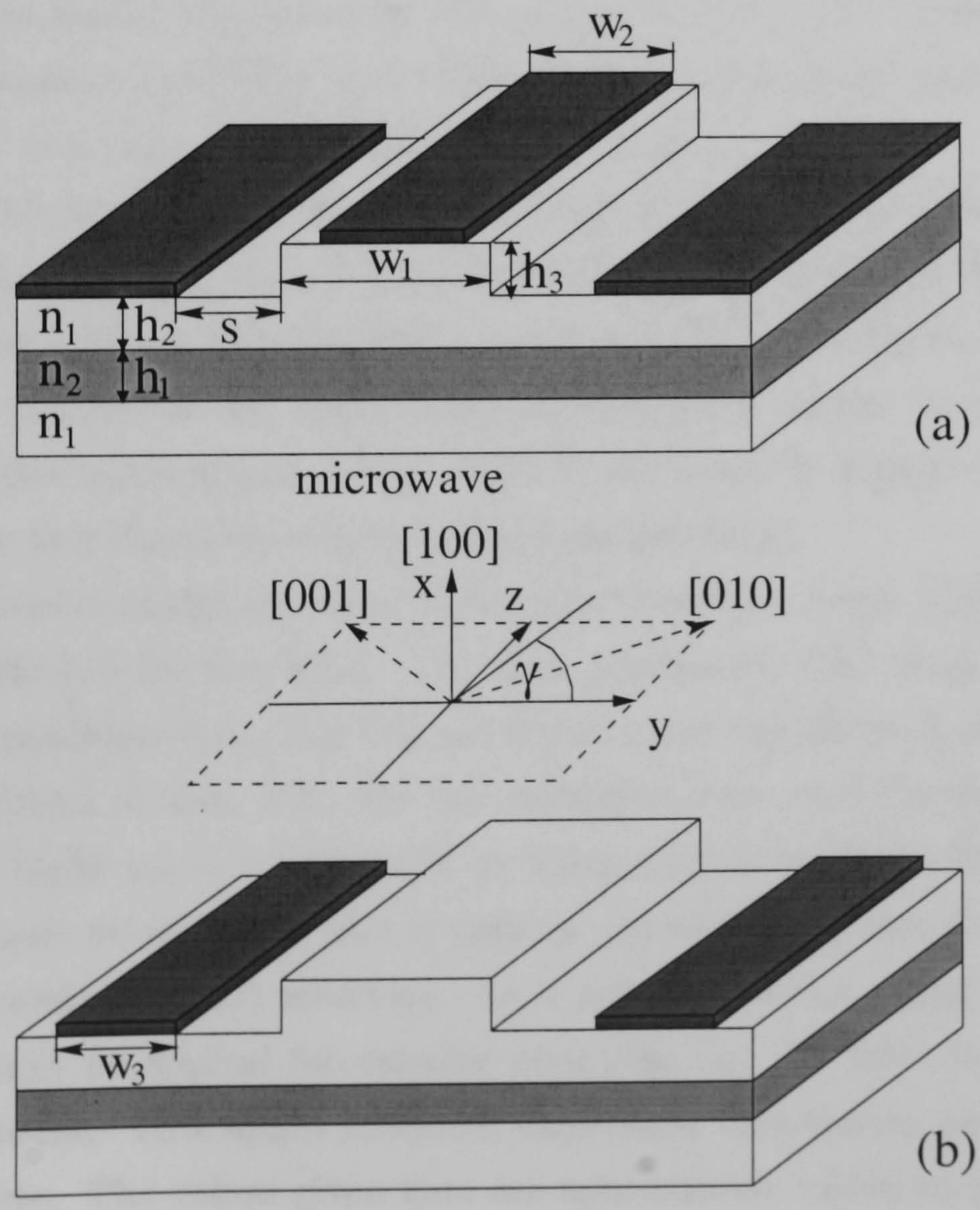

Figure F.1: Sketch of transmission line structures used in calculations: an optical rib waveguide is combined with (a) a coplanar waveguide (CPW) and (b) a coplanar stripline (CPS).

$n_1(0)$	$n_2(0)$	$n_1(\lambda)$	$n_2(\lambda)$	h_1 (μm)	h_2 (μm)	h_3 (μm)	w_1 (μm)
3.49	3.52	3.2509	3.2809	1.5	0.2	0.8	4.0

Table F.1: Parameters of substrate of structures depicted in Fig. F.1; the optical wavelength is $\lambda = 1.6\mu$m; also included is the geometry of the optical rib waveguide.

Quantity	Symbol	Value
effective index	n_{TE}	3.26573
	n_{TM}	3.26548
	$\Delta n = n_{\mathrm{TE}} - n_{\mathrm{TM}}$	0.00025
group index	$n_{\mathrm{TE}}^{\mathrm{gr}}$	3.41797
	$n_{\mathrm{TM}}^{\mathrm{gr}}$	3.41821
	$\Delta n^{\mathrm{gr}} = n_{\mathrm{TE}}^{\mathrm{gr}} - n_{\mathrm{TM}}^{\mathrm{gr}}$	-0.00024
dispersion	D_{TE}	1.233 ps^2/m
	D_{TM}	1.231 ps^2/m

Table F.2: Calculated optical parameters of the example structure at $\lambda = 1.6\mu$m.

is based on the model introduced by Afromowitz in [129]. The values for the zero frequency dielectric constant are obtained by a simple interpolation scheme using the dielectric constants $\varepsilon_{r\mathrm{GaAs}} = 12.9$ and $\varepsilon_{r\mathrm{AlAs}} = 10.0$ as it was done in [63].

The optical parameters of the corresponding optical waveguide have been calculated with the finite difference technique described in Section 4.3.1. All parameters can be found in Tab. F.2. The group indices and dispersion values include mode dispersion. The electrodes are assumed not to influence the mode profile of the optical modes. In a practical device, a thin film of low index material (e.g. SiO_2) might be necessary to separate the optical modes from the electrodes and therefore to prevent high optical losses.

The microwave modes of the example structures have been calculated by the static approach described in Section 4.3.2. The field profiles are then used for the computation of the effective nonlinearities. The line parameters and the corresponding effective nonlinearities can be found in Tab. F.3. For the calculations we used the value of the electro-optic coefficient of GaAs $r_{41} = -1.53\,\mathrm{pm/V}$ at 1.5 μm given in [130]. The dispersion coefficient T_{mic} corresponds to eq. (E.2) and is only an approximate value for modal dispersion in a planar (i.e. without a rib) structure. In a practical device based on AlGaAs, slow wave structures might be applied for velocity matching, e.g. by introduction of gratings in the ground electrodes. This might influence dispersion, attenuation and also overlap integrals of the structure. The values given here are approximate values to get an impression of the physical magnitudes involved.

Quantity	Symbol	Value
effective index	n_{cpwmic}	2.40
	n_{cpsmic}	2.59
impedance	Z_{cpw}	62.4 Ω
	Z_{cps}	108.0 Ω
effective nonlinearity	$\chi_{\text{cpw}}(=\chi_{\text{eff1}})$	1.0×10^{-13} s/m$\sqrt{\text{W}}$
	$\chi_{\text{cps}}(=\chi_{\text{eff2}})$	6.1×10^{-14} s/m$\sqrt{\text{W}}$
	χ_{eff3} (CPW)	1.5×10^{-14} s/m$\sqrt{\text{W}}$
overlap integral	$\Gamma_{\text{cpw}}(=\Gamma_1)$	0.57
	$\Gamma_{\text{cps}}(=\Gamma_2)$	0.38
dispersion	T_{mic}	1.0×10^{-35} s^3/m

Table F.3: Estimated parameters of the example CPW and CPS structures, w_2=3μm, w_3=5μm, s=3μm. Note that $\chi_{\text{eff2}} = 0$ for the symmetric CPW line and $\chi_{\text{eff1}} = \chi_{\text{eff3}} = 0$ for the symmetric CPS line.

Z_0 (m)	T_0 (ps)	A_{mic} ($\sqrt{\text{W}}$)	A_{opt} ($\sqrt{\text{W}}$)	δ ($\Delta n = 0.01$)	ζ	χ
1.5	1.4	0.0057	0.32	37.0	6×10^{-4}	5×10^{-5}

Table F.4: Scaling parameters (see Section 5.3) of example CPW structure.

In Section 5.3, the evolution equations for the scalar interaction between microwave and optical wave are scaled to dimensionless variables. In Tab. F.4 the corresponding scaling parameters for the CPW structure are given. The example value for the variable system parameter δ is given for an assumed velocity mismatch $\Delta n = 0.01$.

Bibliography

[1] M. C. Nuss and J. Orenstein, "Terahertz time-domain spectroscopy," in *Millimeter and submillimeter wave spectroscopy of solids*, Vol. 74 of *Topics in applied physics*, G. Grüner, ed., (Springer-Verlag Berlin, 1998), pp. 7–50.

[2] B. B. Hu and M. Nuss, "Imaging with terahertz waves," Opt. Lett. **20,** 1716–1718 (1995).

[3] U. D. Keil, D. R. Dykaar, A. F. J. Levi, R. F. Kopf, L. N. Pfeiffer, S. B. Darack, and K. W. West, "High-speed coplanar transmission lines," IEEE J. Quantum Electron. **28,** 2333–2342 (1992).

[4] D. H. Auston, "Ultrafast optoelectronics," in *Ultrashort laser pulses and applications*, Vol. 60 of *Topics in applied physics*, W. Kaiser, ed., (Springer Verlag Berlin, 1992), pp. 183–233.

[5] D. H. Auston, "Impulse response of photoconductors in transmission lines," IEEE J. Quantum Electron. **19,** 639–648 (1983).

[6] M. Bass, P. A. Franken, J. F. Ward, and G. Weinreich, "Optical rectification," Phys. Rev. Lett. **9,** 446–448 (1962).

[7] M. Bass, P. A. Franken, and J. F. Ward, "Optical rectification," Phys. Rev. **138,** A534–A542 (1965).

[8] B. N. Morozov and Y. M. Aivazyan, "Optical rectification and its applications (review)," Sov. J. Quantum Electron. **1,** 1–16 (1980).

[9] D. H. Auston, K. P. Cheung, J. A. Valdmanis, and D. A. Kleinman, "Cherenkov radiation from femtosecond optical pulses in electro-optic media," Phys. Rev. Lett. **53,** 1555–1558 (1984).

[10] Y. H. Jin and X. C. Zhang, "Terahertz optical rectification," J. of Nonlinear Opt. Phys. and Materials **4,** 459–495 (1995).

[11] R. Huber, A. Brodschelm, F. Tauser, and A. Leitenstorfer, "Generation and field-resolved detection of femtosecond electromagnetic pulses tunable up to 41 THz," Appl. Phys. Lett. **76,** 3191–3193 (2000).

[12] A. Bonvalet, M. Joffre, J. L. Martin, and A. Migus, "Generation of ultrabroadband femtosecond pulses in the mid-infrared by optical rectification of 15 fs light pulses at 100 MHz repetition rate," Appl. Phys. Lett. **67,** 2907–2909 (1995).

[13] Y. S. Lee, T. Meade, V. Perlin, H. Winful, T. B. Norris, and A. Galvanauskas, "Generation of narrow-band terahertz radiation via optical rectification of femtosecond pulses in periodically poled lithium niobate," Appl. Phys. Lett. **76,** 2505–2507 (2000).

[14] G. I. Stegeman, D. J. Hagan, and L. Torner, "$\chi^{(2)}$ cascading phenomena and their applications to all-Optical signal processing, mode locking, pulse compression and solitons," Opt. Quantum Electron. **28,** 1691–1740 (1996).

[15] C. Etrich, F. Lederer, B. A. Malomed, T. Peschel, and U. Peschel, "Optical solitons in media with a quadratic nonlinearity," in *Progress in Optics*, E. Wolf, ed., (Elsevier Science B.V., Amsterdam, London, New York, 2000), Vol. 41, pp. 485–565.

[16] T. K. Gustafson, J.-P. E. Taran, P. L. Kelley, and R. Y. Chiao, "Self-modulation of picosecond pulses in electro-optic crystals," Opt. Comm. **2,** 17–21 (1970).

[17] C. Bosshard, R. Spreiter, M. Zgonik, and P. Günter, "Kerr nonlinearity via cascaded optical rectification and the linear electro-optic effect," Phys. Rev. Lett. **74,** 2816–2818 (1995).

[18] S. K. Lee and C. S. Yoon, "Nonlinear phase shift by cascaded optical rectification and linear electro-optic effect," Opt. Rev. **6,** 152–154 (1999).

[19] C. Kolleck, "$\chi^{(2)}$ cascading by means of optical rectification in a planar slab waveguide," J. Opt. Soc. Am. B **16,** 1250–1260 (1999).

[20] V. V. Steblina, A. V. Buryak, R. A. Sammut, D. Zhou, M. Segev, and P. Prucnal, "Stable self-guided propagation of two optical harmonics coupled by a microwave or a terahertz wave," J. Opt. Soc. Am. B **17,** 2026–2031 (2000).

[21] T. Iizuka and Y. S. Kivshar, "Optical gap solitons in nonresonant quadratic media," Phys. Rev. E **59,** 7148–7151 (1999).

[22] A. G. Kalocsai and J. W. Haus, "Asymptotic wave-wave processes beyond cascading in quadratic nonlinear optical materials," Phys. Rev. E **52,** 3166–3183 (1995).

[23] M. J. Ablowitz, G. Biondini, and S. Blair, "Multi-dimensional pulse propagation in non-resonant $\chi^{(2)}$ materials," Phys. Lett. A **236,** 520–524 (1997).

[24] M. J. Ablowitz, G. Biondini, and S. Blair, "Nonlinear Schroedinger equations with mean terms in nonresonant multidimensional quadratic materials," Phys. Rev. E **63,** 046605–1–15 (2001).

[25] N. A. F. Jaeger and Z. K. F. Lee, "Slow-wave electrode for use in compound semiconductor electrooptic modulators," IEEE J. Quantum Electron. **28,** 1778–1784 (1992).

[26] R. C. Alferness, "Waveguide electrooptic modulators," IEEE Trans. Microwave Theory Tech. **30,** 1121–1137 (1982).

[27] D. R. Grischkowsky, "Optoelectronic characterization of transmission lines and waveguides by terahertz time-domain spectroscopy," IEEE J. Select. Topics Quantum Electron. **6,** 1122–1135 (2000).

[28] A. Nahata, "Nonlinear optical generation and detection of ultrashort electrical pulses in transmission lines," Opt. Lett. **26,** 385–387 (2001).

[29] A. Nahata and T. F. Heinz, "Generation of subpicosecond electrical pulses by optical rectification," Opt. Lett. **23,** 867–869 (1998).

[30] S. Graf, H. Sigg, and W. Bächtold, "High-frequency electrical pulse generation using optical rectification in bulk GaAs," Appl. Phys. Lett. **76,** 2647–2649 (2000).

[31] P. N. Butcher and D. Cotter, *The Elements of Nonlinear Optics*, Vol. 9 of *Cambridge Studies in Modern Optics* (Cambridge University Press, Cambridge, UK, 1990).

[32] R. W. Boyd, *Nonlinear Optics* (Academic Press, Inc., 1992).

[33] J. A. Armstrong, N. Bloembergen, J. Ducuing, and P. S. Pershan, "Interactions between light waves in a nonlinear dielectric," Phys. Rev. **127,** 1918–1939 (1962).

[34] L. B. Felsen and N. Marcuvitz, *Radiation and scattering of waves* (Prentice-Hall Inc., New Jersey, 1973).

[35] H. Kogelnik, "Theory of optical waveguides," in *Guided-Wave Optoelectronics*, Vol. 26 of *Springer Series in Electronics and Photonics*, T. Tamir, ed., (Springer Verlag Berlin, 1988), pp. 1–88.

[36] U. Peschel, K. Bubke, D. C. Hutchings, J. S. Aitchison, and J. M. Arnold, "Optical rectification in a travelling-wave geometry," Phys. Rev. A **60,** 4918–4926 (1999).

[37] K. Bubke, U. Peschel, and D. C. Hutchings, "Mixed polarization optical rectification in semiconductor waveguides," to be published in J. Opt. Soc. Am. B (2001).

[38] W. F. Ames, *Numerical methods for Partial Differential Equations* (Academic Press, New York, 1977).

[39] A. P. Ansbro and I. Montrosset, "Vectorial finite difference scheme for isotropic dielectric wave guides: transverse electric field representation," IEE Proc. J. **140,** 253–259 (1993).

[40] P. Lüsse, P. Stuwe, J. Schüle, and H. G. Unger, "Analysis of vectorial fields in optical waveguides by a new finite difference method," J. Lightwave Technol. **12,** 484–497 (1994).

[41] B. M. Dillon and J. P. Webb, "A comparison of formulations for the vector finite element analysis of waveguides," IEEE Trans. Microwave Theory Tech. **42,** 308–316 (1994).

[42] A. S. Sudbo, "Improved formulation of the film mode matching method for mode field calculations in dielectric waveguides," Pure Appl. Opt. **3,** 381–388 (1994).

[43] R. Mittra, Y.-L. Hou, and V. Jamnejad, "Analysis of open dielectric waveguides using mode-matching technique and variational methods," IEEE Trans. Microwave Theory Tech. **28,** 36–43 (1980).

[44] C. Vasallo, "1993-1995 Optical Mode Solvers," Opt. Quantum Electron. **29,** 95–114 (1997).

[45] K. Radhakrishnan and W. C. Chew, "Full-wave analysis of multiconductor transmission lines on anisotropic inhomogeneous substrates," IEEE Trans. Microwave Theory Tech. **47,** 1764–1770 (1999).

[46] K. B. Bierwirth, N. Schulz, and F. Arndt, "Finite-difference analysis of rectangular dielectric waveguide structures," IEEE Trans. Microwave Theory Tech. **34,** 1104–1114 (1986).

[47] M. S. Stern, "Semivectorial polarised finite difference method for optical waveguides with arbitrary index profiles," IEE Proc. J **135,** 56–63 (1988).

[48] A. Wexler, "Computation of electromagnetic fields," IEEE Trans. Microwave Theory Tech. **17,** 416–439 (1969).

[49] T. Rozzi, G. Cerri, M. N. Husain, and L. Zapelli, "Variational analysis of the dielectric rib waveguide using the concept of "Transition Function" and including edge singularities," IEEE Trans. Microwave Theory Tech. **39,** 247–256 (1991).

[50] K. J. Maschhoff and D. C. Sorensen, "P_ARPACK: An efficient portable large scale eigenvalue package for distributed memory parallel architectures," in *Applied parallel computing in industrial problems and optimization*, Vol. 1184 of *Lecture Notes in Computer Science*, J. Wasniewsky, J. Dongarra, K. Madsen, and D. Olesen, eds., (Springer-Verlag Berlin, 1996).

[51] K. C. Gupta, R. Garg, and I. J. Bahl, *Microstrip lines and slotlines* (Artech House Inc., Massachusetts, 1979).

[52] H. E. Green, "The numerical solution of some important transmission-line problems," IEEE Trans. Microwave Theory Tech. **13,** 676–692 (1965).

[53] G. Hasnain, A. Dienes, and J. R. Whinnery, "Dispersion of picosecond pulses in coplanar transmission lines," IEEE Trans. Microwave Theory Tech. **34,** 738–741 (1986).

[54] T. Tamir, *Guided-wave optoelectronics*, Vol. 26 of *Springer Series in Electronics and Photonics* (Springer-Verlag Berlin, 1990).

[55] W. H. Knox, J. E. Henry, K. W. Goossen, K. D. Li, B. Tell, D. A. B. Miller, D. S. Chemla, A. C. Gossard, J. English, and S. Schmitt-Rink, "Femtosecond excitonic optoelectronics," IEEE J. Quantum Electron. **25,** 2586–2595 (1989).

[56] D. S. Phatak and A. P. Defonzo, "Dispersion characteristics of optically excited coplanar striplines: pulse propagation," IEEE Trans. Microwave Theory Tech. **38,** 654–661 (1990).

[57] M. Y. Frankel, S. Gupta, J. A. Valdamis, and G. A. Mourou, "Terahertz attenuation and dispersion characteristics of coplanar transmission lines," IEEE Trans. Microwave Theory Tech. **39,** 910–916 (1991).

[58] D. Grischkowsky, I. N. Duling, III, J. C. Chen, and C.-C. Chi, "Electromagnetic shock waves from transmission lines," Phys. Rev. Lett. **59,** 1663–1666 (1987).

[59] C. Fattinger and D. Grischkowsky, "Observation of electromagnetic shock waves from propagating surface-dipole distributions," Phys. Rev. Lett. **62,** 2961 (1989).

[60] D. A. Kleinmann and D. H. Auston, "Theory of electrooptic shock radiation in nonlinear optical media," IEEE J. Quantum Electron. **20,** 964–970 (1984).

[61] D. B. Rutledge, D. P. Neikirk, and D. P. Kasislingham, "Integrated circuit antennas," in *Infrared and millimeter waves*, K. J. Button, ed., (Academic Press, New York, 1983), Vol. 10.

[62] G. Hasnain, K. W. Goossen, and W. H. Knox, "Effect of optical phonons on femtosecond pulse propagation in coplanar striplines," Appl. Phys. Lett. **56,** 515–517 (1990).

[63] S. Adachi, "GaAs, AlAs, and $Al_xGa_{1-x}As$: Material parameters for use in research and device applications," J. Appl. Phys. **58,** R1–R29 (1985).

[64] C. J. Osbahr, B. H. Larsen, T. Hoist, Y. Shen, and S. R. Keiding, "2 THz bandwidth electrical pulses on Au and $Yba_2Cu_3O_x$ transmission lines," Appl. Phys. Lett. **74,** 1892–1894 (1999).

[65] R. J. Dery and E. Kapon, "Low-loss III-V semiconductor optical waveguides," IEEE J. Quantum Electron. **27,** 626–640 (1991).

[66] V. Loyo-Maldonado, personal communications.

[67] K. Noguchi, O. Mitomi, H. Miyazawa, and S. Seki, "A broadband Ti:$LiNbO_3$ optical modulator with a ridge structure," J. Lightwave Technol. **13,** 1164–1168 (1995).

[68] R. G. Walker, "High-speed III-V semiconductor intensity modulators," IEEE J. Quantum Electron. **27,** 654–667 (1991).

[69] F. Rahmatian, N. F. Jaeger, R. James, and E. Berolo, "An ultrahigh-speed AlGaAs-GaAs polarization converter using slow-wave coplanar electrodes," IEEE Photon. Technol. Lett. **10,** 675–677 (1998).

[70] G. K. Gopalakrishnan, W. K. Burns, R. W. McElhanon, C. H. Bulmer, and A. S. Greenblatt, "Performance and modeling of broadband $LiNbO_3$ traveling wave optical intensity modulators," J. Lightwave Technol. **12,** 1807–1819 (1994).

[71] R. Spickermann and N. Dagli, "Experimental analysis of millimeter wave coplanar waveguide slow wave structures on GaAs," IEEE Trans. Microwave Theory Tech. **42,** 1918–1924 (1994).

[72] A. F. Harvey, "Periodic and guiding structures at microwave frequencies," IRE Trans. Microwave Theory Tech. **MTT-8,** 30–61 (1960).

[73] *EMLAB-ISE User's manual* (ISE Integrated Systems Engineering AG, Balgriststrasse 102, CH 8008 Zurich, Switzerland, 2001).

[74] A. Taflove, *Computational electrodynamics; the finite-difference time-domain method* (Artech House, Inc., 1995).

[75] G. P. Agraval, *Nonlinear Fiber Optics* (Academic Press, New York, 1989).

[76] H. J. Bakker, P. C. M. Planken, L. Kuipers, and A. Lagendijk, "Phase modulation in second-order nonlinear-optical processes," Phys. Rev. A **42,** 4085–4100 (1990).

[77] A. Kobyakov and F. Lederer, "Cascading of quadratic nonlinearities: an analytical study," Phys. Rev. A **54,** 3455–3471 (1996).

[78] R. DeSalvo, D. J. Hagan, M. Sheik-Bahae, G. Stegeman, E. W. Van-Stryland, and H. Vanherzeele, "Self-focusing and self-defocusing by cascaded second-order effects in KTP," Opt. Lett. **17,** 28–30 (1992).

[79] F. Shimizu, "Frequency broadening in liquids by a short light pulse," Phys. Rev. Lett. **19,** 1097–1100 (1967).

[80] J. S. Russell, "Report on waves," Rep. 14th Meet. Brit. Assoc. Adv. Sci. pp. 319–320 (1844).

[81] R. K. Dodd, J. C. Eilbeck, J. D. Gibbon, and H. C. Morris, *Solitons and nonlinear wave equations* (Academic Press, New York, 1982).

[82] N. J. Zabusky and M. D. Kruskal, "Interaction of solitons in a collisionless plasma and the recurrence of initial states," Phys. Rev. Lett. **15,** 240–243 (1965).

[83] M. J. Ablowitz and H. Segur, *Solitons and the inverse scattering transform* (SIAM Philadelphia, 1981).

[84] A. Hasegawa and F. Tappert, "Transmission of stationary nonlinear optical pulses in dispersive dielectric fibers. I. Anomalous dispersion," Appl. Phys. Lett. **23,** 142–144 (1973).

[85] L. F. Mollenauer, R. H. Stolen, and J. P. Gordon, "Experimental observation of picosecond pulse narrowing and solitons in optical fibers," Phys. Rev. Lett. **45,** 1095–1098 (1980).

[86] Y. N. Karamzin and A. P. Sukhorukov, "Nonlinear interaction of diffracted light beams in a medium with quadratic nonlinearity: mutual focusing of beams and limitation on the efficiency of optical frequency converters," JETP Lett. **20,** 339–342 (1974).

[87] W. E. Torruellas, Z. Wang, D. J. Hagan, E. W. VanStryland, G. I. Stegeman, L. Torner, and C. R. Menyuk, "Observation of two-dimensional spatial solitary waves in a quadratic medium," Phys. Rev. Lett. **74,** 5036–5039 (1995).

[88] R. Schiek, Y. Baek, and G. I. Stegeman, "One-dimensional spatial solitary waves due to cascaded second-order nonlinearities in planar waveguides," Phys. Rev. E **53,** 1138–1141 (1996).

[89] D. J. Korteweg and G. deVries, "On the change of form of long waves advancing in a rectangular canal, and on a new type of long stationary waves," Phil. Mag. **39,** 422–443 (1895).

[90] A. C. Scott, F. Y. F. Chu, and D. W. McLaughlin, "The soliton: a new concept in applied science," Proc. IEEE **61,** 1443–1483 (1973).

[91] K. E. Lonngren, "Observation of solitons on nonlinear dispersive transmission lines," in *Solitons in action*, A. Lonngren and A. Scott, eds., (Academic Press, New York, New York, San Francisco, London, 1978), pp. 127–152.

[92] T. Kuusela, "Soliton experiments in transmission lines," Chaos, Solitons a. Fractals **5,** 2419–2462 (1995).

[93] A. Scott, *Nonlinear Science* (University Press, Oxford, 1999).

[94] D. J. Benney, "A general theory for interactions between short and long waves," Studies in Appl. Math. **56,** 81–94 (1977).

[95] Y. C. Ma, "The complete solution of the long-wave-short-wave resonance equations," Studies in Appl. Math. **59,** 201–221 (1978).

[96] N. Yajima and M. Oikawa, "Formation and interaction of sonic-Langmuir Solitons," Progr. Theor. Phys. **56,** 1719–1739 (1976).

[97] E. Benilov and S. P. Burtsev, "To the integrability of the equations describing the Langmuir-wave-ion-acoustic-wave interaction," Phys. Lett. A **98,** 256–258 (1983).

[98] T. Yoshinaga and T. Kakutani, "Solitary and E-shock waves in a resonant system between long and short waves," J. Phys. Soc. Jpn. **63,** 445–459 (1994).

[99] T. Yoshinaga, "Oscillatory solitary waves in a resonant system between long gravity and short capillary waves," J. Phys. Soc. Jpn. **66,** 1018–1023 (1997).

[100] T. Kawahara, N. Sugimoto, and T. Kakutani, "Nonlinear interaction between short and long capillary-gravity waves," J. Phys. Soc. Jpn. **39,** 1379–1386 (1975).

[101] K. N. Nishikawa, H. Hojo, K. Mima, and H. Ikezi, "Coupled nonlinear electron-plasma and ion-acoustic waves," Phys. Rev. Lett. **33,** 148–151 (1974).

[102] J. Sakai and T. Kawata, "Nonlinear wave modulation in transmission line," J. Phys. Soc. Jpn. **41,** 1819–1820 (1976).

[103] T. Yoshinaga, N. Sugimoto, and T. Kakutani, "Nonlinear wave interactions on a discrete transmission line," J. Phys. Soc. Jpn. **50,** 2122–2128 (1981).

[104] M. Tabor, *Chaos and integrability in nonlinear dynamics* (John Wiley & Sons, Inc., 1989).

[105] S. Trillo and P. Ferro, "Modulational instability in second-harmonic generation," Opt. Lett. **20,** 438–440 (1995).

[106] H. He, P. D. Drummond, and B. A. Malomed, "Modulational stability in dispersive optical systems with cascaded nonlinearity," Opt. Comm. **123,** 394–402 (1996).

[107] U. Peschel, K. Bubke, D. C. Hutchings, and J. S. Aitchison, "Pulse propagation and soliton formation using optical rectification," In *Nonlinear Guided Waves and Their Applications*, OSA Technical Digest pp. 19–21 (Dijon, France, 1999).

[108] L. Torner, C. R. Menyuk, and G. I. Stegeman, "Bright solitons with second-order nonlinearities," J. Opt. Soc. Am. B **12,** 889–897 (1995).

[109] C. Etrich, U. Peschel, F. Lederer, and B. Malomed, "Collision of solitary waves in media with a second-order nonlinearity," Phys. Rev. A **52,** 3444–3447 (1995).

[110] D. Jäger, "Characteristics of travelling waves along the non-linear transmission lines for monolithic integrated circuits: a review," Int. J. Electronics **58,** 649–669 (1985).

[111] M. J. W. Rodwell *et al.*, "Active and nonlinear wave propagation devices in ultrafast electronics and optoelectronics," Proc. IEEE **82,** 1037–1059 (1994).

[112] G. Schneider, "The long wave limit for a boussinesq equation," SIAM J. Appl. Math. **58,** 1237–1245 (1998).

[113] L. Xu, D. H. Auston, and A. Hasegawa, "Propagation of electromagnetic solitary waves in dispersive nonlinear dielectrics," Phys. Rev. A **45,** 3184–3193 (1992).

[114] K. Bubke, U. Peschel, and D. C. Hutchings, "KdV solitons on GaAs transmission lines due to the intrinsic second order nonlinearity," In *Nonlinear Guided Waves and Their Applications*, OSA Technical Digest pp. 339–341 (Dijon, France, 1999).

[115] D. E. Pelinovsky, A. V. Buryak, and Y. S. Kivshar, "Instability of solitons governed by quadratic nonlinearities," Phys. Rev. Lett. **75,** 591–595 (1995).

[116] D. E. Pelinovsky, J. E. Sipe, and J. Yang, "Generation of soliton oscillations in nonlinear quadratic materials," Phys. Rev. E **59,** 7250–7253 (1999).

[117] C. Etrich, U. Peschel, F. Lederer, B. Malomed, and Y. S. Kivshar, "Origin of the persistent oscillations of solitary waves in nonlinear quadratic media," Phys. Rev. E **54,** 4321–4324 (1996).

[118] R. L. Pego and M. I. Weinstein, "Eigenvalues, and instabilities of solitary waves," Philos. Trans. R. Soc. London A **340,** 47–94 (1992).

[119] D. E. Pelinovsky, Y. S. Kivshar, and V. V. Afanasjev, "Internal modes of envelope solitons," Physica D **116,** 121–142 (1998).

[120] Y. S. Kivshar, D. E. Pelinovsky, T. Cretegny, and M. Peyrard, "Internal modes of solitary waves," Phys. Rev. Lett. **80,** 5032–5035 (1998).

[121] J. Yang, B. A. Malomed, and D. J. Kaup, "Embedded solitons in second-harmonic-generating systems," Phys. Rev. Lett. **83,** 1958–1961 (1999).

[122] D. C. Hutchings, J. M. Arnold, and D. F. Parker, "Stationary mixed-polarization spatial solitons and their stability in semiconductor waveguides," Phys. Rev. E **58,** 6649–6658 (1998).

[123] W. H. Press, S. A. Teukolsky, W. T. Vetterling, and B. P. Flannery, *Numerical Recipes in C: The Art of Scientific Computing* (Cambridge University Press, Cambridge, 1992).

[124] G. Gallot, S. P. Jamison, R. W. McGowan, and D. Grischkowsky, "Terahertz waveguides," J. Opt. Soc. Am. B **17,** 851–863 (2000).

[125] S. P. Jamison, R. W. McGowan, and D. Grischkowsky, "Single-mode waveguide propagation and reshaping of sub-ps terahertz pulses in sapphire fibers," Appl. Phys. Lett. **76,** 1987–1989 (2000).

[126] R. W. McGowan, G. Gallot, and D. Grischkowsky, "Propagation of ultrawideband short pulses of terahertz radiation through submillimeter-diameter circular waveguides," Opt. Lett. **24,** 1431–1433 (1999).

[127] R. Mendis and D. Grischkowsky, "Plastic ribbon THz waveguides," J. Appl. Phys. **88,** 4449–4451 (2000).

[128] M. Börner, R. Müller, R. Schiek, and G. Trommer, *Elements of Integrated Optics* (Teubner, Stuttgart, 1990), in German.

[129] M. A. Afromowitz, "Refractive index of $Ga_{1-x}Al_xAs$," Solid State Comm. **15,** 59–63 (1974).

[130] *Properties of gallium arsenide*, Vol. 2 of *EMIS datareviews series* (INSPEC, London, 1990).

[131] M. Ohashi, T. Kondo, R. Ito, S. Fukatsu, Y. Shiraki, K. Kumata, and S. S. Kano, "Determination of quadratic nonlinear optical coefficients of $Al_xGa_{1-x}As$," J. Appl. Phys. **74,** 596–601 (1993).